A Thesis

entitled

Modeling and Parameter Estimation of Solar Photovoltaic Array

by

ABHISHEK CHAUHAN

Registration No. 951504002

Submitted to the Department of Electrical & Instrumentation Engineering as Fulfilment of the Requirement for the Award of the Degree of

DOCTOR OF PHILOSOPHY

Under the Supervision of

Dr. SURYA PRAKASH

Associate Professor

Department of Electrical & Instrumentation Engineering
Thapar Institute of Engineering and Technology Patiala,
Punjab-India

Thapar Institute of Engineering and Technology
(Deemed-to-be-University)
Patiala (Punjab), India-147004
08 August 2022

“पराभव आशा”

मै मृत्युन: पराभव आशा हूँ.....!

मृदुल मनोरथ मोक्ष मंत्र से मुक्त यह आशा,

प्रत्यक्ष की कुंठा में रूपित है यह आशा,

राग भैरवी सुन शोभित यह अति आशा,

मै मृत्युन: पराभव आशा हूँ.....!

भूत भविष्य की आकुलता से उद्दृत यह आशा,

आधीन की अधीर सी यह आशा,

मरुस्थल में अपार सिंधु सी यह आशा,

मै मृत्युन: पराभव आशा हूँ.....!

क्षणिक चित: की स्थिरता सी यह आशा,

असंभव के संभव होने की यह आशा,

अपार रंगों पर फैली यह धवल आशा,

पुनर्विचार को आमंत्रित यह आशा,

मै मृत्युन: पराभव आशा हूँ.....!

:अभिषेक चौहान

Dedication

“I would like to dedicate this thesis to

my respected Grand Father (Ch. Niranjan Singh), Parents

Sisters (*Vibha & Vinesha*)

and

Loving wife Sonal”

THAPAR INSTITUTE
OF ENGINEERING & TECHNOLOGY
(Deemed to be University)

Electrical & Instrumentation Engineering Department

Thapar Institute of Engineering and Technology

CERTIFICATE

I hereby certify that the work which is being presented in the thesis entitled, "**Modeling and Parameter Estimation of Solar Photovoltaic Array**" is in fulfillment of the requirement for the award of the Degree of **Doctor of Philosophy** submitted in the **Electrical & Instrumentation Engineering Department** of the **Thapar Institute of Engineering & Technology** is an authentic record of my work carried out under the supervision of **Dr. Surya Prakash**, and refer other researcher's work, which is duly listed in the reference section.

The matter presented in this thesis has not been submitted for the award of any other degree of this or any other University.

Abhishek Chauhan
Reg. No. (951504002)

This is to certify that the above statement made by the candidate is correct to the best of my knowledge.

Dr. Surya Prakash
Associate Professor
EIED, Thapar Institute of Engineering and Technology
(Deemed to be University), Patiala, Punjab

Date: 08/08/2022

Abstract

Various advantages allied with the solar PV, also faces numerous challenges that comprise the designing of best possible configurations for solar PV arrays, optimised power converters with converter protocols, optimised maximum power point tracking (MPPT) techniques, and prediction of generated power under real-time environmental conditions. Hence, various simulations are to be executed at specific software platforms through various solar PV electrical models, where modeling of these quantified electrical equivalent models should be reliable, robust, and accurate. In view of this it is important to comprehend that the precision of a commercially available solar PV simulation software resides on the electrical PV model selected, the model parameter extraction technique incorporated, and the preciseness in estimated model parameters through various techniques.

This research aims the assessment of precise solar PV modeling parameters, validated through experimental current-voltage (*I*-*V*) data, and to achieve this goal, the research is divided into three key objectives. The first major contribution of the thesis includes the physical interpretation and behavior of the solar PV, various equivalent models are studied and characterized, where single diode model (SDM), double-diode model (DDM), and three-diode model (TDM) are selected and considered for the implementation of various parameter estimation approaches.

Whereas, the rest two objectives comprise the implementation of five new methodologies for the parameter estimation under different environmental conditions. As the parameter estimation problem is a non-linear engineering problem, where the literature recommends precise results through metaheuristic and hybrid techniques, hence three novel metaheuristic methodologies and two new hybrid approaches are instigated in this research.

Initially, a new Emperor Penguin Optimisation (EPO) based parameter estimation approach for an SDM is presented, that is cohesively analysed under different sets of temperature (*T*) and irradiance (*G*). Validation of the proposed technique is perceived on the analysis of performance characteristics *i.e. I*-*V* and power-voltage (*P*-*V*) of KC200GT, PWP201, and STP6 120-36 PV modules under various simulations conditions. Moreover, estimated results are compared with the experimental data and several established parameter

estimation techniques in the literature for validation and demonstrate the proposed technique with highly precise outcomes having reduced computational cost for the PV model parameter extraction problem. The variations of estimated parameters with variables '*T*' and '*G*' are also been presented for all three modules considered.

Furthermore, six case studies are considered to estimate the parameters of SDM, DDM, and TDM through two metaheuristic techniques *i.e.* Pheromone Value Black Widow Optimisation (*pv*-BWO) and Cannibalism Black Widow Optimisation (*cn*-BWO). The results are compared on the basis of the cost associated with the objective function considered *i.e.* minimum of root mean square error (RMSE), and the convergence speed to the optimal solution, that leads towards the extraction of modeling parameters. Where, it is asserted that *pv*- BWO method gives a more reliable, stable, and precise solution for unknown parameters under investigation, on the other hand, *cn*-BWO exhibits high convergence ability for the parameter estimation problem.

An experimental test is also performed in outdoor environmental conditions, where a 149 point *I*-*V* data of EIL 75 W and SFTI 60P modules are recorded through MECO 9018BT solar PV analyzer, where '*G'* and '*T*' sensor is used to record the irradiance and temperature of the module under test. This experimental data is also incorporated for the validation of proposed techniques.

In literature, hybrid techniques are considered the most recent techniques for parameter estimation problems. Hence, two-hybrid approaches using two new metaheuristic algorithms, *i.e.* the sailfish optimisation (SFO) and spotted hyena optimisation (SHO) framework along with the Newton-Raphson method (NRM) are proposed and compared, to estimate the parameters for SDM, DDM, and TDM of solar PV. Where five case studies are presented for the investigation of the proposed methods, validated and compared through the convergence speed, accuracy of estimated parameters, analysis of *I*-*V*, and *P*-*V* performance characteristics. All the proposed methodologies are state-of-the-art and certainly not implemented for the parameter estimation problem yet in literature, where the comparison with some existing techniques and experimental data exhibits the competence of proposed methodologies. It is important to pronounce that the preciseness of the estimated parameters depends on the closeness of the objective function (OF) to zero. As the information of

exacted parameter values is not accessible, hence the degree of preciseness depends on the experimental data only. Any diminution in the OF *i.e.* RMSE is observed as a significant improvement towards the preciseness of real unknown parameter values, where the same is well observed with the proposed methodologies that exhibits more promising results when compared with the techniques in the literature.

KEYWORDS

Modeling of solar photovoltaic, Environmental conditions, Optimisation, Parameter Estimation, Renewable energy, Solar Photovoltaic.

Acknowledgment

Every research needs a problem to be solved with novel problem-solving approaches, where genuine guidance and gratitude of people makes it easier and one can enjoy this journey of problem-solving. I honestly feel short of words to acknowledge all those who helped me directly and indirectly during this mission.

With due regards and great delight, I convey my heartfelt gratitude and indebtedness to my research supervisor **Dr. Surya Prakash,** Associate Professor, Electrical & Instrumentation Engineering Department, Thapar Institute of Engineering & Technology, Patiala, for his skillful guidance, proficient evaluation, persistent encouragement, and conscientious supervision throughout this research. His vibrant persona, hard-working nature, and methodical directions were a constant source of motivation for me. Due to his able guidance, expertise, inquisitive attitude, and tireless efforts, I found my vision even more broadened. I earnestly thank him from the core of my heart for being a consistent source of inspiration right from the beginning till the end.

I would like to convey my heartiest gratitude to **Dr. Smarajit Ghosh,** Professor, **Dr. Vishal Srivastava,** Assistant Professor, Electrical & Instrumentation Engineering Department and **Dr. Manoj Kumar Sharma,** Professor, School of Physics and Material Sciences, for being the members of the Doctoral Committee and spending their valuable time in reviewing and critically examining the work during regular progress monitoring meetings.

I am also thankful to present Chairman of the Doctoral Committee **Dr. R. S. Kaler**, Senior Professor & Head, and **Dr. Mandeep Singh**, Professor & Ph.D. Coordinator, Electrical & Instrumentation Engineering Department for the much-needed support throughout the work. My heartfelt gratitude to **Dr. Rafat Siddique,** Senior Professor & Dean, Research and Sponsored Projects, and Honourable Director **Dr. Prakash Gopalan** for the encouragement, support, and providing the necessary facilities to carry out and complete this work on a steady course.

I also wish to express my deep sense of gratitude to **Dr. Sanjay Jain, Professor, Dr. Mukesh Singh, Associate Professor, Dr. Saurabh Bhardwaj, Associate Professor, Dr. Prasenjit Basak, Associate Professor, Dr. Manoj Badoni, Associate Professor, Dr.**

Shakti Singh, Assistant Professor, and all faculty and staff members of the Electrical & Instrumentation Engineering Department, who, with their encouraging words, constructive criticism, and suggestions, have contributed directly or indirectly in a significant way towards completion of this work.

I would also express my acknowledgments to **Dr. Krishan Kant Singh Mer**, Director, faculty, and staff of Institute of Technology Gopeshwar, Uttarakhand for the moral support they provide me during my research. Moreover, I am also conveying my words of respect to **Dr. R.C Bansal**, Professor, University of Sharjah, and **Dr. P. Thakur**, Professor, Graphic Era University, Dehradun for continuously reviewing my work and suggesting the required changes.

I wish to especially acknowledge my fellow Ph.D. scholars **Dr. Nagendra Singh**, **Dr. Vinit Kumar**, **Dr. Himanshu Anand**, **Dr. Rituraj Singh Patwal**, and **Dr. Anurag Verma**, for providing a congenial working environment in Lab and for being a critical reviewer. Last but not least, I bow in reverence to Almighty, who showered blessings on me at every step in completing this Thesis and ask forgiveness from those whose efforts and contribution are not acknowledged by me unintentionally.

Abhishek Chauhan

TABLE OF CONTENTS

LIST OF FIGURES

LIST OF TABLES

LIST OF ACRONYMS

ABC	Artificial Bee Colony
ABSA	Aspect based sentiment analysis
ABSO	Advance bee swarm optimisation
ACSF-CR	Adaptively controlled scalling factor and crossover rate
a-DE	Adaptive Differential Evolution
AE-MPP	Absolute Error at Max. PowerPoint
BFO	Bacterial Forging Algorithm
BPFPA	Bee pollinator flower pollination algorithm
CFA	Franklin's and Coulomb's Law Theory
cn-BWO	Cannibalism based- Black Widow Optimisation
CPSO	Comparative Particle Swarm Optimization
CR	Cross-over
CS	Cuckoo Search
CSA	Cuckoo Search Algorithm
CTSA	Chaotic Tunicate Swarm Optimisation
CWOA	Chaotic Whale Optimisation
DDM	Double Diode Model
DEIM	Discrete Empirical Interpolation for Non-Linear Model Reduction
EHA-NMS	Enhance Hybrid ABC Nelder-Mead Simplex
EPO	Emperor Penguin Optimisation
ER-WCA	Evaporation Rate-Water Cycle Algorithm
FPA	Flower Pollination Algorithm
GA	Genetic Algorithm
GCPSO	Guaranteed convergence particle swarm optimization
GWO	Grey Wolf Optimizer
HFP	Hybrid Flower Pollination
HHO	Harris Hawks Optimisation

HS	Harmony Search
H-SA	Hybrid Simulated Annealing
IADE	Improved Adaptive De
IEM	Inborn Errors of Metabolism
ImCSA	Improved Cuckoo Search Algorithm
IMFO	Improved Moth Flames Optimisation
ISCE	Improved Shuffled Complex Evolution Algorithm
ITLBO	Improved Teaching Learning-Based Optimisation
IWOA	Improved Whale Optimisation
JADE	Joint Approximation Diagonalisation of Eigen Matrices (JADE)
LMSA	Least mean square
LW	Lambert W
M-ABC	Modified artificial bee colony
MADE	Memetic Adaptive Differential Evolution
MAE	Mean Absolute Error
MAEP	Mean Absolute Error In Power
MBA	Mine Blast Algorithm
MBE	Mean Bias Error
M-DDM	Modified-Double Diode Model
MDM	Multi diode model
MDmM	Multi-Dimensional Models
MFO	Moth Flame Optimisation
MLBSA	Multi Learning Backtracking Search Algorithm
MPPT	Maximum Power Point Tracking
MPSO	Modified Particle Swarm Optimization
MVO	Multi-Verse Optimisation
NLS	Nonlinear Least Squares
NMM	Nelder-Mead Simplex Method
NMS	Nelder-Mead Simplex
NRM	Newton Raphson Method

OF	Objective Function
Pb-DE	Penalty Based DE
PDE	Partial Differential Equation
PG-JAYA	Performance Guided JAYA Algorithm
PS	Pattern Search
PSO	Particle Swarm Optimisation
PV	Photovoltaic
pv-BWO	Pheromone value-Black Widow Optimisation
RBE	Ranking based elimination
Rcr-IJADE	R_{cr}- crossover rate repairing **s**elf-adaptive **d**ifferential **e**volution
RF	Reduced forms
R-II and R-II	Rao's Algorithm
RMSE	Root Mean Square Error
SA	Simulated Annealing
SDM	Single Diode Model
SF	Scaling Factor
SFO	Sailfish Optimisation
SFS	Stochastic Fractal Search Optimisation
SHADE	Success-History Based Adaptive Differential Evolution
SHO	Spotted Hyena Optimisation
SSA	Salp Differential Equation
STD	Standard Deviation
TDM	Three Diode Model
TLBO	Teaching-Learning Based Optimisation
WC	Worst case algorithm

LIST OF NOTATIONS

I_{lo}	Output current
I_d	Diode current
V_d	Diode voltage
V_{lo}	Output voltage
I_s	Reverse saturation current
V_{th}	Thermal voltage
T	Temperature
q	Charge on electron
α	Ideality factor
k	Boltzmann constant
R_{se}	Series resistance
I_k	Leakage current
R_{sh}	Shunt resistance
C_{jc}	Junction capacitance
V_c	Voltage across capacitor
V_{oc}	Open circuit voltage
I_{sc}	Short circuit current
V_{mpt}	Voltage at maximum power point
I_{mpt}	Current at maximum power point
K_i	Current temperature coefficient
K_v	Voltage temperature coefficient
G	Irradiance
P	Power
R_{seo}	Slope of *I-V* at short circuit current
R_{sho}	Slope of *I-V* at open circuit point
δ	Unknown parameter vector for SDM
ψ	Unknown parameter vector for DDM

ρ	Unknown parameter vector for TDM
N_s	Number of cells in series
N_p	Number of cells in parallel
n	Number of iterations
i	Current iteration
N_{po}	Population
E_{fs}	Error functions
I_{ex}	Experimental current
I_{et}	Estimated current
I_{s2}, I_{s3}	Reverse saturation current for diode D_2 and D_3
α_2, α_3	Ideality factor for diode D_2 and D_3

Chapter 1

INTRODUCTION

1.1 General

Electrical energy exhibits as a magical force, when a simple flipping of switch turns the lights ‘ON’, that adds everyday convenience to the human life and it is a result of a rich history of power generation to power utilisation *i.e.* a journey of about 200 years [1]. This history includes the discovery of electrical power by Benjamin Franklin, and the concept of electrical machines by Michael Faraday, whereas Thomas Edison contributes to the invention of the electric bulb. At the most rudimentary level, electrical power was used for lighting purposes only, but industrialisation in the nineteenth-century brands this magical force as a vital part of human life. Moreover, the socioeconomic fabric of a country is also stitched with the thread of its per capita consumption of power. Hence, to expand the limitless set of applications of electrical power, which includes heating, lighting, communication, transport, computation, and to keep economic competition among countries at its swing, leads the countries toward the identification of various modes of harnessing electrical power, where hydrocarbon-based fuels are more prominent due to industrialisation in the nineteenth century [1].

Industrialisation primes the world to the uncontrolled harnessing of electrical energy from hydrocarbon fuels, which exhibits its toxic behaviour and is responsible for environmental diminution. In fig. 1.1, the sector-wise installed generation in India is represented [2], it is observed that about 60.4% of total installed power is still based on fossil fuels, while about 52.6 % is contributed by coal itself.

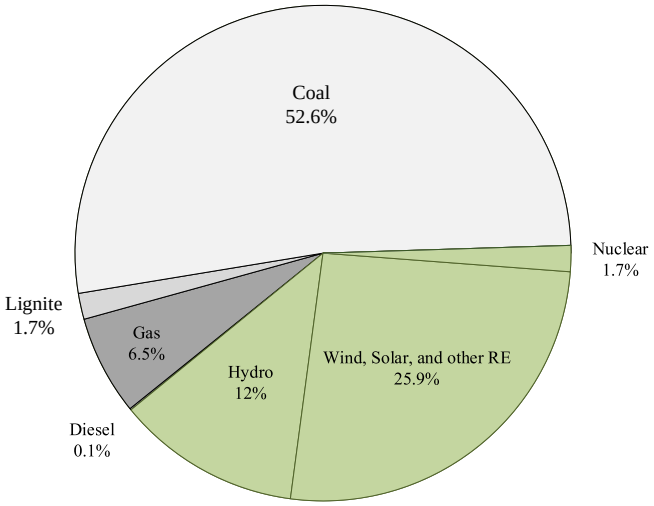

Fig. 1.1 Sector-wise installed generation capacity of India by 31/Aug/2021

Hence, the production of electrical energy from renewable energy sources plays a vigorous role, when the identification of alternate sources of energy is exercised. Renewable energy source selection is important, not only to distress the adverse environmental aspects but also to strengthen the economy of a country by minimising fossil fuel imports [3]-[9]. Solar photovoltaic (PV) gain its popularity among other renewable energy sources due to the abundant availability of solar irradiance, less installation time, and low maintenance [7]- [11].

1.2 Solar PV cell models and its physics

Solar PV cells behavior has been explained as of simple *p-n* junction when it is exposed to sunlight [3], [6], [11].

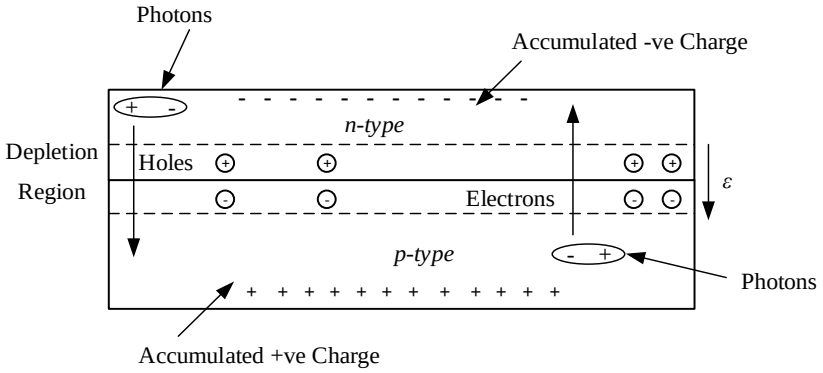

Fig. 1.2 Charge accumulation in *p-n* junction diode

On the basis of Quantum theory, it is elucidated that the electrons in the conduction band are accountable for the current flow, whereas in semiconductor materials the conduction band is empty at absolute zero temperature, moreover only one out of 10^{10} electrons in silicon exist in conduction band at room temperature [3].

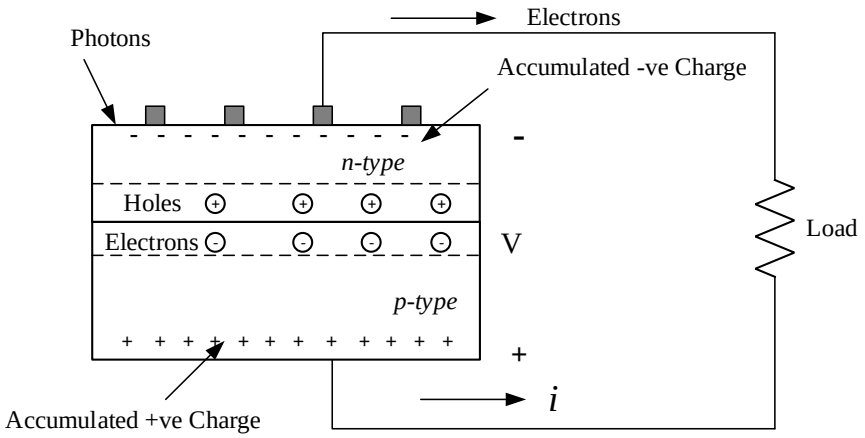

Fig. 1.3 Flow of electrons and conventional current

When the *p-n* junction is exposed to the source of photons *i.e.* sunlight, they are absorbed and hole-electron pair may be formed (as photons have sufficient energy to strike electrons from an atom). When mobile charges reach the vicinity of the junction, the holes in the depletion region will push the holes into the *p*-side and push the electrons into the *n*-side due to the electric field of the depletion region as shown in fig 1.2. The *p*-side accumulates holes and the *n*-side accumulates electrons, which creates a voltage that can be used to deliver current to a load. If electrical contacts are made to the top and bottom of the cell the electrons flow out of the *n*-side into the connecting wire, through the load, and back to the *p*-side [3]. When the electrons reached the *p*-side, they recombine with holes and complete the circuit as shown in fig 1.3.

1.2.1 Equivalent models for solar PV cell

Based on the physical interpretation of PV cell, where specific cell configuration subsequently forms PV module or array, various models are well elucidated in literature as the single diode model (SDM), double-diode model (DDM), multi-diode model (MDM), and a few of multi-dimensional models (MD_mM) like junction capacitances [9].

a) Ideal PV cell model

As PV cells constitute two layers of a differently doped semiconductor, whose *p-n* junction is exposed to photons [3] as shown in fig 1.2. In the absence of solar irradiation, the PV cell behaves as a simple *P-N* junction diode whose *I-V* curve is given by the Shockley equation as below [3]-[11]. Hence, incident photons create a potential difference, and that inturn responsible for the flowing of charge carriers towards the external circuit results in a current *i.e.* denoted by 'I_{lo}'. The ideal PV cell model is well depicted in fig 1.4.

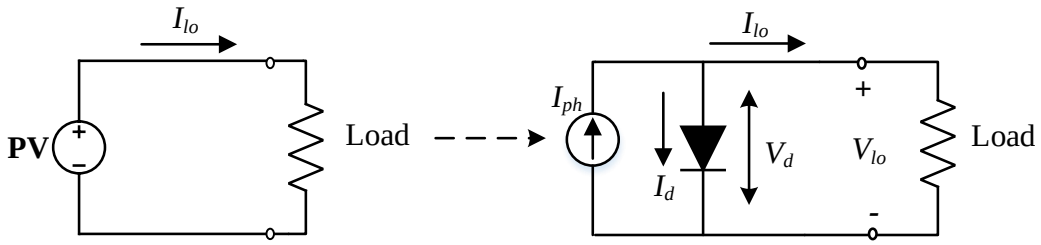

Fig. 1.4 Ideal PV cell model

$$I_d = I_s\left(e^{V_d/V_{th}} - 1\right) \tag{1.1}$$

The expression for diode current is observed in *eq.* 1.1, V_d and I_d are the diode voltage and current respectively, where the saturation current is denoted by I_s. The *I-V* characteristic of PV cell can be drawn by using *eq.* 1.2. The thermal voltage (V_{th}) can be rewritten as, $V_{th} = \frac{\alpha \times k \times T}{q}$, with the ideality factor α, where q is the charge on an electron (1.60217646×10^{-19} *C*), temperature, and Boltzmann constant ($1.380650323\times10^{-23}$ *J/K*), is represented by T and k respectively.

$$I_{lo} = I_{ph} - I_d = I_{ph} - I_s\left(e^{V_d/V_{th}} - 1\right) \tag{1.2}$$

b) Single diode R_{se} model

The R_{se} model of solar PV is more demonstrative if it is compared with the ideal PV cell, as R_{se} model encompasses an important fact as R_{se}, *i.e.* the contact resistance of silicon and connection lead [3], [6]-[7] that can contribute substantial changes in PV characteristic if remained unaddressed. A single diode R_{se} model is represented in fig 1.5.

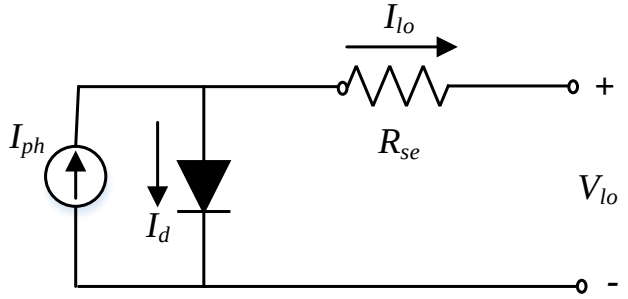

Fig. 1.5 Single diode R_{se} PV model

$$V_d = V_{lo} + I_{lo}R_{se} \tag{1.3}$$

Current *'I_{lo}'* for R_{se} PV model is expressed as,

$$I_{lo} = I_{ph} - I_s\left(e^{\left(\frac{V_{lo}+R_{se}I_{lo}}{V_{th}}\right)} - 1\right) \tag{1.4}$$

c) Single diode R_{sh} model (SDM)

It is important to understand that the generated photocurrent is significantly very sensitive to the presence of light, where under shading conditions, the current through the current source becomes zero and the diode is reversed biased [6]. During this only reverse saturation current passes, hence a simple equivalent circuit gives no power output to the load if any one of the cells

of a module is shaded [3], as explained in fig 1.6. Therefore, to counter this, the equivalent circuit is modified by using a parallel leakage resistance R_{sh}, as shown in fig 1.7, and this showcases that the current delivers to the load through the diode and the R_{sh} [3]-[11]. Suitable transactions among precision and simplicity enable SDM as the most commonly used PV model. The current to the load can be expressed as,

$$I_{lo} = I_{ph} - I_d - I_k \tag{1.5}$$

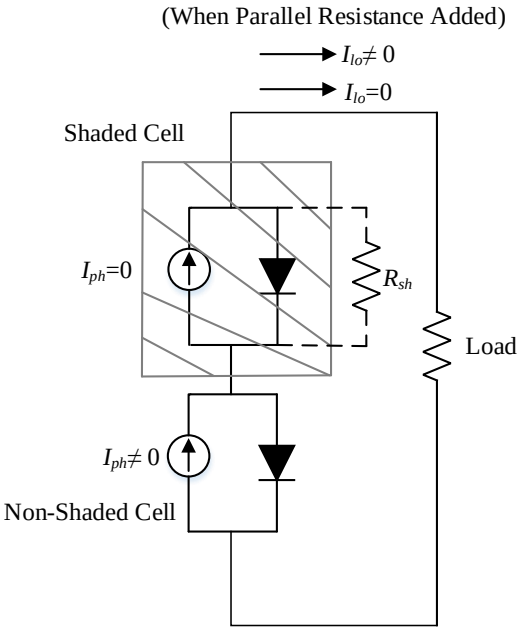

Fig. 1.6 Shaded cell of a module

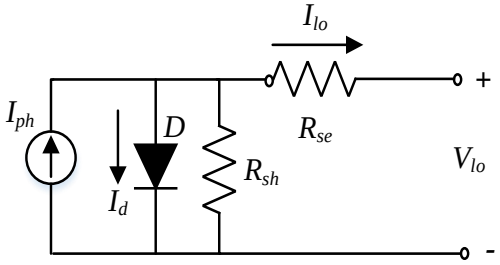

Fig. 1.7 Single diode R_{sh} *PV* model (SDM)

$$I_d = I_s \left(e^{\left(\frac{(V_{lo} + R_{se} I_{lo})}{V_{th}} \right)} - 1 \right) \tag{1.6}$$

$$I_k = \frac{V_{lo} + R_{se} I_{lo}}{R_{sh}} \tag{1.7}$$

leakage current (I_k) is expressed by *eq.* (1.7), while substituting the I_d, and I_k in *eq.* (1.5), it can be rewritten as *eq.* (1.8), *i.e.* output PV current.

$$I_{lo} = I_{ph} - I_s\left(e^{\left(\frac{(V_{lo}+R_{se}I_{lo})}{V_{th}}\right)} - 1\right) - \frac{V_{lo}+R_{se}I_{lo}}{R_{sh}} \tag{1.8}$$

d) Double diode PV model (DDM)

To consider the effect of recombination current loss in the depletion region [6], another diode D_2 is connected in parallel to the SDM. It is important to understand that, at low irradiance conditions the two diode model brings suitable accuracy [6]. The DDM is shown in fig. 1.8 and the current equation for the DDM is realised in *eq.* (1.9), where I_{s1} and I_{s2} are the saturation current for diode *D1* and *D2* respectively, having ideality factor of α_1 and α_2.

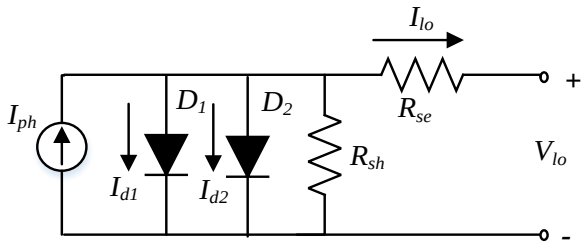

Fig. 1.8 Double diode PV cell model (DDM)

$$I_{lo} = I_{ph} - I_{s1}\left(e^{\left(\frac{V_{lo}+I_{lo}R_{se}}{V_{th}}\right)} - 1\right) - I_{s2}\left(e^{\left(\frac{V_{lo}+I_{lo}R_{se}}{V_{th}}\right)} - 1\right) - \frac{V_{lo}+I_{lo}R_{se}}{R_{sh}} \tag{1.9}$$

e) Three diode PV model (TDM)

In the three diode model, the effect of recombination in the defect regions and grain sites are considered, where, for D_3 the diode saturation current (I_{s3}) and ideality factor (α_3) [6] are the parameters associated with the third diode, an expression for current is given by *eq.* (1.10).

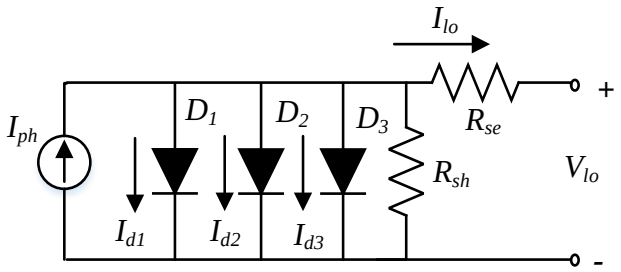

Fig. 1.9 Three diode PV cell model (TDM)

$$I_{lo} = I_{ph} - I_{s1}\left(e^{\left(\frac{V_{lo}+I_{lo}R_{se}}{V_{th}}\right)} - 1\right) - I_{s2}\left(e^{\left(\frac{V_{lo}+I_{lo}R_{se}}{V_{th}}\right)} - 1\right) - I_{s3}\left(e^{\left(\frac{V_{lo}+I_{lo}R_{se}}{V_{th}}\right)} - 1\right) - \frac{V_{lo}+I_{lo}R_{se}}{R_{sh}} \tag{1.10}$$

f) Junction capacitance single diode R_{sh} model

This model is the least considered model for the analysis and simulation of solar-based power systems. This model includes a capacitance that considers the *p-n* junction capacitance (C_{jc}) *i.e.* capacitance of the depletion region [12]. This model is presented in fig 1.10, where the junction capacitance is given by *eq.* (1.11), Δt_i is the instantaneous time duration in μsec, i_{jc} is the mean current flown through the capacitor during transient and ΔV_c is the change in voltage from steady-state charge and discharge of *p-n* junction capacitance *Cjc*.

$$C_{jc} = \frac{\Delta t_i \times \overline{i_{jc}}}{\Delta V_c} \tag{1.11}$$

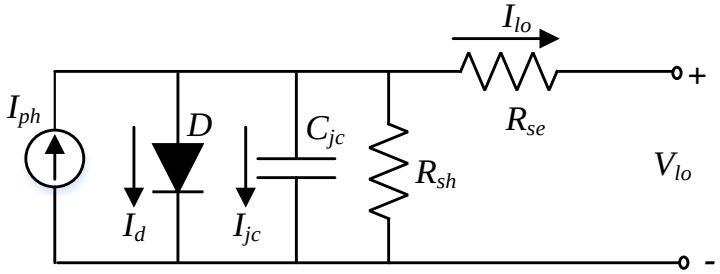

Fig. 1.10 Junction capacitance single diode R_{sh} model

g) Two Capacitance Single Diode R_{sh} Model

In this model two components of capacitances *i.e.* C_{jT} and C_{jD} are considered and that describes the capacitance of the space charge region and neutral region respectively [12]. During reversed bias conditions or during dark, there are few minority carriers available in the neutral region, *i.e.* C_{jD}~0, and there is a negligible drop of voltage across series resistance and this results in a simplified equivalent circuit as shown in fig. 1.11.

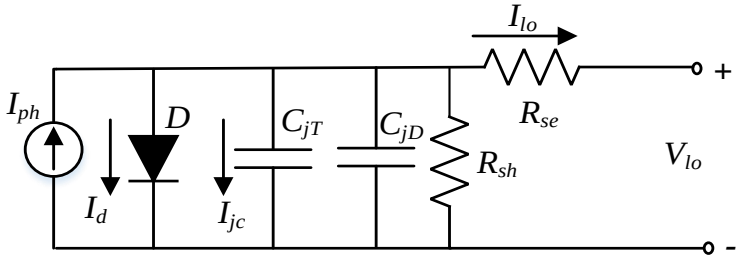

Fig. 1.11 Two capacitance single diode R_{sh} model

the current voltage relationship is expressed by *eq.* 1.12, where, V_{oc} is the open circuit voltage,

$$I_{lo} = R_{se} \times V_{oc} + C_{jT} \times \frac{dV_{oc}}{dt} \tag{1.12}$$

$$\frac{I_{lo} - R_{se} \times V_{oc}}{dV_{oc}/dt} = C_{jT} \tag{1.13}$$

h) Modified double diode model (M-DDM)

The modified double-diode model is shown in fig. 1.12, the R_{se} is divided into three components R_{se1}, $R_{se2,}$ and R_{sb}, where the R_{sb} expresses the consideration of resistance due to substrate and microscopic inhomogeneity of resistivity of grain boundaries [12]. The two diodes D_d and D_r are connected in parallel having $\alpha=1$ and $\alpha=2$ respectively, that separate diffusion and recombination current, effects of grain boundaries are completely reflected by D_r.

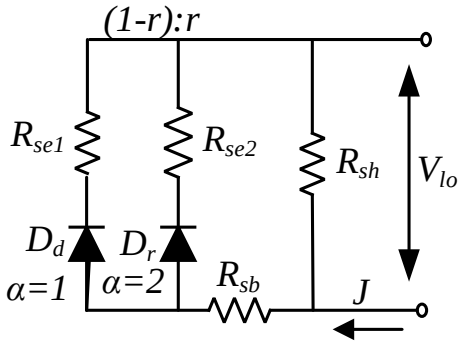

Fig. 1.12 Modified double-diode model (M-DDM)

The equivalent current density for D_d is defined as,

$$J_{od} = q\sqrt{d_c/\tau_n} \times \left(n_i^2/N_A\right) \tag{1.14}$$

where, q, d_c, τ_n, $n_{i,}$ and N_A are the charge on an electron, lifespan of minority carrier, intrinsic carrier density, and acceptor density respectively. Moreover, the equivalent current density for D_r is represented in *eq.* 1.15, where, W_{n_i} is the width of the depletion layer and τ_r is the lifespan of the minority carrier.

$$J_{or} = (qW_{n_i}/2\tau_r) \tag{1.15}$$

1.3 Configuration of solar PV modules and array

Typically, a solar cell gives an output of 0.6 V, and this voltage level feeds only some limited applications like calculators, watches, etc. Whereas, more feasible applications need customisation of PV cells in various configurations. Given this solar PV modules act as the building block for PV applications. PV modules consist of prewired cells in series, cased in robust and weatherproof structure [3]. A module of 36 series cells is designated as a 12 V

module, whereas 72 cell modules are the most commonly used. A series combination of 72 cell configuration results in an output of 24 V, where two parallel strings of 36 cells result in 12 V output. The combination of modules for a particular voltage and current output is known as an array as shown in fig 1.13.

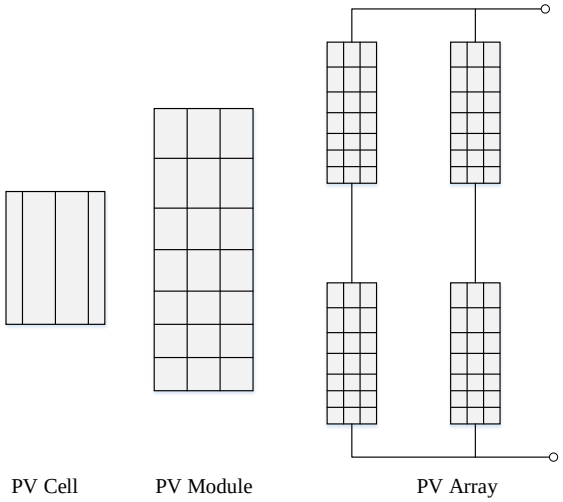

Fig. 1.13 Solar PV cell, module, and array

1.3.1 Cell to the module configuration

When PV cells are connected in a series combination they carry the same current and the voltages add, as shown in fig 1.14, 36 cells are connected in series and the voltage of the modules becomes 36×0.6=21.6 V whereas, the current remains almost the same.

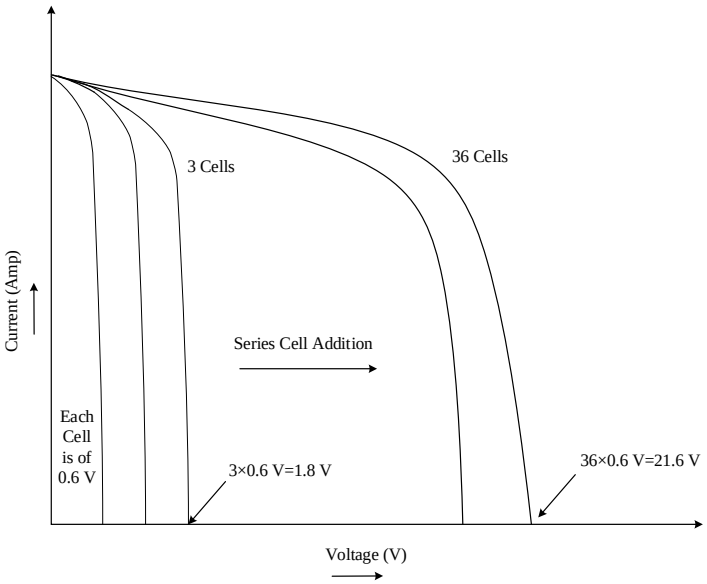

Fig. 1.14 Addition of cell voltage for 36 cell module

1.3.2 Module to the array configuration

When the modules are connected in series/parallel combination then the formation is known as an array as shown in fig 1.15.

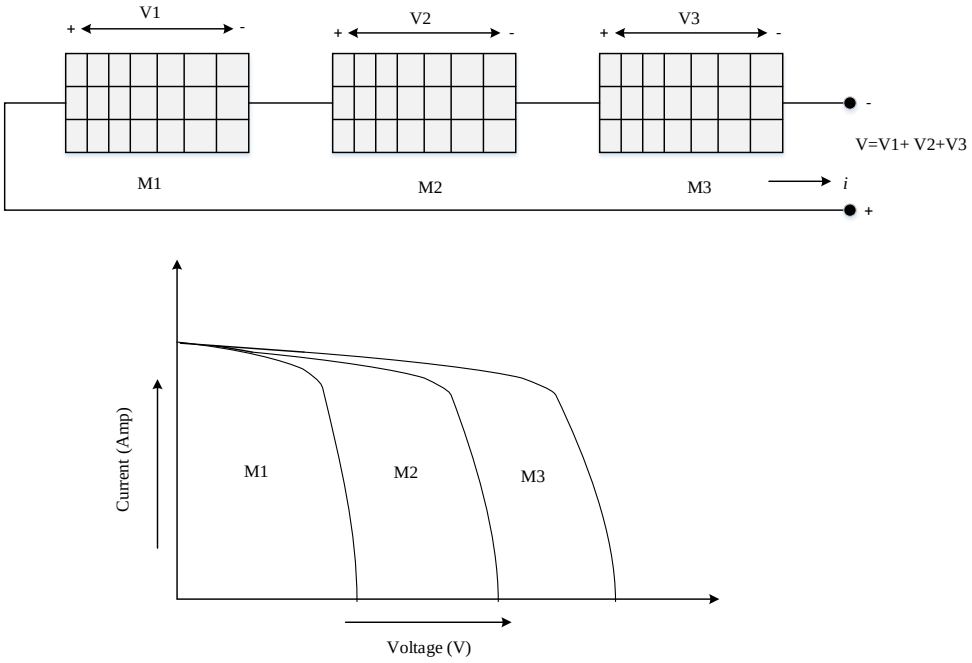

Fig. 1.15 Series module configuration to add voltage for a given current

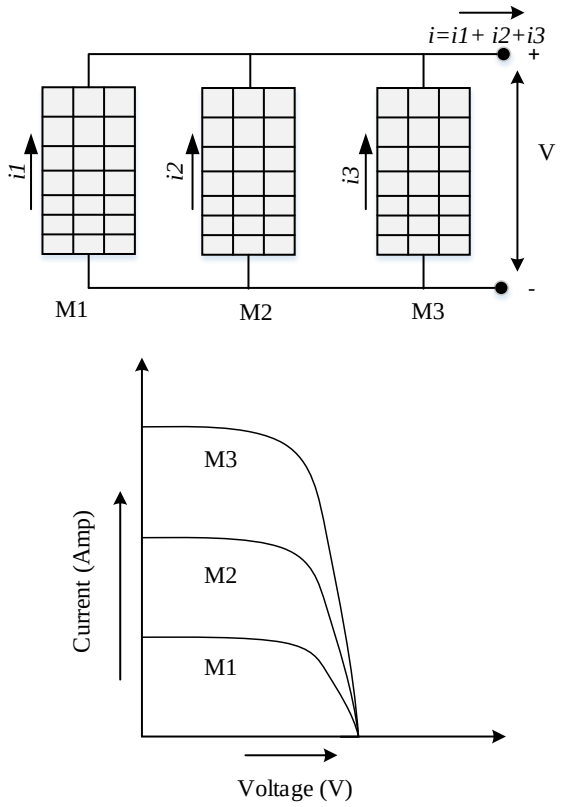

Fig. 1.16 Parallel module configuration to add current for a given voltage

It is also important to know that to increase the voltage the modules are connected in series, whereas for increasing current, the modules are to be connected in parallel [3]. Moreover, for obtaining large powers from an array the modules are connected with some series as well as some parallel connections [13]-[14]. The *I-V* characteristics of the series combination, added along the voltage axis and the total voltage is simply the sum of the voltage of each individual module as exemplified in fig 1.15. Furthermore, the *I-V* characteristic for the parallel combination of modules moves along the current axis and the total current of the array is the algebraic sum of the individual current of each module as shown in fig 1.16.

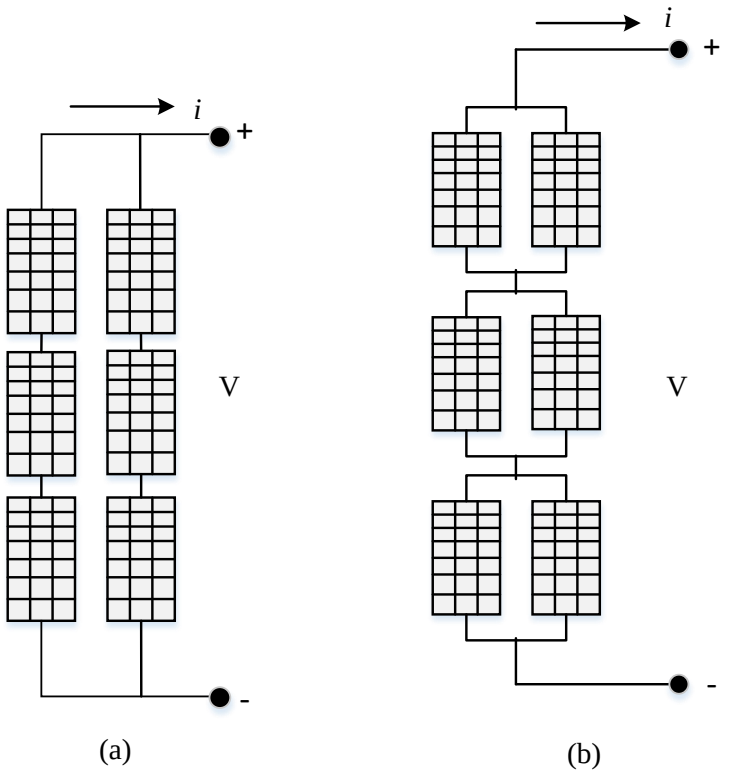

Fig. 1.17 Solar PV array configuration *(a)* Series module strings connected in parallel *(b)* Parallel module string connected in series

The high power configuration needs both series and parallel combinations as explained above and can be classified into two arrangements,

(a) Modules are connected in series to form strings, and the strings are connected in parallel, fig 1.17 (a).

(b) Modules are connected in parallel to form strings and these strings are connected in series as elaborated, fig 1.17 (b).

(c) Configuration (a) of parallel strings is preferred as if a string is removed for service then the system still supplies the same voltage with the reduced current.

1.4 The *I-V* and *P-V* characteristics of solar PV

Let a PV module be exposed to sunlight and no load is connected to the output terminals the voltage across the terminal is the open-circuit voltage *i.e.* V_{oc} only, and the current remains zero.

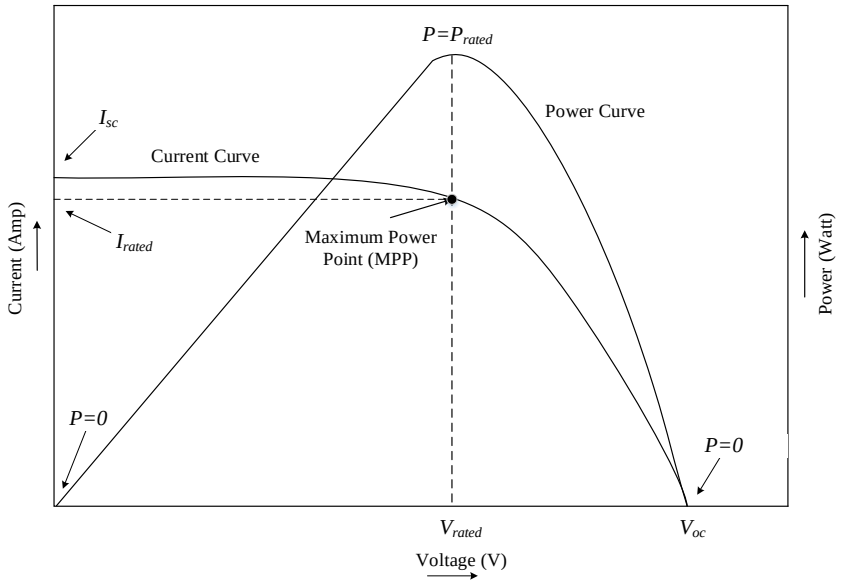

Fig. 1.18 *I-V* and *P-V* curve for a PV module

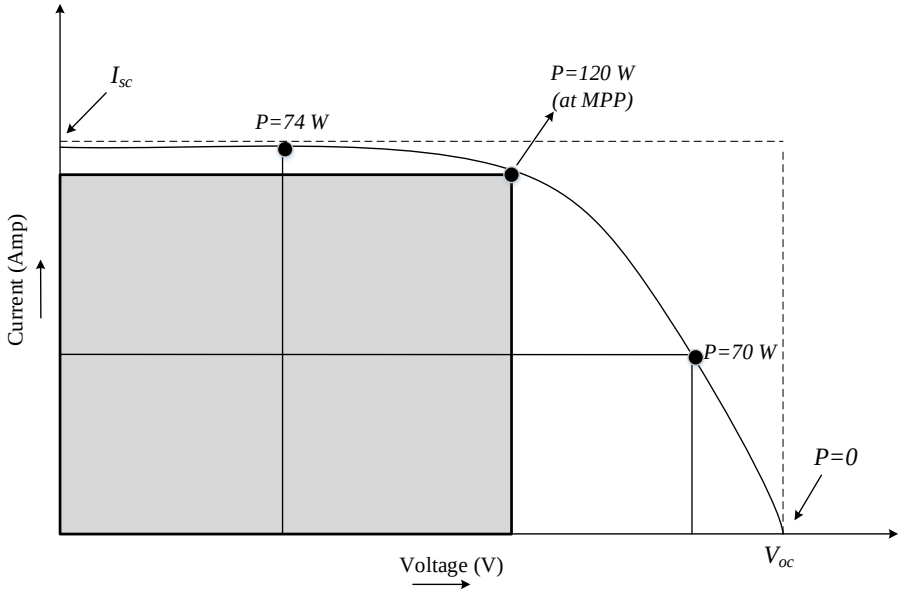

Fig. 1.19 Fill factor

Whereas, if the terminals are short-circuited then only I_{sc} flows and V_{oc} becomes zero, but as the power is the product of *V* and *I*, hence in both cases the power remains zero or in other words,

the power delivered to the load remains zero as shown in fig 1.18. When the actual load is connected to the PV module then it starts extracting the current from the module for a particular voltage and results in power delivered to the load [13], [14]. As shown in fig 1.18, the maximum power point (MPP) is the point where the product of voltage and current is maximum [7], the current and voltage corresponding to MPP are also known as V_{mpt} and I_{mpt}, whereas in ideal test conditions it is known as V_{rated} and I_{rated}.

To locate the MPP the biggest possible rectangle that fits under the *I-V* curve can be considered. As shown in fig 1.19, the side of the rectangle has *V* and *I* as sides, hence the area under the rectangle illustrates the power [3]. Moreover, the fill factor is also used for module performance analysis where,

$$\text{Fill Factor} = \frac{V_{rated} \times I_{rated}}{V_{oc} \times I_{sc}} \tag{1.16}$$

To design the best possible configuration for the solar PV array, the optimised power converter and controller protocol, optimised MPP tracking techniques, and to predict the estimated power under different real-time environmental conditions at specific geographies, various simulations are to be carried out at specific platforms through the electrical model of solar PV, and for this, modelling of solar PV electrical model should be reliable, accurate and robust [4]-[6]. Where, inaccurate modelling of solar PV results in the undermining or oversizing of the converter associated [15] and unrealistic array configuration, which inturn impacts the estimation of payback period and the capital cost associated with solar PV power project. The accuracy of commercially available solar PV simulator software depends on the electrical PV model selected for the simulation and the model parameter extraction technique incorporated.

Table 1.1 Solar PV models and the number of unknown parameters

S. No.	PV Model	Unknown Parameters
1.	Ideal PV	α, I_{ph}, and I_s
2.	Single-diode R_{se} model	α, I_{ph}, R_{se}, and I_s
3.	Single-diode R_{sh} model (SDM)	α, I_{ph}, R_{se}, R_{sh} and I_s
4.	Double-diode model (DDM)	α_1, α_2, I_{ph}, R_{se}, R_{sh}, I_{s1} and I_{s2}
5.	Three-diode model (TDM)	α_1, α_2, α_3, I_{ph}, R_{se}, R_{sh}, I_{s1}, I_{s2} and I_{s3}
6.	Junction capacitance single-diode R_{sh} model	α, I_{lk}, R_{se}, R_{sh}, I_s and C_{jc}

C_{jc} is the junction capacitance.

Due to simplicity, SDM is the most prominently used mathematical model in literature with V_{mpt}, I_{mpt}, current temperature coefficient (K_i), voltage temperature coefficient (K_v), V_{oc} and I_{sc}, are the known parameters available in the manufacturer's datasheet, whereas several parameters

are not available with the manufacturer datasheet are categorised as unknown parameters *i.e.* ideality factor (α), I_{ph}, R_{se}, $R_{sh,}$ and I_s, where, estimation of these unknown parameters for mathematical modelling is acknowledged as parameter estimation problem among researchers [4]-[11].

The number of unknown parameters that are to be estimated is based on the mathematical model selected for the analysis. An SDM model has five unknown parameters, whereas the DDM is characterized by seven unknown parameters. Moreover, there are multi-diode models, where '*d'* is the number of diodes connected in parallel, with 3+2*d* number of unknown parameters [9]. Table 1.1, showcases the number of unknown parameters for various models considered in the literature [6]. It is important to comprehend that the parameter estimation problem is a non-linear and constrained problem, whose estimation is reviewed in literature through various methodologies *i.e.* analytical, metaheuristic and hybrid, a critical literature review is also highlighted in chapter 2, where various merits of optimisation approaches over-analytical approaches for parameter estimation problem are underlined [6].

1.5 Research objectives

The research work presented with the tittle "Modeling and Parameter Estimation of Solar Photovoltaic Array" holds the following research objective,

1) To consider different models of PV array for parameter estimation.
2) To analyse the impact of different environmental factors on parameter estimation.
3) To implement different techniques for parameter estimation of PV array.

1.6 Thesis organisation

This thesis represents cohesive research on modelling and parameter estimation of the solar PV cell, module, or array. The thesis is well organised into six chapters, where each chapter contributes to the accomplishment of the above-stated research objectives. The chapters are outlined as,

Chapter 1: Introduction

This chapter incorporates the advantages of renewable energy sources over conventional energy sources and the decision factors for the selection of solar PV among other renewable energy sources. Moreover, the need for modelling and parameter estimation of solar PV along with various solar PV models are presented. Numerous design configurations of solar PV cells, modules, and arrays are also discussed, where special prominence is given to the *I-V* and *P-V*

characteristics associated with the performance analysis. This chapter also enlists the research objectives considered and the aspects in which the thesis is organised.

Chapter 2: Literature Review

A critical review of various modelling and parameter estimation techniques are highlighted in this chapter, where the literature is broadly classified into analytical, metaheuristic, and hybrid approaches. Moreover, various sets of conditions designed for the modelling of solar PV are also represented. In the later part of the chapter, the author describes the contribution to the parameter estimation problem.

Chapter 3: Emperor penguin optimisation for parameter estimation problem and impact of environmental conditions

This chapter elaborates a new Emperor Penguin Optimisation (EPO) based parameter estimation approach for an SDM of solar PV, that is cohesively analysed under different sets of temperature and irradiances (G). Validation of the proposed technique is perceived on the analysis of performance characteristics *i.e.* current-voltage (I-V) and power-voltage (P-V) under various simulation conditions. Moreover, estimated results are compared with the experimental data and several established estimation techniques in the literature for validation and demonstrate the proposed technique with highly precise outcomes having reduced computational cost for the PV model parameter extraction problem.

Chapter 4: Pheromone value and cannibalism based black widow optimisation approaches

In this chapter two metaheuristic approaches, *i.e.* Pheromone Value Black Widow Optimisation (*pv*-BWO) and Cannibalism Black Widow Optimisation (*cn*-BWO) are proposed to model and estimate accurate modeling parameters for six different PV modules using the SDM, DDM, and TDM. The suggested techniques are validated through the experimental I-V and P-V performance characteristics of all the six case studies considered. A real-time I-V and P-V data is also recorded for two modules to affirm the suitability of the proposed methodology under real implementation. Furthermore, a comparison of *cn*-BWO and *pv*-BWO methods of parameter estimation results is also carried out on the basis of various error functions and performance characteristics. The real-time I-V and P-V data is also presented in the chapter, where the data is logged with the help of a solar PV analyser.

Chapter 5: Implementation of two new hybrid approaches using sailfish and spotted hyena optimisers

This chapter exhibits two-hybrid approaches using two new metaheuristic algorithms, *i.e.* the sailfish optimisation (SFO) and spotted hyena optimisation (SHO) framework along with the Newton-Raphson method (NRM) are proposed and compared, to estimate the parameters for the SDM, DDM, and TDM of solar PV. Five case studies are presented for the investigation of the proposed methods, validated and compared through the convergence speed, accuracy of estimated parameters, analysis of *I-V*, and *P-V* performance characteristics.

Chapter 6: Conclusions and future scope

This chapter represents the conclusion of the studies considered in the thesis as per the research objectives framed. Moreover, some future aspects of further researches are also listed.

1.7 Chapter summary

This chapter enables us to understand the criterion for the selection of solar-based energy conversion over other renewable energy sources. The basic physics associated with the solar PV cell that are further articulated into modules and arrays are discussed along with the modelling of solar PV. Various models for the modelling of solar PV are critically analysed, that includes the SDM, DDM, TDM, and numerous capacitance models, where the importance of the parameter estimation approach is also highlighted.

Chapter 2

LITERATURE REVIEW

2.1 General

The selection of solar-based energy sources over other available renewable energy sources [4]-[7] due to various outstanding advantages is already emphasized in chapter 1. Where it is asserted that the parameter estimation problem is a concern among researchers when various softwares are employed for the modelling and simulation of solar PV. In literature, various methodologies are suggested for solar PV parameter estimation problem, where the classification is carried out broadly in three categories, *i.e.* analytical, metaheuristic, and hybrid approaches.

2.2 Analytical methods

Analytical methods are the mathematical equation-based problem-solving approaches, articulated through elementary functions, congruently applied to several points on *I-V* and *P-V* characteristics through approximations, that convert the equation into a more precise format, for instance, the Lambert *W* function. As it is evident that parameter estimation is a non-linear problem, where, the solution of non-linear equations with an increase in the number of unknown parameters became difficult by using analytical approaches [6]. In analytical approaches, the equations or mathematical relations are to be designed for the parameter estimation, and it is in complete congruence with the model considered. For the parameter estimation, various sets of conditions considered to design the strategy for different PV models by using the analytical approaches are listed below as,

2.2.1 Analytical approaches for the single-diode R_{se} model

As the single-diode R_{se} model have four unknown parameters *i.e.* I_{ph}, α, I_s, and R_{se}, then it requires four distinct equations for their estimation, whereas the combination of open circuit point, short circuit point, the power derivative to the voltage at maximum power point that sets to zero and slope of *I-V* curve at open circuit point are most prominently used [8], [16], [17], where the ideality factor is arbitrarily kept 1. The set of conditions considered to structure four different equations are prescribed as [9],

under open-circuit conditions, $I = 0$, and *eq.* (1.4), can be rewritten as,

$$0 = I_{ph} - I_s \left(e^{\left(\frac{V_{oc}}{V_{th}}\right)} - 1 \right) \tag{2.1}$$

where, $V_{th} = \dfrac{\alpha \times k \times T}{q}$

eq. (2.1), can be rewritten as,

$$I_{ph} = I_s \left(e^{\left(\frac{V_{oc}}{V_{th}}\right)} - 1 \right) \tag{2.2}$$

short-circuit of load terminals, where, $V = 0$ and *eq*. (1.4), can be modified as,

$$I_{sc} = I_{ph} - I_s \left(e^{\left(\frac{R_{se} I_{sc}}{V_{th}}\right)} - 1 \right) \tag{2.3}$$

eq. (2.3), can be rewritten as,

$$I_{ph} = I_{sc} + I_s \left(e^{\left(\frac{R_{se} I_{sc}}{V_{th}}\right)} - 1 \right) \tag{2.4}$$

by using *eq*. (2.2) and *eq*. (2.4), we have

$$I_s \left(e^{\left(\frac{V_{oc}}{V_{th}}\right)} - 1 \right) = I_{sc} + I_s \left(e^{\left(\frac{R_{se} I_{sc}}{V_{th}}\right)} - 1 \right) \tag{2.5}$$

hence, the saturation current can be calculated using,

$$I_s = \frac{I_{sc}}{e^{\left(\frac{V_{oc}}{V_{th}}\right)} - e^{\left(\frac{R_{se} I_{sc}}{V_{th}}\right)}} \tag{2.6}$$

where, the photo-current can be estimated by substituting *eq*. (2.6) in *eq*. (2.4)

$$I_{ph} = I_{sc} \left[1 + \frac{I_{sc} \left(e^{\left(\frac{R_{se} I_{sc}}{V_{th}}\right)} - 1 \right)}{e^{\left(\frac{V_{oc}}{V_{th}}\right)} - e^{\left(\frac{R_{se} I_{sc}}{V_{th}}\right)}} \right] \tag{2.7}$$

In [75]-[77], it is observed that I_{ph} and I_{sc} are taken equal, moreover *eq*. (1.4), at maximum power point condition, gives,

$$I_{mpt} = I_{ph} - I_s \left(e^{\left(\frac{(v_{mpt} + R_{se} I_{mpt})}{V_{th}}\right)} - 1 \right) \tag{2.8}$$

where the output power derivative with the voltage should be zero and evaluated as,

$$\left. \frac{dP}{dV_{lo}} \right|_{Max.pp} = \frac{d(V_{lo} I_{lo})}{dV_{lo}} = V_{lo} \frac{d(I_{lo})}{dV_{lo}} + I_{lo} = 0 \tag{2.9}$$

further can be obtained as,

$$\left.\frac{dI_{lo}}{dV_{lo}}\right|_{Max.pp} = -\frac{I_{mpt}}{V_{mpt}} \tag{2.10}$$

on differentiating *eq.* (1.4), with respect to 'V_{lo}', *eq.* (2.11) is obtained as,

$$\left.\frac{dI_{lo}}{dV_{lo}}\right|_{Max.pp} = \left[\frac{\frac{I_s}{V_{th}} e^{\left(\frac{V_{lo}+R_{se}I_{lo}}{V_{th}}\right)}}{\frac{R_{se}}{V_{th}} e^{\left(\frac{V_{lo}+R_{se}I_{lo}}{V_{th}}\right)} - 1}\right] \tag{2.11}$$

eq. (2.10) and *eq.* (2.11) can be equated and written as,

$$\left[\frac{\frac{I_s}{V_{th}} e^{\left(\frac{V_{mpt}+R_{se}I_{mpt}}{V_{th}}\right)}}{\frac{R_{se}}{V_{th}} e^{\left(\frac{V_{mpt}+R_{se}I_{mpt}}{V_{th}}\right)} - 1}\right] = -\frac{I_{mpt}}{V_{mpt}} \tag{2.12}$$

Furthermore, a derivative of current with respective voltage *i.e.* slope of *I-V* characteristic near short circuit current is given by,

$$\left.\frac{dI_{lo}}{dV_{lo}}\right|_{I=I_{sc}} = \frac{\frac{I_s}{V_{th}} e^{\left(\frac{R_{se}I_{sc}}{V_{th}}\right)}}{\frac{R_{se}}{V_{th}} R_{se}V_{th} e^{\left(\frac{R_{se}I_{sc}}{V_{th}}\right)} - 1} = -\frac{1}{R_{seo}} \tag{2.13}$$

There are two distinct sets of equations that can be employed for the estimation of four unknown parameters of the single diode R_{se} model, *i.e.* by using *eq.* (2.6)-*eq.* (2.8), along with *eq.* (2.12) or by using *eq.* (2.6)-*eq.* (2.8), along with *eq.* (2.13).

2.2.2 Analytical approaches for the SDM

In the case of SDM five unknown parameters *i.e.* I_{ph}, α, I_s, $R_{se,}$ and R_{sh} are to be estimated, by using five distinct equations, where in some cases 'α' is arbitrarily considered as in the range of [1, 2.5]. To formulate the condition and to select five potential equations various researchers use a different set of conditions *i.e.* mentioned in table 2.1, whereas the modelling of these equations are formulated using,

the open-circuit conditions, where $I_{lo} = 0$, *eq.* (1.8), can be rewritten as,

$$0 = I_{ph} - I_s\left(e^{\left(\frac{V_{oc}}{V_{th}}\right)} - 1\right) - \frac{V_{oc}}{R_{sh}} \tag{2.14}$$

and can be rewritten as,

$$I_{ph} = I_s\left(e^{\left(\frac{V_{oc}}{V_{th}}\right)} - 1\right) + \frac{V_{oc}}{R_{sh}} \tag{2.15}$$

whereas, in the short-circuit *eq*. (1.8), can be modified as,

$$I_{sc} = I_{ph} - I_s\left(e^{\left(\frac{R_{se}I_{sc}}{V_{th}}\right)} - 1\right) - \frac{R_{se}I_{sc}}{R_{sh}} \tag{2.16}$$

eq. (2.16), can be restructured as,

$$I_{ph} = I_{sc} + I_s\left(e^{\left(\frac{R_{se}I_{sc}}{V_{th}}\right)} - 1\right) + \frac{R_{se}I_{sc}}{R_{sh}} \tag{2.17}$$

by using *eq*. (2.15) and *eq*. (2.17), we have

$$I_s\left(e^{\left(\frac{V_{oc}}{V_{th}}\right)} - 1\right) + \frac{V_{oc}}{R_{sh}} = I_{sc} + I_s\left(e^{\left(\frac{R_{se}I_{sc}}{V_{th}}\right)} - 1\right) + \frac{R_{se}I_{sc}}{R_{sh}} \tag{2.18}$$

hence, the saturation current can be calculated using,

$$I_s = \frac{I_{sc} + \frac{R_{se}I_{sc}}{R_{sh}} - \frac{V_{oc}}{R_{sh}}}{e^{\left(\frac{V_{oc}}{V_{th}}\right)} - e^{\left(\frac{R_{se}I_{sc}}{V_{th}}\right)}} \tag{2.19}$$

where, by using *eq*. (2.19), in *eq*. (2.15),

$$I_{ph} = \left[\frac{\left(I_{sc} + \frac{R_{se}I_{sc}}{R_{sh}} - \frac{V_{oc}}{R_{sh}}\right)\left(e^{\left(\frac{R_{se}I_{sc}}{V_{th}}\right)} - 1\right)}{e^{\left(\frac{V_{oc}}{V_{th}}\right)} - e^{\left(\frac{R_{se}I_{sc}}{V_{th}}\right)}}\right] - \frac{V_{oc}}{R_{sh}} \tag{2.20}$$

by using the maximum power point condition, *eq*. (1.8), can be rewritten as,

$$I_{mpt} = I_{ph} - I_s\left(e^{\left(\frac{(v_{mpt} + R_{se}I_{mpt})}{V_{th}}\right)} - 1\right) - \frac{V_{mpt} + R_{se}I_{mpt}}{R_{sh}} \tag{2.21}$$

$$\frac{dI_{lo}}{dV} = \frac{-\left[\frac{I_s}{V_{th}}\left(e^{\left(\frac{(V+R_{se}I_{lo})}{V_{th}}\right)}\right) + \frac{1}{R_{sh}}\right]}{\left[\frac{R_{se}I_s}{V_{th}}\left(e^{\left(\frac{(V+R_{se}I_{lo})}{V_{th}}\right)}\right) + \frac{R_{se}}{R_{sh}} + 1\right]} \tag{2.22}$$

further, on differentiating 'I_{lo}' concerning 'V_{lo}' at maximum power point *eq*. (2.23) is obtained as,

$$\left.\frac{dI_{lo}}{dV_{lo}}\right|_{Max.pp} = -\frac{I_{mpt}}{V_{mpt}} = \frac{\left[\frac{I_s}{V_{th}}\left(e^{\left(\frac{(v_{mpt}+R_{se}I_{mpt})}{V_{th}}\right)}\right)+\frac{1}{R_{sh}}\right]}{\left[\frac{R_{se}I_s}{\alpha kT}\left(e^{\left(\frac{(v_{mpt}+R_{se}I_{mpt})}{V_{th}}\right)}\right)+\frac{R_{se}}{R_{sh}}+1\right]} \tag{2.23}$$

the slope of *I-V* characteristic near short circuit current and slope at open circuit point is given by *eq*. (2.24) and *eq*. (2.25) respectively,

$$\left.\frac{dI_{lo}}{dV_{lo}}\right|_{I=I_{sc}} = \frac{-\left[\frac{I_s}{V_{th}}e^{\left(\frac{R_{se}I_{sc}}{V_{th}}\right)}+\frac{1}{R_{sh}}\right]}{\left[\frac{R_{se}I_s}{\alpha kT}e^{\left(\frac{R_{se}I_{sc}}{V_{th}}\right)}+\frac{R_{se}}{R_{sh}}+1\right]} = -\frac{1}{R_{se0}} \tag{2.24}$$

$$\frac{-\left[\frac{I_s}{V_{th}}e^{\left(\frac{V_{oc}}{R_{sh}}\right)}+\frac{1}{R_{sh}}\right]}{\left[\frac{R_{se}I_s}{\alpha kT}e^{\left(\frac{V_{oc}}{V_{th}}\right)}+\frac{R_{se}}{R_{sh}}+1\right]} = -\frac{1}{R_{sh0}} \tag{2.25}$$

Table 2.1 Condition sets used for formulating equations

References	V_{oc}	I_{sc}	V_{mpt}	I_{mpt}	R_{seo}	R_{sho}	$dp/dv=0$
[18]-[25]	✓	✓	✓	✓	✓	✓	-
[23]	✓	✓	-	-	✓	✓	✓
[24]	✓	✓	✓	✓		✓	✓
[25]	✓	✓	✓	✓	✓	-	-
[26]	✓	✓	✓	✓	-	-	✓

Few researchers consider analytical approaches for the solar PV parameter estimation are well covered in [26]-[30], whereas [18], [19], consider the R_{seo} and R_{sho} for the parameter extraction that are not so commonly used, moreover [19] records, a comparative analysis under various sets of temperature and irradiance.

2.2.3 Analytical approaches for the DDM

As DDM has seven unknown parameters *i.e.*, R_{se}, R_{ph}, I_{ph} α_1, α_2, I_{s1}, and I_{s2}, and to formulate seven unknown parameters seven distinguish equations are required [6], where five equations are the same as those used for SDM, whereby setting the derivative of power with voltage to zero gives the sixth equation, and in some researches like [31] seventh equation coined by keeping the sum of α_1 and α_2 to 3.

In contrast to analytical approaches,

1) An increase in the number of parameters results in more number required equations that add more complexity and these transcendent equations are very difficult to be solved.
2) By keeping the ideality factor fixed to either 1 or 2 or the sum to 3, the precise output from the estimated parameters-based simulation is difficult to obtain and should be eradicated.
3) In some cases, some assumptions are considered to simplify the process of parameter estimation which inturn reduces the expected accuracy.
4) The need of specifying the initial guesses might result in premature convergence.

To mitigate the few issues with analytical approaches numerical approaches are introduced by the researchers. The numerical method exhibits more precise outcomes than analytical methods [32]. Where, [25], [33], Newton Raphson (NR) [5], [34], and Gauss-Seidel [4], [5], [22] are the most popularly used numerical technique for solar PV parameter estimation problem. Numerical methods also exhibit a problem of premature convergence, to local minima despite global minima, if the initial guesses for the unknown parameters are not predicted well, a large number of unknown parameters also leads to high computational time.

2.3 Metaheuristic Approaches

Convergence and involvement of initial parameter substitution are the prominent problems that are faced by the researchers while using analytical and numerical approaches [35], [6]. This results in the shift of parameter estimation problems towards optimisation problems. Probabilistic and population-based optimization is the main core of metaheuristic techniques, these techniques hold the nature-based inspiration that is efficient enough to solve non-linear engineering problems, hence it is also popularly used to identify the solution for the parameter estimation problem of solar PV. Various literature follows different indexes *i.e. eq.* (2.26) - *eq.* (2.29), for performance analysis [8], [10]. In other words, it can be established that the parameter estimation problem is a minimisation of error problem, *i.e.* minimisation of error among the experimental and estimated current, where $'\delta'$ is the vector of unknown parameters.

Sum squared error (SSE),

$$\mathrm{SSE} = \sum_{i=1}^{n}\left(I_{(i)} - \hat{I}_{(V_i,\delta)} \right)^2, \tag{2.26}$$

Absolute error (AE),

$$\mathrm{AE} = \sum_{i=1}^{n}\left| I_{(i)} - \hat{I}_{(V_i,\delta)} \right|, \tag{2.27}$$

Mean absolute error (MAE),

$$\mathrm{MAE} = \frac{1}{n}\sum_{i=1}^{n}\left| I_{(i)} - \hat{I}_{(V_{(i)},\delta)} \right|, \tag{2.28}$$

Root mean square error (RMSE),

$$\mathrm{RMSE} = \sqrt{\frac{1}{n}\sum_{i=1}^{n}\left(I_{(i)} - \hat{I}_{(V_{(i)},\delta)} \right)^2}, \tag{2.29}$$

In [36], parameters are estimated for SDM and DDM of RTC France by using artificial bee colony (ABC) optimization, the experimental *I-V* data is referred from [37], where RMSE is considered as the objective function for the estimation of optimised parameters, the proposed method in [38], signifies improved performance in the context of robustness and preciseness, when compared with genetic algorithm (GA), harmony search (HS), bacterial foraging optimization algorithm (BFOA), particle swarm optimization (PSO). Whereas, in [39], an improved ABC (*i*-ABC), is proposed for SDM and DDM, and it exhibits improved results when compared with chaotic PSO, simulated annealing (SA), HS, pattern search (PS), and GA. In [40], an adaptive differential evolution (*a*-DE), is proposed, where two control parameters *i.e.* the crossover (CR) and scaling factor (*SF*) are considered with RMSE as the objective function, and experimental *I-V* characteristic is used for the validation of the proposed method, where the performance of proposed method exhibits better results when compared with a penalty based (*pb*-DE) [41]. In the *pb*-DE [41], the results are analyzed for thin-film, mono-crystalline, and poly-crystalline solar modules, where it outperformed SA and PSO on the basis of convergence speed and preciseness. It is interesting to understand that in a few metaheuristic approaches, the researchers improve the performance of existing parameter estimation techniques by incorporating new penalty and adaptive constraints, as shown in [40]-[42]. In [42], an improved JADE (*i*-JADE) is proposed for the parameter estimation problem, where a repaired adaptive crossover rate, strategy for the scaling factor along with ranking-based mutation is considered.

Table 2.2 Literature of Metaheuristic techniques for parameter estimation

Ref.	Objective function	Optimisation technique	Data considered	Equivalent Model Considered	Contribution
[36]	RMSE	ABC	Experimental *I-V*	SDM	Parameters are estimated by using the ABC algorithm and conclude the outperformance of ABC over GA, PSO, BFOA, and HS based on sturdiness and accurateness.
[4]	RMSE	SA, NR	Manufacturer's datasheet	SDM	Performance characteristic *i.e. I-V* is drawn under diverse irradiance conditions. Error plots are drawn for simulated and experimental module current. The selection criterion for the SDM is elaborated and compared with other existing mathematical models. It is highlighted that other mathematical models diverge from the real value at low irradiance conditions.
[36]	RMSE	M-ABC	Experimental *I-V*	SDM, DDM	M-ABC algorithm is used for parameter estimation problem solution and observes its importance over PS, HS, SA, and chaotic PSO. Fitness of SDM over DDM based on performance, *i.e.* only 0.79%.

[41]	RMSE	PBDE	Two diode synthetic model datasheet	DDM	Mono-crystalline, thin filmed, and multi-crystalline, solar modules are considered for analysis. Improved convergence, when compared with GA, SA, and PSO.
[40]	RMSE	ACSF-CR	Manufacturer's datasheet	SDM	The impact of irradiance on parameters is explained, and extract different parameters under different irradiance conditions. More superior results are obtained when compared with the penalty-based approach.
[45]	RMSE	DE, ACSF-CR	---	SDM	This adaptive DE doesn't need any control parameter tuning.
[6]	RMSE	LW function	Manufacturer's datasheet	SDM	A combination of iterative and approximation methods is presented. A more realistic approach is presented when exposed to *'α'* variations.
[42]	MAE	Curve fitting algorithm	Manufacturer's datasheet	SDM	The proposed method estimates MAE between *P-V* curves for the proposed model and the *P-V* curves from manufacturers' datasheets under different environmental conditions. *P-V* curves are considered for parameter estimation despite of *I-V* curves. MAEP, a new error benchmark is considered.
[46]	RMSE, MBE, AEMPP	MFO	Experimental *I-V*	DDM, TDM, MDM	Observe the improved performance of MFO on TDM for a more precise depiction of the physical behaviour of multi-crystalline solar PV modules. High convergence speed, *i.e.* comparable with DEIM and FPA.

[47]	RMSE and MAE	MVO	Experimental *I-V*	SDM	Initial values are calculated through the conventional approximate mathematical method, whereby using MVO, optimised parameters are extracted, outperforming MBA, CSA, and PSO.
[48]	RMSE	I-JAYA	Experimental *I-V*	SDM, DDM	To tune the affinity of identifying the best solution and elimination of the worst solution a self-adaptive weight is introduced. I-JAYA is implemented for parameter estimation problem and observed promising results while compared with experimental *I-V* data points.
[49]	RMSE, MRE, MAE	ER-WCA	Experimental *I-V*	SDM, DDM	Parameters are estimated for three modules, where results are found comparable with experimental data, TLBO, ABC, and IADE.
[50]	RMSE	Im-CSA	Experimental *I-V*	SDM, DDM	In the initialization step of CSA, a QOBL approach is employed. Develop a dynamic adaptive scheme for step size selection. A probability function P_a is introduced to amplify search ability and to make an alliance between exploration and exploitation.
[51]	RMSE	IWOA	Experimental *I-V*	SDM, DDM	To improve the performance of WOA, two prey strategies are proposed, the performance validation is expressed by comparing the results with WOA, CWOA, and PSO-WOA.
[52]	RMSE	(R-II), R-III)	Experimental *I-V*	SDM, DDM, TDM	The high conversion speed is observed while comparing with ABC, PSO, CS, and TLBO.

[16]	MAE, AE, RMSE	SFS	Experimental *I-V*	SDM, DDM	SFS is proposed for the parameter estimation problem, with three different modules. A 43 point dataset is also recorded for ESP-160 PPW PV module.
[53]	RE, RMSE, IAE	NMS-OL-MFO	Experimental *I-V*	SDM, DDM, PVM	A novel hybrid approach is proposed, where search performance is improved.
[54]	AE, RMSE, STD, MBE	IEM	Experimental *I-V*	SDM	Observed improved convergence speed and accuracy. The accuracy and convergence speed is improved, where AE=0.19%, TS=0.53, and STD=0.19%. The performance is validated through the experimental data and few existing techniques, like EM, SSA, IADE, PSO, and PDE.
[55]	---	---	Experimental *I-V*	Capacitance SDM	A new parasitic capacitance-based SDM is proposed, where the impact of capacitance on the *I-V* characteristic is observed experimentally.
[56]	RMSE	IMFO	Experimental *I-V*	SDM, DDM	An improved local exploration and global exploitation are exercised through the double flame generation strategies with a moths-flames optimization.
[57]	-	CTSA	Experimental *I-V*	DDM, TDM	An outstanding mathematical model of adaptive weights are considered, outperformed HHO and PSO on the basis of computational time.

Table 2.3 Literature of Hybrid techniques for parameter estimation

Ref.	Objective function	Optimisation technique	Data considered	Equivalent Model Considered	Contribution
[58]	MAE	GA	Manufacturer's datasheet	SDM, DDM	GA is used for parameter estimation under different environmental conditions, whereas, I_{ph} and I_s are analytically analysed.
[59]	-	Hybrid GA-IP	Manufacturer's datasheet	SDM	Illustrate the dominance of GA-IP over PSO.
[60]	-	BFOA	Manufacturer's datasheet	SDM	In the context of sturdiness and precision, the BFOA showcases its pre-eminence over GA and AIS.
[61]	RMSE, MAE	GWO	Experimental *I-V*	SDM	Suitability of GWO over PSO, NR, and NLS. R_{sh}, $R_{se,}$ and α are estimated by using GWO where I_{ph} and I_s analytically analyzed.
[8]	RMSE	GCPSO	Experimental *I-V*	SDM, DDM	Showcase the outperformance of GCPSO over PSO, ABC-DE, FPA, SA, PS, and TLBO.
[62]	RMSE	PG-JAYA	-	SDM, DDM	A self-adaptive chaotic perturbation mechanism is introduced, analysis is observed with different sets of populations, irradiance, and temperatures.

[63]	RMSE	HFP	Experimental *I-V*	SDM, DDM	Incorporate the Nelder-Mead simplex method (NMM) with the flower pollination algorithm and the opposition-based learning method is generalized. Tests are performed on Multi-crystalline, thin-film, and mono-crystalline modules reported with stability and high convergence speed. Observed improved results when compared with CPSO, LMSA, PS, ABC, and ABSO.
[9]	MPE, RMSE, NRMSE,	Hybrid SA	Experimental *P-V*	SDM	Parameters are estimated for two different modules *i.e.* KC200GT and PWP201. Characteristic equations are derived in terms of R_{se} and α, where SA is used along with these characteristic equations to estimate these unknown parameters, whereas, R_{sh}, $I_{ph,}$ and I_s are analytically estimated through NR.
[64]	RMSE	MADE	Experimental *I-V*	SDM, DDM	SHADE, NMM, and RBE are incorporated together for parameter estimation. Precise guess for initial values, acceleration in convergence speed and elimination of worse solutions are the features of SHADE, NMM, and RBE, that are combined and incorporated to formulate MADE.
[65]	RMSE	ISCE	Data available in datasheet	SDM, DDM	Shown suitable results when compared with EHA-NMS and Rcr-IJADE, in terms of computational efficiency.

Furthermore, in [43], PSO approach is implemented, for the extraction of parameters for DDM and the three-diode model (TDM) by using the manufacturer's datasheet. Here, MAE *i.e. eq.* 2.28, is considered as, the objective function, and it is concluded that TDM exhibits more reliable results when compared with DDM. About nine modeling parameters are to be estimated for the TDM, where in [43], $I_{ph}=I_{sc}$, and the ideality factors 'α_1' and 'α_2' are considered as 1 and 2 respectively, hence only the remaining six parameters are to be estimated in [43]. A novel technique is also showcased in [44], for modified DDM through Harris Hawks optimisation (HHO). The most recent literature is reviewed in table 2.2, where the model considered, decision standards, approaches used and findings are consolidated.

2.4 Hybrid Approaches

It is also important to underline that the metaheuristic algorithms undergo few trade-offs in global and local optima, where exploration and exploitation balance should be enhanced. High exploration and exploitation result in convergence problems and trapping in local optima respectively, hence a new hybrid approach *i.e.* a combined arrangement of analytical or numerical and metaheuristic approaches are introduced in the literature to improve the overall efficiency of the solution [6], [66]. For instance, [9] employed NR and SA together for the parameter estimation, where R_{se} and α are estimated through SA, and I_s, I_{ph}, and R_{sh} are numerically estimated by using NR. A series of researches are well emphasised in table 2.3, where the data considered, techniques implemented along with the PV models used, and objective functions considered for the estimation problem are listed. Hybrid approaches are also considered for various solar PV problems that also include the designing of MPPT strategies [67].

2.5 Chapter summary

A critical review of literature is presented, where it is divided on the basis of techniques implemented for the solution *i.e.* analytical, metaheuristic, and hybrid approaches. The preciseness of the parameters to be estimated depends on the closeness of the objective function (OF) to zero. Where the information of exact parameter values is not available, hence the degree of preciseness rests on the experimental data only. Any diminution in the OF *i.e.* RMSE is observed as a substantial enhancement towards the preciseness of real unknown parameter values, where the same is well observed with the proposed methodologies that exhibits more promising results when compared with the techniques in the literature.

Chapter 3

EMPEROR PENGUIN OPTIMISATION FOR PARAMETER ESTIMATION PROBLEM AND IMPACT OF ENVIRONMENTAL CONDITIONS

3.1 General

It is important to apprehend that solar PV is very sensitive to environmental changes, where '*T*' and '*G*' are the environmental parameters that make a substantial impact on the performance of solar PV. Hence, the impact of environmental conditions on the performance characteristics of solar PV is well studied in this chapter, moreover, a new Emperor Penguin Optimisation (EPO) [68] based parameter estimation approach for an SDM of solar PV is presented that is cohesively analysed under different sets of '*T*' and '*G*' for three case studies having three different multi-crystalline solar PV modules, *i.e.* KC200GT, PWP201, and STP6 120-36. As it is concluded in chapter 2 SDM is the simplest and most accurate mathematical model, which it is widely accepted in literature. Hence, in the proposed Emperor Penguin Optimisation approach for parameter estimation, SDM is considered for analysis. The preciseness of the parameter estimation problem resides in the superimposition of extracted *I-V* over the experimental *I-V* characteristic, as the exact parameter's values are not known, hence these parameters are also known as the unknown modelling parameters.

3.2 Impact of environmental conditions on solar PV

The performance characteristics of solar PV are subtle towards the change in environmental conditions, *i.e.* the ambient temperature and solar irradiance, for instance in fig. 3.1 the performance characteristic of the KC200GT module is presented in fig. 3.1 (a). Where an appreciable change in the current is observed under a different set of irradiances, whereas for constant irradiance, voltage changes with the temperature change. This shows that modules/arrays performed well at high irradiances and comparatively low temperatures. The irradiance and temperature make an appreciable impact on I_{ph}, I_{sc}, I_s, V_{oc}, $V_{mpt,}$ and I_{mpt} *i.e.* well observed from *eq.* (3.1)-(3.6), [3].

$$I_{ph} = \left[I_{ph}^{STC} + K_i dt \right] \frac{G}{G_{STC}} \tag{3.1}$$

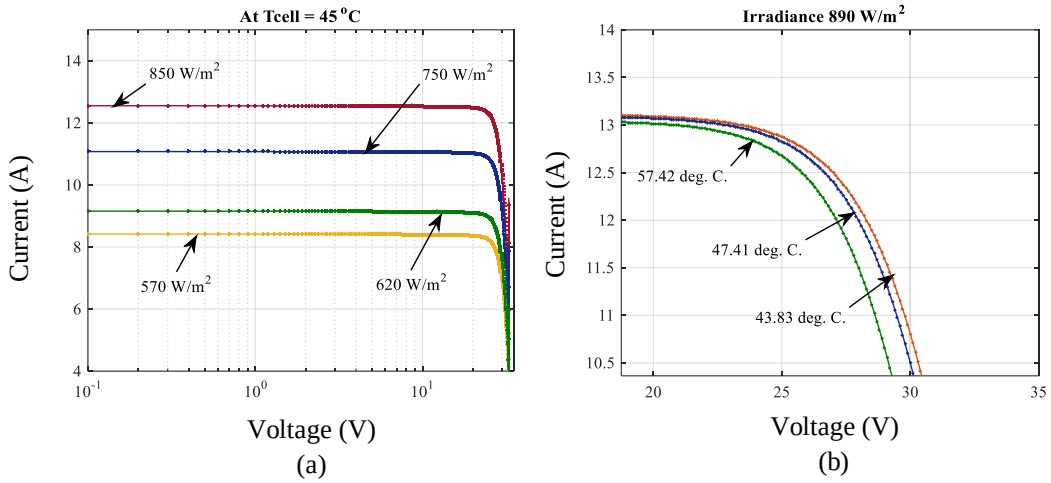

Fig. 3.1 *I-V* characteristic of KC200GT under different sets of environmental conditions

$$I_{sc} = \left[I_{sc}^{STC} + K_i dt \right] \frac{G}{G_{STC}} \tag{3.2}$$

$$I_s = \frac{I_{sc,STC} + K_i dt}{\exp\left(\frac{V_{oc,\,STC} + K_v dt}{V_{th}} \right) - 1} \tag{3.3}$$

$$V_{oc} = V_{oc,STC} + V_{th} \ln\left(\frac{G}{G_{STC}} \right) + K_v dt \tag{3.4}$$

$$V_{mpt} = V_{mpt,STC} + V_{th} \ln\left(\frac{G}{G_{STC}} \right) + K_v dt \tag{3.5}$$

$$I_{mpt} = I_{mpt,STC} \ln\left(\frac{G}{G_{STC}} \right) \left(1 + K_i dt \right) \tag{3.6}$$

I_{ph}^{STC}, I_s^{STC}, K_v and K_i are the photo and reverse saturation current at Standard test condition (STC) *i.e.* 25° *C* and *G* of 1000 *W/m*^{2}, and the voltage and current co-efficient of temperature respectively. Moreover, *dt* = *T*-T_{STC} *i.e.* the difference between *T* (ambient temperature) and the T_{STC} (STC temperature).

3.3 Problem formulation

Here, only SDM is considered for the analysis, hence vector δ = [I_{ph}, I_s, α, R_{se}, and R_{sh}] is to be estimated. The RMSE *i.e. eq.* 3.7, is considered as the objective function, where the error among the estimated current value and experimental current value is to be minimised, the

boundary conditions for all the three case studies are listed in table 3.1, the estimated current as a function of 'δ' is given by $\hat{I}_{lo(V_{lo(i)},\delta)}$.

$$\text{Min OF}(\delta) \text{ for SDM}=\sqrt{\frac{1}{n}\sum_{i=1}^{n}\left(I_{lo(i)}-\hat{I}_{lo(V_{lo(i)},\delta)}\right)^2}, \tag{3.7}$$

It is important to understand that the parameters are estimated for the cell, where the realisation of estimated parameters for the module or array can be further carried on the basis of the number of series and parallel cells connected, hence for the array *eq.* (1.8), can be written as *eq.* (3.8), and the same is also considered in chapter 4 for SDM, where N_s and N_p are the numbers of cells connected in series and parallel respectively, the function of current is given by *eq.* (3.9).

$$I_{lo(V_{lo(i)},\delta)}=N_p\left\{I_{ph}-I_s\left(\exp\left[\frac{\left(V_{lo}+I_{lo}R_{se}\left(\frac{N_s}{N_p}\right)\right)}{N_sV_{th}}\right]-1\right)\right\}-\frac{\left(V_{lo}+\left(\frac{N_s}{N_p}\right)I_{lo}R_{se}\right)}{\left(\frac{N_s}{N_p}\right)R_{sh}} \tag{3.8}$$

$$f\left(\hat{I}_{lo(V_{lo(i)},\delta)}\right)=I_{lo}-N_p\left\{I_{ph}-I_s\left(e^{\left[\frac{\left(V_{lo}+I_{lo}R_{se}\left(\frac{N_s}{N_p}\right)\right)}{N_sV_{th}}\right]}-1\right)\right\}+\frac{\left(V_{lo}+\left(\frac{N_s}{N_p}\right)I_{lo}R_{se}\right)}{\left(\frac{N_s}{N_p}\right)R_{sh}} \tag{3.9}$$

3.4 Proposed methodology

Proposed methodology practice, the EPO algorithm *i.e.* explained in [68], for the solution of the parameter estimation problem. EPO is a bio-inspired population-based metaheuristic algorithm, to formulate the solution for both constraint and unconstraint problems [68].

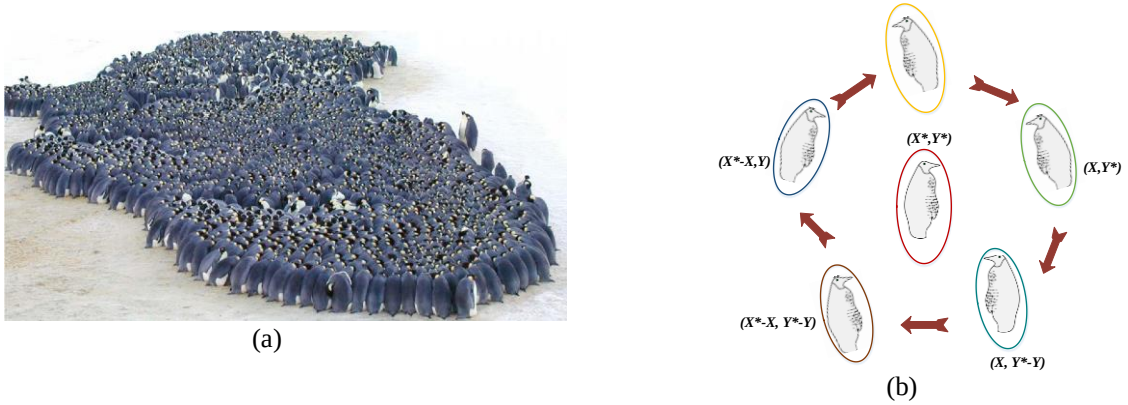

(a) (b)

Fig. 3.2 (a) Huddle of Emperor penguins, (b) Huddling behaviour of emperor penguins [68]

This algorithm instigates from the social huddling behaviour of emperor penguins (largest and heaviest among all penguin species) during their breeding season in Antarctic winter, while breeding thousands of these flightless emperor penguins come onshore to lay eggs. In fig. 3.2 (a), a huddle of emperor penguins is showcased, whereas, in fig. 3.2 (b), it is observed that the penguin *(X*, Y*),* can appraise its location to other penguins and can reach different locations about the current position. There are four phases of huddling by emperor penguins that are configured in a mathematical model and used to solve parameter estimation problem, four phases are classified as,

a) Generation and determination of emperor penguin's huddle boundary

In this algorithm, the emperor penguins are the search agents, and the identification of an effective mover or achieving an optimised solution is the main objective. Here, it is assumed that the huddle is a two-dimensional *L*-shaped polygon plane, while obtaining the best solution, the position of the mover is updated and the boundary is also recomputed accordingly [68]. During this process, the penguins will select two random neighbours in the huddle as showcased in fig. 3.2 (b), where the huddle boundary around the polygon is formulated based on the flow of air around the huddle, the flow of air is considered for huddle boundary prediction, as when airflow towards the huddle it spreads around the huddle as per the shape configuration and this spread can easily draw down the boundary of the huddle.

Let, the wind velocity defines by 'ϕ' with gradient 'ψ', observed in *eq.* (3.10) as,

$$\psi = \nabla \phi \tag{3.10}$$

To generate analytical function *'f'* on the polygon plane and to generate complex potential, 'ϕ' is used along with the vector Ω, expressed in *eq.* (3.11),

$$f = \phi + i\Omega \tag{3.11}$$

The idea is to advance the mover *i.e.* search penguins in such a way that they discover a multidimensional search space *i.e.* within the huddle boundary for an optimal solution. In the context of the parameter estimation problem, the parameters I_{ph}, I_{lo}, I_s, V_{lo}, V_{th}, N_s, N_p, R_{se}, α, and R_{sh}, are initialised. Where constraints are generated, based on the minimum and maximum of PV modelling ranges mentioned as lower and upper boundary constraints. In this paper, the boundary conditions are furnished in table 3.1 as,

Table 3.1 Boundary conditions for SDM

Parameter	Case study 1 (KC200GT)		Case study 2 (STP6-120/36)		Case study 3 (PWP-201)	
	LB	UB	LB	UB	LB	UB
I_{ph} [A]	0	50	0	2	0	8
I_s [A]	0	2	0	50	0	50
α	1	50	1	50	1	50
R_{se} [Ω]	0	2	0	2	0	10
R_{sh} [Ω]	0	1000	0	2000	0	1500

$$f_{cons} = \begin{cases} R_{se(\min)} \le R_{se} \le R_{se(\max)} \\ R_{sh(\min)} \le R_{sh} \le R_{sh(\max)} \\ \alpha_{\min} \le \alpha \le \alpha_{\max} \end{cases} \tag{3.12}$$

b) Calculation of temperature around the huddle

To survive, the emperor penguins create the huddle and maximize the temperature inside the huddle, that is according to the temperature outside the huddle ($T_h^{'}$). The $T_h^{'}$ is modelled by using *eq.* 3.13 and 3.14. It is assumed that temperature T_h =1, if polygon radius R_{hb} > 1, and T_h = 0 if R_{hb} < 1.

$$T_h^{'} = \left(T_h - \frac{n}{i-n} \right) \tag{3.13}$$

$$T_h = \begin{cases} 1, \text{ if } R_{hb} < 1 \\ 0, \text{ if } R_{hb} > 1 \end{cases} \tag{3.14}$$

where *i* is the current iteration and '*n'* expresses the maximum number of iterations. For the PV parameter estimation problem, the decision conditions are temperature and irradiance.

c) Formulation of distance among emperor penguins during huddling

As the emperor penguins huddle together, hence there is a need to model mathematically the component to avoid collision with neighbour penguins, and for this vector $\vec{A}$ and $\vec{C}$ are utilised, expressed by *eq.* (3.15) and *eq.* (3.16).

$$\vec{A} = \left(M \times \left(T_h^{'} + P_{gr}\left(Acc\right) \right) \times Rand() \right) - T_h^{'} \tag{3.15}$$

$$\vec{C} = Rand() \tag{3.16}$$

$$P_{gr}\left(Acc\right) = Abs\left(\vec{P} - \vec{P}_{ep} \right) \tag{3.17}$$

Where *M* represents the movement parameter, responsible to maintain the gap among the search agents that in turn inhibit the collision, the value of *M* is fixed to 2, $P_{gr}\left(Acc\right)$ indicates the accuracy of the polygon, $\vec{P}$ implies the fittest emperor penguin *i.e.* optimal solution, $\vec{P}_{ep}$ expresses the position vector of other emperor penguins and *Rand*() is the random function in the range [0,1].

By using the vector $\vec{A}$ and $\vec{C}$ the distance between the emperor penguin and the fittest search agent can be calculated, expressed as $\vec{D_{ep}}$ in *eq.* (3.18).

$$\vec{D}_{ep} = Abs\left(S(\vec{A}).\vec{P}(i) - \vec{C}.\vec{P}_{ep}\left(i\right)\right) \tag{3.18}$$

Where, *S*() elaborates on the social forces which stimulate the emperor penguins to move towards the optimal search agent, with f_c and l_c as control parameters with a range of [2,3] and [1.5, 2] respectively, and expressed in *eq.* (3.19).

$$S(A) = \left(\sqrt{\vec{f_c e^{\frac{-i}{l_c}}}} - e^{-i} \right)^2 \tag{3.19}$$

To estimate the optimised unknown parameters, the *eq.* (3.18) for $\vec{D_{ep}}$, is used to find the distance between the emperor penguin holding optimal solution for I_{lo} *i.e.*($\vec{P}$), by using *eq.* (3.9) and the search penguin ($\vec{P}_{ep}$). If the best optimal solution for *eq.* (3.9) is obtained from the iteration i_x, then the obtained solution will be updated.

d) Effective mover relocation

The mover is the best attained optimal solution, to attain the best optimal solution, the emperor penguins continuously change their current position according to the mover that in turn continuously changes the huddle configuration. By using *eq.* (3.20), the next updated position of the emperor penguin is estimated,

$$\vec{P}_{ep}\left(i+1\right) = \left(\vec{P}(i) - \vec{A}.\vec{D}_{ep} \right) \tag{3.20}$$

where, $\vec{P}_{ep}\left(i+1\right)$ is the next updated emperor penguin's position, *i.e.* relocation of penguin as per the best optimal solution of I_{lo} from *eq.* (3.9). The flow diagram for the proposed methodology of parameter estimation using EPO is elucidated in fig. 3.3, along with the pseudo-code.

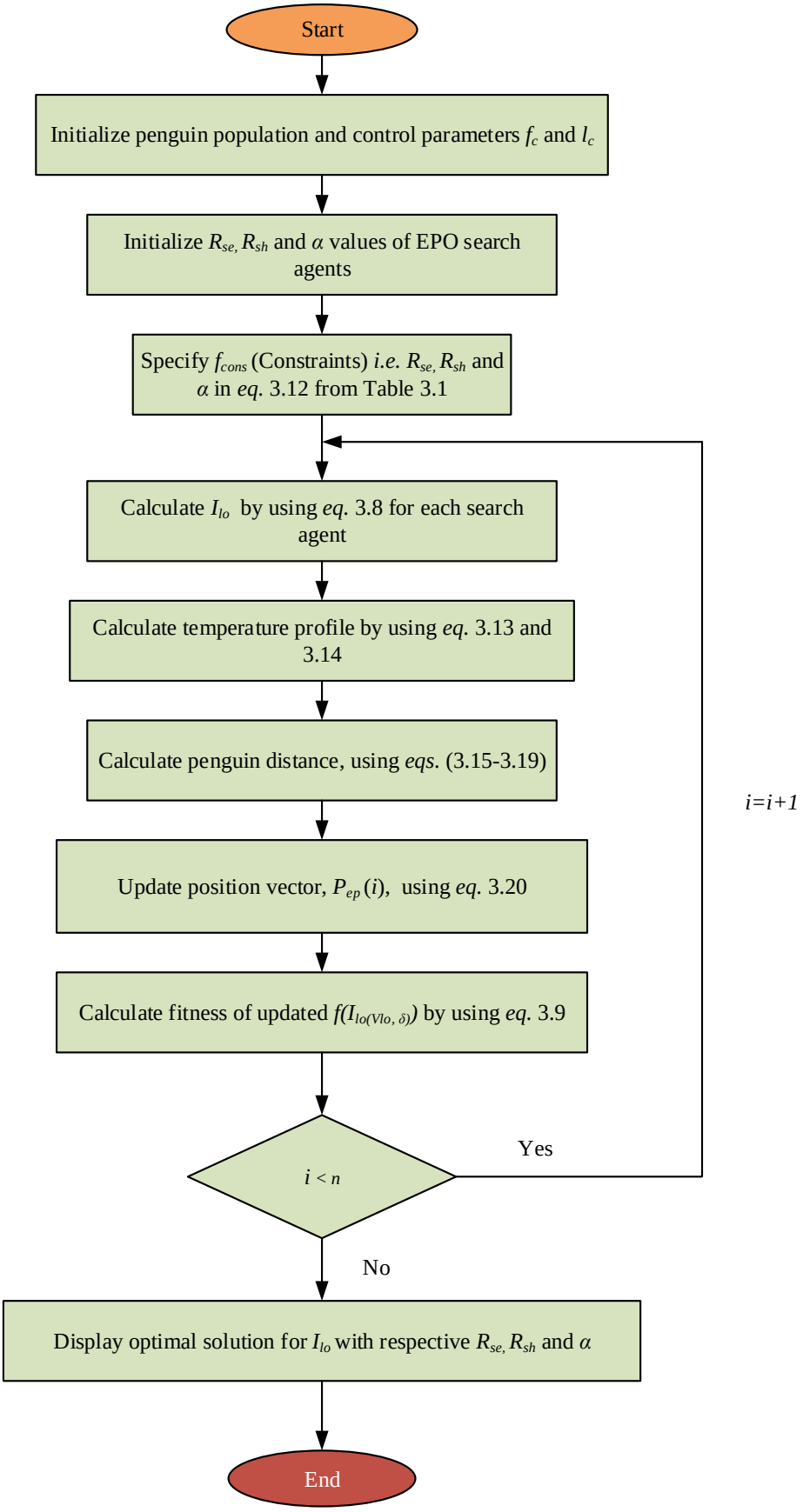

Fig. 3.3 Implementation of EPO for solar PV parameter estimation problem

**pseudo-code for proposed parameter estimation approach using EPO*

$\vec{P}_{ep}(i)$ $(i \leftarrow 1, 2, ..., n)$ **emperor penguin population*

Initialize the unknown parameters R_{se}, R_p and α

While ($i < n$) do

fitness ()

rand()

if (R<1) then

$T_h \leftarrow 0$

else

$T_h \leftarrow 1$

end if

$T_h^{'} \leftarrow$ Compute temperature profile **for temperature round the huddle*

for $i \leftarrow 1$ to n do

for $j \leftarrow 1$ to n do

compute equations (3.15)-(3.19) **distance between penguins*

update position using (3.20) **effective mover*

end for

end for

update $T_h^{'}$, $\vec{A}$, $\vec{C}$, S ()

**search agent beyond the search space region*

fitness $f\left(\hat{I}_{lo(V_{lo(i)},\delta)}\right)$ **fitness function, eq. 3.9*

update best fitness

$i \leftarrow i+1$

end while

end

Fitness procedure

for $i \leftarrow 1$ to n do

$f\left(\hat{I}_{lo(V_{lo(i)},\delta)}\right) \leftarrow$ fitness function

end for

$f\left(\hat{I}_{lo(V_{lo(i)},\delta)}\right)_{best} \leftarrow best\left[f\left(\hat{I}_{lo(V_{lo(i)},\delta)}\right)\right]$

return $f\left(\hat{I}_{lo(V_{lo(i)},\delta)}\right)_{best}$

end

procedure $best\left[f\left(\hat{I}_{lo(V_{lo(i)},\delta)}\right)\right]$

best $\leftarrow f(0)$

for $i \leftarrow 1$ to n do

if $\left(f\left(\hat{I}_{lo(V_{lo(i)},\delta)}\right) < best\right)$ *then*

$best \leftarrow f\left(\hat{I}_{lo(V_{lo(i)},\delta)}\right)$

end if

end for

return best

end

3.5 Results and discussion

To check the efficacy of the proposed parameter estimation method, three multi-crystalline solar PV modules have been considered, the manufacturer's data for the modules are summarised in table 3.2. As manufacturer's specifications in table 3.2, are not sufficient to model the characteristics of the solar PV module or array and there is a need for unknown parameter vector $\delta = [I_{ph}, I_s, \alpha, R_{se,}$ and $R_{sh}]$, to minimise the complexity associated the vector $\delta = [R_{se}, R_p, \alpha]$ is estimated by using EPO where I_{ph} and I_s are analytically analysed. For optimisation problems, the initial guess of parameters is very critical, and for EPO and analytical analysis, the upper and lower bounds are randomly chosen based on their physical significance, showcased in table 3.1. For EPO, a population size (N_{po}) of 100 is chosen with iterations (n)=100. By using initial guesses from table 3.1, the MATLAB program is simulated for the EPO algorithm. Results are classified into two sections as,

Table 3.2 Specifications of modules from the manufacturer's datasheet

S. No.	Solar PV modules		Known parameters from the manufacturer's datasheet						
		V_{mpt} (V)	I_{mpt} (A)	V_{oc} (V)	I_{sc} (A)	N_s	P_{max} (W)	*Temp* ($^{\circ}C$)	K_i ($A/^{\circ}C$)
1.	Kyocera, KC200GT	26.3	7.61	32.9	8.21	54	200.143	25	0.0032
2.	Schutten Solar, STP6 120-36	14.93	6.83	21.24	7.33	36	120	55	0.0042
3.	Photowatt, PWP201	12.6	0.89	16.78	1.031	36	12	45	0.00178

3.5.1 Comparative analysis of proposed technique

Here, the simulation of the above-mentioned modules by using estimated parameters, analysis of *I-V* and *P-V* characteristics, and comparison with the results observed in recent literature *i.e.* PG-Jaya algorithm [62], MPSO algorithm [69], WC algorithm [49], ABSA method [9], ITLBO algorithm [70], ImCSA [50], ISCE [65] and hybrid BPFPA [71] is showcased. The efficacy of the proposed work is established by reducing the RMSE values and selecting the optimal set of unknown parameters for gathering optimal I_{lo} for maximum power.

Table 3.3-3.5, showcases, the parameters that are estimated for KC200GT, STP6 120/36, and PWP 201 at T=25$^{\circ}C$, T=55$^{\circ}C$, and T=45$^{\circ}C$ respectively, with an irradiance of G=1000W/m^2.

Furthermore, table 3.3-3.5, also depicts the parameters extracted for all three cases and expresses improved results by using the proposed EPO method. In most of the scenarios, the estimated parameters offer lesser RMSE *i.e.* calculated by *eq.* (3.7), for I_{lo}, which is based on measured and estimated values, when compared with several parameter extraction techniques in the literature. Where experimental values are referred from [52] for KC200GT and from [54] for

STP6 120/36 and PWP 201. It is also observed that the estimated parameters are in decent concurrence with the theoretical estimation of smaller R_{se} and larger R_{sh}.

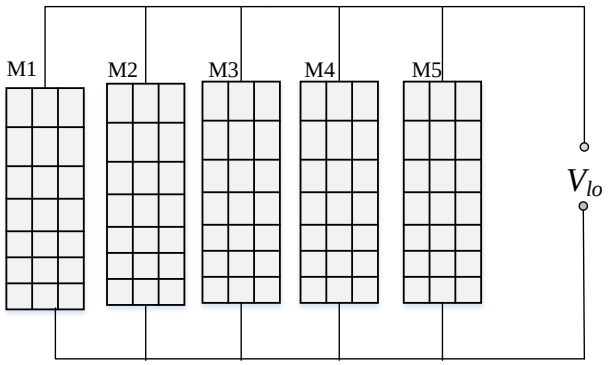

Fig. 3.4 Array with five modules of KC200GT and PWP 201 connected in parallel

Table 3.3 Comparison of parameters estimated by using EPO with existing techniques for Kyocera KC200GT at G=1000W/m^2, T=25$^{\circ}C$

Techniques	**Kyocera, KC200GT**			
	R_p **(Ω)**	R_{se} **(Ω)**	α	***RMSE***
Proposed	50.018	0.0343	1.077	0.0015
PG-Jaya	773.811	0.3569	1.0367	$2.425e^{-03}$
MPSO	753.21	0.344	1.072	0.0014
WC	176.62	0.322	1.078	$1.78e^{-3}$
ABSA	895.797	0.2109	1.8766	0.023

Table 3.4 Comparison of parameters estimated by using EPO with existing techniques for Schutten solar STP6 120/36 at G=1000W/m^2, T=55$^{\circ}C$

Techniques	**Schutten Solar, STP6 120-36**			
	R_p **(Ω)**	R_{se} **(Ω)**	α	***RMSE***
Proposed	9.478	3.5612	1.0224	0.0132
ITLBO	22.2199	0.0046	1.2601	0.0166
ImCSA	10.00	5.3870	1.1977	0.0158
ISCE	22.21991	4.5946	1.2601	0.0166

Table 3.5 Comparison of parameters estimated by using EPO with existing techniques for Photowatt PWP 201 at G=1000W/m^2, T=45$^{\circ}C$

Techniques	**Photowatt, PWP 201**			
	R_p **(Ω)**	R_{se} **(Ω)**	α	***RMSE***
Proposed	982.45	1.172	48.472	0.0022
PG-Jaya	981.85	1.201	48.642	0.0024
MPSO	762.90	1.238	47.47	0.020
WC	961.05	1.1963	48.789	0.0023
ABSA	616.75	1.338	1.2482	0.1203

By using the proposed method, parameters are extracted for all three cases and summarised in table 3.3-3.5. Moreover, based on extracted parameters two arrays are modelled by assembling five, KC200GT and PWP 201 modules in parallel, where the configuration is showcased in fig. 3.4. Whereas, in the case of STP6 120/36, the comparison with experimental data is carried out only for a single module.

$$R_{se-a} = \frac{N_s \times R_{se}}{N_p} \tag{3.21}$$

$$R_{p-a} = \frac{N_s \times R_{se}}{N_p} \tag{3.22}$$

$$I_{ph-a} = \left(N_p \times I_{ph}\right) \tag{3.23}$$

$$I_{s-a} = \left(N_p \times I_{s1}\right) \tag{3.24}$$

In other words, it can be stated that the PV array is a long chain of series and parallel combinations of cells, arranged to obtain the required voltage and power [3] as shown in fig. 3.5. To increase the overall voltage, the cells are connected in series, whereas an increase in parallel strings results in higher currents, *i.e.* also highlighted in chapter 1.

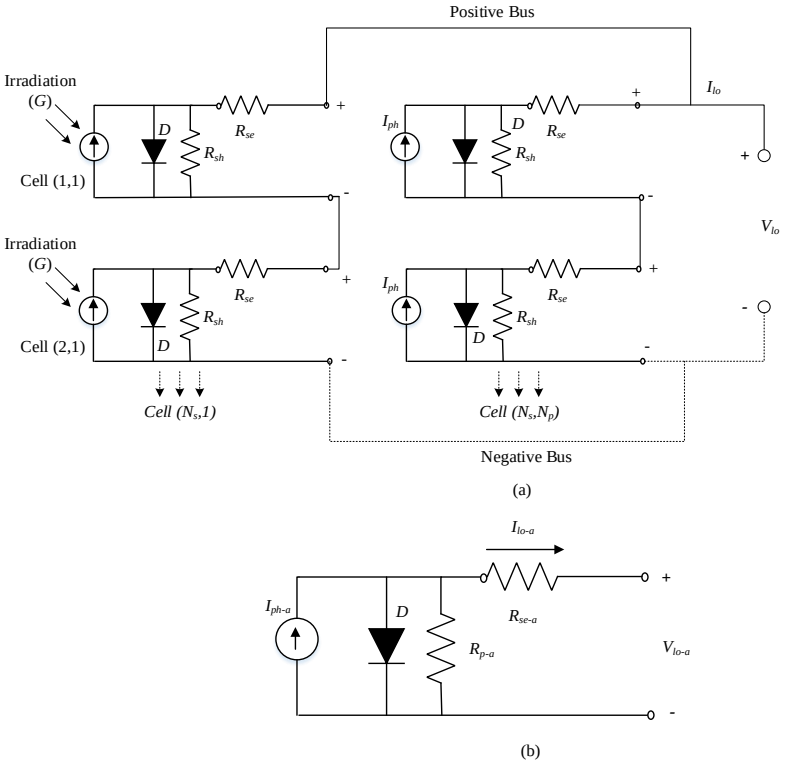

Fig. 3.5 Modelling of PV array (a) Lumped circuit of an array by using SDM, (b) Equivalent array model

In fig. 3.5 (a), an array is modelled with N_s and N_p, numbers of series and parallel strings respectively. Arrays can be considered as a single cell with suitable multipliers that are completely compliant with the number of series-parallel strings of cells in the array. Parameters for an array can easily be estimated if the parameter of a single-cell or module is obtained, hence in our study, we estimate the parameters for the modules that can be simply multiplied by the multipliers for the array parameters. The lumped resistances can be calculated by using *eq.* 3.21 and *eq.* 3.22, where $I_{ph\text{-}a}$ and $I_{s\text{-}a}$ can be realised from *eq.* 3.33 and *eq.* 3.34 respectively. The movement of the emperor penguin for the optimal solution is showcased in fig. 3.6, where fig. 3.7 and fig. 3.9, showcases the *I-V* and *P-V* characteristics for KC200GT and PWP 201 arrays, that are drawn by using estimated parameters. These characteristics exhibit superior performance over PG-JAYA [49], MPSO [62], WC [69] and ABSA [9].

Table 3.6 Comparison of experimental values of *V*, *I*, and *W*, with estimated values for Schutten solar STP6 120/36

S. No.	**Experimental [70]**			**Estimated power parameters by using estimated PV model parameters through EPO**		**Absolute Error (AE)**
	Voltage (V)	Current (A)	Power (W)	Current (A)	Power (W)	
1	17.65	3.83	67.5995	3.658	64.5637	0.172
2	17.41	4.29	74.6889	4.112	71.58992	0.178
3	17.25	4.56	78.66	4.401	75.91725	0.159
4	17.1	4.79	81.909	4.67	79.857	0.12
5	16.9	5.07	85.683	4.935	83.4015	0.135
6	16.76	5.27	88.3252	5.30	88.828	0.03
7	16.34	5.75	93.955	5.526	90.29484	0.224
8	16.08	6.00	96.48	5.73	92.1384	0.27
9	15.71	6.36	99.9156	6.301	98.98871	0.059
10	15.39	6.58	101.2662	6.689	102.9437	0.109
11	14.93	6.83	101.9719	6.825	101.8973	0.005
12	14.58	6.97	101.6226	7.068	103.0514	0.098
13	14.17	7.1	100.607	7.227	102.4066	0.127
14	13.59	7.23	98.2557	7.41	100.7019	0.18
15	13.16	7.29	95.9364	7.565	99.5554	0.275
16	12.74	7.34	93.5116	7.724	98.40376	0.384
17	12.36	7.37	91.0932	7.874	97.32264	0.504
18	11.81	7.38	87.1578	7.989	94.35009	0.609
19	11.17	7.41	82.7697	8.078	90.23126	0.668
20	10.32	7.44	76.7808	8.174	84.35568	0.734
21	9.74	7.42	72.2708	8.206	79.92644	0.786
22	9.06	7.45	67.497	8.221	74.48226	0.771
Integral Absolute Error (IAE)						6.597

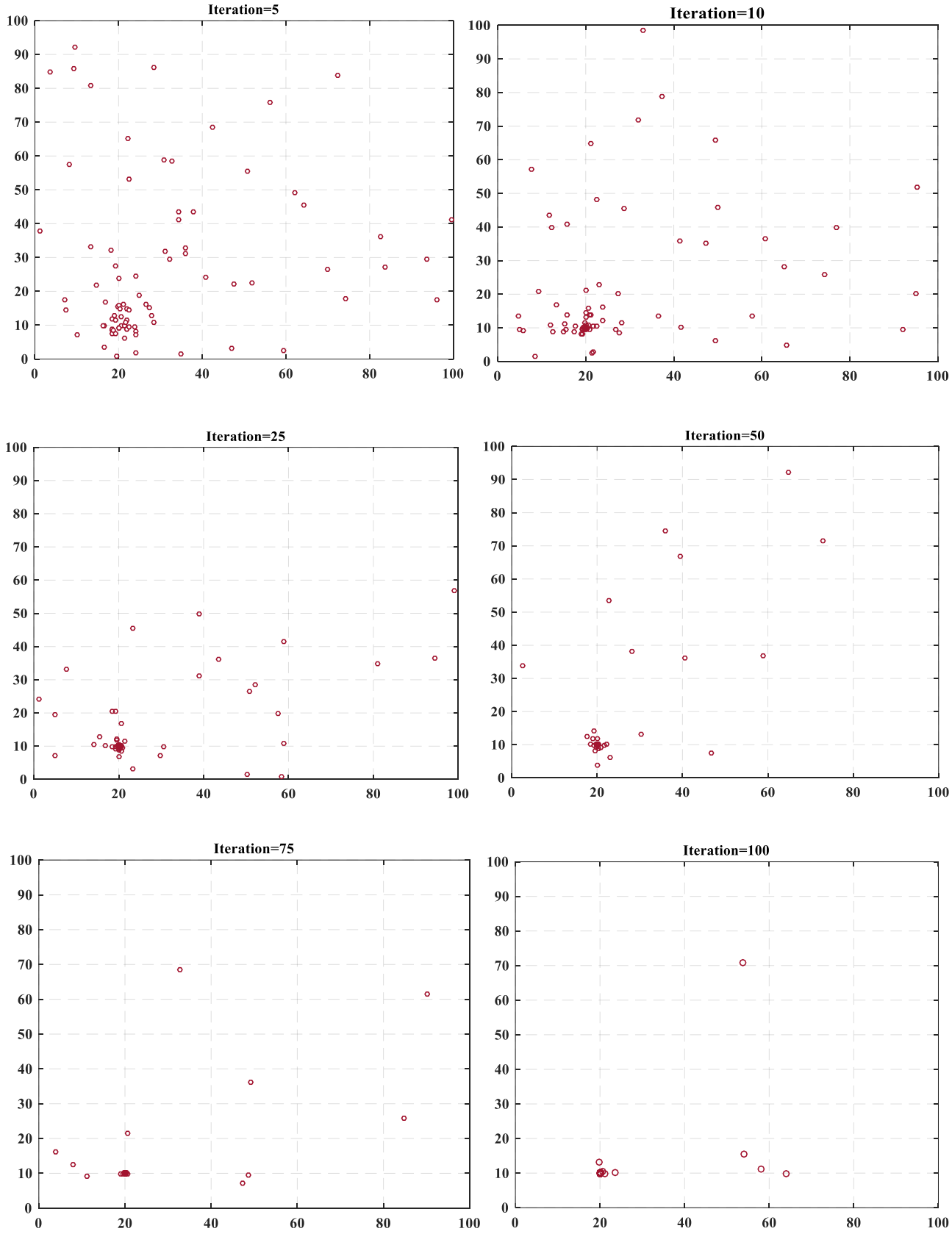

Fig. 3.6 Swarm behaviour of emperor penguins for parameter search with N_{po} =100 and n=100

Moreover, the *I-V* and *P-V* characteristics of the STP6 120/36 module, *i.e.* shown in fig. 3.8 are also drawn, which showcases that the characteristics are very much in concurrence with the experimental data. Hence, it can be stated that the parameters estimated by using the proposed EPO method, are more accurate if compared with the techniques mentioned in the comparison curves and its accuracy is also validated.

Table 3.7 Comparison of experimented maximum power, with the estimated maximum power obtained through different techniques in literature

Modules	Techniques	Experimented maximum power P_{max} (W)	Estimated maximum power $P_{e,max}$ (W)	Relative power error $E_r = \frac{P_{\max} - P_{e,\max}}{P_{\max}} \times 100\%$
KC200GT ($1000 W/m^2$, T=25°C)	**Proposed**	**200.143**	**200.124**	**9.4932E-3**
	Hybrid BPFPA	200.143	199.75	1.9635E-1
	ABSA	200.143	200.096	2.8479E-2
STP6-120/36 ($1000 W/m^2$, T=55°C)	**Proposed**	**101.9719**	**101.9579**	**1.3729E-2**
	ITLBO	101.9719	101.74586	2.2166E-1
	ImCSA	101.9719	101.81639	1.5250E-1
	ISCE	101.9719	101.7459	2.2162E-1
	ABSA	101.9719	101.9368	3.442E-2
PWP201 ($1000 W/m^2$, T=45°C)	**Proposed**	**11.54032**	**11.53571**	**3.9946E-2**
	PG-Jaya	11.54032	11.5289	9.8957E-2
	ITLBO	11.54032	11.5316	7.5561E-2
	ImCSA	11.54032	11.5316	7.5561E-2
	ISCE	11.54032	11.5316	7.5561E-2

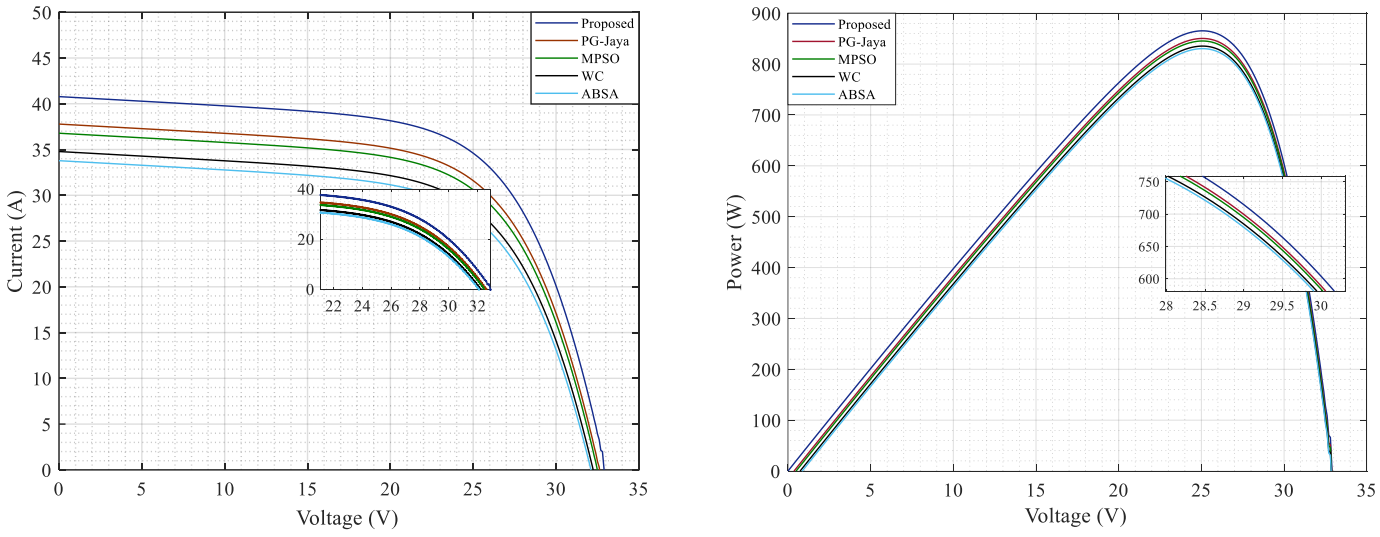

(a) (b)

Fig. 3.7 Array by using KC200GT module, at G=1000W/m^2, T=25°C (a) *I-V* characteristic (b) *P-V* characteristic

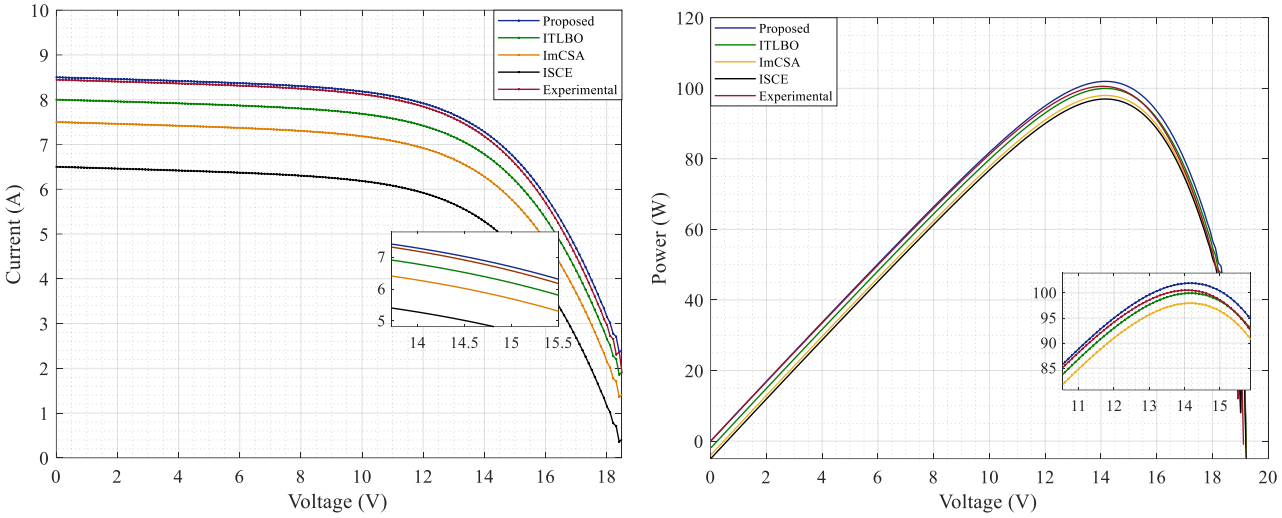

(a) (b)

Fig. 3.8 STP6 120/36, at G=1000W/m^2, T=55$^{\circ}C$ (a) *I-V* characteristic (b) *P-V* characteristic

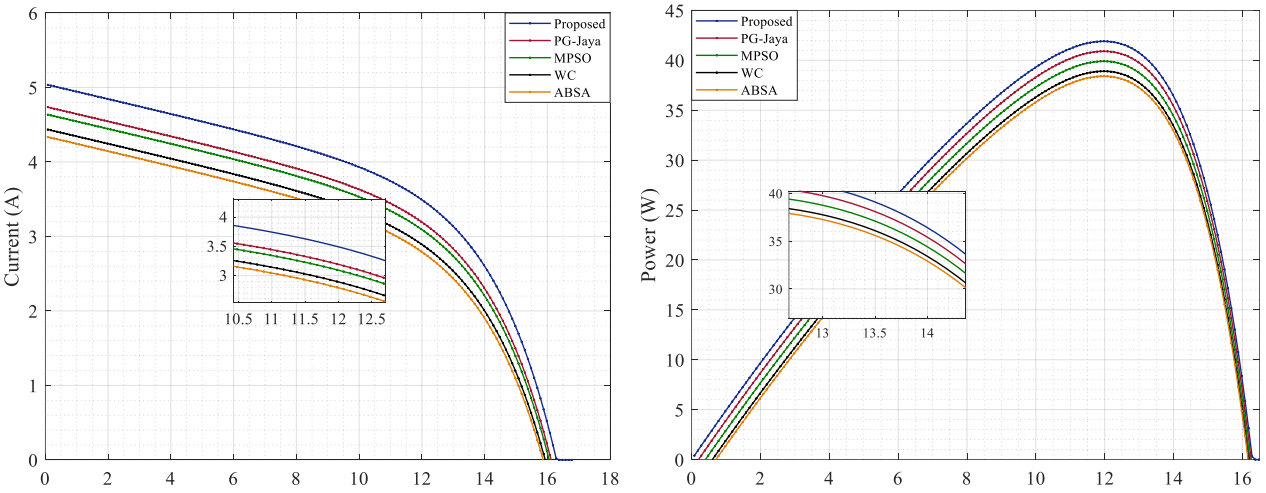

(a) (b)

Fig. 3.9 Array by using PWP 201 module, at G=1000W/m^2, T=45$^{\circ}C$ (a) *I-V* characteristic (b) *P-V* characteristics

3.5.2 Impact of different environmental conditions on parameters estimation

Table 3.6, illustrates the comparison of experimental and estimated values of *V*, *I*, and *W* for the STP6 120/36 module with an IAE of 6.597. Whereas, table 3.7, concludes that, the relative error, *i.e.* the difference among experimented and estimated power, observed from different estimation techniques in literature, the proposed method exhibits minimum error in all the three cases considered. This elucidates that, while modelling the PV module with the parameters

estimated through the proposed method gives very near to practical results *i.e.* with less relative error. As the performance of solar PV is very subtle to the environmental conditions, hence, the impact of different environmental conditions on the estimated parameters are also relevant and to be analysed.

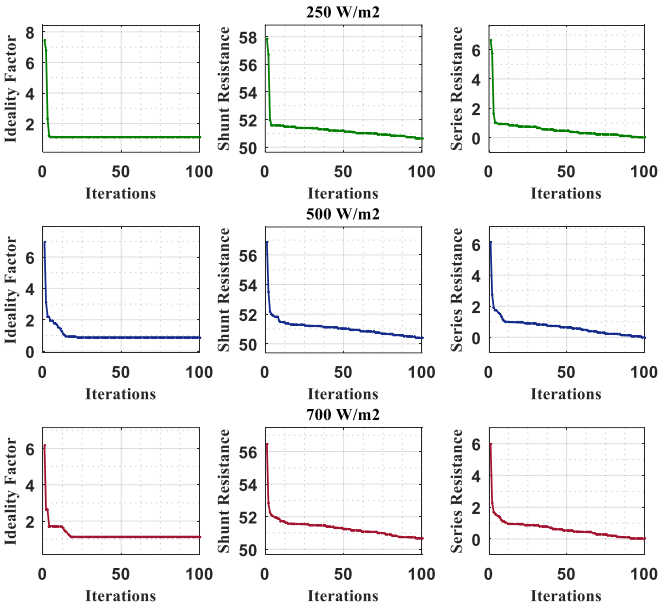

KC200GT at T=25$^{\circ}C$
3.10 (a)

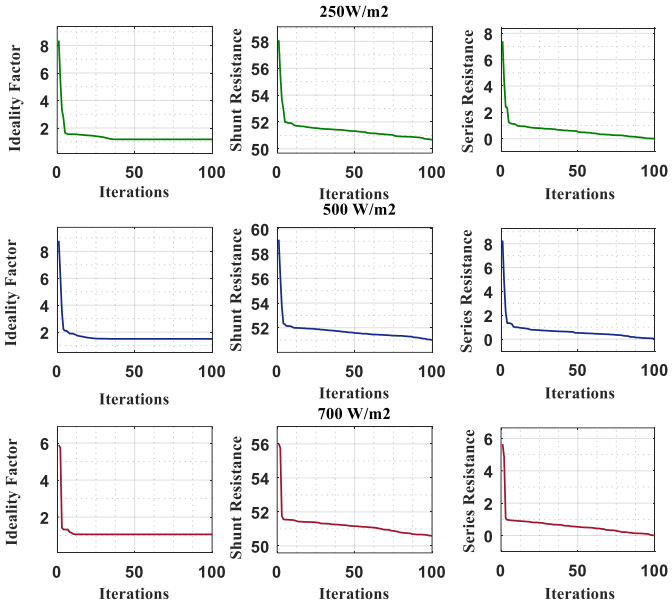

STP6 120/36 at T=55$^{\circ}C$
3.10 (b)

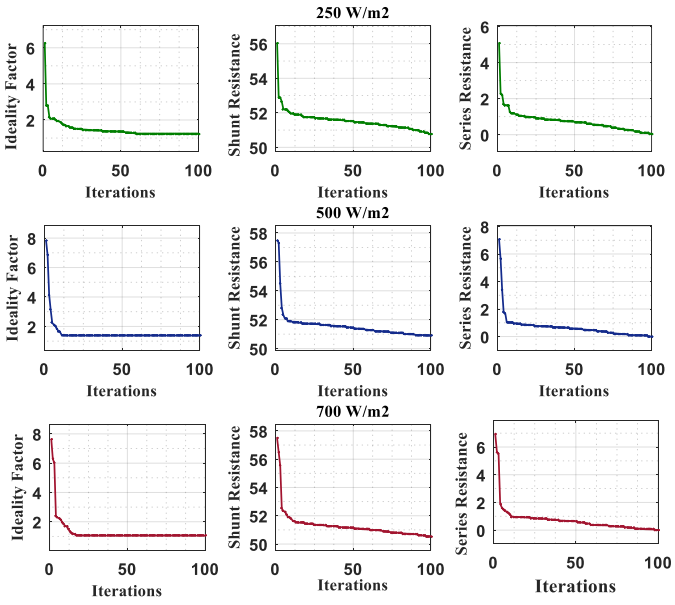

PWP 201 at T=45$^{\circ}C$
3.10 (c)

Fig. 3.10 Variation of α, R_{sh} and R_{se}, and its convergence to optimised values for n =100 under different irradiance conditions

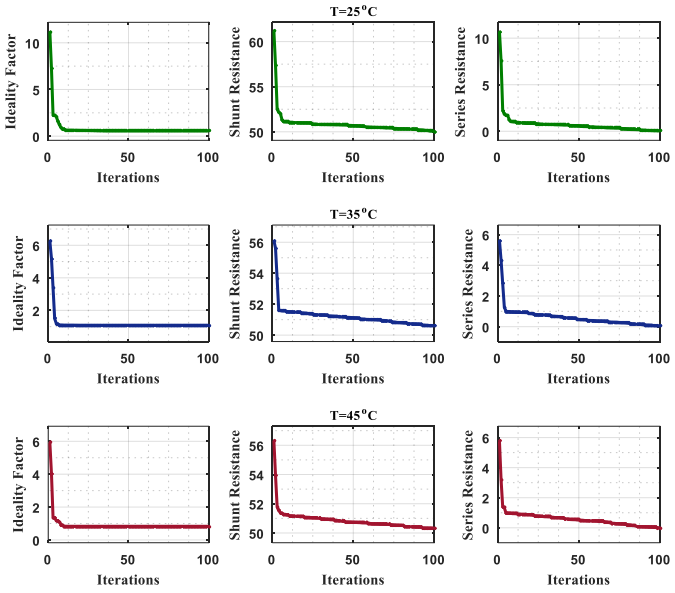

KC200GT at *G=1000 W/m²*
3.11 (a)

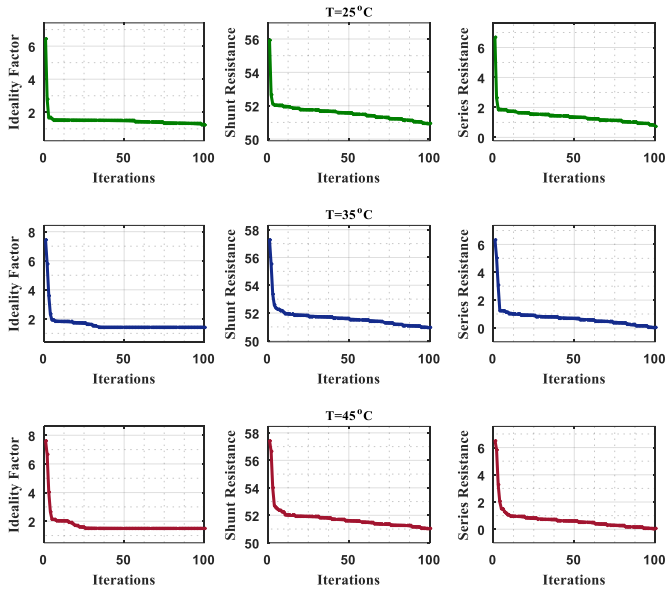

STP6 120-36 at *G=1000 W/m²*
3.11 (b)

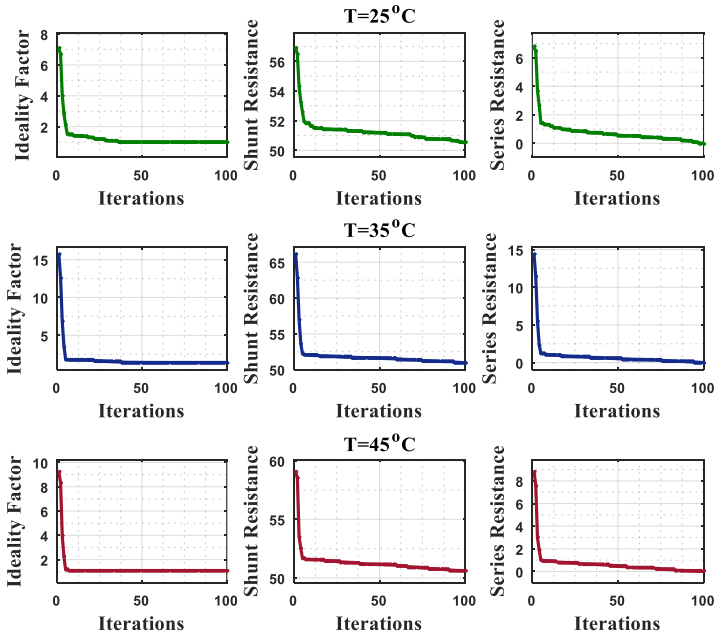

PWP 201 at *G=1000 W/m²*
3.11 (c)

Fig. 3.11 Variation of α, R_{sh} and R_{se}, and its convergence to optimized values for n =100 under different temperature conditions

In this section, the impact of different irradiance and temperature conditions on the convergence of optimal parameter values is analysed. In fig. 3.10, the convergence of parameters with optimal values is observed for all three cases where, the temperature remains unchanged and curves are

drawn for irradiance of 250, 500, and 700 W/m^2. Whereas, the impact of different temperature conditions *i.e.* 25° *C*, 35° *C*, and 45° *C* on the convergence of optimal parameter values are recorded in fig. 3.11, where the irradiance remains constant at 1000 W/m^2 for all the cases considered. Moreover, the estimated parameters under these different environmental conditions are observed in table 3.8 with RMSE and MAE

Table 3.8 Variations in estimated parameters under different sets of irradiances and temperatures

Modules	**Environmental conditions**		**Parameters Estimated**						
			I_{ph} (A)	I_s (A)	R_p (Ω)	R_{se} (Ω)	α	RMSE	MAE
KC200GT	$T^\circ C$	25 $^\circ C$	8.194	5.03 e^{-5}	50.36	0.0013	0.858	6.49e^{-6}	3.57e^{-7}
		35 $^\circ C$	8.226	9.74 e^{-5}	50.78	0.0382	1.274	7.83e^{-6}	4.30e^{-7}
		45 $^\circ C$	8.258	1.80 e^{-5}	50.60	0.0198	1.094	1.26e^{-5}	6.97e^{-7}
	G (W/m^2)	250	2.048	5.03 e^{-5}	50.43	0.0019	0.915	4.45e^{-5}	2.45e^{-8}
		500	4.113	9.74 e^{-5}	50.18	0.0024	0.682	1.45 e^{-5}	8.02e^{-8}
		700	5.7806	1.80 e^{-5}	50.26	0.224	0.694	5.32 e^{-6}	2.92e^{-7}
STP6 120/36	$T^\circ C$	25 $^\circ C$	7.354	9.37 e^{-5}	50.55	0.0013	1.057	2.18 e^{-5}	1.56 e^{-6}
		35 $^\circ C$	7.396	1.81 e^{-4}	50.46	0.0178	0.955	2.23 e^{-5}	1.60 e^{-6}
		45 $^\circ C$	7.438	3.35 e^{-4}	50.57	0.0015	1.077	1.33 e^{-5}	9.56 e^{-7}
	G (W/m^2)	250	1.838	9.37 e^{-5}	50.42	0.0035	0.913	5.77 e^{-6}	4.14 e^{-7}
		500	3.698	1.81 e^{-4}	50.19	0.0042	0.662	1.37 e^{-5}	9.88 e^{-7}
		700	5.2066	3.35 e^{-4}	50.51	0.0085	1.016	4.39 e^{-5}	3.15 e^{-6}
PWP201	$T^\circ C$	25 $^\circ C$	0.9954	5.84 e^{-5}	50.49	0.0276	0.994	4.66 e^{-5}	3.59 e^{-6}
		35 $^\circ C$	1.013	1.13 e^{-5}	50.40	0.0047	0.895	8.45 e^{-6}	6.50 e^{-7}
		45 $^\circ C$	1.031	2.09 e^{-5}	50.58	0.0563	1.035	4.45 e^{-5}	3.43 e^{-6}
	G (W/m^2)	250	0.2488	5.84 e^{-5}	50.98	0.0197	1.471	2.90 e^{-5}	2.23 e^{-6}
		500	0.5066	1.13 e^{-5}	50.33	0.0015	0.826	3.05 e^{-6}	2.35 e^{-7}
		700	0.7217	2.09 e^{-5}	50.85	0.0072	1.314	9.08 e^{-5}	6.98 e^{-6}

3.6 Chapter summary

This chapter proposed a novel technique employing EPO for the precise estimation of solar PV parameters α, R_{se}, R_p, I_s and I_{ph} for an SDM, three multi-crystalline PV modules KC200GT, STP6 120/36, and PWP 201 are considered for the parameter estimation. The accuracy in estimation and robustness under different sets of environmental conditions make this method of parameter estimation novel. Whereas, statistical error, RMSE is calculated and it is highlighted that these statistical errors are minimal when compared with the PG-Jaya algorithm [62], MPSO algorithm [69], WC algorithm [49], ABSA method [9], ITLBO algorithm [70], ImCSA [50], ISCE [65] and hybrid BPFPA [71]. The *I-V* and *P-V* characteristics are drawn for the arrays configured, by using KC200GT and PWP 201, where it is pragmatic that the characteristics

possess superior results when compared with the above-mentioned techniques. Moreover, the *I-V* and *P-V* characteristics of the STP6 120/36 cases express a very near relationship with the experimental curve. Here, it is also observed that with the set of extracted parameters, a more optimised power can be extracted from all the three cases under consideration, where the impact of environmental conditions on the parameters, as well as on the performance characteristics are also underlined. Hence, it is stated that the proposed EPO method for parameter estimation is one of the improved methods for parameter estimation when compared with existing methods.

Chapter 4

PHEROMONE VALUE AND CANNIBALISM BASED BLACK WIDOW OPTIMISATION APPROACHES

4.1 General

In this chapter, two new metaheuristic approaches for the estimation of mathematical model parameters of PV cell, modules, or array through Pheromone value black widow optimisation (*pv*-BWO) and Cannibalism black widow optimisation (*cn*-BWO) algorithms, by using the experimental data under numerous set of conditions is presented. The proposed methodologies evade the problem of premature conversion to local minima. Six case studies are considered, for six different PV modules that are modeled using SDM, DDM, and TDM where the validation of the results is carried out through the experimental datasets. Moreover, 149 pair *I-V* data is also recorded for SFTI-60P and EIL-75W modules in the outdoor experimental environment to assess the prominence of *pv*-BWO and *cn*-BWO methods in real implementation.

4.2 Problem formulation

The main objective of solar PV modelling is the estimation of the unknown parameters for the electrical equivalent models. The vector δ = [I_{ph}, I_s, α, $R_{se,}$ and R_{sh}] is to be estimated for SDM, ψ = [I_{ph}, I_{s1}, $I_{s2,}$ α_1, α_2, $R_{se,}$ and R_{sh}], for DDM, and ρ= [I_{ph}, I_{s1}, I_{s2}, $I_{s3,}$ α_1, α_2, $\alpha_{3,}$ $R_{se,}$ and R_{sh}] for TDM. The objective is to minimize the variance between experimental and estimated data or the minimisation of error as already discussed in chapter 3. Hence, it is important to quantify an OF that enables the degree of concurrence among the set of parameters (under defined boundary conditions) that characterize the experimental dataset and the model. In the proposed approach RMSE is considered the OF, for SDM, DDM, and TDM.

$$\text{Min OF1}(\delta) \text{ for SDM} = \sqrt{\frac{1}{n}\sum_{i=1}^{n}\left(I_{lo(i)} - \hat{I}_{lo(V_{lo(i)},\delta)}\right)^2}, \tag{4.1}$$

$$\text{Min OF2}(\psi) \text{ for DDM} = \sqrt{\frac{1}{n}\sum_{i=1}^{n}\left(I_{lo(i)} - \hat{I}_{lo(V_{lo(i)},\psi)}\right)^2}, \tag{4.2}$$

$$\text{Min OF3}(\rho) \text{ for TDM} = \sqrt{\frac{1}{n}\sum_{i=1}^{n}\left(I_{lo(i)} - \hat{I}_{lo(V_{lo(i)},\rho)}\right)^2}, \tag{4.3}$$

Where, n is the set of empirical (I_i, V_i) points, $i \in n$, the $\hat{I}_{lo(V_{lo(i)},\delta)}$, $\hat{I}_{lo(V_{lo(i)},\psi)}$, and $\hat{I}_{lo(V_{lo(i)},\rho)}$ are the estimated current values as the function of unknown vectors 'δ', 'ψ', *and* 'ρ', modeled using *eq.* (4.1)-*eq.* (4.3). The preciseness of the parameters estimated depends on the closeness of the OF to zero, as the information of exacted parameter values is not accessible, hence the degree of preciseness depends on the experimental data only, where any diminution in the OF *i.e.* RMSE, observed as a significant improvement towards the preciseness of real unknown parameter values.

As discussed in chapter 1, the solar cell is the fundamental building block of a solar PV system, where various series-parallel configuration results in the formation of a module [5], further various modules are again configured to form long solar PV arrays. For the arrays, *eq.* (1.8), *eq.* (1.9) and *eq.* (1.10) can be rewritten as *eq.* (4.4), *eq.* (4.5) and *eq.* (4.6) respectively, where N_s and N_p are the numbers of cells connected in series and parallel respectively.

$$I_{lo(V_{lo(i)},\delta)} = N_p \left\{ I_{ph} - I_s \left(\exp\left(\frac{\left(V_{lo} + I_{lo} R_{se} \left(\frac{N_s}{N_p} \right) \right)}{N_s V_{th}} \right) - 1 \right) \right\} - \frac{\left(V_{lo} + \left(\frac{N_s}{N_p} \right) I_{lo} R_{se} \right)}{\left(\frac{N_s}{N_p} \right) R_{sh}} \tag{4.4}$$

$$I_{lo(V_{lo(i)},\psi)} = N_p \left\{ I_{ph} - I_{s1} \left(\exp\left(\frac{\left(V_{lo} + I_{lo} R_{se} \left(\frac{N_s}{N_p} \right) \right)}{N_s V_{th}} \right) - 1 \right) - I_{s2} \left(\exp\left(\frac{\left(V_{lo} + I_{lo} R_{se} \left(\frac{N_s}{N_p} \right) \right)}{N_s V_{th}} \right) - 1 \right) \right\} - \frac{\left(V_{lo} + \left(\frac{N_s}{N_p} \right) I_{lo} R_{se} \right)}{\left(\frac{N_s}{N_p} \right) R_{sh}} \tag{4.5}$$

$$I_{lo(V_{lo(i)},\rho)} = N_p \left\{ I_{ph} - I_{s1} \left(\exp\left(\frac{\left(V_{lo} + I_{lo} R_{se} \left(\frac{N_s}{N_p} \right) \right)}{N_s V_{th}} \right) - 1 \right) - I_{s2} \left(\exp\left(\frac{\left(V_{lo} + I_{lo} R_{se} \left(\frac{N_s}{N_p} \right) \right)}{N_s V_{th}} \right) - 1 \right) I_{s3} \left(\exp\left(\frac{\left(V_{lo} + I_{lo} R_{se} \left(\frac{N_s}{N_p} \right) \right)}{N_s V_{th}} \right) - 1 \right) \right\} - \frac{\left(V_{lo} + \left(\frac{N_s}{N_p} \right) I_{lo} R_{se} \right)}{\left(\frac{N_s}{N_p} \right) R_{sh}} \tag{4.6}$$

A single current function for the calculation of estimated current values is obtained by equating *eq.* (4.4), *eq.* (4.5) and *eq.* (4.6) as *eq.* (4.7), *eq.* (4.8) and *eq.* (4.9) respectively, that is used for the calculation of OF through *pv*-BWO and *cn*-BWO.

$$f\left(\hat{I}_{lo(V_{lo(i)},\delta)} \right) = I_{lo} - N_p \left\{ I_{ph} - I_s \left(e^{\left(\frac{\left(V_{lo} + I_{lo} R_{se} \left(\frac{N_s}{N_p} \right) \right)}{N_s V_{th}} \right)} - 1 \right) \right\} + \frac{\left(V_{lo} + \left(\frac{N_s}{N_p} \right) I_{lo} R_{se} \right)}{\left(\frac{N_s}{N_p} \right) R_{sh}} \tag{4.7}$$

$$f\left(\hat{I}_{lo(V_{lo(i)},\psi)}\right)=I_{lo}-N_p\left\{I_{ph}-I_{s1}\left(\exp\left(\frac{\left(V_{lo}+I_{lo}R_{se}\left(\frac{N_s}{N_p}\right)\right)}{N_sV_{th}}\right)-1\right)+I_{s2}\left(\exp\left(\frac{\left(V_{lo}+I_{lo}R_{se}\left(\frac{N_s}{N_p}\right)\right)}{N_sV_{th}}\right)-1\right)\right\}+\frac{\left(V_{lo}+\left(\frac{N_s}{N_p}\right)I_{lo}R_{se}\right)}{\left(\frac{N_s}{N_p}\right)R_{pl}} \tag{4.8}$$

$$f\left(\hat{I}_{lo(V_{lo(i)},\rho)}\right)=I_{lo}-N_p\left\{I_{ph}-I_{s1}\left(\exp\left(\frac{\left(V_{lo}+I_{lo}R_{se}\left(\frac{N_s}{N_p}\right)\right)}{N_sV_{th}}\right)-1\right)+I_{s2}\left(\exp\left(\frac{\left(V_{lo}+I_{lo}R_{se}\left(\frac{N_s}{N_p}\right)\right)}{N_sV_{th}}\right)-1\right)+I_{s3}\left(\exp\left(\frac{\left(V_{lo}+I_{lo}R_{se}\left(\frac{N_s}{N_p}\right)\right)}{N_sV_{th}}\right)-1\right)\right\}+\frac{\left(V_{lo}+\left(\frac{N_s}{N_p}\right)I_{lo}R_{se}\right)}{\left(\frac{N_s}{N_p}\right)R_{sh}} \tag{4.9}$$

4.3 Proposed methodology

Proposed methodologies exercises, the *pv*-BWO, and *cn*-BWO algorithms *i.e.* elucidated in [72] and [73] respectively for the minimisation of OF1(δ), OF2(ψ), and OF3 (ρ) and the estimation of unknown parameters for SDM, DDM, and TDM of solar PV.

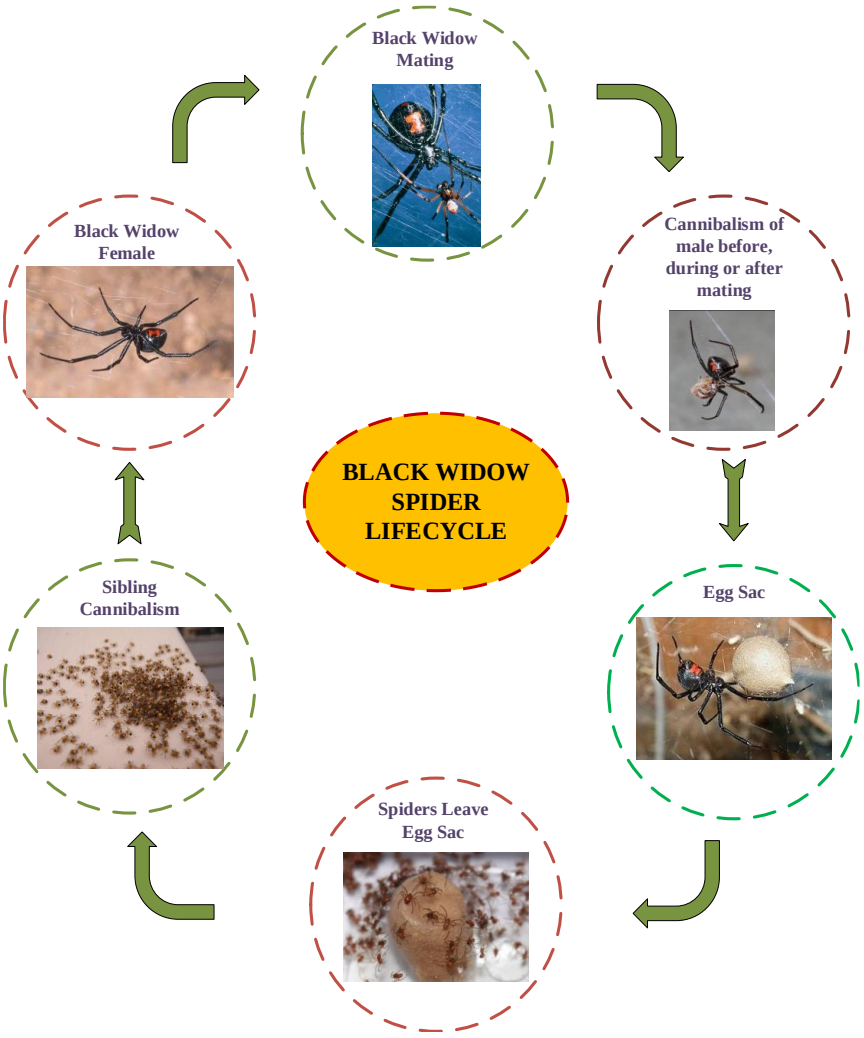

Fig. 4.1 Black Widow Spider Lifecycle

The *pv*-BWO and *cn*-BWO are nature-inspired population-based metaheuristic algorithms, that are considered for solutions to non-linear engineering or non-engineering problems. In these algorithms, the bizarre lifecycle of black widow spiders *i.e.* the reproduction style is modeled and instigated. The life cycle of the Black widow spider is well explained in fig. 4.1, where it can be further explained as,

4.3.1 *pv*-BWO algorithm

In this algorithm the process of identifying the best mating female partner by the male *L. Hesperus* Black widow spider is exercised *i.e.* stage 1 observed in fig. 4.1, here the male spider considers the concentration of sex pheromones to identify the mating status of the female black widow spider. Where, the male has shown low or no curiosity towards the starved and poorly fed female, as the female exhibits cannibalistic behavior [74], [75]. This algorithm exhibits the two most significant stages *i.e.* the movement and the pheromones strategy, that are aligned with the solar PV modelling and for the solution of the parameter estimation problem. These two stages are explained as,

a) Movement and position strategy

Two movement configurations of the spider *i.e.* linear and circular are modeled by using *eq.* (4.10) and *eq.* (4.11) respectively, where the new position of the black widow spider is given by the $\vec{B}_{wi}(x+1)$, where the best position from the previous iteration is given by $\vec{B}_{w(best)}(x)$. A floating variable '*m*' is randomly generated for an interval [0.4, 0.9], 'r_1', showing the integer for interval 1 to a maximum number of search agents, where $\vec{B}_{wr1}(x)$ is the 'r_1^{th}' selected, search agent. The 'α' represents the random floating number generated with the interval [-1.0, 1.0], with $\vec{B}_{wi}(x)$ as current black widow search agent, in other words, where, *i* is the current iteration and '*n'* expresses the maximum number of iterations.

$$\vec{B}_{wi}(x+1)=\left\{\vec{B}_{w(best)}(x)-m\times\vec{B}_{wr1}(x), \text{if rand}() \le 0.3\right\} \tag{4.10}$$

$$\vec{B}_{wi}(x+1)=\left\{\vec{B}_{w(best)}(x)-\cos(2\pi\alpha)\times\vec{B}_{wi}(x), \text{ other cases}\right\} \tag{4.11}$$

b) Strategy for pheromones

In the case of *L. Hesperus*, BW spiders, a change in pheromones concentration is concluded in [31], [32] which also impacts the quality and the quantity of the web silk. A well-nourished female produces more web silk when compared with the malnourished females.

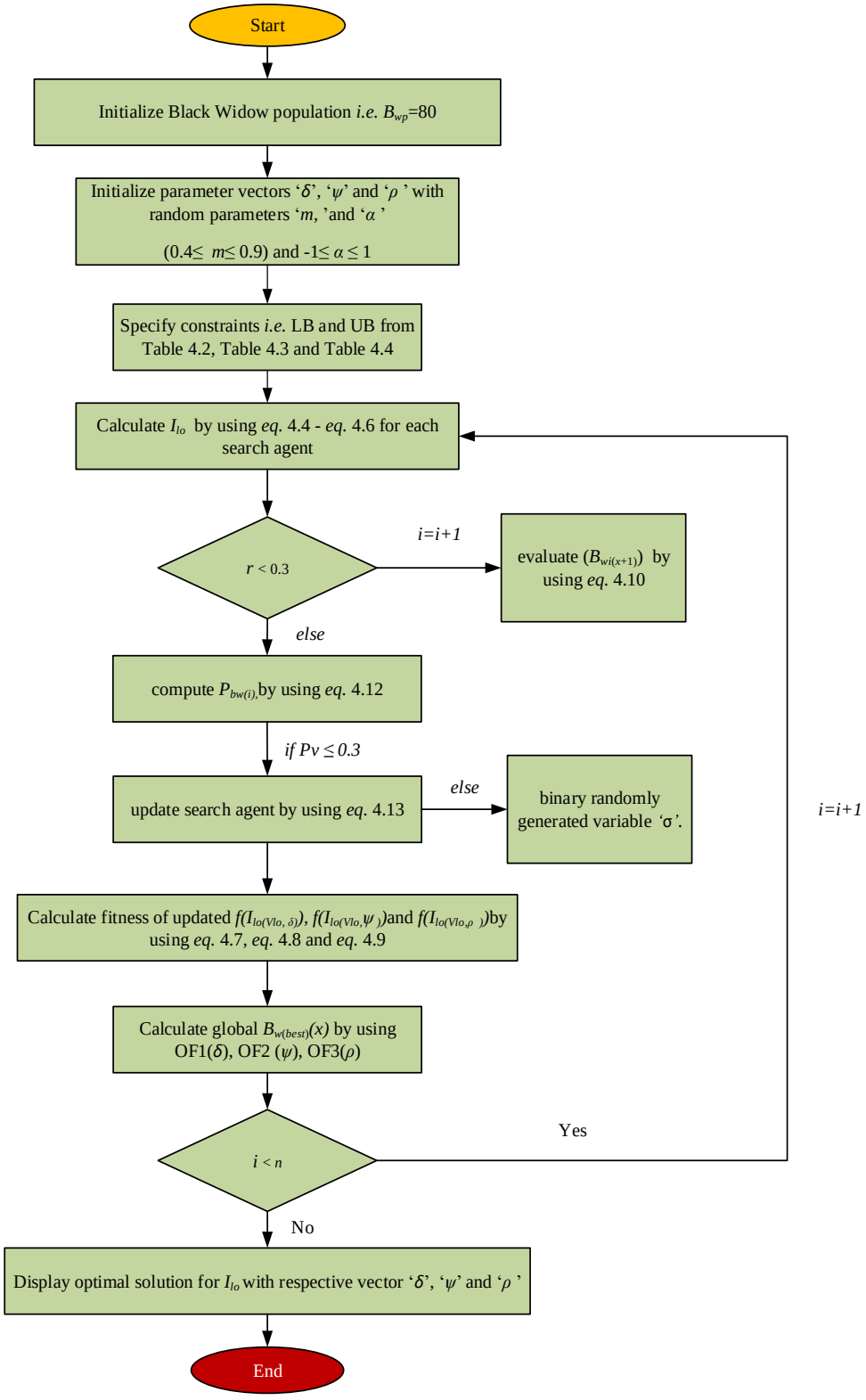

Fig. 4.2 Block diagram for *pv*-BWO methodology

It is important to understand that the male BW spiders are more receptive to well-nourished females, due to the benefit of a high fertility rate and less probability of female cannibalism during, before, and after mating [74], [75].

$$P_{bw(i)} = \frac{BW_{f.\max} - BW_{f(i)}}{BW_{f.\max} - BW_{f.\min}} \tag{4.12}$$

The *eq.* (4.12), is the pheromone vector with the best and the worst-case fitness function of BW, for low concentration of pheromones *i.e.* ≤ 0.3, *eq.* (4.13), is considered or pheromone procedure and this female is replaced by another female BW to avoid cannibalism.

$$\vec{B}_{wi}(x) = \vec{B}_{w(best)}(x) + \frac{1}{2}\left\{\vec{B}_{wr1}(x) - (-1)^{\sigma} \times \vec{B}_{wr2}(x)\right\} \tag{4.13}$$

where, $\vec{B}_{wr1}(x), \vec{B}_{wr2}(x)$ are the r_1^{th} and r_2^{th} search agent selected, with a binary randomly generated variable *'σ'*. By using, *eq.* (4.4)-(4.9), the $P_{bw(i)}$ is calculated, based on which the optimal solution for OF1(δ), OF2(ψ), and OF3 (ρ) is assessed with parameter vectors 'δ', 'ψ' and 'ρ'. The hierarchy of the *pv*-BWO methodology is also well explained in fig. 4.2.

4.3.2 *cn*-BWO algorithm

This methodology exercises, the *cn*-BWO algorithm *i.e.* elucidated in [73], in this algorithm the reproduction style and cannibalism are modeled and instigated. It is asserted in [73], that the female spider eats the male partner before, during, or after the mating process, where the cost of sacrifice conferred the fortuitous of fertilizing more eggs. Moreover, it is also evident that the female lays an egg to the egg sac, and after 11 days the spiderlings hatch out, where sibling cannibalism is initiated. The sibling eats out their mother and their siblings, where the fittest spreads out and leads towards further reproduction, as also shown in fig. 4.1. Here, four stages are considered for black widow spiders that are aligned with the solar PV modelling and for the solution of the parameter estimation problem. These four stages are explained as follows,

a) Widow initial population

In BWO the widows are the search agents, the foremost purpose is to detect the fittest widow for a global optimized or potential solution.

$$\text{Widow array} = \left[w_1, w_2, w_3 \ldots\ldots w_{Nv}\right] \tag{4.14}$$

A widow array is showcased in *eq.* (4.14), for an N_v, dimensional problem, where a fitness function f_w, illustrates the fitness of each widow.

$$f_w = f\left(w_1, w_2, w_3 \ldots\ldots w_{Nv}\right) \tag{4.15}$$

So, the algorithm is initiated through the population initialization, where the matrix for the solution is given by,

$$\text{Population matrix} = N_{pl} \times N_{vr} \tag{4.16}$$

For the next stage *i.e.* procreation stage, a pair of two widows are randomly selected. Here the initial population of 80 widows is initialized, and the unknown parameter vectors 'δ', 'ψ' and 'ρ' are also initialized through the boundary condition shown in table 4.2-table 4.4.

b) Procreation of widow

Here, two conditions are underlined, firstly, as the widow pairs are independent, hence they may mate together to reproduce the subsequent generation, or in the later case, they may mate with other individuals at their respective web, where only the fittest offspring survived. So, procreation can be modeled as,

$$w_{o1} = \sigma \times w_{p1} + (1-\sigma) \times w_{p2} \tag{4.17}$$

$$w_{o2} = \sigma \times w_{p2} + (1-\sigma) \times w_{p1} \tag{4.18}$$

Where, σ is the array, having w_{o1} and w_{o2} are the two offspring in which, w_{p1} and w_{p2} are the parent widows. In order to evade the duplicity in randomly selected widows, this process is repeated by $N_{vr}/2$. The array is continuously updated by adding the female parent and offspring *i.e.* organized by the fitness values, whereby using cannibalism rating (CR), the fittest widows are updated in the freshly generated population. The OF1, OF2, and OF3 are evaluated for the optimal solution, where $I_{lo(V_{lo(i)},\delta)}$, $I_{lo(V_{lo(i)},\psi)}$ and $I_{lo(V_{lo(i)},\rho)}$ are estimated through *eq.* (4.4), *eq.* (4.5) and *eq.* (4.6) respectively.

c) Incorporation of cannibalism

As it is already asserted that cannibalism is one of the most important facts of BW lifecycle, and is characterized by three types *i.e.* sexual, spiderling, and female parent. So, to calculate the number of survivors, a CR is introduced in this algorithm. Where the strength or weakness of the widow is asserted by using the fitness values.

d) Mutation and convergence

Here, the number of individual widows (M_p), is randomly selected, where each of the selected solutions randomly exchanges the two elements in the array, as in *eq.* (4.19), w_3 and w_n are selected, where, M_p depends on the mutation rate.

Moreover, for the convergence, no appreciable change in fitness value of the global solution, fixed number of iterations, and attaining quantified accuracy rate can be considered, here for the

parameter estimation problem 200 iterations are considered to access the convergence and optimal solution. The *cn*-BWO methodology is explained in fig. 4.3.

$$\left[W_1, W_2, W_3 \ldots\ldots W_{Nv}\right] \rightarrow \left[W_1, W_2, W_n \ldots W_3, \ldots W_{Nv}\right] \tag{4.19}$$

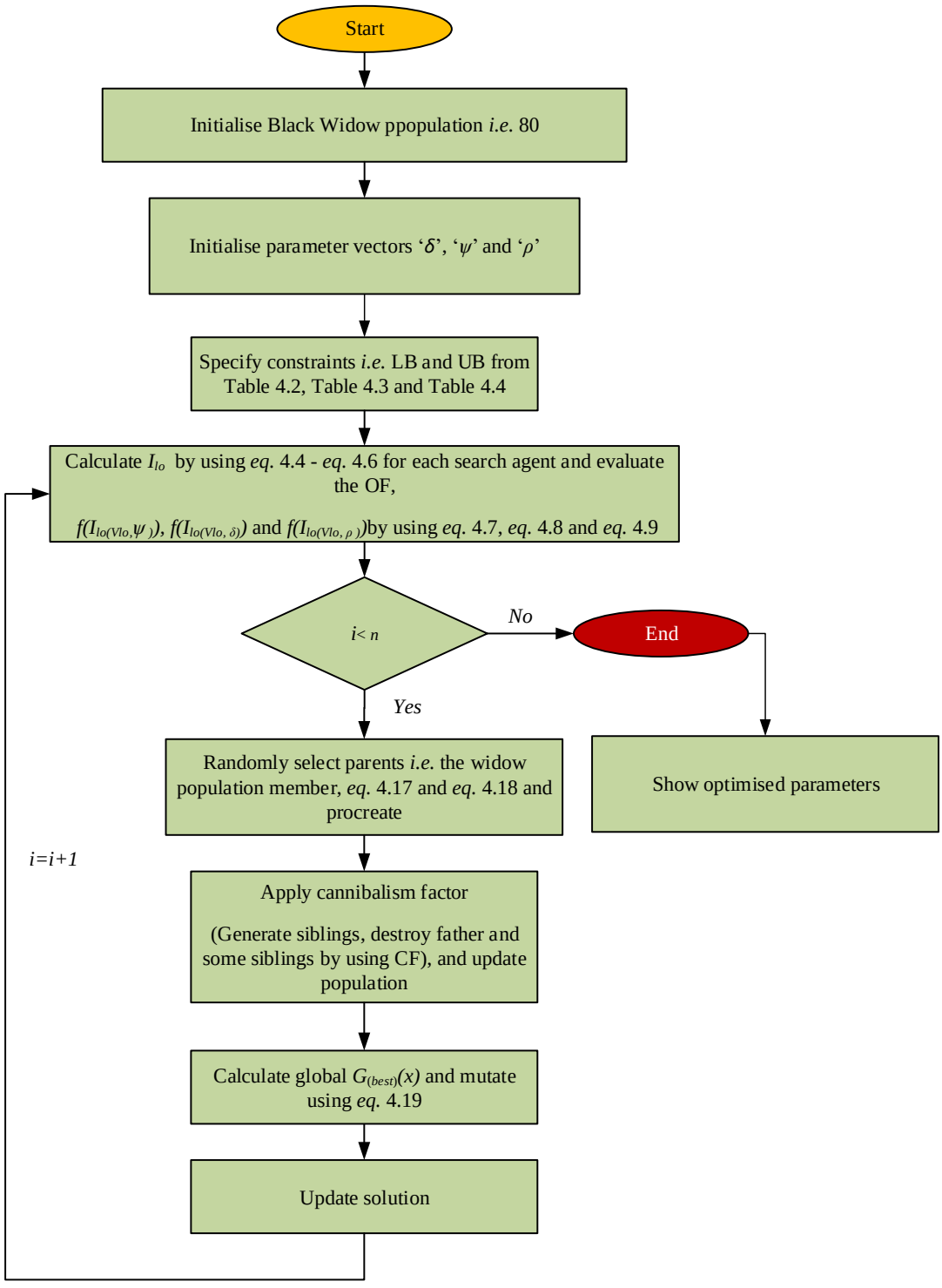

Fig. 4.3 Block diagram for *cn*-BWO methodology

4.4 Results and discussion

The performance of *pv*-BWO and *cn*-BWO methods for the solar PV model parameter extraction problem is critically evaluated, compared, and analyzed in this section, where the SDM, DDM, and TDM are considered for the analysis. To validate the proposed methods, experimental data of six different PV, acquired under a particular set of irradiance and temperature are considered.

Table 4.1 Manufacturer's datasheet

S. No.	Solar PV modules	Known parameters from the manufacturer's datasheet						
		V_{mpt} (V)	I_{mpt} (A)	V_{oc} (V)	I_{sc} (A)	N_s	P_{max} (W)	Temp (^oC)
1	RTC France (*Monocrystalline*)	0.4507	0.6894	0.5728	0.7603	01	-	33
2	PWP-201 (*Polycrystalline*)	12.6	0.89	16.78	1.031	36	12	45
3	ESP -160 PPW (*Polycrystalline*)	19.26	8.33	22.82	8.87	36	160	47
4	Sharp ND-R250A5 (*Polycrystalline*)	30.9	8.1	37.6	8.68	60	250	47.5
5	EIL75W (*Polycrystalline*)	18.14	4.13	22.34	4.48	36	75	25
6	SFTI-60P (*Polycrystalline*)	31.60	8.23	37.14	8.73	60	260	25

The dataset for the RTC France cell and the PWP-201 module is originally proposed in [76], where various researchers [48], [56], [77], [78] consider the same for the assessment of effectiveness and robustness of methods instigated for solar PV parameter extraction problem. Moreover, the experimental data for ESP-160 PPW and Sharp ND-R250A5 is proposed in [8] and [10] respectively. Whereas, in the fifth and sixth cases *i.e.* EIL-75W and SFTI-60P module, the real data is experimentally recorded by the authors, to validate the proposed method's explicit performance under real implementation.

Case study 1, referred to an RTC France commercially used monocrystalline silicon PV cell with a diameter of 57 mm, under G=1000W/m^2 and T=33°C [76], case study 2 and case 3 refers to polycrystalline PWP-201 and ESP-160 PPW modules respectively, where 36 cells are connected in series to form a single module. The Sharp ND-R250A5 a 250 W polycrystalline module with 60 series cells is referred to as case 4. The manufacturer's datasheet of all the considered PV modules is given in table 4.1. The results of each case study are computed through 200 independent iterations, case 1-case 6 is analyzed for SDM and DDM, whereas case 2 to case 5 is also computed for TDM.

The computation is carried out in a Matlab® environment, with Intel® core *i*7-8550U CPU @1.80GHz, 16 GB RAM, and Windows 10 Professional 64-bit operating system.

Table 4.2 Boundary conditions for DDM

Parameter	Case study 1 (RTC France)		Case study 2 (PWP-201)		Case study 3 (ESP-160 PPW)		Case study 4 (Sharp ND-R250A5)		Case study 5 (EIL-75W)		Case study 6 SFTI-60P	
	LB	UB	LB	UB	LB	UB	LB	UB	LB	UB	LB	UB
I_{ph} [A]	0	1	0	1	0	10	0	10	0	10	0	1
I_{s1} [A]	1E−12	1E−5	1E−12	1E−5	1E−12	1E−5	1E−12	1E−5	1E−12	1E−5	1E−12	1E−5
I_{s2} [A]	1E−12	1E−5	1E−12	1E−5	1E−12	1E−5	1E−12	1E−5	1E−12	1E−5	1E−12	1E−5
α_1	0.5	2.5	0.5	2.5	0.5	2.5	0.5	2.5	0.5	2.5	0.5	2.5
α_2	0.5	2.5	0.5	2.5	0.5	2.5	0.5	2.5	0.5	2.5	0.5	2.5
R_{se} [Ω]	0.001	2	0.001	2.5	0.001	3	0.001	2	0.001	2.5	0.001	50
R_{sh} [Ω]	0.001	120	0.001	2000	0.001	1000	0.001	5000	0.001	600	0.001	3000

Table 4.3 Boundary conditions for SDM

Parameter	Case study 1 (RTC France)		Case study 2 (PWP-201)		Case study 3 (ESP-160 PPW)		Case study 4 (Sharp ND-R250A5)		Case study 5 (EIL-75W)		Case study 6 SFTI-60P	
	LB	UB	LB	UB	LB	UB	LB	UB	LB	UB	LB	UB
I_{ph} [A]	0	1	0	1	0	10	0	10	0	10	0	1
I_s [A]	1E−12	1E−5	1E−12	1E−5	1E−12	1E−5	1E−12	1E−5	1E−12	1E−5	1E−12	1E−5
α	0.5	2.5	0.5	2.5	0.5	2.5	0.5	2.5	0.5	2.5	0.5	2.5
R_{se} [Ω]	0.001	2	0.001	2.5	0.001	3	0.001	2	0.001	2.5	0.001	50
R_{sh} [Ω]	0.001	120	0.001	2000	0.001	1000	0.001	5000	0.001	600	0.001	3000

Table 4.4 Boundary conditions for TDM

Parameter	Case study 2 (PWP-201)		Case study 3 (ESP-160 PPW)		Case study 4 (SHARP-160 PPW)		Case study 5 (EIL-75W)	
	LB	LB	LB	UB	LB	UB	LB	UB
I_{ph} [A]	0	0	0	10	0	10	0	10
I_{s1} [A]	1E−12	1E−12	1E−12	1E−5	1E−12	1E−5	1E−12	1E−5
I_{s2} [A]	1E−12	1E−12	1E−12	1E−5	1E−12	1E−5	1E−12	1E−5
I_{s3} [A]	1E−12	1E−12	1E−12	1E−5	1E−12	1E−5	1E−12	1E−5
α_1	0.5	0.5	0.5	2.5	0.5	2.5	0.5	2.5
α_2	0.5	0.5	0.5	2.5	0.5	2.5	0.5	2.5
α_3	0.5	0.5	0.5	2.5	0.5	2.5	0.5	2.5
R_{se} [Ω]	0.001	0.001	0.001	3	0.001	2	0.001	2.5
R_{sh} [Ω]	0.001	0.001	0.001	1000	0.001	5000	0.001	600

4.4.1 Case study 1: Comparison of STC France (SDM and DDM) using *pv*-BWO and *cn*-BWO methodologies

Based on 20 pair experimental *I-V* data of RTC France at G=1000W/m^2 and T=33 ℃, parameter vectors 'δ' and 'ψ' for SDM and DDM, where $\delta \in P_+^5$ and $\psi \in P_+^7$ are to be extracted. The results are evaluated by using *pv*-BWO and *cn*-BWO and compared below based on computational cost, convergence, and other performance characteristics.

a) Comparison of results and analysis for SDM

For the SDM the five extracted parameters are showcased in table 4.5 with some other existing techniques which are acquired under the boundary conditions mentioned in table 4.3, where the convergence of OF1 using *pv*-BWO and *cn*-BWO is observed in fig. 4.4(e) and fig. 4.4(f) respectively. It is observed that the *pv*-BWO method exhibits a low convergence rate to the best solution *i.e.* near the 65th iteration that takes a total time of 44.151s for the convergence, with a low RMSE cost of 0.0026, when compared to the *cn*-BWO method with RMSE error of 0.0071. Moreover, the *pv*-BWO exhibits more promising results when compared with *cn*-BWO based on other various error functions (E_f) as shown in table 4.7 and also when compared with the few other existing techniques listed in table 4.8.

The comparison of *I-V* and *P-V* characteristics drawn through *pv*-BWO and *cn*-BWO techniques, with experimental characteristics and few existing techniques like SFS [79], I-JAYA [48], IMFO [46], HS [76], and GA [77], are showcased in fig. 4.4 (a)-fig. 4.4 (d). In fig. 4.4 (a) and fig. 4.4 (c), the *I-V* and *P-V* obtained using *pv*-BWO are observed to be in very close congruence with the experimental *I-V* and *P-V* characteristics, and exhibit more near results when compared with *cn*-BWO in fig. 4.4 (b) and fig. 4.4 (d), and other listed techniques. In other words, from fig. 4.4 (c) the *P-V* witnessed better power output when compared with the listed techniques, where a peak power of 0.307943 W is achieved from the *pv*-BWO method, with an error of 0.002111 W, while compared with the experimental peak power value.

The values of estimated current (I_{et}) is also compared with the experimental current (I_{ex}) in table 4.6, where *pv*-BWO illustrates an IAE of 0.0419 *i.e.* lower by 0.0935 when compared with the IAE given by *cn*-BWO.

b) Comparison of results and analysis for DDM

For the DDM, the seven extracted parameters are shown in table 4.5, with the boundary conditions cited in table 4.2, here it is important to highlight that with the increase in

complexity related to the DDM, having $\psi \in \mathcal{P}_{+}^{7}$, the rate of convergence is slowed down to 80th iteration as shown in fig. 4.5 (e), while compared with the convergence in SDM *i.e.* 65th iteration as shown in fig. 4.4 (e). In other words, the multi-diode model results in high computation cost along with a higher value of error functions when compared with SDM, and the same is well observed in table 4.7. Moreover, it is also underlined that in the context of DDM, the convergence is faster in *cn*-BWO when compared with the counterpart using *pv*-BWO, which can be easily observed in fig. 4.5 (e) and fig. 4.5 (f).

Where the computational cost is higher in *cn*-BWO when compared with *pv*-BWO, and the same along with other E_f can be observed from table 4.7. While comparing the *I-V* and *P-V* performance characteristics a close-fitting is observed with the experimental characteristics by *pv*-BWO when compared with *cn*-BWO, as shown in fig. 4.5 (a)-fig. 4.5(d). Moreover, the I_{et} is also calculated for DDM by using *pv*-BWO and *cn*-BWO, and recorded in table 4.6.

Table 4.5 Estimated parameters for SDM and DDM, RTC France

DDM								
S.No.	**Method**	I_{ph}	I_{s1}	I_{s2}	α_1	α_2	R_{se}	R_{sh}
1	*cn*-BWO	0.7659	6.1198e-06	1.4131e-06	1.9028	1.8966	0.0201	64.1277
2	*pv*-BWO	0.759529	1.68464e-07	1.3948e-06	1.7522823	1.6995565	0.02922	2420.0395
3	SFS	0.7608	2.183e-07	3.681e-07	1.450	1.820	0.03675	54.5464
4	HS	0.76176	1.2545e-07	2.547e-07	1.49439	1.49989	0.03545	46.82696
5	I-JAYA	0.7601	5.0445e-09	7.5094e-07	1.2186	1.6247	0.0376	77.8519
6	IMFO	0.76078	2.335e-07	6.8372e-07	1.45374	2	0.03671	55.2997
SDM								
1	*cn*-BWO	0.7678	4.2538e-06	-	1.8456	-	0.0247	76.7124
2	*pv*-BWO	0.761084	9.94694e-07	-	1.64813	-	0.0309642	73.0401
3	SFS	0.7609	3.167e-07	-	1.47918	-	0.03648	53.2805
4	GA	0.7619	8.087e-07	-	1.5751	-	0.0299	42.372
5	HS	0.7619	3.049e-07	-	1.47538	-	0.03663	53.5946
6	IJAYA	0.7608	3.228e-07	-	1.4811	-	0.0364	53.7595
7	IMFO	0.76078	3.2296e-07	-	1.48117	-	0.03638	53.71456

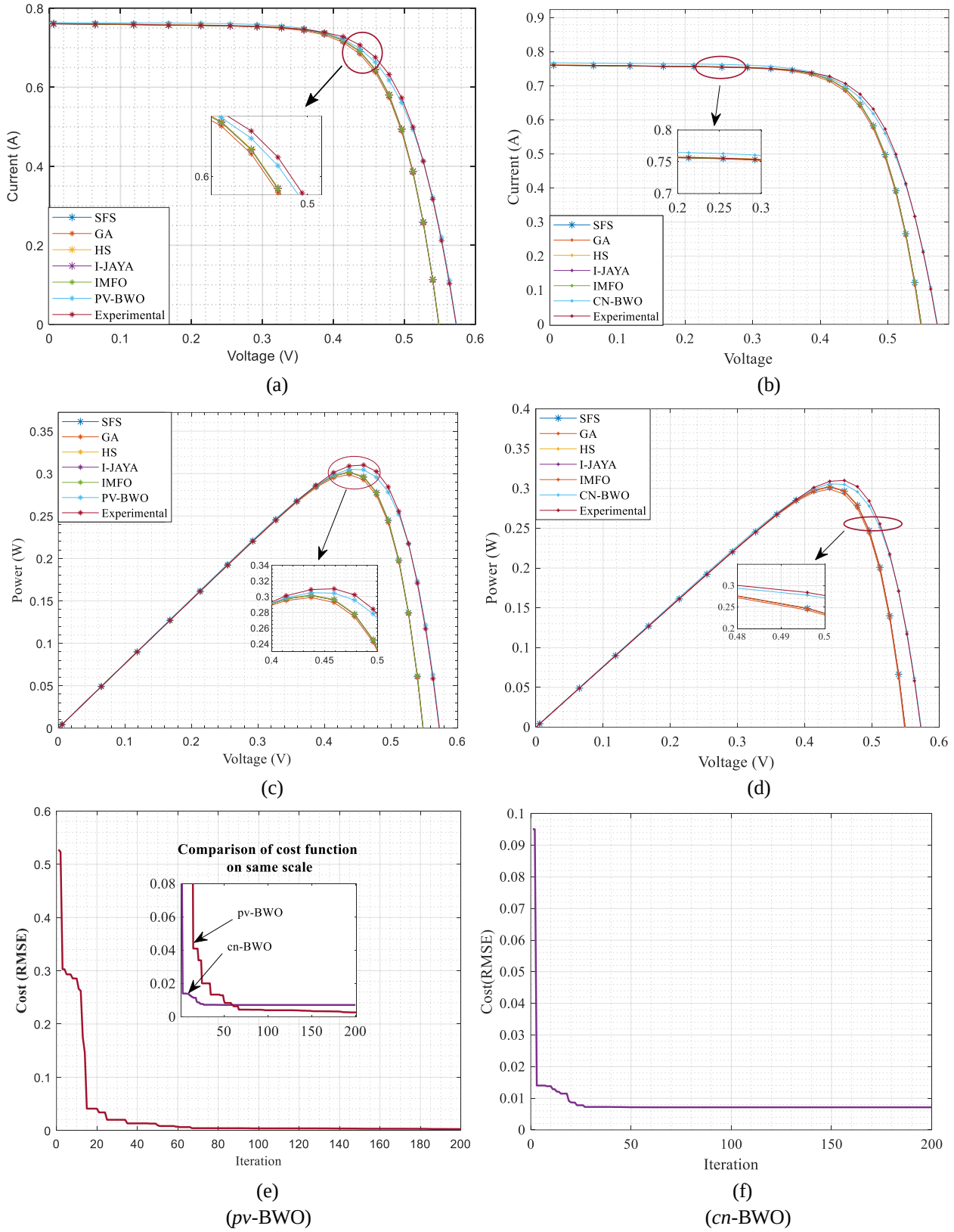

Fig. 4.4 Comparison for SDM of RTC France performance, (a) *I-V* using *pv*-BWO, (b) *I-V* using *cn*-BWO, (c) *P-V* using *pv*-BWO, (d) *P-V* using *cn*-BWO, (e) Cost RMSE, *pv*-BWO, (f) Cost RMSE, *cn*-BWO

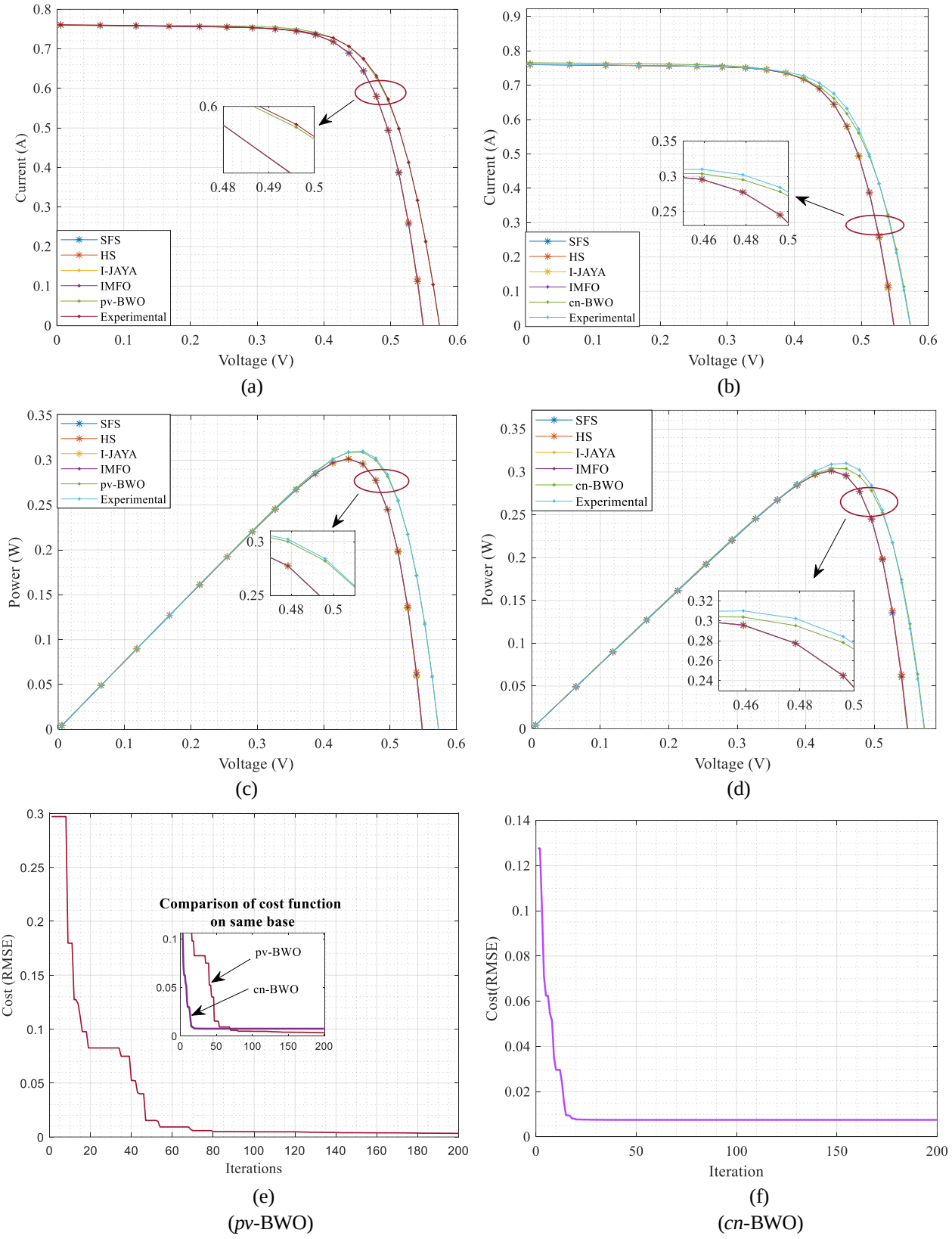

Fig. 4.5 Comparison for DDM of RTC France performance, (a) *I-V* using *pv*-BWO, (b) *I-V* using *cn*-BWO, (c) *P-V* using *pv*-BWO, (d) *P-V* using *cn*-BWO, (e) Cost RMSE, *pv*-BWO, (f) Cost RMSE, *cn*-BWO

Table 4.6 Comparison of estimated and experimental current for SDM and DDM, RTC France

S.No.	I_{ex}	I_{et}	AE	I_{et}	AE	I_{et}	AE	I_{et}	AE
		(SDM)		(DDM)		(SDM)		(DDM)	
		(*pv*-BWO)				(*cn*-BWO)			
1	0.76050	0.76070	0.0002	0.7595	0.00100	0.7675	0.00700	0.7656	0.00510
2	0.76000	0.75990	0.0001	0.7595	0.00050	0.7667	0.00670	0.7646	0.00460
3	0.75900	0.75910	0.0001	0.7594	0.00040	0.7660	0.00700	0.7636	0.00460
4	0.75700	0.75840	0.0014	0.7593	0.00230	0.7652	0.00820	0.7626	0.00560
5	0.75700	0.75760	0.0006	0.7591	0.00210	0.7642	0.00720	0.7615	0.00450
6	0.75550	0.75660	0.0011	0.7585	0.00300	0.7629	0.00740	0.7599	0.00440
7	0.75400	0.75500	0.0010	0.7573	0.00330	0.7608	0.00680	0.7575	0.00350
8	0.75050	0.75240	0.0019	0.7549	0.00440	0.7571	0.00660	0.7536	0.00310
9	0.74650	0.74770	0.0012	0.7501	0.00360	0.7508	0.00430	0.7470	0.00050
10	0.73850	0.73940	0.0009	0.7415	0.00300	0.7404	0.00190	0.7364	0.00210
11	0.72800	0.72530	0.0027	0.7270	0.00100	0.7238	0.00420	0.7198	0.00820
12	0.70650	0.70360	0.0029	0.7046	0.00190	0.6994	0.00710	0.6959	0.01060
13	0.67550	0.67090	0.0046	0.6713	0.00420	0.6644	0.01110	0.6618	0.01370
14	0.63200	0.62620	0.0058	0.6261	0.00590	0.6183	0.01370	0.6171	0.01490
15	0.57300	0.56810	0.0049	0.5678	0.00520	0.5600	0.01300	0.5607	0.01230
16	0.49900	0.49740	0.0016	0.4972	0.00180	0.4903	0.00870	0.4930	0.00600
17	0.41300	0.41370	0.0007	0.4138	0.00080	0.4086	0.00440	0.4131	0.00010
18	0.31650	0.31970	0.0032	0.3202	0.00370	0.3172	0.00070	0.3229	0.00640
19	0.21200	0.21600	0.0040	0.2169	0.00490	0.2161	0.00410	0.2220	0.01000
20	0.10350	0.10650	0.0030	0.1076	0.00410	0.1088	0.00530	0.1134	0.00990
			IAE		IAE		IAE		IAE
			0.0419		0.0571		0.1354		0.1301

Table 4.7 Comparison of error functions for SDM and DDM, RTC France

S.No.	Error Function (E_f)	SDM	DDM	SDM	DDM
		(*pv*-BWO)		(*cn*-BWO)	
1	Mean Absolute Error (MAE)	0.0021	0.0029	0.0064	0.0065
2	Root Mean Square Error (RMSE)	0.0026	0.0033	0.0071	0.0075
3	Mean Biased Error (MBE)	0.0002	0.0002	0.0014	0.0003
4	Sum of Squares (SSE)	0.0002	0.0003	0.0013	0.0015
5	Normalised RMSE (NRME)	0.0027	0.0034	0.0073	0.0077

Table 4.8 Comparison of error functions with existing techniques for RTC France SDM

S. No.	Method	RMSE	MAE	AE
1	*pv*-BWO	0.00260	0.0021	0.0419
2	*cn*-BWO	0.0071	0.0064	0.1354
3	GA	0.00476	0.0031277	0.081320
4	TLBO [80]	0.0058554	0.003717	0.096653
5	NRM [81]	0.0096964	---	---
6	RF 2A [82]	0.01388	0.0094014	---
7	MBA [83]	0.07620	0.044495	1.156900
8	PS [84]	0.0028547	0.00215	0.055993
9	Method [85]	0.0058668	0.0037242	0.096830
10	Method [86]	0.0061149	0.0038939	0.10124
11	Method [87]	0.003161	0.001786	---

4.4.2 Case study 2: Comparison of PWP-201 (SDM and DDM) using *pv*-BWO and *cn*-BWO methodologies

Based on 25 pair experimental *I-V* data of PWP-201 at G=1000W/m^2 and T=45℃, parameter vector 'δ' and 'ψ', are to be extracted, for SDM and DDM, where the boundary conditions are taken from table 4.3 and table 4.2 respectively. Table 4.9, witness the E_f observed by using *cn*-BWO, which records high computational cost when compared with the *pv*-BWO. In the context of the OF considered, *pv*-BWO records 68.57 percent less computational cost, whereas the *cn*-BWO exhibits fast convergence speed when compared with the *pv*-BWO, in the case of SDM it is well observed in fig. 4.6 (e) and fig. 4.6 (f).

Due to fewer computational errors, the *I-V* and *P-V* characteristics are in much congruence with the experimental *I-V* and *P-V* characteristics for *pv*-BWO while compared with *cn*-BWO, the same is well observed in fig. 4.6 (a)-fig. 4.6 (d) for SDM. For the DDM, the suitability of *pv*-BWO over *cn*-BWO is observed from table 4.9, as the OF and other E_f showcase comparatively higher error for *cn*-BWO, and due to this the *I-V* and *P-V* characteristics of *pv*-BWO establish more near relationship with the experimental characteristics and the same can be observed in fig. 4.7 (a)-fig. 4.7 (d).

Table 4.9 Comparison of error functions for SDM and DDM, PWP 201

S.No	E_f	PWP 201			
		SDM	DDM	SDM	DDM
		(*pv*-BWO)		(*cn*-BWO)	
1	MAE	0.0029	0.0042	0.0052	0.0054
2	RMSE	0.0035	0.0050	0.0059	0.0051
3	MBE	-	-	0.0002	0.0004
4	SSE	0.0003	0.0006	0.0009	0.0008
5	NRME	0.0026	0.0037	0.0044	0.0039
6	IAE	0.0729	0.1061	0.1289	0.1151

Table 4.10 Estimated parameters for SDM and DDM, PWP-201

PWP 201 (DDM)							
Method	I_{ph}	I_{s1}	I_{s2}	α_1	α_2	R_{se}	R_{sh}
cn-BWO	1.0330	3.8709e-06	5.7577e-06	1.6182	1.4255	1.0945	1275.1
pv-BWO	1.038914	3.877097e-06	3.479066e-06	1.614638	1.484221	1.102028	571.7099
PWP 201 (SDM)							
cn-BWO	1.0424	6.7709e-06	-	1.4286	-	1.0855	461.4783
pv-BWO	1.03274	6.5633e-06	-	1.519067	-	1.118267	997.6883

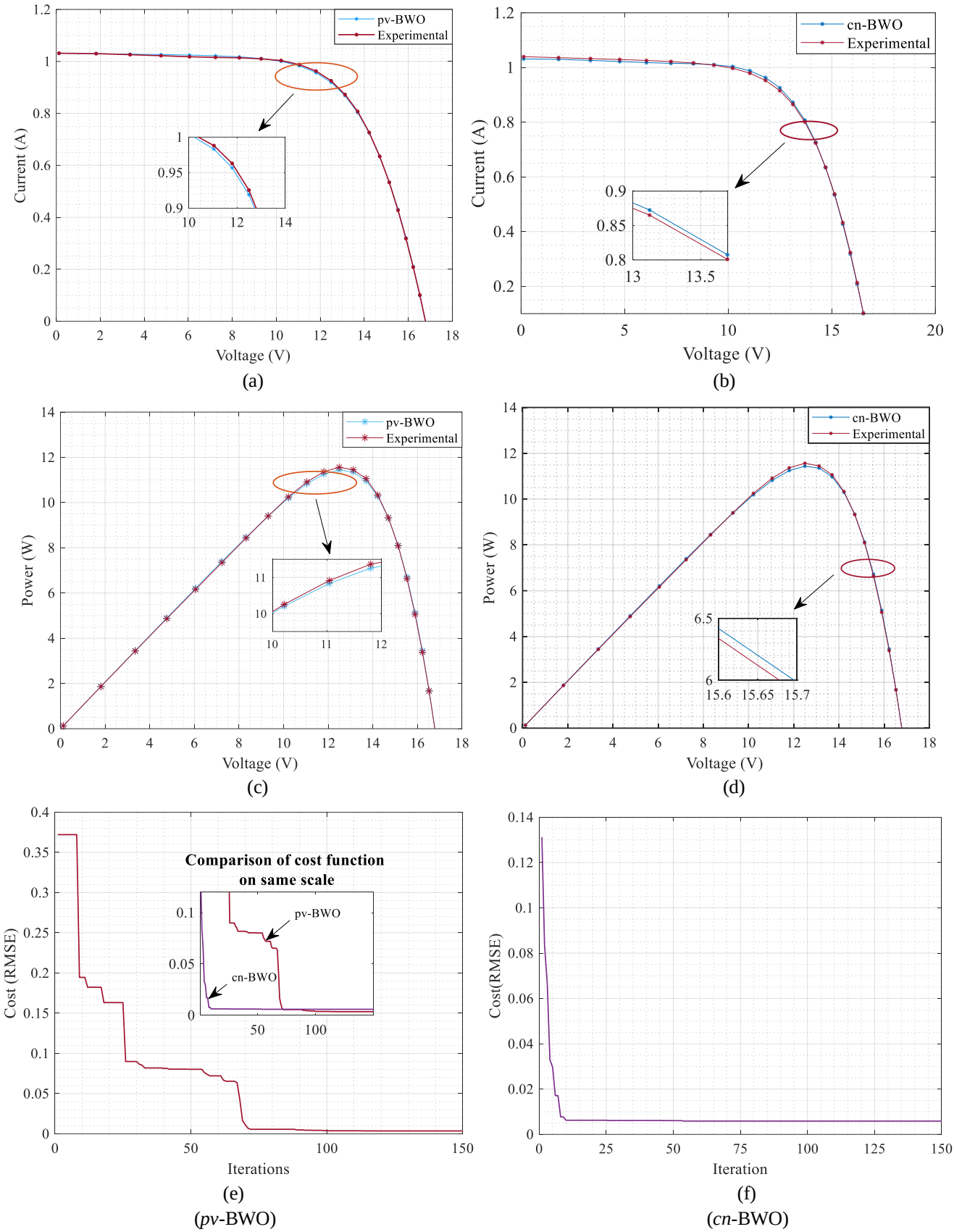

Fig. 4.6 Comparison for SDM of PWP-201 performance, (a) *I-V* using *pv*-BWO, (b) *I-V* using *cn*-BWO, (c) *P-V* using *pv*-BWO, (d) *P-V* using *cn*-BWO, (e) Cost RMSE, *pv*-BWO, (f) Cost RMSE, *cn*-BWO

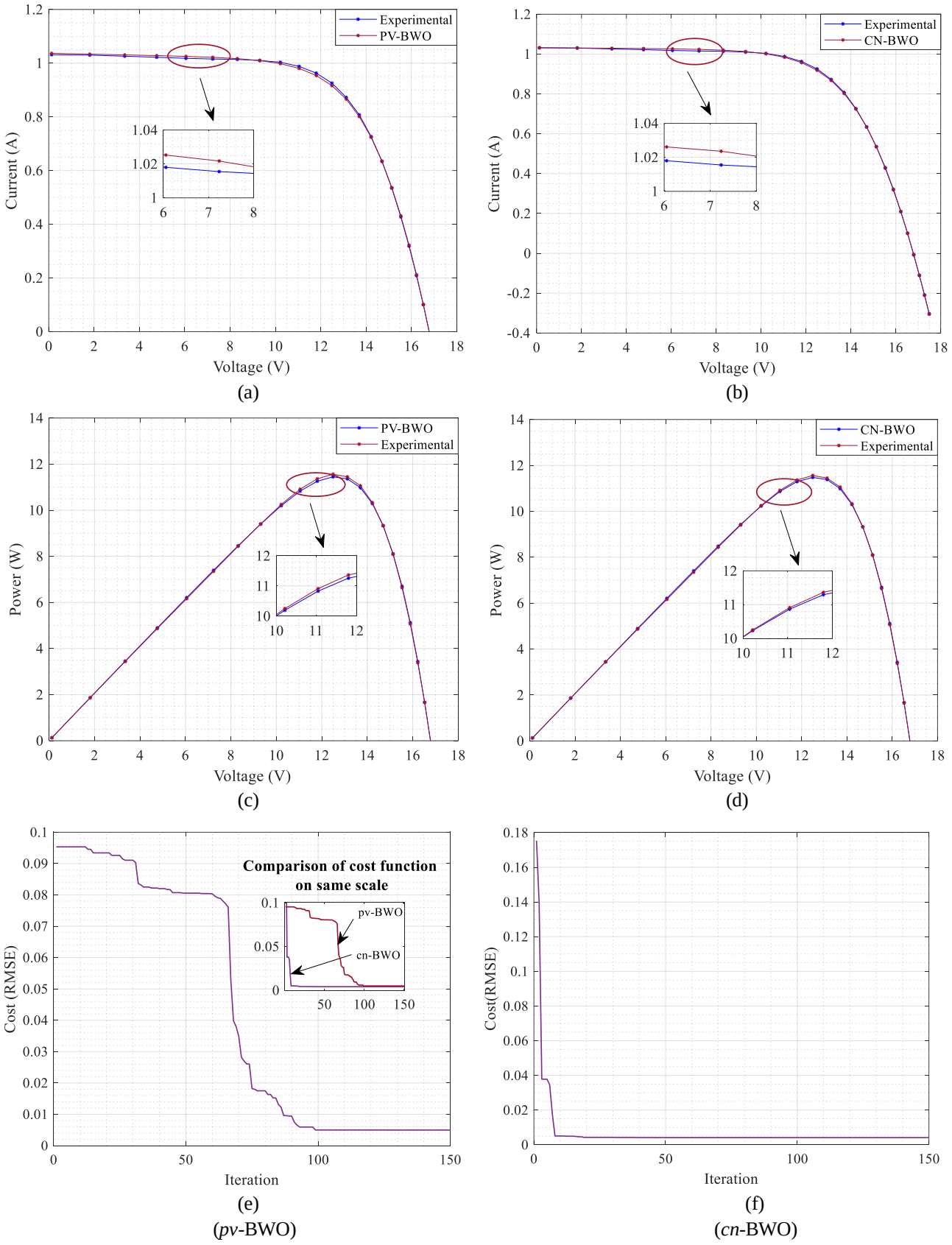

Fig. 4.7 Comparison for DDM of PWP-201 performance, (a) *I-V* using *pv*-BWO, (b) *I-V* using *cn*-BWO, (c) *P-V* using *pv*-BWO, (d) *P-V* using *cn*-BWO, (e) Cost RMSE, *pv*-BWO, (f) Cost RMSE, *cn*-BWO

Whereas, *cn*-BWO exhibits high convergence when compared with the *pv*-BWO which can be well explored in fig. 4.7 (e) and fig. 4.7 (f), all the extracted parameters for SDM and DDM are well listed in table 4.10.

4.4.3 Case study 3: Comparison of ESP 160 PPW (SDM and DDM) using *pv*-BWO and *cn*-BWO methodologies

A 41 pair experimental *I-V* data from [10], is chosen for ESP-160PPW module analysis at G=1000W/m^2 and T=47 ℃, the performance analysis and parameter estimation for SDM and DDM is discussed below,

a) Comparison of results and analysis for SDM

From fig. 4.8 (a)-fig. 4.8 (d), the exactness of the *pv*-BWO method over *cn*-BWO is observed through the congruence of *I-V* and *P-V* with the experimental *I-V* and *P-V* characteristics, where the cost function is recorded to 0.0810, whereas *cn*-BWO records comparatively higher cost function to 0.0829 with better convergence *i.e.* 25 iterations, shown in fig. 4.8 (e) and fig. 4.8 (f), along with table 4.13. All the estimated parameters are listed in table 4.11, by using the boundary conditions defined in table 4.3. Moreover, the variance of I_{st} with I_{ex} is also furbished in table 4.12, whereby using *pv*-BWO the peak power of 78.7712 W can be extracted through the estimated current, with an error of 0.4288 W when compared with the experimental peak power.

b) Comparison of results and analysis for DDM

Here while comparing convergence in fig. 4.9 (e) and fig. 4.9 (f), the convergence for the DDM *pv*-BWO takes more than 75 iterations for obtaining the minimum error, *i.e.* 0.0867 still higher than the OF of SDM and *cn*-BWO. Whereas, *cn*-BWO recorded higher values for E_{fs} on comparing with the *pv*-BWO, *i.e.* depicted well in table 4.13. The *I-V* and *P-V* curves still show prominence with the experimental curves in fig. 4.9 (a)-fig. 4.9 (d), the seven estimated parameters are listed in table 4.11, where the AE for each experimental data is consolidated in table 4.12.

Table 4.11 Comparison of estimated parameters for ESP-160PPW SDM and DDM

DDM								
S.No.	**Method**	I_{ph}	I_{s1}	I_{s2}	α_1	α_2	R_{se}	R_{sh}
1	*cn*-BWO	5.4848	9.0389e-06	5.8174e-06	1.7211	1.7764	0.1366	249.9684
2	*pv*-BWO	5.50995	6.907142e-06	7.572571e-06	2.20062	1.658471	0.1460715	117.1784
SDM								
3	*cn*-BWO	5.4755	8.7504e-06	-	1.6708	-	0.1555	320.8297
4	*pv*-BWO	5.51681	7.73825e-06	-	1.65767	-	0.146206	99.0132

In the case of *pv*-BWO the peak power extracted is 78.8528 W having an error of 0.3472 on comparing it with the experimental peak power.

Table 4.12 Comparison of estimated and experimental current for SDM and DDM, ESP-160PPW

S.No.	I_{ex}	I_{et}	AE	I_{et}	AE	I_{et}	AE	I_{et}	AE
		(SDM)		(DDM)		(SDM)		(DDM)	
		(*pv*-BWO)				(*cn*-BWO)			
1	0.090	0.1072	0.0172	0.1073	0.017	0.1127	0.0227	0.1042	0.0142
2	0.150	0.2457	0.0957	0.2453	0.095	0.2506	0.1006	0.2405	0.0905
3	0.200	0.2876	0.0876	0.287	0.087	0.2913	0.0913	0.2827	0.0827
4	0.250	0.3617	0.1117	0.3608	0.111	0.3645	0.1145	0.3561	0.1061
5	0.300	0.4346	0.1346	0.4335	0.134	0.4367	0.1367	0.4285	0.1285
6	0.370	0.5287	0.1587	0.5273	0.157	0.5297	0.1597	0.522	0.152
7	0.510	0.5584	0.0484	0.557	0.047	0.5557	0.0457	0.555	0.045
8	0.650	0.6494	0.0006	0.6477	0.002	0.6437	0.0063	0.6474	0.0026
9	0.750	0.6658	0.0842	0.6641	0.086	0.6575	0.0925	0.6662	0.0838
10	0.900	0.8391	0.0609	0.8369	0.063	0.8289	0.0711	0.8387	0.0613
11	1.100	0.8995	0.2005	0.8971	0.203	0.8847	0.2153	0.9028	0.1972
12	1.300	1.2881	0.0119	1.2847	0.015	1.2746	0.0254	1.2859	0.0141
13	1.510	1.6633	0.1533	1.6590	0.149	1.6515	0.1415	1.6567	0.1467
14	1.780	1.8053	0.0253	1.8009	0.021	1.7904	0.0104	1.8014	0.0214
15	2.200	2.2136	0.0136	2.2087	0.009	2.1993	0.0007	2.2094	0.0094
16	2.500	2.5158	0.0158	2.5108	0.011	2.5036	0.0036	2.5113	0.0113
17	2.700	2.7294	0.0294	2.7245	0.024	2.7196	0.0196	2.7246	0.0246
18	2.900	3.0043	0.1043	2.9995	0.099	2.993	0.0993	2.9987	0.0987
19	3.100	3.1811	0.0811	3.1766	0.077	3.1787	0.0787	3.1763	0.0763
20	3.250	3.2883	0.0383	3.2839	0.034	3.2873	0.0373	3.2844	0.0344
21	3.400	3.3516	0.0484	3.3474	0.053	3.3508	0.0492	3.349	0.051
22	3.500	3.4594	0.0406	3.4554	0.045	3.4609	0.0391	3.4571	0.0429
23	3.650	3.5875	0.0625	3.5839	0.066	3.5918	0.0582	3.5862	0.0638
24	3.850	3.7726	0.0774	3.7695	0.081	3.7813	0.0687	3.7727	0.0073
25	4.120	4.0610	0.0590	4.0592	0.061	4.078	0.042	4.0639	0.0561
26	4.580	4.5511	0.0289	4.5524	0.028	4.5842	0.0042	4.5626	0.0174
27	4.950	4.9232	0.0268	4.9283	0.022	4.969	0.019	4.9464	0.0036
28	5.150	5.1323	0.0177	5.1402	0.010	5.1837	0.0337	5.1644	0.0144
29	5.300	5.3157	0.0157	5.326	0.026	5.365	0.065	5.3547	0.0547
30	5.380	5.3808	0.0008	5.3906	0.011	5.42	0.04	5.416	0.036
31	5.390	5.4159	0.0259	5.4234	0.033	5.441	0.051	5.4411	0.0511
32	5.440	5.4444	0.0044	5.4484	0.008	5.4524	0.0124	5.4554	0.0154
33	5.470	5.4743	0.0043	5.474	0.004	5.4621	0.0079	5.468	0.002
34	5.480	5.4839	0.0039	5.4821	0.002	5.4652	0.0148	5.4719	0.0081
35	5.490	5.4853	0.0047	5.4833	0.007	5.4656	0.0244	5.4724	0.0176
36	5.490	5.4859	0.0041	5.4838	0.006	5.4658	0.0242	5.4727	0.0173
37	5.500	5.4890	0.0110	5.4864	0.014	5.4667	0.0333	5.4739	0.0261
38	5.510	5.4905	0.0195	5.4877	0.022	5.4672	0.0428	5.4745	0.0355
39	5.500	5.5021	0.0021	5.4975	0.003	5.4708	0.0292	5.4791	0.0209
40	5.500	5.5072	0.0072	5.5018	0.002	5.4724	0.0276	5.4811	0.0189
41	5.510	5.5087	0.0013	5.5031	0.007	5.4728	0.0372	5.4817	0.0283
			IAE		IAE		IAE		IAE
			1.9393		1.952		2.1968		2.4509

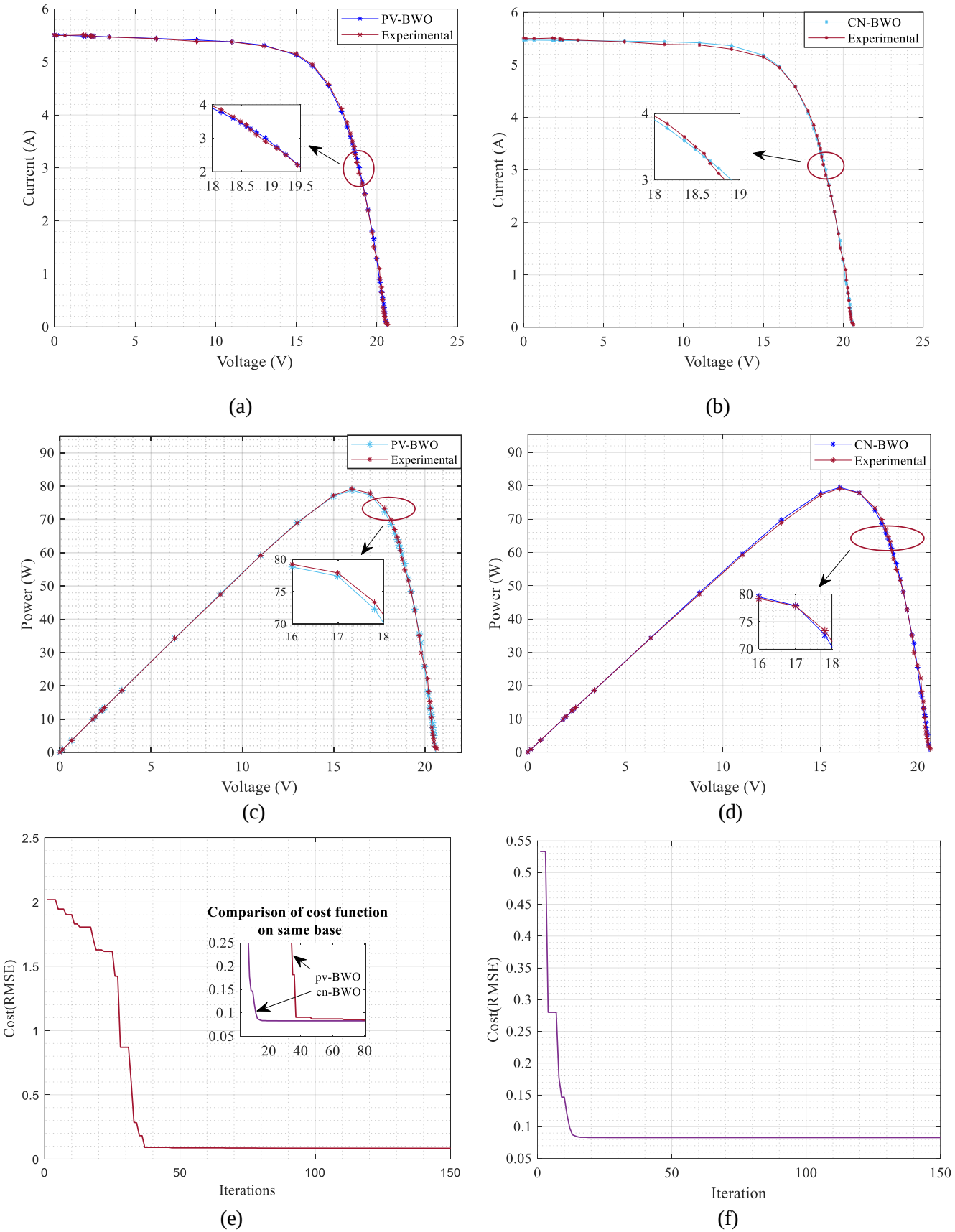

Fig. 4.8 Comparison for SDM of ESP 160PPW performance, (a) *I-V* using *pv*-BWO, (b) *I-V* using *cn*-BWO, (c) *P-V* using *pv*-BWO, (d) *P-V* using *cn*-BWO, (e) Cost RMSE, *pv*-BWO, (f) Cost RMSE, *cn*-BWO

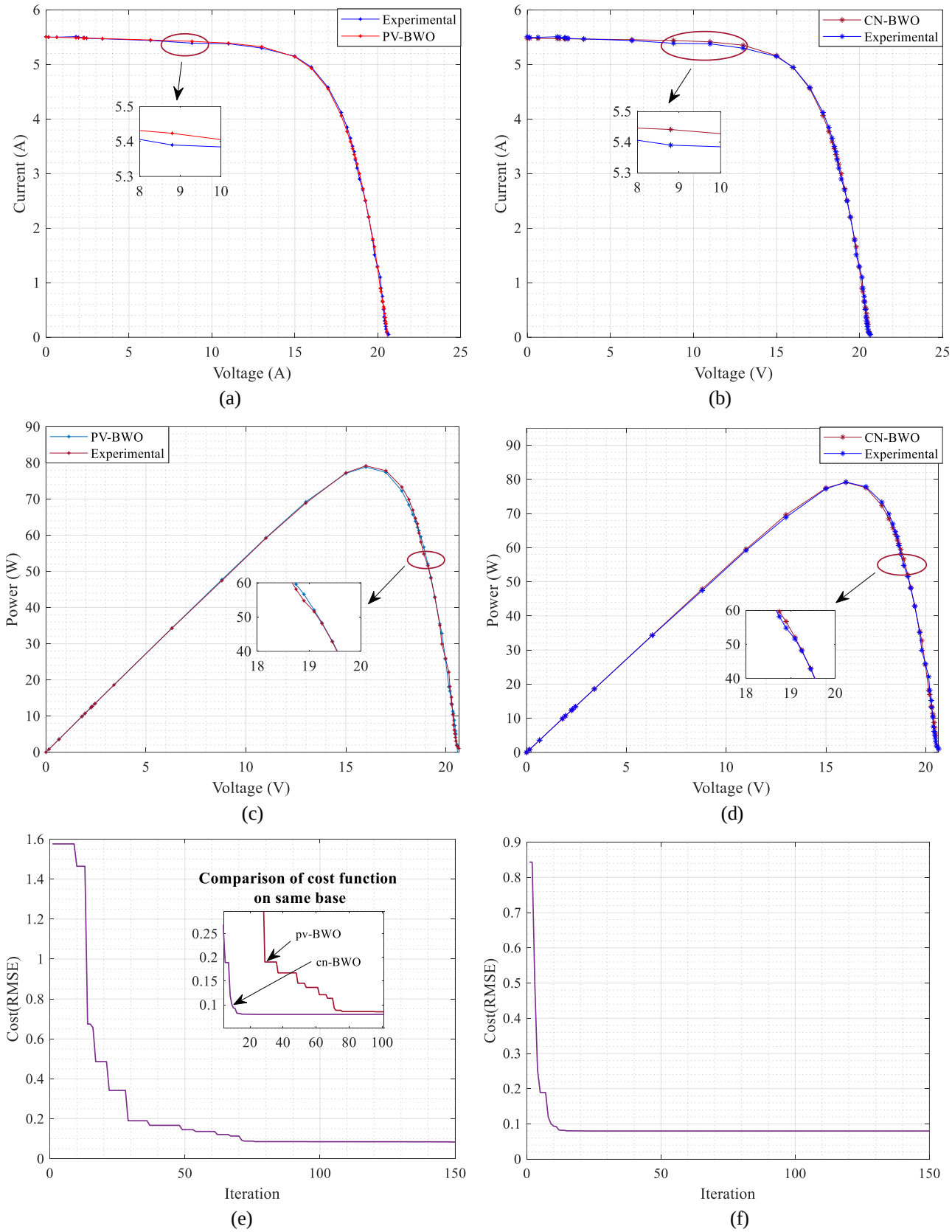

Fig. 4.9 Comparison for DDM of ESP 160PPW, (a) *I-V* using *pv*-BWO, (b) *I-V* using *cn*-BWO, (c) *P-V* using *pv*-BWO, (d) *P-V* using *cn*-BWO, (e) Cost RMSE, *pv*-BWO, (f) Cost RMSE, *cn*-BWO

Table 4.13 Comparison of error functions for ESP-160PPW SDM and DDM

S. No.	Error Function (E_f)	SDM	DDM	SDM	DDM
		(*pv*-BWO)		(*cn*-BWO)	
1	Mean Absolute Error (MAE)	0.0544	0.0546	0.0602	0.0570
2	Root Mean Square Error (RMSE)	0.0810	0.0867	0.0829	0.0891
3	Mean Biased Error (MBE)	0.0005	0.0007	0.0003	0.0008
4	Sum of Squares (SSE)	0.2820	0.2860	0.2954	0.2893
5	Normalised RMSE (NRME)	0.0148	0.0148	0.0152	0.0146
6	Integral Absolute Error (IAE)	1.9393	1.9520	2.1968	2.4509

4.4.4 Case study 4: Comparison of Sharp ND-R250A5 (SDM and DDM) using *pv*-BWO and *cn*-BWO methodologies

A 36-pair experimental *I-V* data of Sharp ND-R250A5 at G=1000W/m^2 and T=59 ℃, parameters are to be extracted for SDM and DDM. All the estimated parameters for SDM and DDM are well detailed in table 4.15.

a) Comparison of results and analysis for SDM

As observed in previous cases similar results are highlighted for this case study, where, for SDM the *cn*-BWO exhibits high convergence speed *i.e.* nearly in 25 iterations whereas, *pv*-BWO takes about 50 iterations for the convergence *i.e.* is well observed from fig. 4.10 (e) and fig. 4.10 (f) for SDM. Even though the *I-V* and *P-V* characteristics are in congruence with the experimental characteristics in *pv*-BWO and *cn*-BWO as shown in fig. 4.10 (a)-fig. 4.10 (d), where high RMSE is observed with *cn*-BWO *i.e.* 0.0592 when compared with the RMSE for *pv*-BWO *i.e.* 0.0117, moreover the same is observed with other E_f in table 4.14.

b) Comparison of results and analysis for DDM

Comparatively, high RMSE is recorded for the DDM when compared with the SDM, *i.e.* 0.0202 for *pv*-BWO whereas, *cn*-BWO exhibits an RMSE of 0.0857 for the DDM, due to which the *I-V* and *P-V* characteristic through proposed *pv*-BWO is more nearly aligned with the experimental characteristics when compared with the *cn*-BWO as shown in fig. 4.11 (a)-fig. 4.11 (d).

Table 4.14 Comparison of error functions for SHARP SDM and DDM

S.No.	Error Function (E_f)	SDM	DDM	SDM	DDM
		(*pv*-BWO)		(*cn*-BWO)	
1	Mean Absolute Error (MAE)	0.0094	0.0179	0.0516	0.0710
2	Root Mean Square Error (RMSE)	0.0117	0.0202	0.0592	0.0857
3	Mean Biased Error (MBE)	0.0002	0.0003	0.0179	0.0015
4	Sum of Squares (SSE)	0.0049	0.0147	0.1260	0.2647
5	Normalised RMSE (NRME)	0.0013	0.0022	0.0065	0.0094
6	Integral Absolute Error (IAE)	0.3387	0.6451	1.8582	2.5546

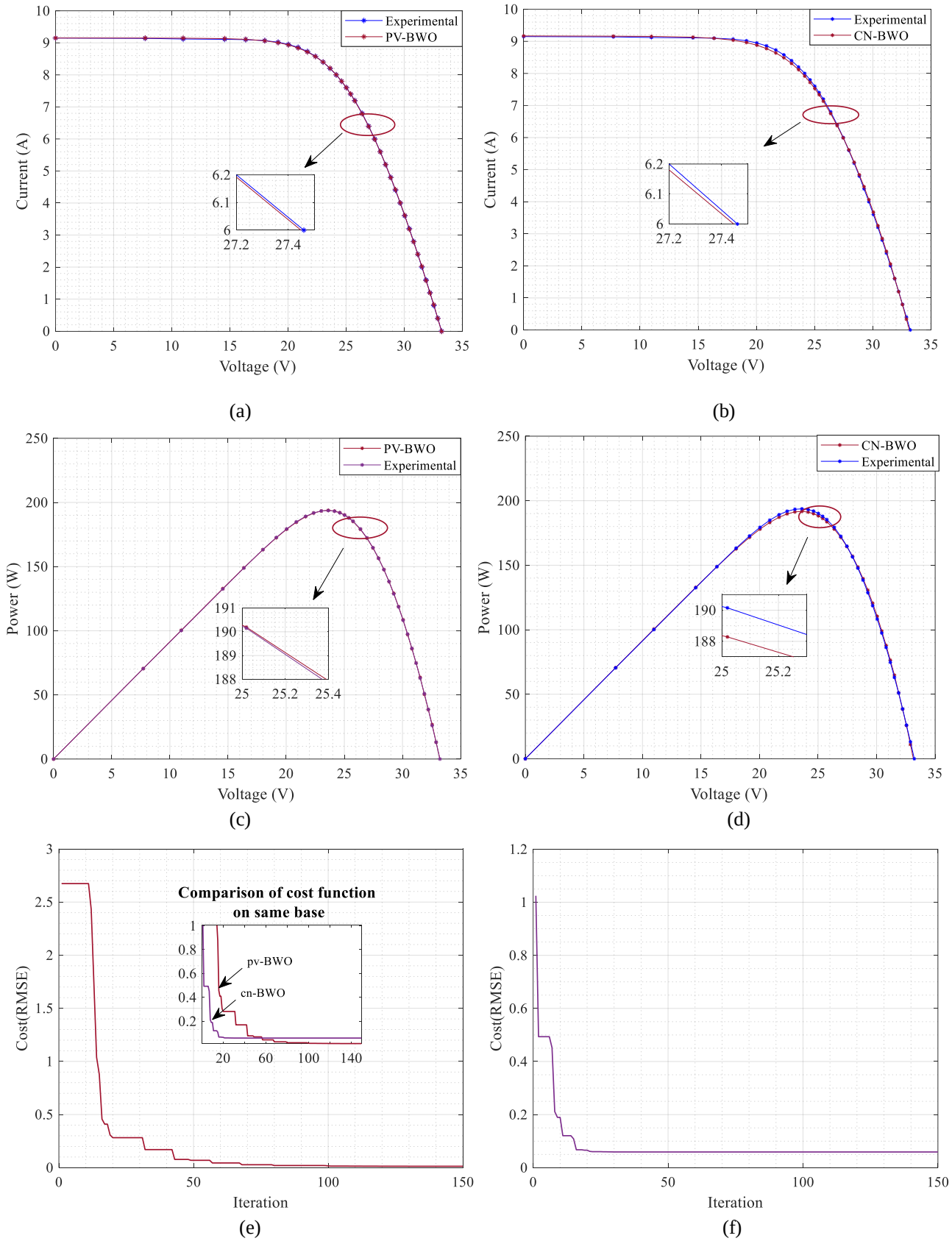

Fig. 4.10 Comparison for SDM of SHARP performance, (a) *I-V* using *pv*-BWO, (b) *I-V* using *cn*-BWO, (c) *P-V* using *pv*-BWO, (d) *P-V* using *cn*-BWO, (e) Cost RMSE, *pv*-BWO, (f) Cost RMSE, *cn*-BWO

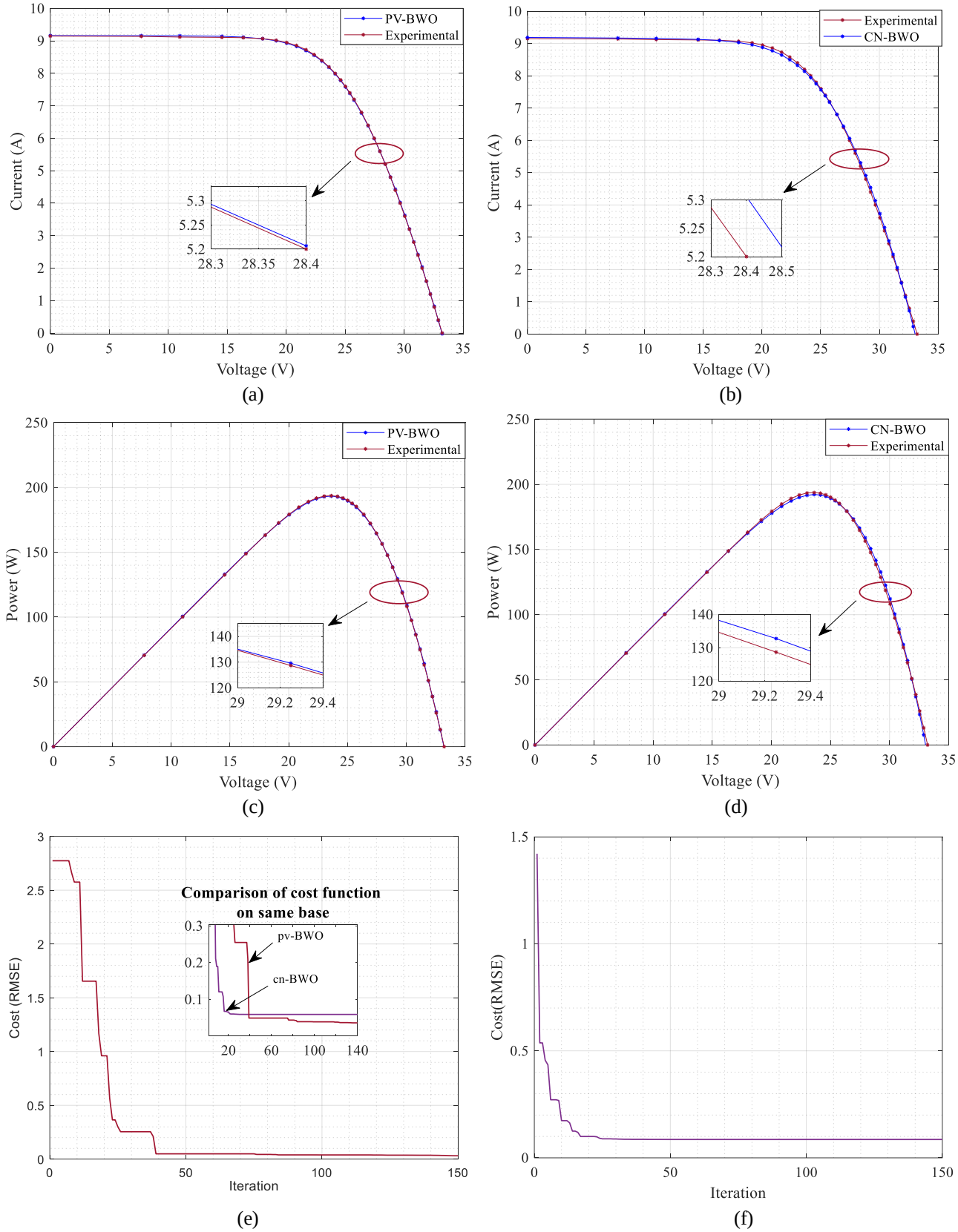

Fig. 4.11 Comparison for DDM of SHARP, (a) *I-V* using *pv*-BWO, (b) *I-V* using *cn*-BWO, (c) *P-V* using *pv*-BWO, (d) *P-V* using *cn*-BWO, (e) Cost RMSE, *pv*-BWO, (f) Cost RMSE, *cn*-BWO

Table 4.15 Comparison of estimated parameters for SHARP SDM and DDM

DDM								
S.No.	**Method**	I_{ph}	I_{s1}	I_{s2}	α_1	α_2	R_{se}	R_{sh}
1	*cn*-BWO	9.1956	6.0344e-06	4.7478e-06	1.4312	1.3982	0.5090	495.1486
2	*pv*-BWO	9.16536	1.9939834e-08	2.2529613e-06	1.87918	1.41657	0.57312	4964.177
SDM								
1	*cn*-BWO	9.1724	8.6275e-06	-	1.3937	-	0.5317	1452.6
2	*pv*-BWO	9.1518617	1.244643e-06	-	1.363666	-	0.58690	4700.589

4.4.5 Case study 5: Comparison of EIL 75W (SDM and DDM) using *pv*-BWO and *cn*-BWO methodologies

An experimental test is a setup in outdoor environmental conditions, where a 149 pair of EIL 75 W *I-V* data is recorded through MECO 9018BT solar PV analyzer at 897 W/m^2 and T=60.4℃. The irradiance and temperature are recorded by the irradiance and temperature sensor, all the components of the setup are shown in fig. 4.12. The recorded data is used for the parameter estimation and analyzing the results for EIL 75W SDM and DDM, where all the estimated parameters are recorded in table 4.17.

a) Comparison of results and analysis for SDM

The superimposition of proposed *I-V* and *P-V* characteristics over experimental *I-V* and *P-V* characteristics is shown in fig. 4.13 (a)-fig. 4.13(d), where a closer relationship is observed with *pv*-BWO having an RMSE of 0.0380 when compared with *cn*-BWO having a high-cost function of 0.0441. It is important to understand that even with the real recorded data by the authors, *cn*-BWO exhibits a high convergence speed that takes 15 iterations when compared with *pv*-BWO, as shown in fig. 4.13 (e) and fig. 4.13 (f). Moreover, for the *pv*-BWO technique the peak I_{ex} is 4.2090, wherein in response the peak I_{et} of 4.1595 is recorded, *i.e.* an AE of 0.0495. The convergence of population to the optimal solution *i.e.* towards the estimated parameters with the progress in iterations for *pv*-BWO is witnessed in fig. 4.15 (a) to fig. 4.15 (e).

b) Comparison of results and analysis for DDM

It is important to understand that to process 149 data points *pv*-BWO take approximately 125 iterations with a cost of 0.0455 *i.e.* somewhere equal to the cost delivered by *cn*-BWO with high convergence as observed in fig. 4.14 (e) and fig. 4.14 (f). Moreover, table 4.16 showcases high E_{fs} values over SDM, whereas, the estimated *I-V* and *P-V* are validated by the experimental *I-V* and *P-V* as shown in fig. 4.14 (a) to fig. 14 (d). A peak power of 57.41 W is extracted

through *pv*-BWO in the given environmental condition which is 1.55608 W less than the peak experimental power.

Fig. 4.12 Outdoor experimental setup

Table 4.16 Comparison of error functions for EIL-75W SDM and DDM

S.No.	Error Function (E_f)	SDM	DDM	SDM	DDM
		(*pv*-BWO)		(*cn*-BWO)	
1	Mean Absolute Error (MAE)	0.0283	0.0361	0.0349	0.0368
2	Root Mean Square Error (RMSE)	0.0380	0.0455	0.0441	0.0459
3	Mean Biased Error (MBE)	0.0017	0.0001	0.0002	0.0036
4	Sum of Squares (SSE)	0.2155	0.3081	0.2898	0.3142
5	Normalised RMSE (NRME)	0.0096	0.0115	0.0111	0.0116
6	Integral Absolute Error (IAE)	4.2131	5.3769	5.1936	5.4891

Table 4.17 Comparison of estimated parameters for EIL-75W SDM and DDM

DDM								
S.No.	**Method**	I_{ph}	I_{s1}	I_{s2}	α_1	α_2	R_{se}	R_{sh}
1	*cn*-BWO	4.1739	5.5739e-06	5.2966e-06	1.6038	1.4542	0.2654	831.8480
2	*pv*-BWO	4.17713	5.664128e-06	5.492524e-06	2.01389	1.6019	0.2863969	504.5037
SDM								
1	*cn*-BWO	4.1616	7.5575e-06	-	1.4644	-	0.2782	2082.6
2	*pv*-BWO	4.161629	1.408631e-06	-	1.449671	-	0.3494873	742.3116

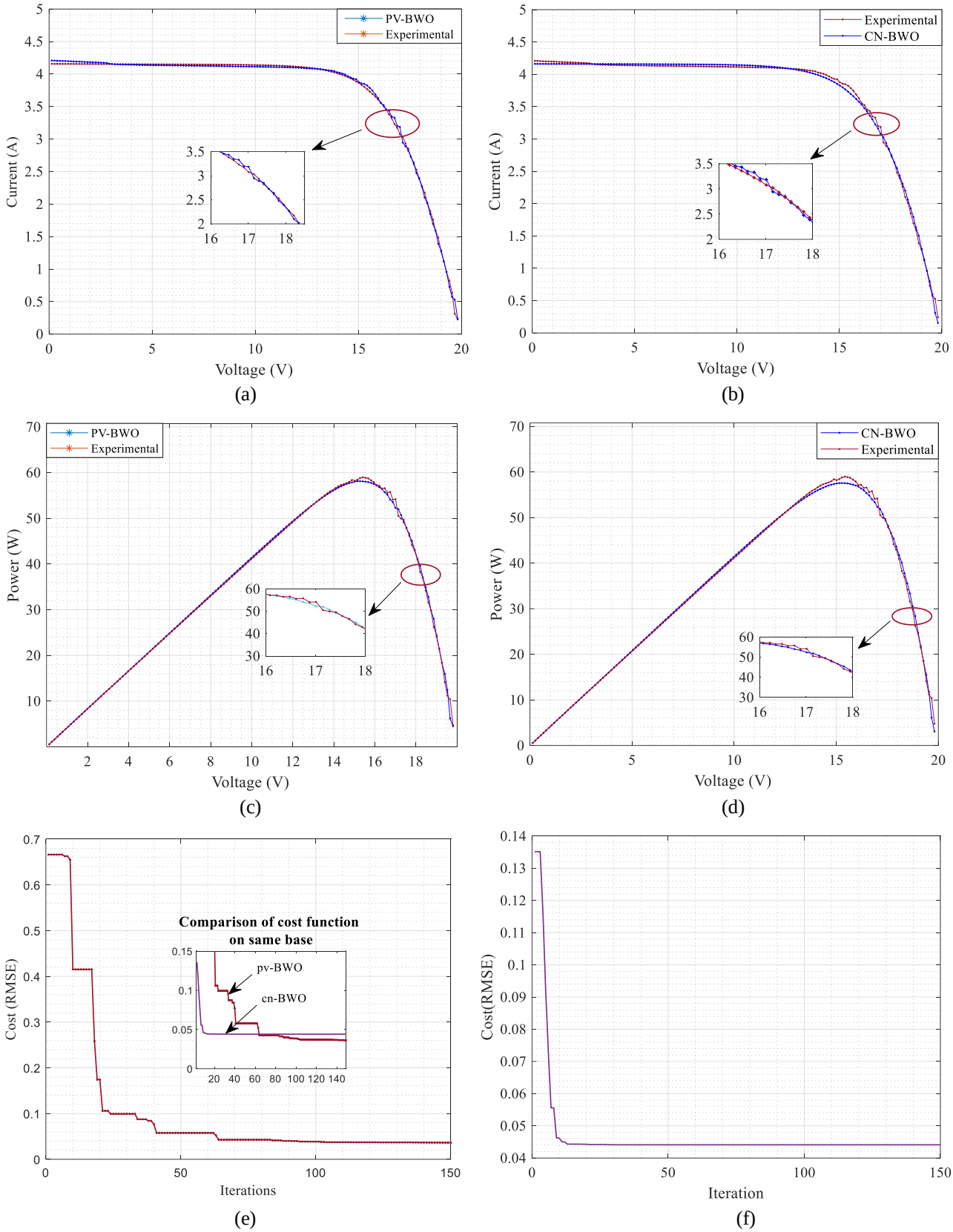

Fig. 4.13 Comparison for SDM of EIL-75W performance, (a) *I-V* using *pv*-BWO, (b) *I-V* using *cn*-BWO, (c) *P-V* using *pv*-BWO, (d) *P-V* using *cn*-BWO, (e) Cost RMSE, *pv*-BWO, (f) Cost RMSE, *cn*-BWO

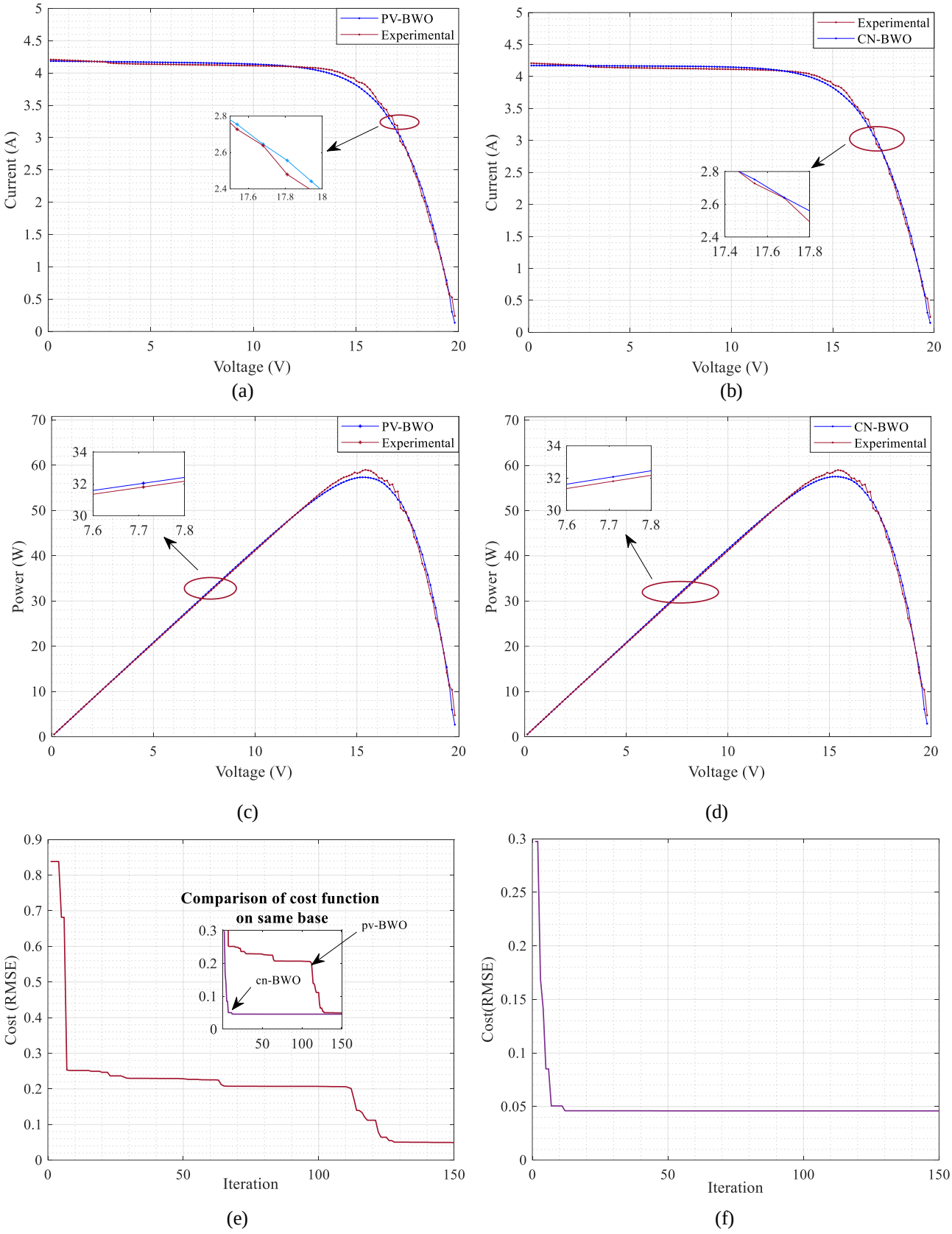

Fig. 4.14 Comparison for DDM of EIL-75W performance, (a) *I-V* using *pv*-BWO, (b) *I-V* using *cn*-BWO, (c*) P-V* using *pv*-BWO, (d) *P-V* using *cn*-BWO, (e) Cost RMSE, *pv*-BWO, (f) Cost RMSE, *cn*-BWO

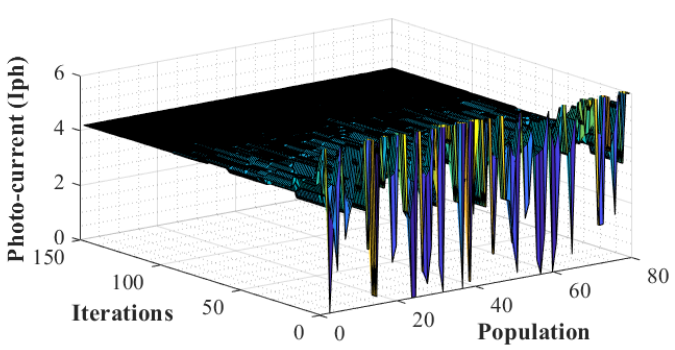

(a)

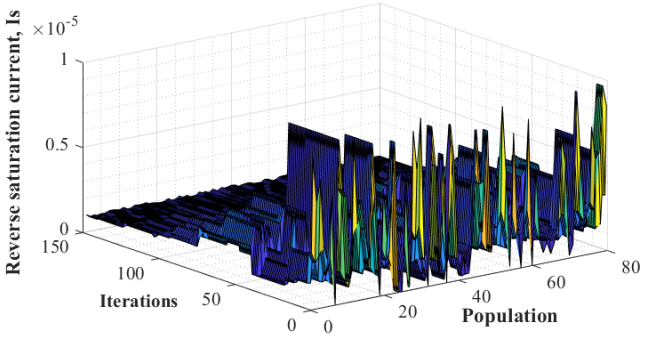

(b)

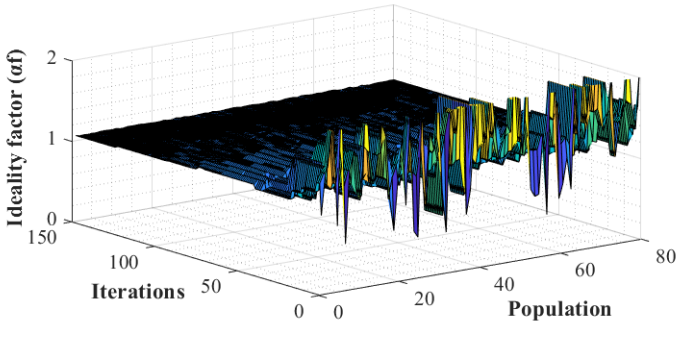

(c)

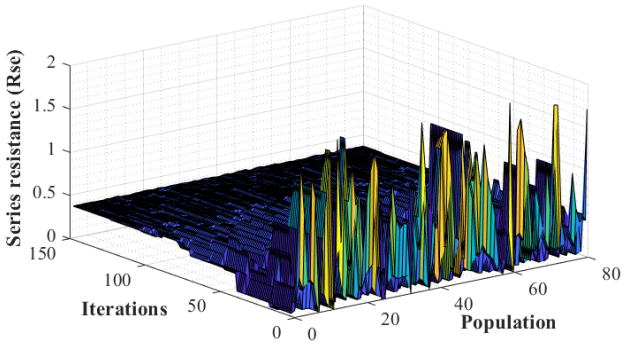

(d)

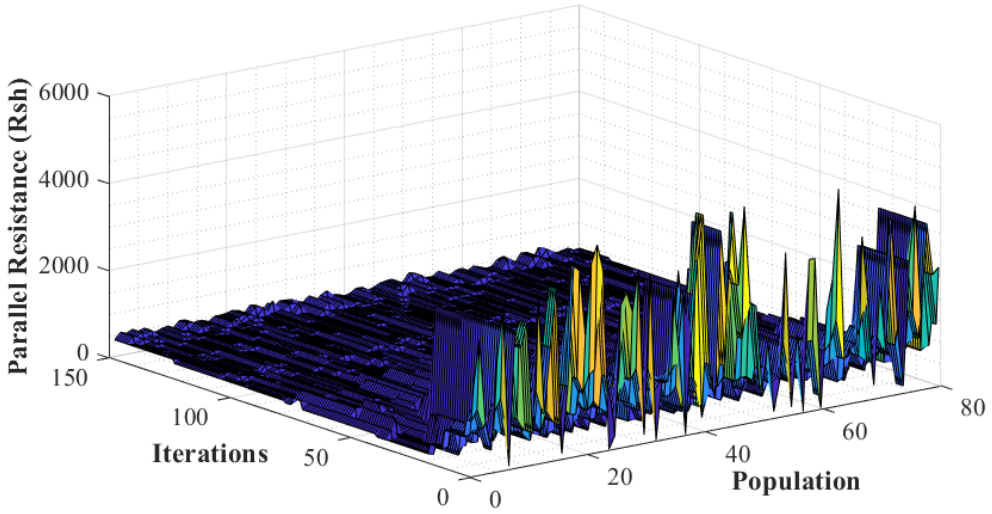

(e)

Fig. 4.15 Convergence of population with change in iteration for optimal solution of EIL-75W SDM, (a) I_{ph} (b) I_s (c) α (d) R_{se} (e) R_{sh}

4.4.6 Case study 6: Comparison of SFTI 60 P (SDM and DDM) using *pv*-BWO and *cn*-BWO methodologies

An experimental test is setup in outdoor environmental conditions, where a 149 pair of SFTI-60P *I-V* data is recorded through MECO 9018BT solar PV analyzer at 983 W/m^2 and T=51 ˚C, by using the same setup shown in fig. 4.12. The recorded data is used for the parameter estimation and analyzing the results for SFTI-60P, SDM, and DDM.

a) Comparison of results and analysis for SDM

The superimposition of proposed *I-V* characteristics over experimental *I-V* for SFTI 60 P, SDM, by using *pv*-BWO and *cn*-BWO is shown in fig. 4.16 (a) and fig. 4.16 (b) respectively, where *pv*-BWO approach exhibits more near results to the experimental *I-V* and can be compared while observing table 4.18. Where, *cn*-BWO has shown better convergence speed *i.e.* near to 15 iterations when compared with the *pv*-BWO convergence curve that takes about 80 iterations to observe the optimal result, as shown in fig. 4.16 (e) and fig. 4.16 (f). All the estimated parameters for the SDM and DDM are listed in table 4.19, whereas the *P-V* characteristic is compared in fig. 4.16 (c) and fig. 4.16 (d). Where *pv*-BWO delivers a high peak current when compared with *cn*-BWO.

a) Comparison of results and analysis for DDM

Similar results are observed for the DDM as of SDM, where high convergence is given by the *cn*-BWO, as shown in fig. 4.17 (e) and fig. 4.17 (f). Whereas *cn*-BWO exhibits high RMSE when compared with *pv*-BWO, and the same is well observed with other E_f in table 4.18. The *I-V* and *P-V* characteristics are also compared with the experimental *I-V* and *P-V*, where a more near relationship with the experimental characteristics is observed with *pv*-BWO, as shown in fig. 4.17 (a)-fig. 4.17 (d).

Table 4.18 Comparison of error functions for SFTI-60P SDM and DDM

S.No.	Error Function (E_f)	SDM	DDM	SDM	DDM
		(*pv*-BWO)		(*cn*-BWO)	
1	Mean Absolute Error (MAE)	0.0416	0.0423	0.0713	0.0653
2	Root Mean Square Error (RMSE)	0.0744	0.0726	0.0935	0.0884
3	Mean Biased Error (MBE)	0.0005	0.0001	0.0073	0.0086
4	Sum of Squares (SSE)	0.8240	0.7852	1.3014	1.1635
5	Normalised RMSE (NRME)	0.0107	0.0104	0.0134	0.0127
6	Integral Absolute Error (IAE)	6.1999	6.3055	10.616	9.7289

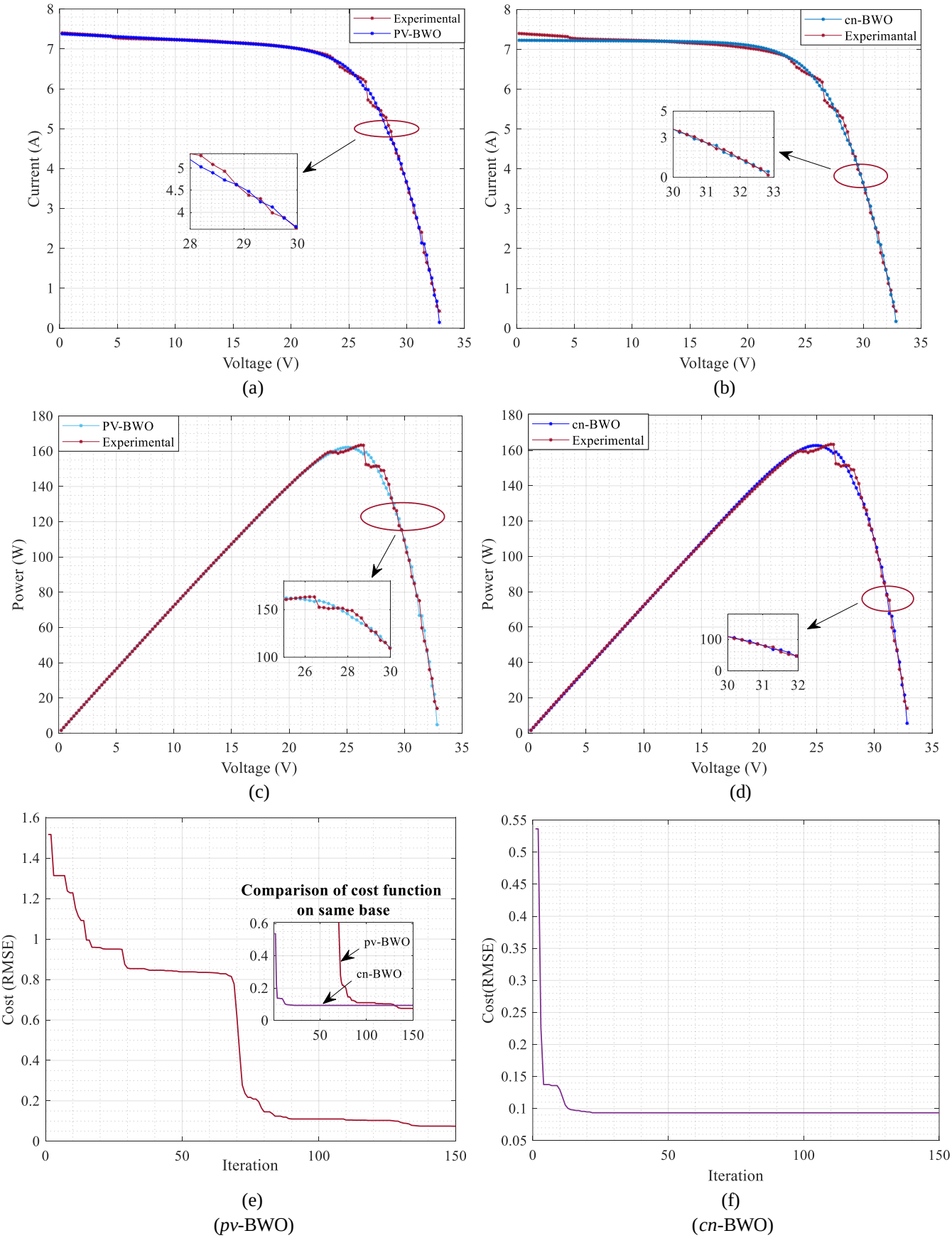

Fig. 4.16 Comparison for SDM of SFTI 60-P performance, (a) *I-V* using *pv*-BWO, (b) *I-V* using *cn*-BWO, (c) *P-V* using *pv*-BWO, (d) *P-V* using *cn*-BWO, (e) Cost RMSE, *pv*-BWO, (f) Cost RMSE, *cn*-BWO

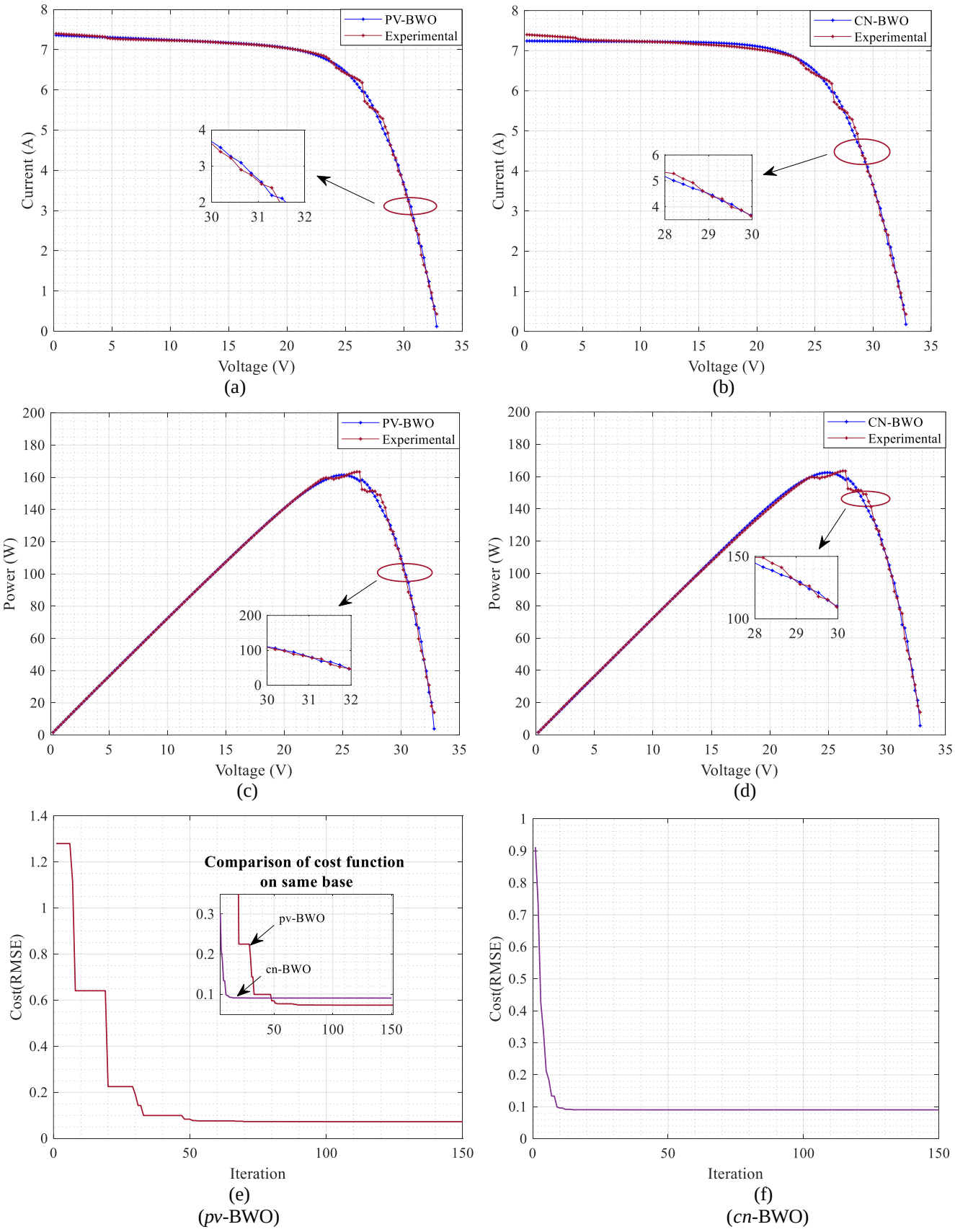

Fig. 4.17 Comparison for DDM of SFTI 60-P performance, (a) *I-V* using *pv*-BWO, (b) *I-V* using *cn*-BWO, (c) *P-V* using *pv*-BWO, (d) *P-V* using *cn*-BWO, (e) Cost RMSE, *pv*-BWO, (f) Cost RMSE, *cn*-BWO

Table 4.19 Comparison of estimated parameters for SFTI-60P SDM and DDM

SFTI-60P (DDM)							
Method	I_{ph}	I_{s1}	I_{s2}	α_1	α_2	R_{se}	R_{sh}
cn-BWO	7.2481	5.9645e-06	5.4900e-06	1.5038	1.4024	21.3971	2518
pv-BWO	7.39539	3.47013e-06	5.01464e-06	1.90315	1.26291	0.356869	81.9335
SFTI-60P (SDM)							
cn-BWO	7.2332	7.2126e-06	-	1.3939	-	0.39670	61.344
pv-BWO	7.42553	79.71515e-07	-	1.21645	-	0.414485	67.477

4.4.7 Estimation of parameters for TDM using *pv*-BWO and *cn*-BWO methodology

As in the previous section the parameters are extracted for the SDM and DDM, where it is asserted that the multi-diode models exhibit higher errors when compared with the SDM. Similarly, for the TDM, higher errors are observed in table 4.21, when compared with the errors for SDM and DDM. For instance, in case 2, *i.e.* for PWP 201, from table 4.9, it is evident that the RMSE for the SDM using *pv*-BWO 0.0035, whereas from table 4.21 it is observed that for the TDM the RMSE rises to 0.0048. In this section, parameters are estimated using TDM for case 2, case 3, case 4, and case 5, under the boundary conditions given in table 4.4. There are about nine parameters for each case, *i.e.* listed in table 4.20, whereas various E_f is also recorded under a set of boundary and environmental conditions, and listed in table 4.21. As observed in previous cases of SDM and DDM, *pv*-BWO exhibits more precise results when compared *cn*-BWO, whereas *cn*-BWO exhibits high convergence speed, and the same is observed in fig. 4.18-fig. 4.21.

Table 4.20 Estimated parameters for TDM

***cn*-BWO**					
S.No.	**Parameters**	**PWP-201**	**ESP 75W**	**EIL 75W**	**Sharp ND-R250A5**
1	I_{ph}	1.0372	5.4847	4.1762	9.1821
2	I_{s1}	5.5304e-06	6.1635e-06	4.6214e-06	4.8291e-06
3	I_{s2}	5.5143e-06	5.1077e-06	5.1485e-06	4.5460e-06
4	I_{s3}	6.7390e-06	7.1236e-06	5.7369e-06	4.7332e-06
5	α_1	1.7258	1.8338	1.5354	1.6901
6	α_2	1.7381	1.7862	1.5350	1.3976
7	α_3	1.4540	1.7238	1.5732	1.4143
8	R_{se}	1.0242	0.1314	0.2396	0.5219
9	R_{sh}	903.1559	273.2176	800.4345	1149.6
***pv*-BWO**					
1	I_{ph}	1.03604	5.46144	4.187191	9.1750742
2	I_{s1}	2.1569e-06	6.004136e-06	1e-12	9.5680098e-06
3	I_{s2}	2.2682e-06	8.655162e-06	1.0622e-06	2.5268593e-06
4	I_{s3}	5.39168e-06	3.02063e-06	9.4108e-06	1.8086547e-06
5	α_1	1.875279	1.625332	0.672249	2.3215188
6	α_2	1.405315	2.442775	1.70901	2.4998433
7	α_3	1.467366	1.645532	1.662155	1.2537776
8	R_{se}	1.083005	0.1559871	0.5434128	0.57711493
9	R_{sh}	767.3599	1864.6915	259.1338	9.1750742

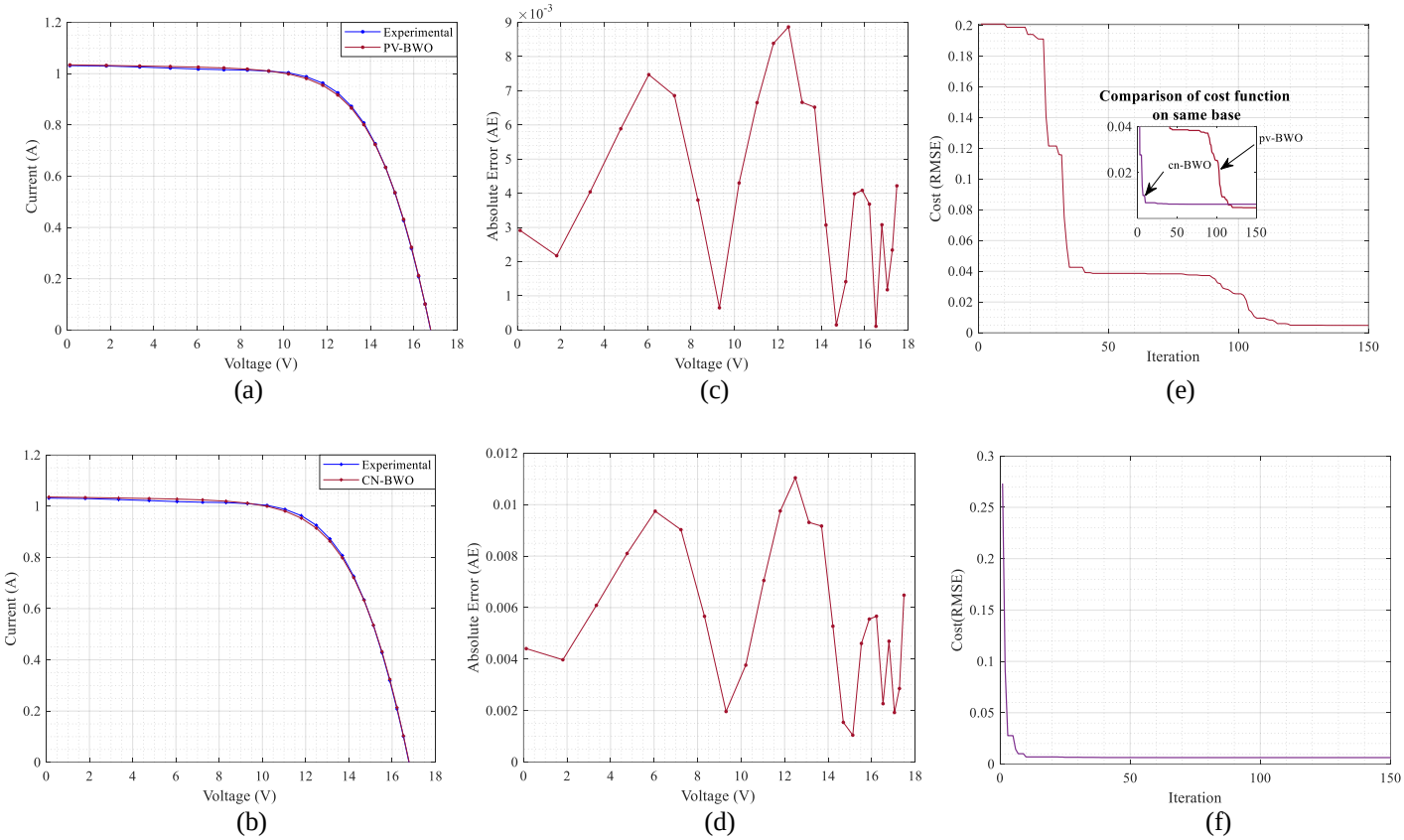

Fig. 4.18 Comparison for TDM of PWP 201, (a) *I-V* using *pv*-BWO, (b) *I-V* using *cn*-BWO, (c*)* Absolute error using *pv*-BWO (d) Absolute error using *cn*-BWO (e) Cost RMSE, *pv*-BWO, (f) Cost RMSE, *cn*-BWO

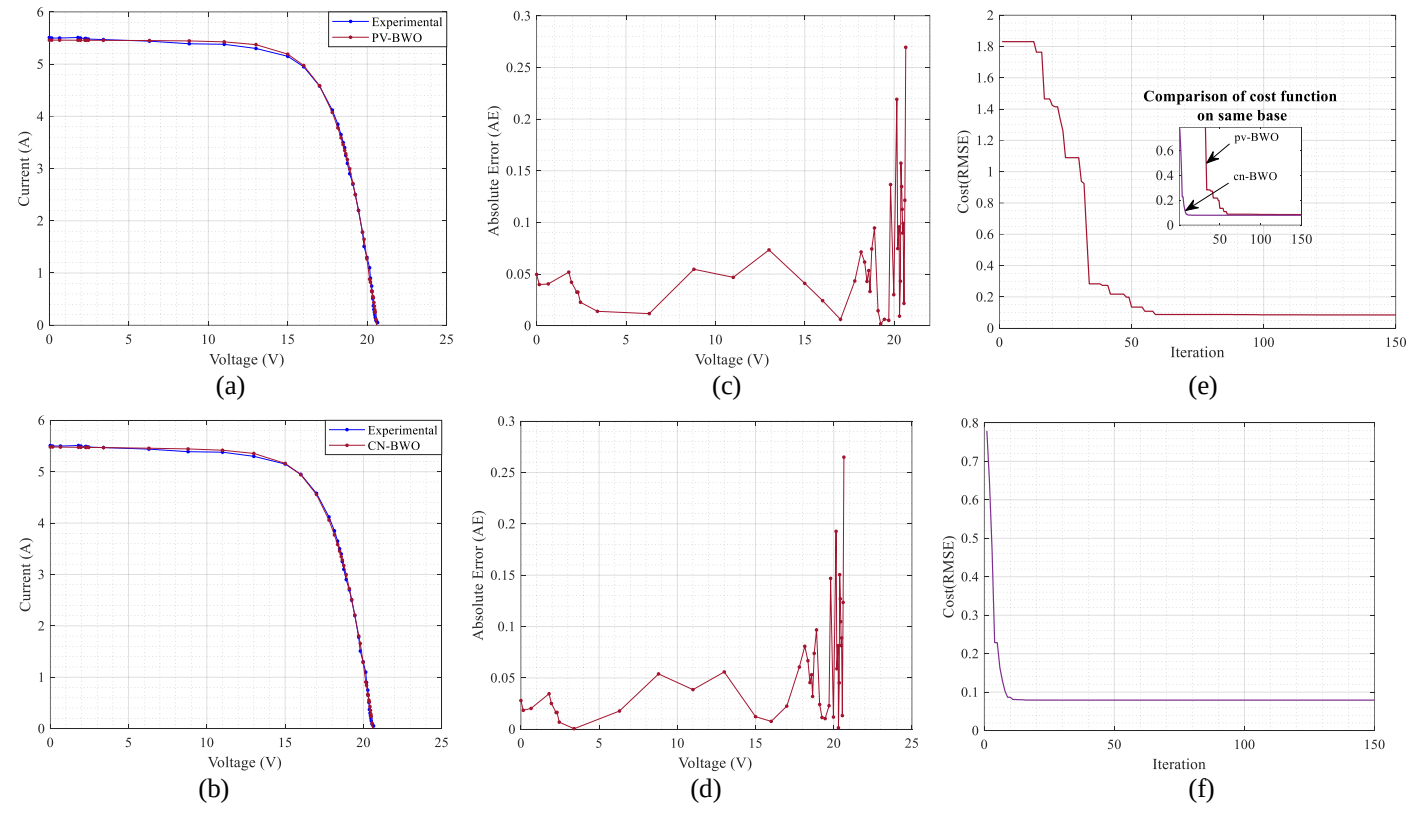

Fig. 4.19 Comparison for TDM of ESP 160PPW, (a) *I-V* using *pv*-BWO, (b) *I-V* using *cn*-BWO, (c*)* Absolute error using *pv*-BWO (d) Absolute error using *cn*-BWO (e) Cost RMSE, *pv*-BWO, (f) Cost RMSE, *cn*-BWO

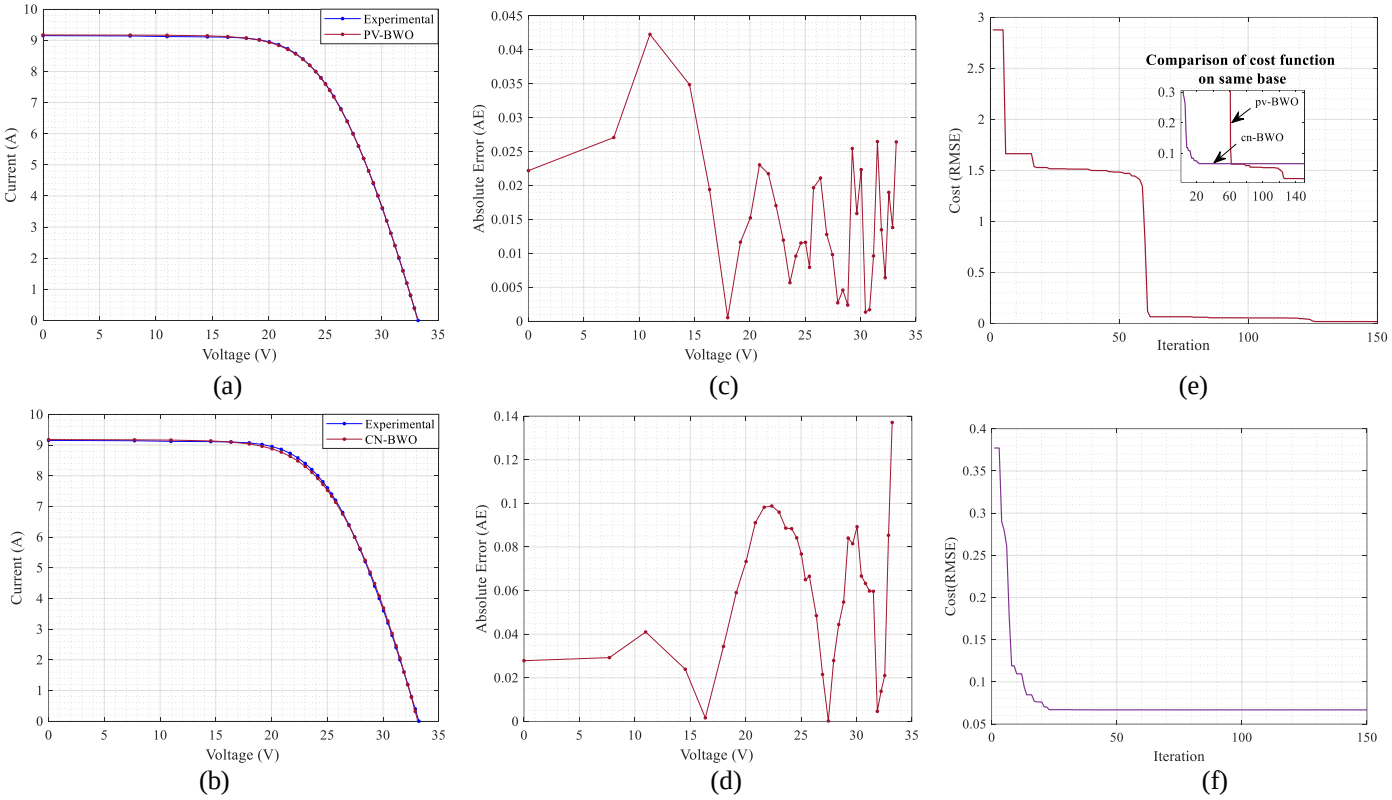

Fig. 4.20 Comparison for TDM of Sharp, (a) *I-V* using *pv*-BWO, (b) *I-V* using *cn*-BWO, (c*)* Absolute error using *pv*-BWO (d) Absolute error using *cn*-BWO (e) Cost RMSE, *pv*-BWO, (f) Cost RMSE, *cn*-BWO

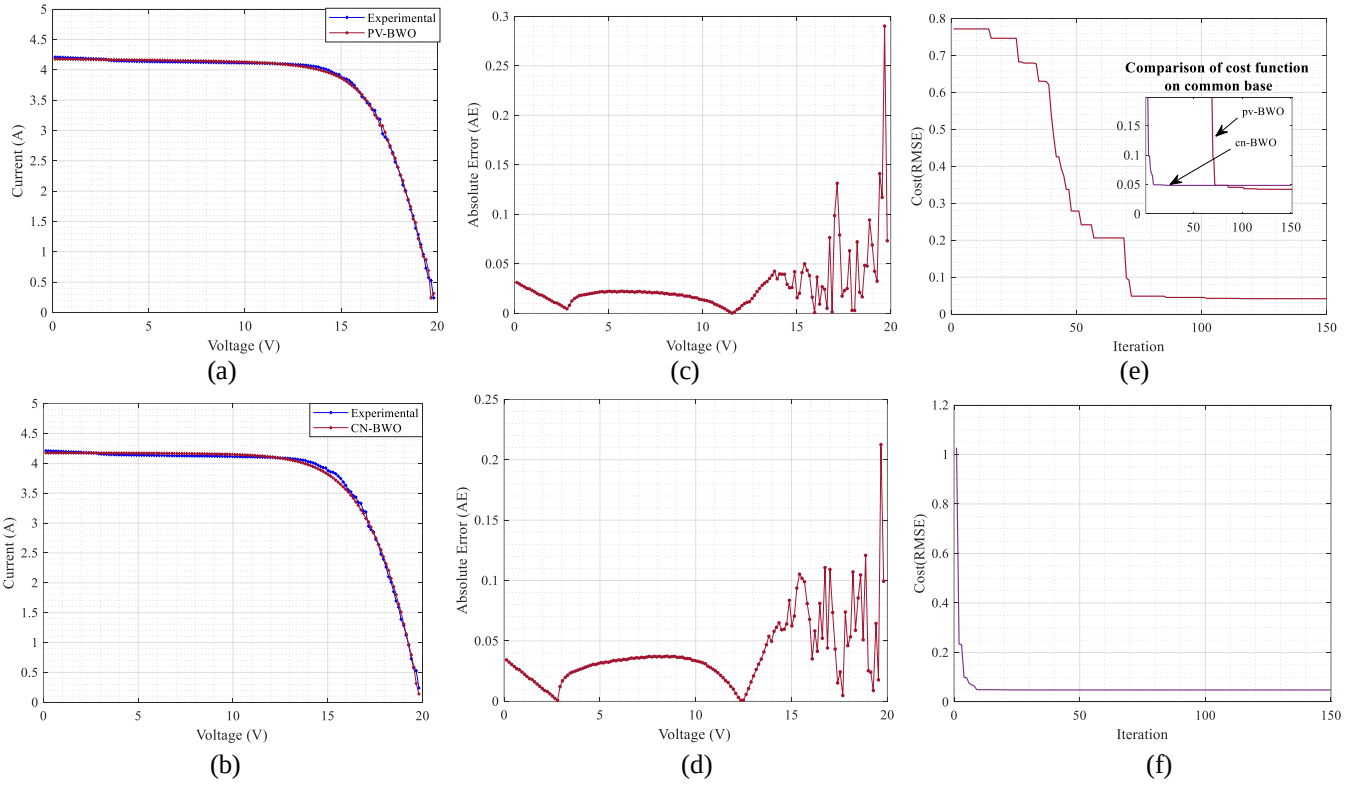

Fig. 4.21 Comparison for TDM of EIL 75W, (a) *I-V* using *pv*-BWO, (b) *I-V* using *cn*-BWO, (c*)* Absolute error using *pv*-BWO (d) Absolute error using *cn*-BWO (e) Cost RMSE, *pv*-BWO, (f) Cost RMSE, *cn*-BWO

Table 4.21 Comparison of error functions for TDM

***pv*-BWO**							
S.No.	**PV Module**	**MAE**	**RMSE**	**MBE**	**SSE**	**NRME**	**IAE**
1	PWP 201	0.0041	0.0048	0.0000	0.0006	0.0036	0.1025
2	ESP160PPW	0.0628	0.0639	0.0035	0.3028	0.0154	2.6992
3	Sharp	0.0152	0.0180	0.0001	0.0117	0.0020	0.5483
4	EIL 75W	0.0272	0.0414	0.0008	0.2553	0.0104	4.0475
***cn*-BWO**							
1	PWP 201	0.0056	0.0063	0.0003	0.0010	0.0047	0.1410
2	ESP160PPW	0.0569	0.0792	0.0007	0.2701	0.0145	2.4456
3	Sharp	0.0585	0.0668	0.0164	0.1607	0.0073	2.1075
4	EIL 75W	0.0389	0.0485	0.0027	0.3500	0.0122	5.7971

4.5 Chapter summary

This chapter presents a comparative analysis of two metaheuristic approaches based on the *pv*-BWOA and *cn*-BWO to estimate, precisely and quickly, the unknown parameter set for various solar PV models. Both approaches were implemented by using the experimental data, to estimate the unknown parameters of the SDM, DDM, and TDM. The validation of the proposed methodologies was carefully carried out through six different case studies, four case studies are extensively analyzed in various literature, whereas to examine the proposed methodology the fifth and sixth case study is performed in a real outdoor experimental environment. For case study 1, the RMSE values of SDM are compared with *cn*-BWO and a few existing techniques in the literature and observed that the *pv*-BWO methodology exhibits more promising results. The *I-V* and *P-V* characteristics of both SDM, DDM, and TDM that are carried out through *pv*-BWO, match more closely with the experimental data when compared with *cn*-BWO, which showcases the preciseness of *pv*-BWO methodology. Whereas *cn*-BWO exhibits high convergence when compared with *pv*-BWO, the same is observed with cases 1 to case 6. With these case studies, we conclude that the *pv*-BWO and *cn*-BWO are among the newest, modern, and precisely tuned methods for the mathematical model parameter estimation of solar PV, where *cn*-BWO exhibits high converging ability, whereas, the *pv*-BWO gives less erroneous results, under the same sets of boundary and environmental conditions.

Chapter 5

IMPLEMENTATION OF TWO NEW HYBRID APPROACHES USING SAILFISH AND SPOTTED HYENA OPTIMISERS

5.1 General

In the literature cited in chapter 2, parameter estimation is characterised majorly by three categories *i.e.* analytical, metaheuristic, and hybrid approaches. Where hybrid approaches are considered the most advanced techniques for the parameter estimation problem. It is also important to underline that in most of the methodologies implemented in literature for the parameters estimation of SDM and DDM the current values are to be estimated with the least errors. As the current equations for the SDM and DDM do not admit explicit solutions, hence there are significant limitations associated with the explicit simulation and parameter estimation. Moreover, there are few constraints observed in metaheuristic approaches in the context of global and local optima, where improvement in exploitation and exploration is a matter of concern [6], [88], which is also well explained for hybrid solar PV systems [89]. Hence, to improve the preciseness of estimated parameters a hybrid arrangement is constituted *i.e.* an association of analytical or numerical or metaheuristic approaches together, to improve the overall efficiency of the parameter estimation problem.

In this chapter, two new hybrid approaches are introduced for solar PV parameter estimation, using Sailfish optimisation (SFO) and Spotted hyena optimisation (SHO), along with the Newton-Raphson method (NR) through experimental *I-V* datasets. The proposed hybrid methodologies minimises the premature convergence to local minima, and a balance of exploration and exploitation is presented through the proposed methodologies. Five cases are considered, where the validation of the methodologies is carried out with the help of experimental datasets, whereas in the fourth and fifth cases 149 pairs of the experimental *I-V* datasets are considered that are recorded by the authors and also referred to in chapter 4. Moreover, a critical comparison of hybrid SFO (*h*-SFO) and hybrid SHO (*h*-SHO) is also carried out for all the above-mentioned cases and asserted that the *h*-SHO performs well when compared with *h*-SFO, in terms of converging speed, various error functions, and most importantly the objective function considered, later the analysis is also carried for TDM by using *h*-SHO.

5.2 Problem formulation

As explained in chapter 4, the objective is same as to estimate vector $\delta = [I_{ph}, I_s, \alpha, R_{se}, R_{sh}]$ for SDM, $\psi = [I_{ph}, I_{s1}, I_{s2}, \alpha_1, \alpha_2, R_{se}, R_{sh}]$, for DDM, and $\rho = [I_{ph}, I_{s1}, I_{s2}, I_{s3}, \alpha_1, \alpha_2, \alpha_3, R_{se}, R_{sh}]$ for

TDM. Where the objective is also referred to in chapter 4 *i.e.* minimisation of the variance between experimental and estimated data or the minimisation of error. Hence, here also the *eq.* 4.1, *eq.* 4.2 and *eq.* 4.3 are considered the objective function for the SDM, DDM, and TDM respectively.

5.2.1 Problem formulation for SDM

The optimised parameters are assessed through the estimated current that gives the least error when compared with the experimental current value. As for the case of SDM, it is observed that *eq.* (1.8), does not give an explicit solution for the precise parameter estimation, hence these limitations can be minimised by using numerical methods like NR and Lambert *W* method [6].

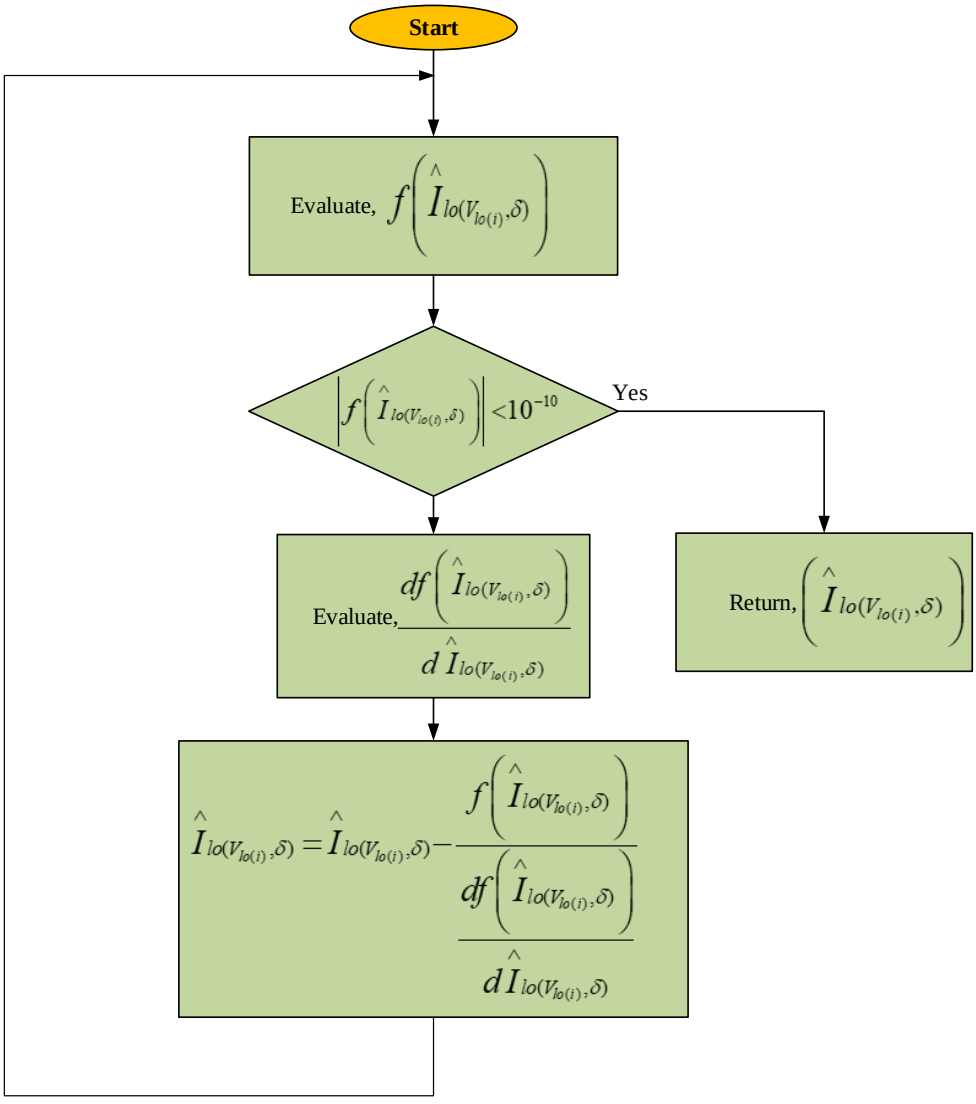

Fig. 5.1 Evaluation of estimated current using Newton-Raphson method

In the suggested approach, the current is estimated through the NR method by following the steps shown in fig. 5.1. The solution for the function $f\left(\hat{I}_{lo(V_{lo(i)},\delta)}\right)$, *i.e.* the eq. (4.7) is evaluated till the function value satisfies the stopping constraint $\left|f\left(\hat{I}_{lo(V_{lo(i)},\delta)}\right)\right|<10^{-10}$. As shown in fig. 5.1, the derivative of $f\left(\hat{I}_{lo(V_{lo(i)},\delta)}\right)$ concerning $\hat{I}_{lo(V_{lo(i)},\delta)}$ in *eq.* (5.1), is evaluated for each successive iteration. Whereas, the boundary conditions for the SDM are given in table 5.1.

$$\frac{df\left(\hat{I}_{lo(V_{lo(i)},\delta)}\right)}{d\,\hat{I}_{lo(V_{lo(i)},\delta)}}=-\left(\frac{I_s\times R_{se}\left(e^{\frac{\left(V_{lo}+\hat{I}_{lo(V_{lo(i)},\delta)}\times R_{se}\right)}{V_{tr}}}\right)}{V_{th}}\right)-\frac{R_{se}}{R_{sh}}-1 \tag{5.1}$$

5.2.2 Problem formulation for DDM

For the DDM, the estimated current is evaluated by using *eq.* (1.9), the current function is given by $f\left(\hat{I}_{lo(V_{lo(i)},\psi)}\right)$, for the estimation of seven unknown parameters, here also the flow diagram in fig. 5.1 is considered, where the derivative of *eq.* (4.8), can be written as *eq.* (5.2), where the boundary condition for the DDM parameters are given in table 5.2.

$$\frac{df\left(\hat{I}_{lo(V_{lo(i)},\psi)}\right)}{d\,\hat{I}_{lo(V_{lo(i)},\psi)}}=-\left(\frac{I_{s1}\times R_{se}\left[e^{\frac{\left(V_{lo}+\hat{I}_{lo(V_{lo(i)},\psi)}\times R_{se}\right)}{V_{th}}}\right]}{V_{th}}\right)-\left(\frac{I_{s2}\times R_{se}\left[e^{\frac{\left(V_{lo}+\hat{I}_{lo(V_{lo(i)},\psi)}\times R_{se}\right)}{V_{th}}}\right]}{V_{th}}\right)-\frac{R_{se}}{R_{sh}}-1 \tag{5.2}$$

5.2.3 Problem formulation for TDM

For the TDM, *eq.* (5.3), is considered for the estimation of current through NR method, where *eq.* (1.10) and *eq.* (4.9) is used to formulate *eq.* (5.3). The fig. 5.1, is to be followed for the estimation of current, where the current function is given by $f\left(\hat{I}_{lo(V_{lo(i)},\rho)}\right)$, and nine parameters are to be estimated. The derivative of *eq.* (4.9), can be written as *eq.* (5.3), where the boundary condition for the DDM parameters are given in table 5.3.

$$\frac{df\left(\hat{I}_{lo(V_{lo(i)},\rho)}\right)}{d\,\hat{I}_{lo(V_{lo(i)},\rho)}} = -\left(\frac{I_{s1}\times R_{se}\left[e^{\frac{\left(V_{lo}+\hat{I}_{lo(V_{lo(i)},\rho)}\times R_{se}\right)}{V_{th}}}\right]}{V_{th}}\right) - \left(\frac{I_{s2}\times R_{se}\left[e^{\frac{\left(V_{lo}+\hat{I}_{lo(V_{lo(i)},\rho)}\times R_{se}\right)}{V_{th}}}\right]}{V_{th}}\right) - \left(\frac{I_{s2}\times R_{se}\left[e^{\frac{\left(V_{lo}+\hat{I}_{lo(V_{lo(i)},\rho)}\times R_{se}\right)}{V_{th}}}\right]}{V_{th}}\right) - \frac{R_{se}}{R_{sh}} - 1 \tag{5.3}$$

5.3 Proposed methodologies

In this chapter two methodologies *i.e.* the sailfish optimisation [90] and spotted hyena optimisation [91] framework is elucidated, for the parameter estimation problem through the minimisation of objective functions given in *eq.* (4.1), *eq.* (4.2) and *eq.* (4.3) for SDM, DDM, and TDM respectively. The SFO is a nature-inspired metaheuristic approach that imitates the sailfish hunting strategy, whereas, the SHO is inspired by the hunting behaviour of spotted hyenas. Here, the current is estimated through the Newton-Raphson method expressed in fig. 5.1, and the estimated current is incorporated with these two proposed metaheuristic methodologies to estimate the optimised parameters through *eq.* (4.1)-*eq.* (4.3).

5.3.1 *Methodology 1:* Sailfish optimisation (SFO)

The SFO algorithm is a nature-based metaheuristic approach initially proposed in [90], where the alteration in the group hunting strategy of sailfish is modelled for the solution of various engineering problems. Sailfish are considered the fastest fish that reach a speed of 100km/hr, they hunt for small active sardine fishes in groups. The active movement of sardine fishes became a challenge for the sailfish, to mitigate this active maneuver by the sardine fishes, the sailfish continuously alter their attacking strategy of hunting.

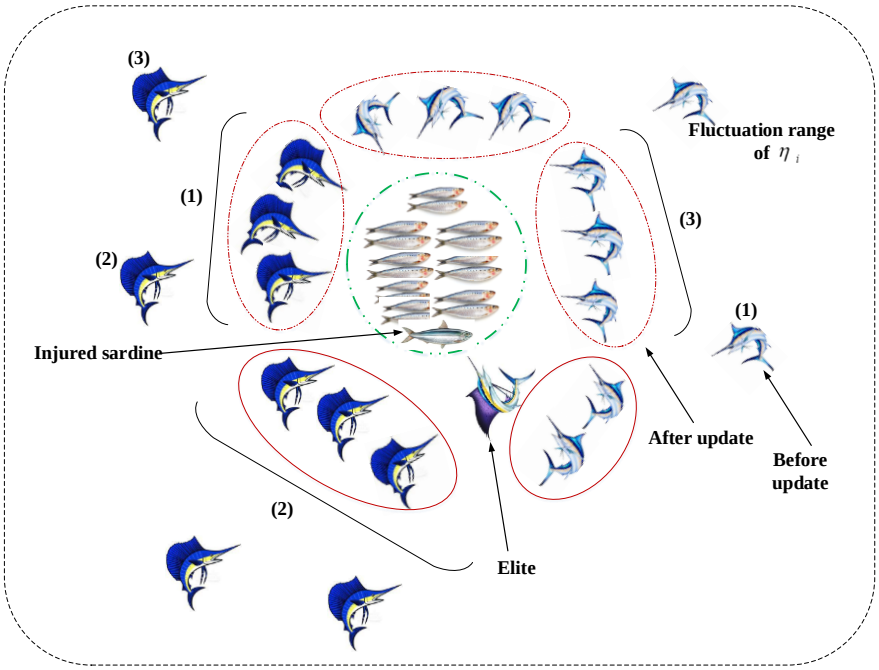

Fig. 5.2 Methodology for Sailfish optimisation

Various stages of strategies are well shown in fig. 5.2, and further explained in four stages as,

a) Initialisation

In the randomly generated population, the candidate solution is signified by the sailfish, whereas the problem variable is given by the position of the sailfish. In a multi-dimensional search space, the i^{th} sailfish member having f^{th} searching instant, the current position can be represented by, $Sf_{s(i,f)} \in R_n(1, 2, 3,\ldots..,r)$. The position matrix for each sailfish is given by *eq.* (5.4), whereas the fitness matrix *i.e.* the objective function value saved throughout the optimisation process is witnessed by the matrix in *eq.* (5.5). Moreover, the herd of sardine fishes is also playing a significant role in the proposed methodology, where it is assumed that the sardine fishes are also floating in the search space. Hence the position and the fitness matrix for the sardine fishes are modeled in *eq.* (5.6) and *eq.* (5.7), where *k* is the number of sardines fishes, and *'d'* is the number of variables.

$$Sf_{s(p)} = \begin{bmatrix} Sf_{s(1,1)} & Sf_{s(1,2)} & \ldots & Sf_{s(1,d)} \\ Sf_{s(2,1)} & Sf_{s(2,2)} & \ldots & Sf_{s(2,d)} \\ \vdots & \vdots & \vdots & \vdots \\ Sf_{s(r,1)} & Sf_{s(r,2)} & \ldots & Sf_{s(r,d)} \end{bmatrix} \tag{5.4}$$

$$Sf_{s(f)} = \begin{bmatrix} f(Sf_{sf(1,1)} & Sf_{sf(1,2)} & \ldots & Sf_{sf(1,d)}) \\ f(Sf_{sf(2,1)} & Sf_{sf(2,2)} & \ldots & Sf_{sf(2,d)}) \\ \vdots & \vdots & \vdots & \vdots \\ f(Sf_{sf(r,1)} & Sf_{sf(r,2)} & \ldots & Sf_{sf(r,d)}) \end{bmatrix} = \begin{bmatrix} Ft_{(1)} \\ Ft_{(2)} \\ \vdots \\ Ft_{(r)} \end{bmatrix} \tag{5.5}$$

$$Srf_{(p)} = \begin{bmatrix} Srf_{(1,1)} & Srf_{(1,2)} & \dots & Srf_{(1,d)} \\ Srf_{(2,1)} & Srf_{(2,2)} & \dots & Srf_{(2,d)} \\ \vdots & \vdots & \vdots & \vdots \\ Srf_{(k,1)} & Srf_{(k,2)} & \dots & Srf_{(k,d)} \end{bmatrix} \tag{5.6}$$

$$Srf_{(f)} = \begin{bmatrix} f(Srf_{(1,1)} & Srf_{(1,2)} & \dots & Srf_{(1,d)}) \\ f(Srf_{(2,1)} & Sf_{sf(2,2)} & \dots & Srf_{2,d)}) \\ \vdots & \vdots & \vdots & \vdots \\ f(Srf_{(k,1)} & Srf_{(k,2)} & \dots & Srf_{(k,d)}) \end{bmatrix} = \begin{bmatrix} Ft_{(s1)} \\ Ft_{(s2)} \\ \vdots \\ Ft_{(sk)} \end{bmatrix} \tag{5.7}$$

It is important to understand that sailfish and the sardines fishes are the corresponding factors responsible for the optimal solution, as the sailfish position is scattered in the search space, where sardines fishes lead to achieving the best possible position of sailfish.

b) Elitism factor

With each iteration, the best sailfish position is saved and considered as an elite sailfish identified so far, which in turn impacts the manoeuvrability and movement of sardines fishes during the attack. Whereas the sardines fish may injure by the slashing motion of the rostrum during hunting, hence it is important to store the position of injured sardine as the finest target, $P^{i}_{el(Sf_s)}$ and $P^{i}_{inj(Srf)}$ the position of elite sailfish and injured sardine respectively have the highest fitness value at i^{th} iteration.

c) Alternation strategy during an attack

The sailfish attack from all possible directions and change their position around the best solution, *i.e.* a sphere around the best solution. Whereas, every new position of sailfish is updated through *eq.* (5.8), where $P^{i}_{nw(Sf_s)}$ is the new position, $P^{i}_{cu(Sf_s)}$ is the current position of the sailfish, and η_i, is the coefficient for *i*th iteration.

$$P^{i}_{nw(Sf_s)} = P^{i}_{el(Sf_s)} - \eta_i \times \left(rand(0,1) \times \left(\frac{P^{i}_{el(Sf_s)} + P^{i}_{inj(Srf)}}{2} \right) - P^{i}_{cu(Sf_s)} \right) \tag{5.8}$$

$$\eta_i = 2 \times rand(0,1) \times P_d \tag{5.9}$$

Prey density (P_d), exhibits the number of prey in each iteration, during the hunting process the number of prey decreases, where 'P_d' plays a vital role in updating the sailfish position, N_{Sf_s} and N_{Srf} the number of sailfish and sardine fishes respectively.

$$P_d = 1 - \left(\frac{N_{Sf_s}}{N_{Sf_s} + N_{Srf}} \right) \tag{5.10}$$

'P_d' ranges from -1 to 1, which depends on the number of prey, P_d =1 exhibits *rand* (0,1) > 0.5, P_d = -1, implies *rand* (0,1) < 0.5 and *rand* (0,1) = 0.5 for P_d = 0. Hence, given this, the variation of 'P_d' mathematically model the divergence among sailfish and convergence around the prey *i.e.* sardine fishes.

d) Hunting of prey

It is important to highlight that in most cases a complete carnage of sardines is not commonly observed, where a prominent sardine population undergoes injury. Initially, both the sardine and sailfish are energetic, which enables high escape movement by the sardine, whereas, over time the hunting ability of sailfish weakens and the sardine's escape maneuver also deteriorates. So, to model this effect, the sardine position is updated based on the current sailfish position and the power of hunting with each incrimination in iteration. The new position of sardine is given by *eq.* (5.11), where $P^i_{ol(Srf)}$ is the current position with sailfish attack power P_{wr}, where a_t and μ are the coefficient to regulate the P_{wr} from a_t to 0.

$$P^i_{nw(Srf)} = r \times \left(P^i_{el(Sf_s)} - P^i_{ol(Srf)} + P_{wr} \right) \tag{5.11}$$

$$P_{wr} = a_t \times \left(1 - 2 \times Itr \times \mu \right) \tag{5.12}$$

Whereas, the P_{wr} responsible for the sardine fish position updation *i.e.* given by using factor $\alpha = P_{wr} \times N_{Srf_s}$, and $\beta = d_i \times N_{Sf_s}$, the d_i are the variables at *i*th iterations. So, in the proposed methodology, the position of hunter fish and prey fish are randomly generated, where injured prey and the elite hunter are responsible to update the position of each hunter sailfish. The probability of hunting new prey can be maximized by using *eq.* (5.13).

$$P^i_{(Sf_s)} = P^i_{(Srf)} \text{ if } f(Srf_i) < f(Sf_i) \tag{5.13}$$

Where at *i*th iteration sardine position is given by $P^i_{(Srf)}$, the sailfish position at *i*th iteration is given by $P^i_{(Sf_s)}$. The position of the prey fish is updated based on the power of the hunter fish, after updation of the position, the proposed objective function is calculated. If any of the prey fish shows more fitness value than any other hunter fish update with the same position, where the hunted prey will have been removed from the prey population.

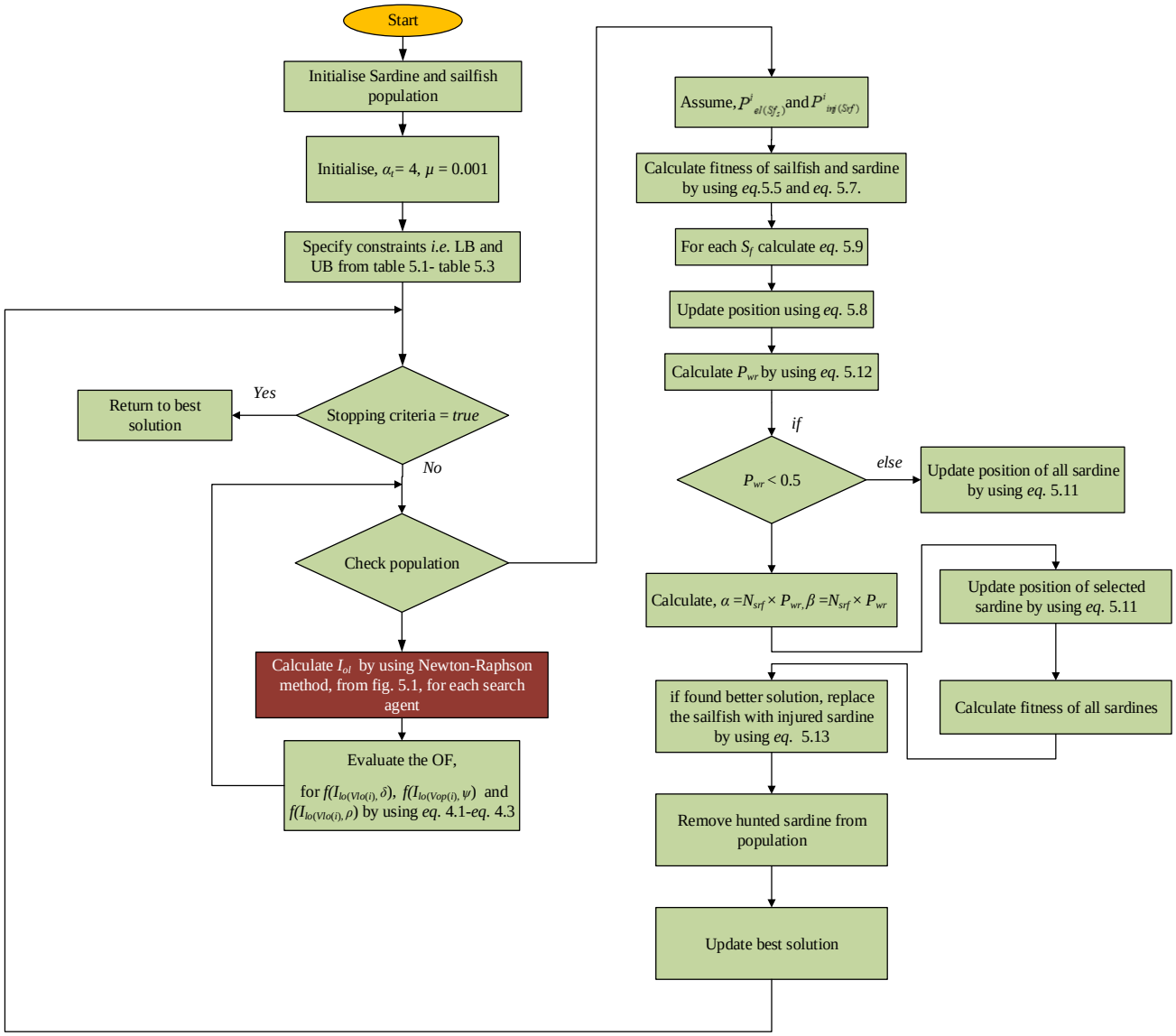

Fig. 5.3 Proposed methodology for parameter estimation using Sailfish optimisation

5.3.2 *Methodology 2:* Spotted hyena optimisation (SFO)

This methodology incorporates the social behaviour of spotted hyenas, especially skillful hunting, *i.e.* well explained in [91]. Hyenas are the hefty carnivores of the dog species, they communicate among members through various social calls and signals. The hunting behaviour of spotted hyenas is modeled in four steps, *i.e.* searching and tracking, encircling prey, hunting, and attacking prey, where two-dimensional position vectorization for hunting is showcased in fig. 5.4.

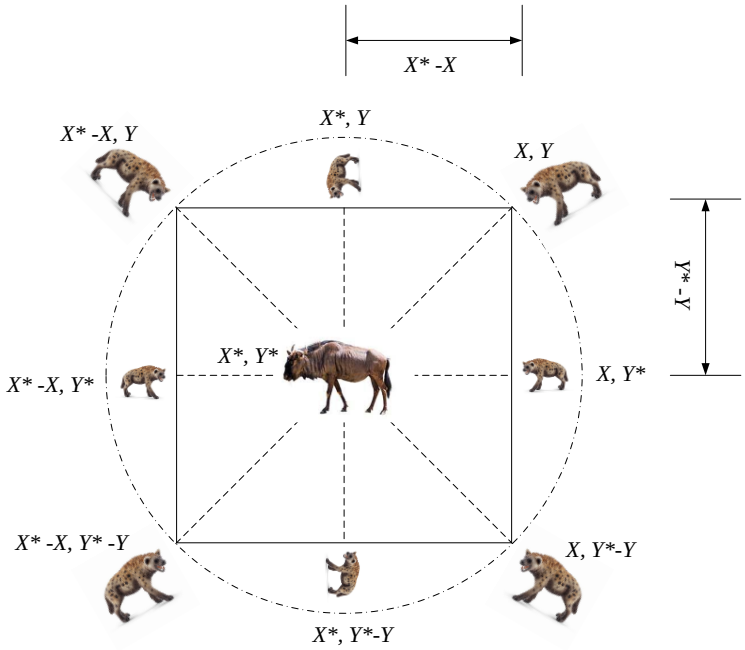

Fig. 5.4 Two-dimensional vectorization of Spotted Hyena

a) Encircling prey

Here, target prey is considered as the best candidate solution, *i.e.* the objective which is near to the optimum solution, where the other search population update positions, according to the solution of the best search candidate.

$$\vec{d}_{hy} = \left| \vec{U} . \vec{P}_r(x) - \vec{P}_h(x) \right| \tag{5.14}$$

$$\vec{P}(x+1) = \vec{P}_h(x) - \vec{g} . \vec{d}_{hy} \tag{5.15}$$

Distance between prey and the spotted hyena is given by $\vec{d}_{hy}$, where '*x*' is the current iteration, $\vec{U}$ and $\vec{g}$ are the coefficient vectors considered, whereas, $\vec{P}_r$ and $\vec{P}_h$ are the position vector of the prey and spotted hyena respectively.

$$\vec{U} = 2.r\vec{d}_1 \tag{5.16}$$

$$\vec{g} = 2\,\vec{j} . r\vec{d}_2 - \vec{j} \tag{5.17}$$

$$\vec{j} = 5 - (i \times (5/n)) \tag{5.18}$$

To balance the ability of the proposed methodology for exploration and exploitation, ' $\vec{j}$ ' is linearly decreased to 0 from 5, till '*n*'. In fig. 5.4, it is observed that the position of the hyena

i.e. (*X*, *Y*) continuously updated as per the position of the prey *i.e.* (X^*, Y^*), by using *eq.* (5.14) and *eq.* (5.15).

b) Prey hunting

Spotted hyenas hunt in groups, and align the hunt with the network of other trusted hyenas groups to identify the location of prey. Here it is assumed that the location of prey is already known to the optimum value search agent, whereas the trusted network search population update its position as per the position of the best search agent and saved the best solution with the increment in iterations.

$$\vec{d}_{hy} = \left| \vec{U} . \vec{P}_{bh} - \vec{P}_k \right| \tag{5.19}$$

$$\vec{P}_k = \left| \vec{P}_{bh} - \vec{g} . \vec{d}_{hy} \right| \tag{5.20}$$

$$\vec{G}_k = \vec{P}_k + \vec{P}_{k+1} + ... + \vec{P}_{k+N} \tag{5.21}$$

$\vec{G}_k$ is the group, where *N*, exhibits the number of spotted hyenas, $\vec{P}_{bh}$ is the position of the first best hyena, and the position of other hyenas are signified by $\vec{P}_k$. The computed hyenas 'N_h' is given by *eq.* (5.22). Where N_{sl} are the number of solutions and M_h is a random vector within [0.5, 1].

$$\vec{N}_h = N_{sl} (\vec{P}_h + \vec{P}_{h+1} + ... + (\vec{P}_h + \vec{M}_h)) \tag{5.22}$$

c) Attack on prey

The variation in vector '*j*', *i.e. eq.* (5.18), promises a change in *eq.* (5.17) *i.e.* vector '*g*', where |g|<1 exhibits the forcing of hyena group towards prey, where $\vec{P}(x+1)$ stores the best solution, and the position of other hyenas in the group is also updated accordingly.

The attack phenomenon explains the exploitation ability of the proposed method,

$$\vec{P}(x+1) = \frac{\vec{G}_k}{N} \tag{5.23}$$

where vector '*g*', enables the global search of prey, | *g* | > 1, that exhibits the movement of hyenas away from the prey, hence, the exploration is exercised through *eq.* (5.16) - *eq.* (5.18).

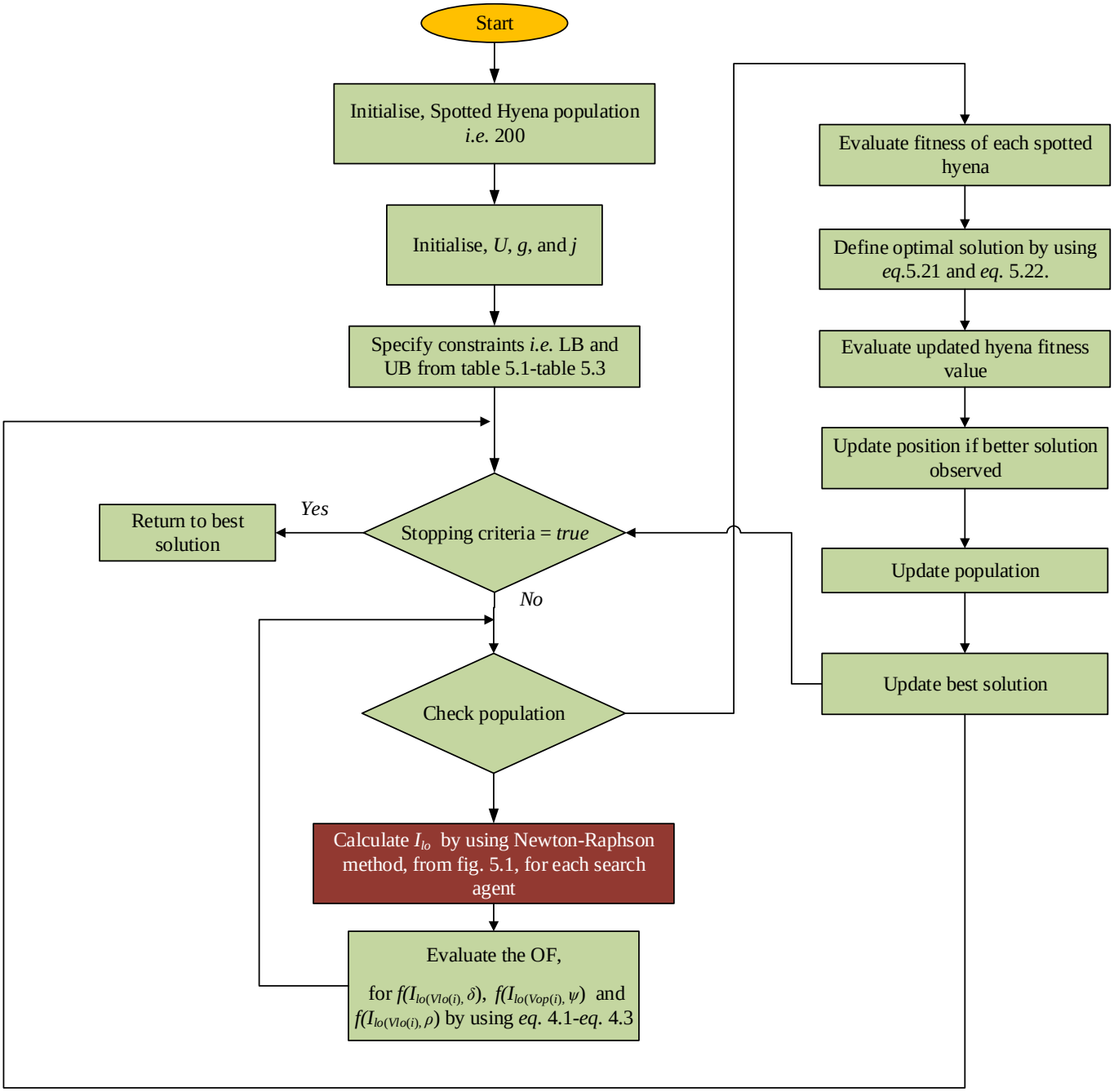

Fig. 5.5 Proposed methodology for parameter estimation using Spotted Hyena optimisation

5.4 Result and analysis

The analysis of *h*-SHO and *h*-SFO approaches for parameter estimation of solar PV are carried out in this section, where the results are evaluated for SDM, DDM, and TDM. Experimental data of five different PV are considered, *i.e.* acquired under a particular set of environmental conditions. The RTC France, PWP-201, Sharp ND-R250A5, EIL 75 W, and SFTI 60P are the five modules considered and each module is considered as a case study.

All the datasets considered are already referred to in section 4.4 along with the manufacturer's datasheet, all the set of conditions for each case is the same as explained in chapter 4. The computation is carried out in a Matlab® environment, with Intel® core *i7*-8550U CPU @1.80GHz, 16 GB RAM, and Windows 10 Professional 64-bit operating system.

Table 5.1 Boundary conditions for SDM

Parameter	**Case study 1 (RTC France)**		**Case study 2 (PWP-201)**		**Case study 3 (Sharp ND-R250A5)**		**Case study 4 (EIL-75W)**		**Case study 5 SFTI-60P**	
	LB	UB	LB	UB	LB	UB	LB	UB	LB	UB
I_{ph} [A]	0	1	0	10	0	10	0	10	0	10
I_s [A]	1E−12	1E−5	1E−12	1E−5	1E−12	1E−5	1E−12	1E−5	1E−12	1E−5
α	0.5	2.5	0.5	2.5	0.5	2.5	0.5	2.5	0.5	2.5
R_{se} [Ω]	0.001	2.5	0.001	3	0.001	2	0.001	3	0.001	50
R_{sh} [Ω]	0.001	100	0.001	1000	0.001	5000	0.001	1000	0.001	3000

Table 5.2 Boundary conditions for DDM

Parameter	**Case study 1 (RTC France)**		**Case study 2 (PWP-201)**		**Case study 3 (Sharp ND-R250A5)**		**Case study 4 (EIL-75W)**		**Case study 5 SFTI-60P**	
	LB	UB	LB	UB	LB	UB	LB	UB	LB	UB
I_{ph} [A]	0	1	0	10	0	10	0	10	0	10
I_{s1} [A]	1E−12	1E−5	1E−12	1E−5	1E−12	1E−5	1E−12	1E−5	1E−12	1E−5
I_{s2} [A]	1E−12	1E−5	1E−12	1E−5	1E−12	1E−5	1E−12	1E−5	1E−12	1E−5
α_1	0.5	2.5	0.5	2.5	0.5	2.5	0.5	2.5	0.5	2.5
α_2	0.5	2.5	0.5	2.5	0.5	2.5	0.5	2.5	0.5	2.5
R_{se} [Ω]	0.001	2	0.001	2.5	0.001	2	0.001	3	0.001	50
R_{sh} [Ω]	0.001	120	0.001	2000	0.001	5000	0.001	1000	0.001	3000

Table 5.3 Boundary conditions for TDM

Parameter	**Case study 1 (RTC France)**		**Case study 2 (PWP-201)**		**Case study 3 (Sharp ND-R250A5)**		**Case study 4 (EIL-75W)**		**Case study 5 SFTI-60P**	
	LB	UB	LB	UB	LB	UB	LB	UB	LB	UB
I_{ph} [A]	0	1	0	10	0	10	0	10	0	10
I_{s1} [A]	1E−12	1E−5	1E−12	1E−5	1E−12	1E−5	1E−12	1E−5	1E−12	1E−5
I_{s2} [A]	1E−12	1E−5	1E−12	1E−5	1E−12	1E−5	1E−12	1E−5	1E−12	1E−5
I_{s3} [A]	1E−12	1E−5	1E−12	1E−5	1E−12	1E−5	1E−12	1E−5	1E−12	1E−5
α_1	0.5	2.5	0.5	2.5	0.5	2.5	0.5	2.5	0.5	2.5
α_2	0.5	2.5	0.5	2.5	0.5	2.5	0.5	2.5	0.5	2.5
α_3	0.5	2.5	0.5	2.5	0.5	2.5	0.5	2.5	0.5	2.5
R_{se} [Ω]	0.001	2	0.001	2.5	0.001	2	0.001	3	0.001	50
R_{sh} [Ω]	0.001	120	0.001	2000	0.001	5000	0.001	1000	0.001	3000

5.4.1 Case study 1: Comparison of STC France (SDM and DDM) using *h*-SHO and *h*-SFO methodologies

In 300 iterations, the best optimised results with a min of RMSE, and the computational cost is presented. For the SDM the five extracted parameters through the proposed *h*-SHO and *h*-SFO techniques are showcased in table 5.4, which are acquired under the boundary conditions mentioned in table 5.1. In fig. 5.6 (c), it is observed that *h*-SHO exhibits high convergence ability at low RMSE *i.e.* 0.0025 when compared with *h*-SFO having RMSE of 0.0120. Moreover, *h*-SHO also exhibits better results when compared with other techniques in literature and based on other error functions like MAE and AE, shown in table 5.5. The I_{et} for each experimental data point is given in table 5.7, for *h*-SHO and *h*-SFO, where *h*-SHO targets a low AE of 0.0433 when compared with an AE of 0.2190 for *h*-SFO.

Table 5.4 Estimated parameters for SDM and DDM

RTC France (DDM)							
Method	I_{ph}	I_{s1}	I_{s2}	α_1	α_2	R_{se}	R_{sh}
h-SHO	0.75887	8.573158e-06	9.999181e-06	2.109867	2.102244	0.00167	111.1799
h-SFO	0.77108	5.43844e-06	5.84383e-06	1.91460	2.22945	0.00774	84.40040
RTC France (SDM)							
h-SHO	0.76277	8.59755e-07	--	1.631059	--	0.03127	45.74371
h-SFO	0.76161	1.76682e-07	--	1.46335		0.04814	34.41282
PWP 201 (DDM)							
h-SHO	1.02802	1.76991e-06	8.20242e-06	1.38559	1.84410	1.20918	1699.67902
h-SFO	1.07586	3.77378e-06	8.70294e-06	1.54687	1.48642	1.29326	403.77044
PWP 201 (SDM)							
h-SHO	1.02841	2.29298e-06	--	1.39603	--	1.26118	1110.94310
h-SFO	1.02316	5.01700e-06	--	1.44731	--	1.08774	4179.36947
Sharp ND-R250A5 (DDM)							
h-SHO	9.16286	1.66903e-06	1.57790e-12	1.38910	2.46550	0.57802	1842.27336
h-SFO	9.18577	8.37770e-06	1.50784e-06	1.54820	2.02865	0.53912	4234.55737
Sharp ND-R250A5 (SDM)							
h-SHO	9.15709	1.98897e-06	--	1.40470	--	0.57214	4769.69124
h-SFO	9.08869	1.11991e-06	--	1.35397		0.55364	690.52681
EIL 75W (DDM)							
h-SHO	4.19871	4.02193e-06	5.47324e-06	1.98691	1.19475	0.26429	191.47575
h-SFO	4.20147	1.65093e-06	3.78663e-06	1.95491	1.16904	0.32158	781.18759
EIL 75W (SDM)							
h-SHO	4.16996	8.57139e-07	--	1.05218	--	0.36063	372.92251
h-SFO	4.18423	3.76824e-06	--	1.15263	--	0.14905	303.24485
SFTI 60P (DDM)							
h-SHO	7.2681	1.05695e-12	2.41654e-06	2.1655	1.2014	0.4272	281.5792
h-SFO	7.3902	6.22869e-07	3.54943e-06	1.1132	1.4957	0.6815	328.6026
SFTI 60P (SDM)							
h-SHO	7.2582	9.88636e-06	--	1.3244	--	0.3664	452.7809
h-SFO	7.3266	7.72928e-06	--	1.3213	--	0.5710	402.4716

Moreover, the *I-V* and *P-V* characteristics are also drawn for SDM by using *h*-SHO and *h*-SFO, where the characteristics are also compared with the experimental characteristics and a few well-established techniques *i.e.* SFS [79], I-JAYA [48], IMFO [46], HS [76], and GA [77], as shown in fig. 5.6 (a) and fig. 5.6 (b) respectively. Where, it is evident that the *I-V* and *P-V* characteristics exhibit a nearer and more precise relationship with the experimental characteristic in other words more correct results are achieved through the *h*-SHO technique, while compared with other referred techniques along with *h*-SFO.

Moreover, the results are also validated for the DDM, where, *h*-SHO showcases high convergence with low AE, as shown in fig. 5.7 (c) and fig. 5.7 (d). From table 5.6, it is observed that the SFO exhibits the RMSE of 0.0179 which is higher if compared with *h*-SHO *i.e.* 0.0074. Table 5.6 also asserted that low E_f is observed for SDM rather than DDM for both *h*-SFO and *h*-SHO techniques, which concludes that more precise results are achieved for SDM rather than DDM, due to the complexity associated with DDM, where *h*-SHO gives more conclusive results *i.e.* near to the experimental values. The *I-V* and *P-V* characteristics *i.e.* fig. 5.7 (a) and fig. 5.7 (b) for DDM are further drawn and compared with the referred techniques in the literature, where the proposed *h*-SHO is nearly in concurrence with the experimental values when compared with SFS [15], I-JAYA [25], IMFO [20], HS [24], and GA [26].

Table 5.5 Comparison of error functions with existing techniques for SDM, RTC France

S. No.	Method	RMSE	MAE	AE
1	*h*-SHO	0.0025	0.0021	0.0433
2	*h*-SFO	0.0120	0.0087	0.219
3	GA	0.00476	0.0031277	0.081320
4	TLBO [80]	0.0058554	0.003717	0.096653
5	NRM [81]	0.0096964	---	---
6	RF 2A [82]	0.01388	0.0094014	---
7	MBA [83]	0.07620	0.044495	1.156900
8	PS [84]	0.0028547	0.00215	0.055993
9	Method [85]	0.0058668	0.0037242	0.096830
10	Method [86]	0.0061149	0.0038939	0.10124
11	Method [87]	0.003161	0.001786	---
12	PS+GRG [92]	0.0026100	---	---
13	CPSO [93]	0.002650	0.001680	---

The boundary condition considered for the DDM is given in table 5.2, where all the seven estimated parameters for DDM are listed in table 5.4, the I_{et} for each experimental data point is given in table 5.7, where *h*-SHO exhibits an AE of 0.132, and *h*-SFO targets an AE of 0.2763, which is much higher when compared with *h*-SFO.

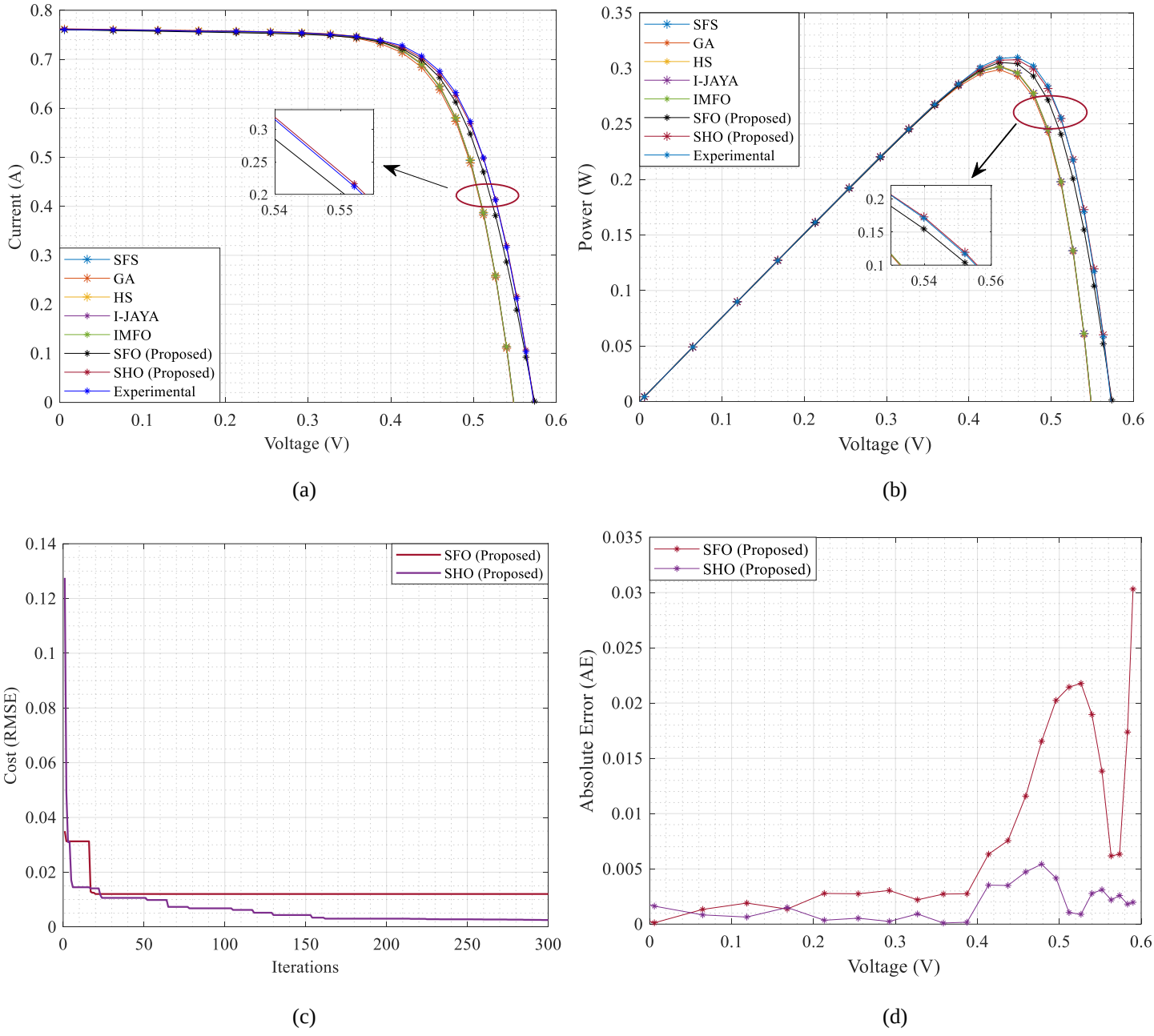

Fig. 5.6 Performance characteristics for RTC France SDM (a) Comparison of *I-V* with experimental and existing techniques, (b) *P-V* characteristic comparison (c) Variation of OF with iterations, (d) Absolute error

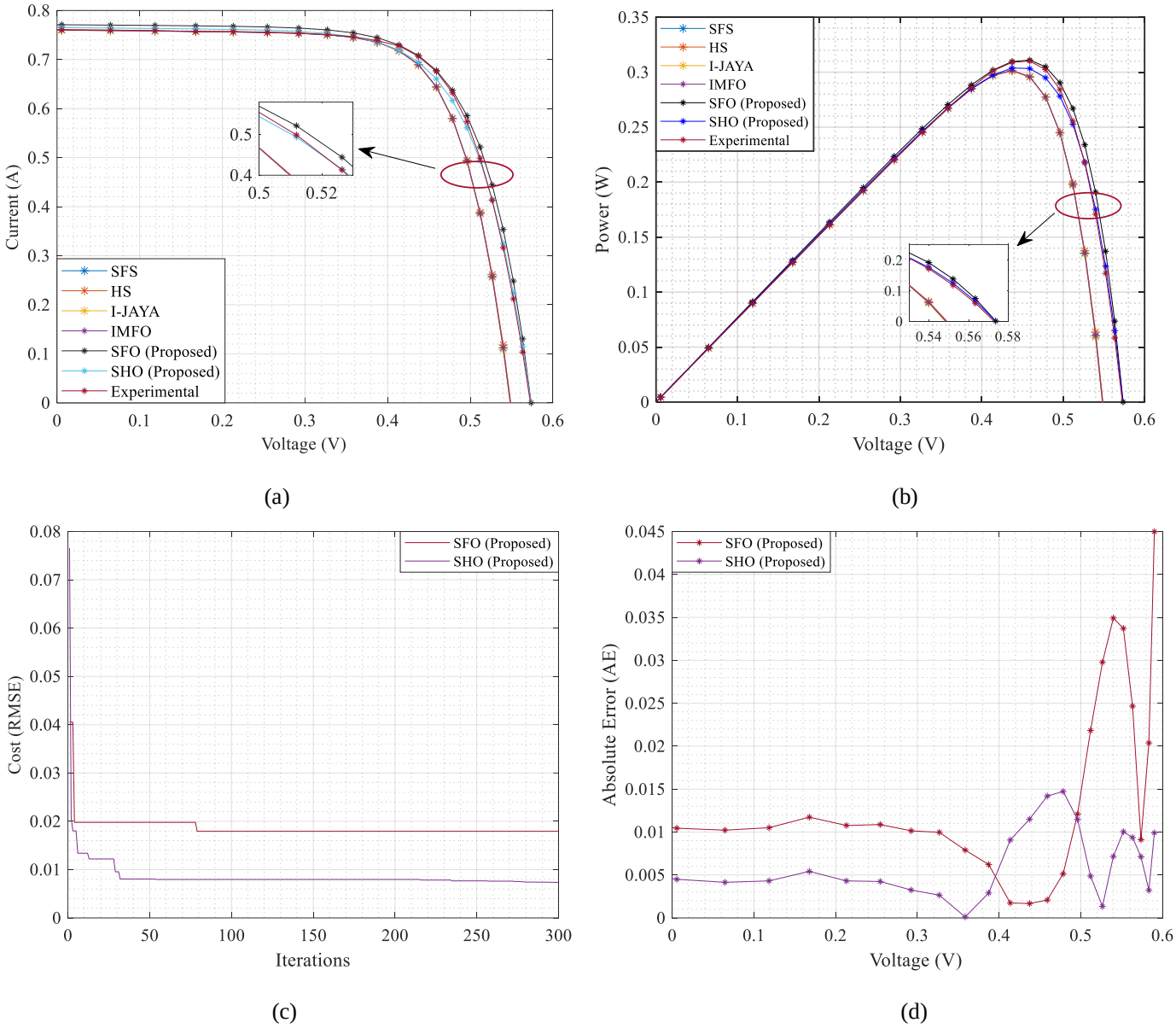

Fig. 5.7 Performance characteristics for RTC France DDM (a) Comparison of *I-V* with experimental and existing techniques, (b) *P-V* characteristic comparison (c) Variation of OF with iterations, (d) Absolute error

Table 5.6 Comparison of error functions for SDM and DDM, of RTC France

E_f	RTC France			
	SDM	DDM	SDM	DDM
	(*h*-SHO)		(*h*-SFO)	
MAE	0.0021	0.0063	0.0087	0.0063
RMSE	0.0025	0.0074	0.0120	0.0179
MBE	0.0001	0.0001	0.0040	0.0093
SSE	0.0002	0.0014	0.0038	0.0084
NRME	0.0026	0.0075	0.0124	0.0184

Table 5.7 Comparison of estimated and experimental current for SDM and DDM, RTC France

S. No.	V_{ex}	I_{ex}	(*h*-SHO)				(*h*-SFO)			
			(SDM)		(DDM)		(SDM)		(DDM)	
			I_{et}	AE	I_{et}	AE	I_{et}	AE	I_{et}	AE
1	0.00570	0.76050	0.7621	0.0016	0.7650	0.0045	0.7604	1E-04	0.7709	0.0104
2	0.06460	0.76000	0.7608	0.0008	0.7641	0.0041	0.7587	0.0013	0.7702	0.0102
3	0.11850	0.75900	0.7596	0.0006	0.7633	0.0043	0.7571	0.0019	0.7695	0.0105
4	0.16780	0.75700	0.7585	0.0015	0.7624	0.0054	0.7556	0.0014	0.7687	0.0117
5	0.21320	0.75700	0.7574	0.0004	0.7613	0.0043	0.7542	0.0028	0.7678	0.0108
6	0.25450	0.75550	0.756	0.0005	0.7597	0.0042	0.7528	0.0027	0.7664	0.0109
7	0.29240	0.75400	0.7542	0.0002	0.7573	0.0033	0.7509	0.0031	0.7642	0.0102
8	0.32690	0.75050	0.7514	0.0009	0.7532	0.0027	0.7483	0.0022	0.7605	0.01
9	0.35850	0.74650	0.7466	1E-04	0.7464	0.0001	0.7438	0.0027	0.7544	0.0079
10	0.38730	0.73850	0.7383	0.0002	0.7356	0.0029	0.7357	0.0028	0.7447	0.0062
11	0.41370	0.72800	0.7244	0.0036	0.7188	0.0092	0.7214	0.0066	0.7297	0.0017
12	0.43730	0.70650	0.7029	0.0036	0.6947	0.0118	0.6985	0.008	0.7082	0.0017
13	0.45900	0.67550	0.6705	0.005	0.6608	0.0147	0.6627	0.0128	0.6776	0.0021
14	0.47840	0.63200	0.6261	0.0059	0.6165	0.0155	0.6126	0.0194	0.6372	0.0052
15	0.49600	0.57300	0.5683	0.0047	0.5607	0.0123	0.5476	0.0254	0.5854	0.0124
16	0.51190	0.49900	0.4977	0.0013	0.4937	0.0053	0.47	0.029	0.5216	0.0226
17	0.52650	0.41300	0.4141	0.0011	0.4145	0.0015	0.3812	0.0318	0.4442	0.0312
18	0.53980	0.31650	0.3202	0.0037	0.3248	0.0083	0.2865	0.03	0.3536	0.0371
19	0.55210	0.21200	0.2164	0.0044	0.224	0.012	0.1883	0.0237	0.2484	0.0364
20	0.56330	0.10350	0.1067	0.0032	0.1151	0.0116	0.0922	0.0113	0.1306	0.0271
				IAE		IAE		IAE		IAE
				0.0433		0.138		0.2190		0.2763

5.4.2 Case study 2: Comparison of PWP 201 (SDM and DDM) using *h*-SHO and *h*-SFO methodologies

Based on 25 pair experimental *I-V* data of PWP-201 at G=1000W/m^2 and T=45 ℃, parameter vectors 'δ' and 'ψ' are to be extracted. Table 5.8, witnesses the high computational cost of using *h*-SFO over *h*-SHO *i.e.* 0.0073 and 0.0023 respectively for SDM of PWP 201, similarly, for the DDM the OF recorded as 0.0024 and 0.0252. While referring to fig. 5.8 (c), fig. 5.8 (d), fig. 5.9(c) and fig. 5.9(d), it is perceived that for both SDM and DDM the *h*-SHO showcases fast convergence speed with low error results, while compared with *h*-SFO. In fig. 5.9(c), a very deprived convergence is observed by *h*-SFO with a very high error function, for DDM. With this, it is asserted that DDM requires more iterations along with a longer execution time, due to the complexity associated with the DDM. Due to fewer computational errors, the *I-V* and *P-V* characteristics for SDM and DDM are in much congruence with the experimental *I-V* and *P-V* characteristics for *h*-SHO on comparing with *h*-SFO, the same is well observed in fig. 5.8 (a) and fig. 5.8 (b) for SDM, fig. 5.9 (a) and fig. 5.9 (b) for DDM. The estimated parameter for the SDM and DDM is well illustrated in table 5.4, whereas, various E_f for the SDM and DDM are well compared in table 5.8. The IAE of 0.0439 and 0.1298 is recorded for SDM, where a comparatively high IAE of 0.0506 and 0.6015 is observed in table 5.9, for DDM when calculated through *h*-SHO and *h*-SFO respectively.

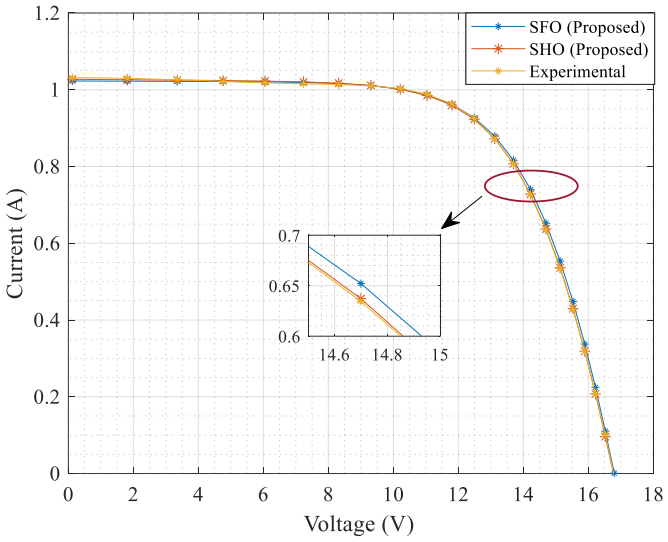

(a)

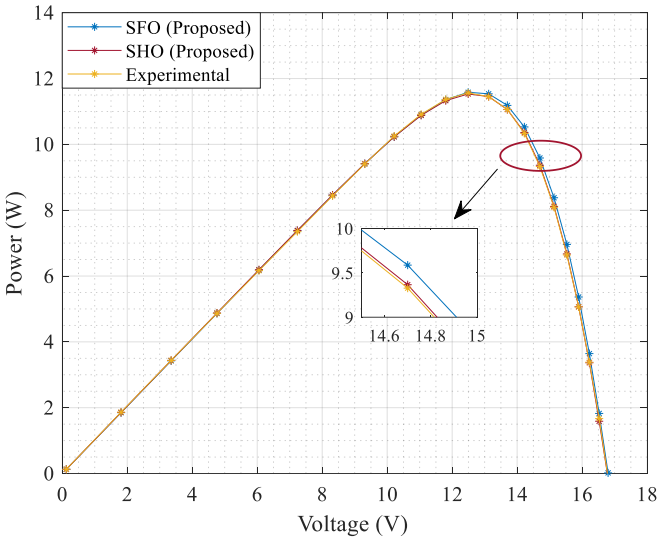

(b)

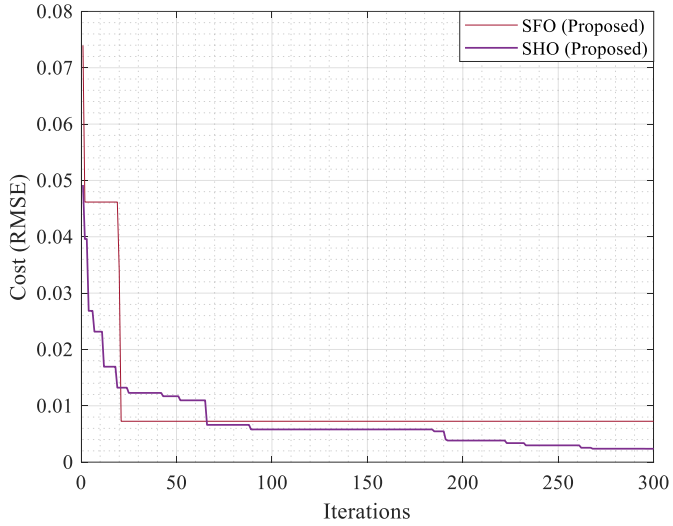

(c)

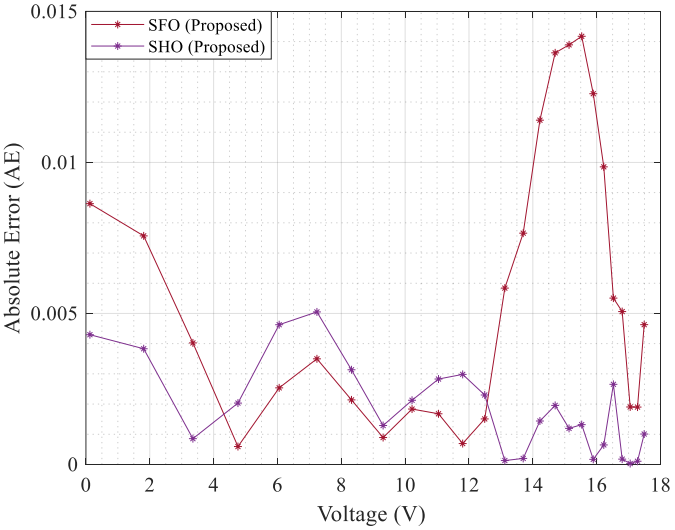

(d)

Fig. 5.8 Performance characteristics for PWP 201 SDM (a) Comparison of *I-V* with experimental characteristic, (b) *P-V* characteristic comparison (c) Variation of OF with iterations, (d) Absolute error curve

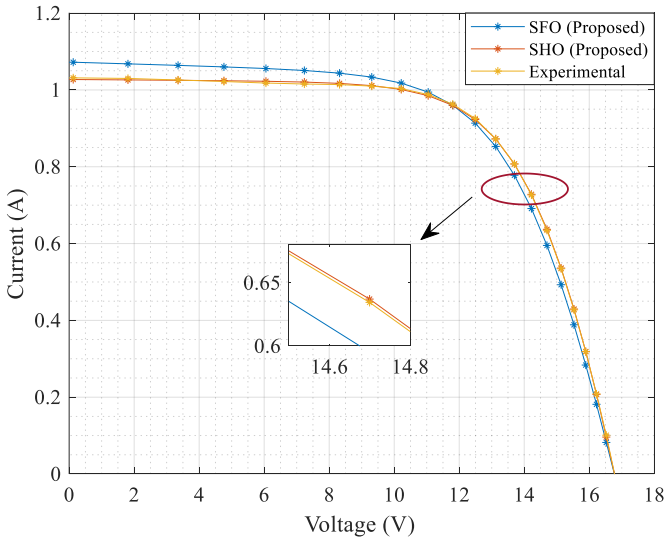

(a)

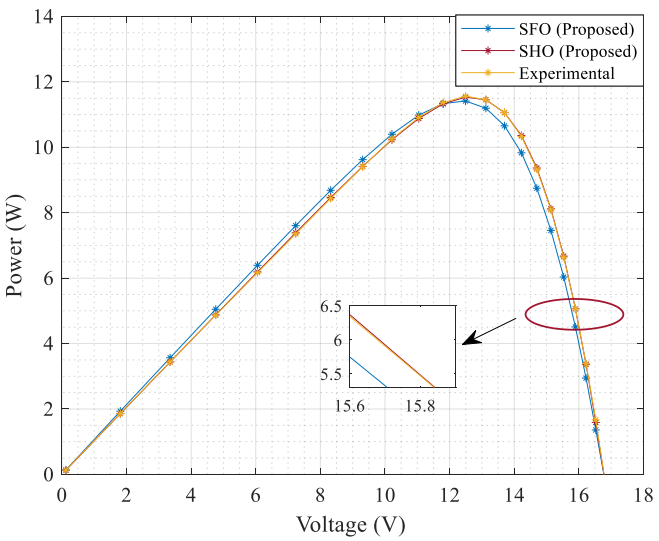

(b)

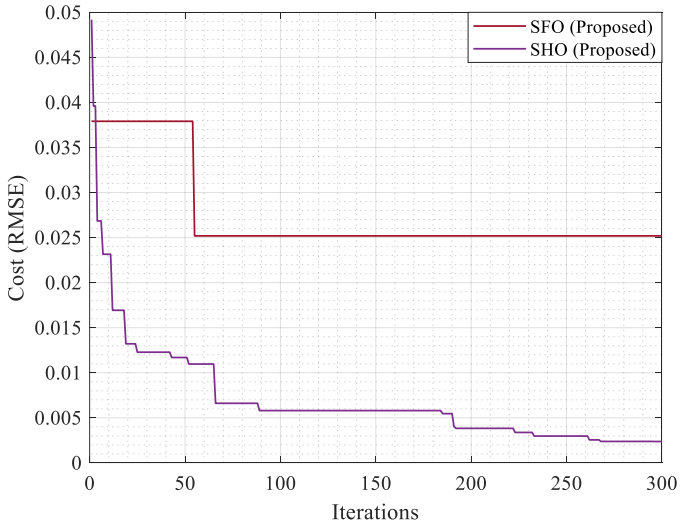

(c)

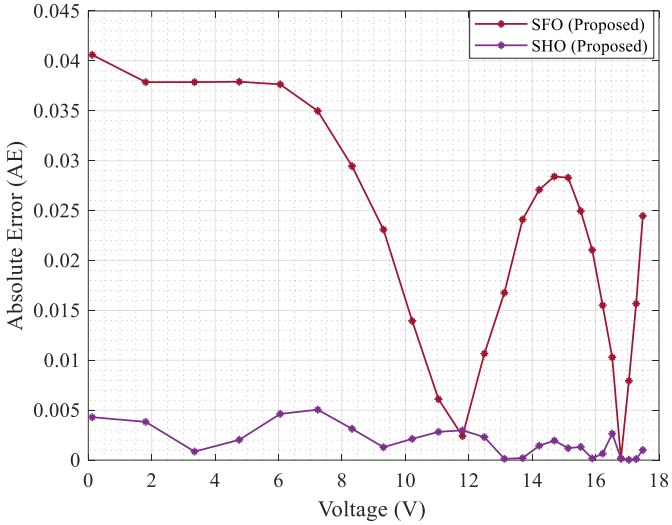

(d)

Fig. 5.9 Performance characteristics for PWP 201 DDM (a) Comparison of *I-V* with experimental characteristic, (b) *P-V* characteristic comparison (c) Variation of OF with iterations, (d) Absolute error

Table 5.8 Comparison of error functions for SDM and DDM, of PWP-201

E_f	PWP-201			
	SDM	DDM	SDM	DDM
	(*h*-SHO)		(*h*-SFO)	
MAE	0.0019	0.0019	0.0057	0.0223
RMSE	0.0023	0.0024	0.0073	0.0252
MBE	0.0001	0.0001	0.0032	0.0055
SSE	0.0001	0.0001	0.0013	0.0159
NRME	0.0018	0.0018	0.0054	0.0189

Table 5.9 Comparison of estimated and experimental current for SDM and DDM, PWP 201

S. No.	V_{ex}	I_{ex}	(*h*-SHO)				(*h*-SFO)			
			(SDM)		(DDM)		(SDM)		(DDM)	
			I_{et}	AE	I_{et}	AE	I_{et}	AE	I_{et}	AE
1	0.1248	1.0315	1.0359	0.0044	1.0272	0.0043	1.0401	0.0086	1.0722	0.0407
2	1.8093	1.03	1.0344	0.0044	1.0262	0.0038	1.0376	0.0076	1.068	0.038
3	3.3511	1.026	1.0278	0.0018	1.0251	0.0009	1.03	0.004	1.064	0.038
4	4.7622	1.022	1.0227	0.0007	1.024	0.002	1.0226	0.0006	1.0601	0.0381
5	6.0538	1.018	1.0211	0.0031	1.0226	0.0046	1.0205	0.0025	1.0558	0.0378
6	7.2364	1.0155	1.0191	0.0036	1.0206	0.0051	1.019	0.0035	1.0507	0.0352
7	8.3189	1.014	1.0159	0.0019	1.0172	0.0032	1.0161	0.0021	1.0438	0.0298
8	9.3097	1.01	1.0105	0.0005	1.0113	0.0013	1.0109	0.0009	1.0335	0.0235
9	10.2163	1.0035	1.0056	0.0021	1.0013	0.0022	1.0053	0.0018	1.0178	0.0143
10	11.0449	0.988	0.9899	0.0019	0.9851	0.0029	0.9897	0.0017	0.9944	0.0064
11	11.8018	0.963	0.9643	0.0013	0.9599	0.0031	0.9637	0.0007	0.9604	0.0026
12	12.4929	0.9255	0.9266	0.00011	0.923	0.0025	0.927	0.0015	0.9136	0.0119
13	13.1231	0.8725	0.8751	0.0026	0.8726	1E-04	0.8783	0.0058	0.853	0.0195
14	13.6983	0.8075	0.8093	0.0018	0.8073	0.0002	0.8152	0.0077	0.7779	0.0296
15	14.2221	0.7265	0.7292	0.0027	0.7283	0.0018	0.7379	0.0114	0.6912	0.0353
16	14.6995	0.6345	0.6368	0.0023	0.6371	0.0026	0.6481	0.0136	0.5951	0.0394
17	15.1346	0.5345	0.5351	0.0006	0.5362	0.0017	0.5484	0.0139	0.4928	0.0417
18	15.5311	0.4275	0.4278	0.0003	0.4295	0.002	0.4417	0.0142	0.3885	0.039
19	15.8929	0.3185	0.32	0.0015	0.3188	0.0003	0.3308	0.0123	0.2837	0.0348
20	16.2229	0.2085	0.2108	0.0023	0.2074	0.0011	0.2184	0.0099	0.1815	0.027
21	16.5241	0.101	0.105	0.004	0.0961	0.0049	0.1065	0.0055	0.0821	0.0189
				IAE		IAE		IAE		IAE
				0.0439		0.0506		0.1298		0.6015

Table 5.10 Comparison of error functions with existing techniques for SDM, PWP 201

Method	AE	MAE	OF (RMSE)
h-SHO	0.0435	0.0019	2.3000E−3
h-SFO	0.1298	0.0057	0.0073
IADE [94]	NA	NA	2.4000E−3
ABC-DE [42]	NA	NA	2.4000E−3
R*cr*-IJADE[95]	4.1773E−2	NA	2.4250E−3
MPCOA [96]	3.9770E−2	NA	2.4250E−3
EHA-NMS [63]	4.1788E−2	NA	2.4250E−3
rbcNM (implicit)[97]	NA	NA	2.4251E−3
GOFPANM [98]	NA	NA	2.4251E−3
SATLBO [99]	NA	NA	2.4251E−3
CARO [100]	4.1970E−2	NA	2.4270E−3
CS [78]	NA	1.7284E−3	2.4300E−3
LI [101]	NA	1.8461E−3	2.4777E−3
SA [78]	5.0710E−2	2.0300E−3	2.6600E−3
Method in[102]	NA	NA	NA
PS [84]	5.6883E−2	2.2753E−3	3.0494E−3
Method in[103]	6.0079E−2	2.3107E−3	3.4527E−3
TLBO (a) [80]	1.1556E−1	4.4447E−3	5.4902E−3
Method in[22]	1.3185E−1	5.0710E−3	5.7485E−3
Method in[86]	NA	3.4840E−3	6.1300E−3
CPSO [104]	NA	5.0670E−3	6.2440E−3
Method in[33]	1.4648E−1	5.6337E−3	6.3402E−3
GA [77]	1.5348E−1	6.1392E−3	6.9829E−3

It is also important to understand that the proposed *h*-SHO method showcases more precise results, with less RMSE when compared with various existing techniques which are observed in table 5.10.

5.4.3 Case study 3: Comparison of Sharp ND-R250A5 (SDM and DDM) using *h*-SHO and *h*-SFO methodologies

As observed in previous cases similar results are highlighted for the third case study, where, for SDM the *h*-SHO exhibits high convergence speed *i.e.* nearly 50 iterations whereas, *h*-SFO takes about 80 iterations for the convergence *i.e.* is well observed from fig. 5.10 (c), for the SDM and fig. 5.11 (c) for DDM. Whereas for SDM the RMSE is recorded as 0.0127 and 0.0675 for *h*-SHO and *h*-SFO respectively, and 0.0113 and 0.0576 for DDM.

In contrast, higher-order errors are observed for *h*-SFO over *h*-SHO in fig. 5.10 (d) and fig. 5.11 (d), for SDM and DDM respectively, due to which the *I-V* and *P-V* characteristic through proposed *h*-SHO is more nearly aligned with the experimental characteristics when compared with the *h*-SFO, as shown in fig. 5.10 (a) and fig. 5.10 (b), for SDM, and fig. 5.11 (a) and fig. 5.11 (b) for DDM. Moreover, the estimated parameters for the SDM and DDM through *h*-SHO and *h*-SFO are listed in table 5.4, whereas various E_f values are also compared for SDM and DDM in table 5.11, which establishes the validation of the superiority of *h*-SHO over *h*-SFO technique for parameter estimation.

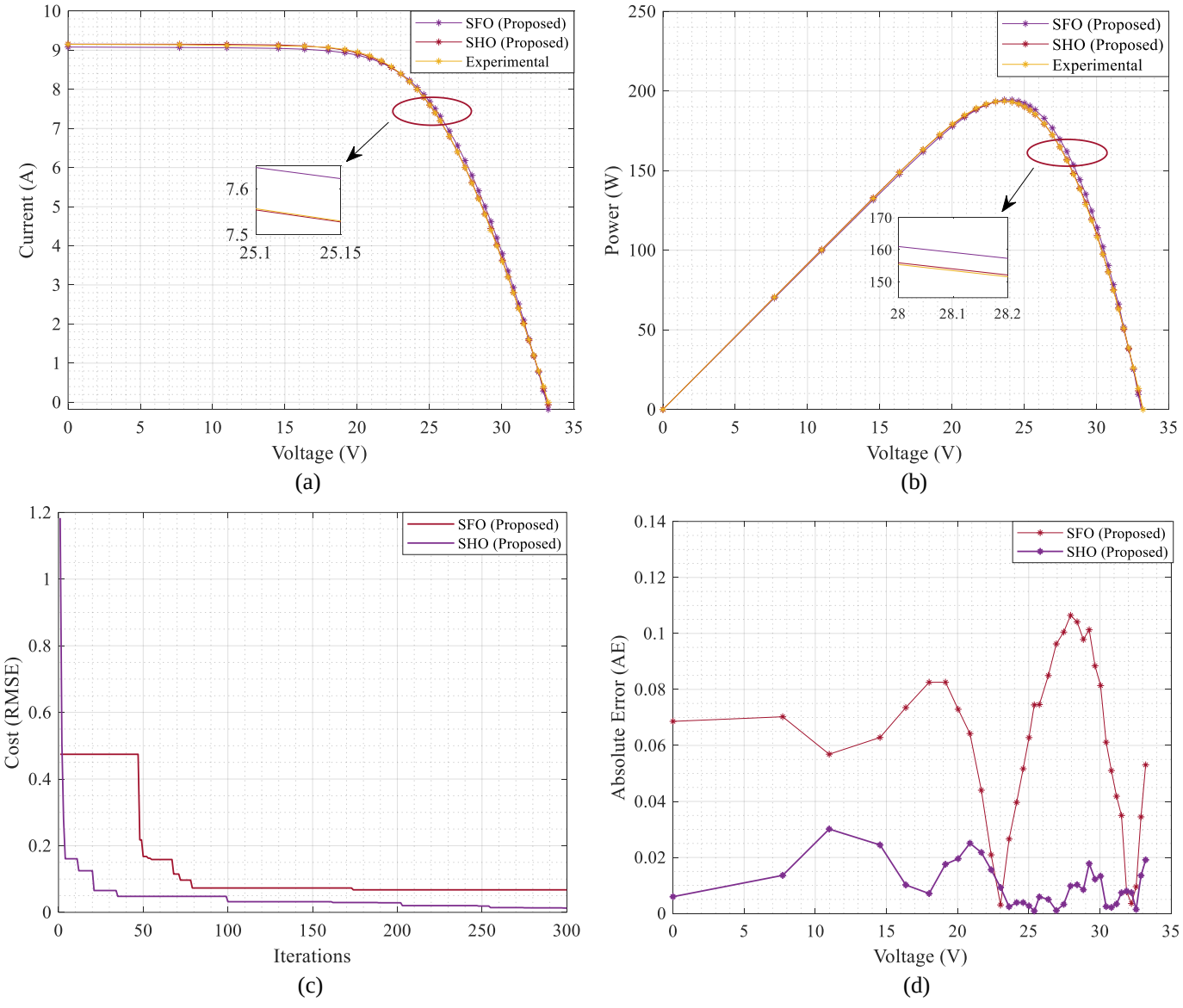

Fig. 5.10 Performance characteristics for Sharp ND-R250A5, SDM (a) Comparison of *I-V* with experimental characteristic, (b) *P-V* characteristic comparison (c) Variation of OF with iterations, (d) Absolute error curve

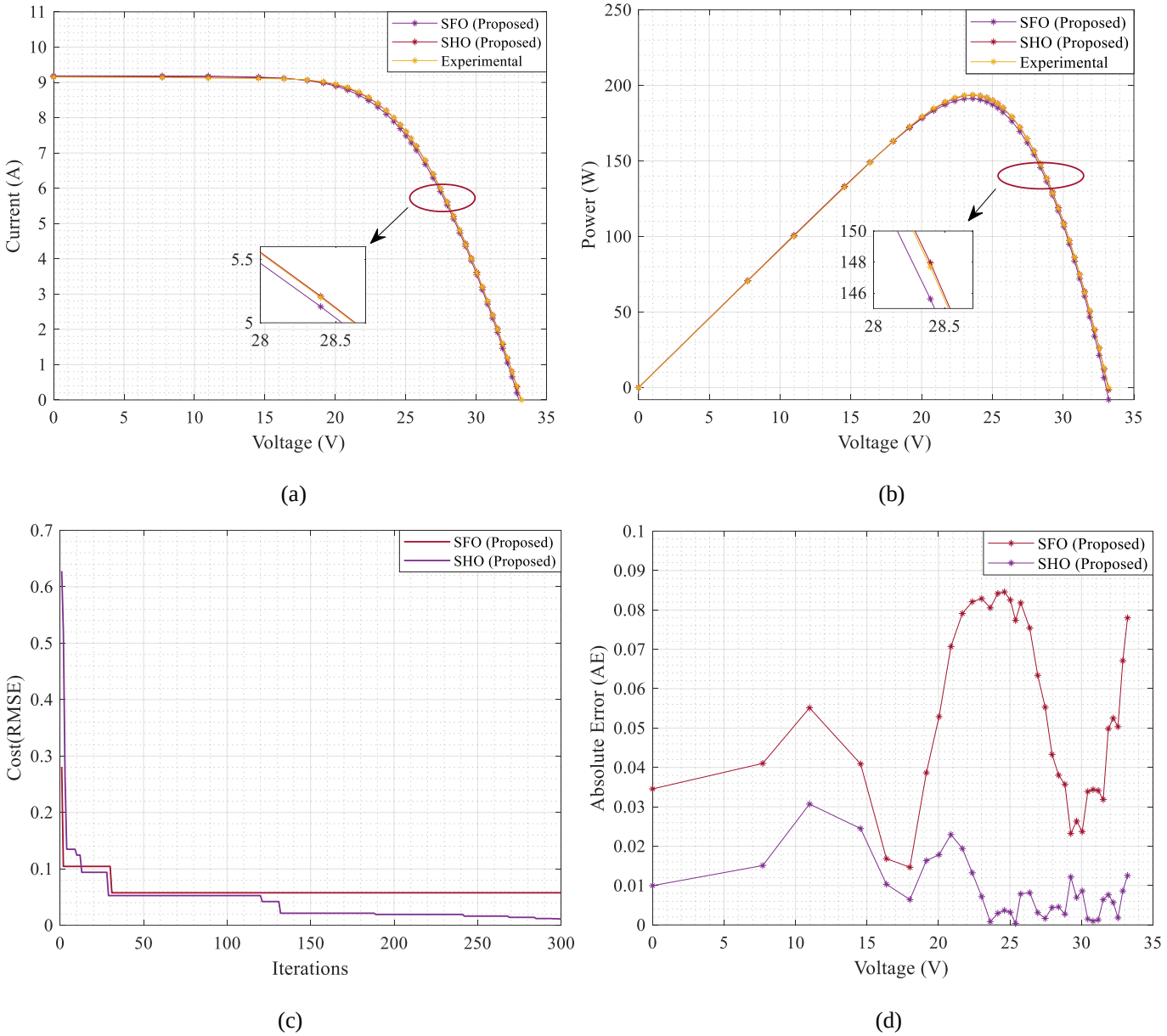

(a) (b)

(c) (d)

Fig. 5.11 Performance characteristics for Sharp ND-R250A5, DDM (a) Comparison of *I-V* with experimental characteristic, (b) *P-V* characteristic comparison (c) Variation of OF with iterations, (d) Absolute error

Table 5.11 Comparison of error functions for SDM and DDM, of sharp ND-R250A5

E_f	Sharp ND-R250A5			
	SDM	DDM	SDM	DDM
	(*h*-SHO)		(*h*-SFO)	
MAE	0.0102	0.0087	0.0609	0.0532
RMSE	0.0127	0.0113	0.0675	0.0576
MBE	0.0003	0.0009	0.0164	0.0428
SSE	0.0058	0.0046	0.1642	0.1195
NRME	0.0014	0.0012	0.0074	0.0063

5.4.4 Case study 4: Comparison of EIL 75W (SDM and DDM) using *h*-SHO and *h*-SFO methodologies

The experimental data for this case study is recorded by the authors and also referred to in chapter 4. In fig. 5.12 (a) and fig. 5.12 (b), the exactness of the proposed *h*-SHO method is observed through the congruence of *I-V* and *P-V* from the proposed *h*-SHO method with the experimental *I- V* and *P-V*, where the cost function is recorded as 0.0273 converged in approximately 30 iterations. As shown in fig. 5.12 (c), *h*-SFO takes about 150 iterations for convergence with an RMSE of 0.0848. Similarly, the performance of *h*-SHO outperforms the *h*-SFO technique of parameter estimation *i.e.* validated for DDM through fig. 5.13 (a) and fig. 5.13 (b), where a similar congruence of *h*-SHO with experimental *I-V* and *P-V* is observed. The

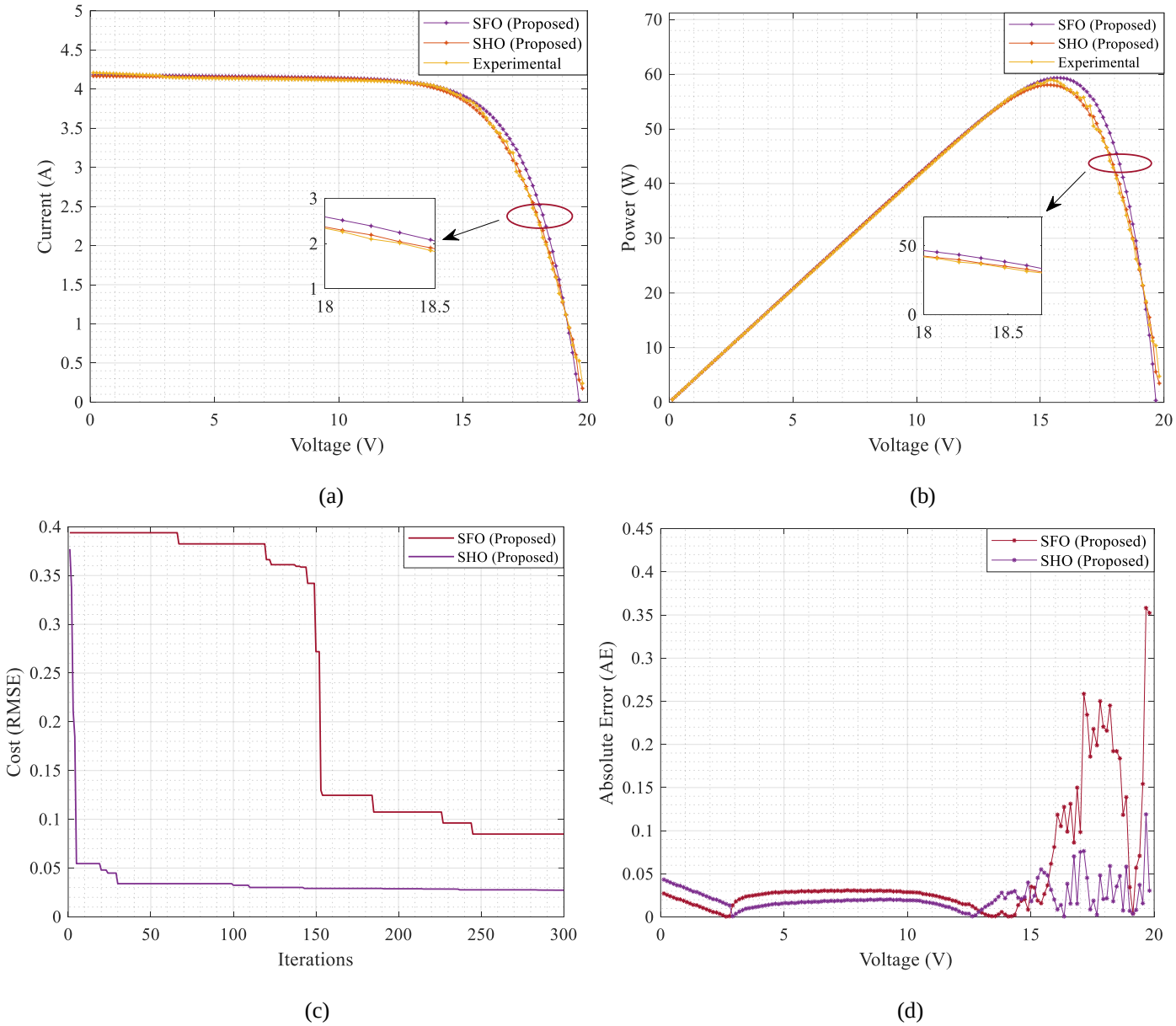

Fig. 5.12 Performance characteristics for EIL 75 W SDM (a) Comparison of *I-V* with experimental characteristic, (b) *P-V* characteristic comparison (c) Variation of OF with iterations, (d) Absolute error

convergence for the DDM takes 50 iterations for obtaining the minimum error, *i.e.* 0.0392 over the error of 0.0607, recorded through the *h*-SFO. The estimated parameters for the SDM and DDM are listed in table 5.4, whereas various E_{fs} are also listed in table 5.12, to exhibit the performance of the proposed method for the parameter estimation of EIL 75 W, SDM, and DDM.

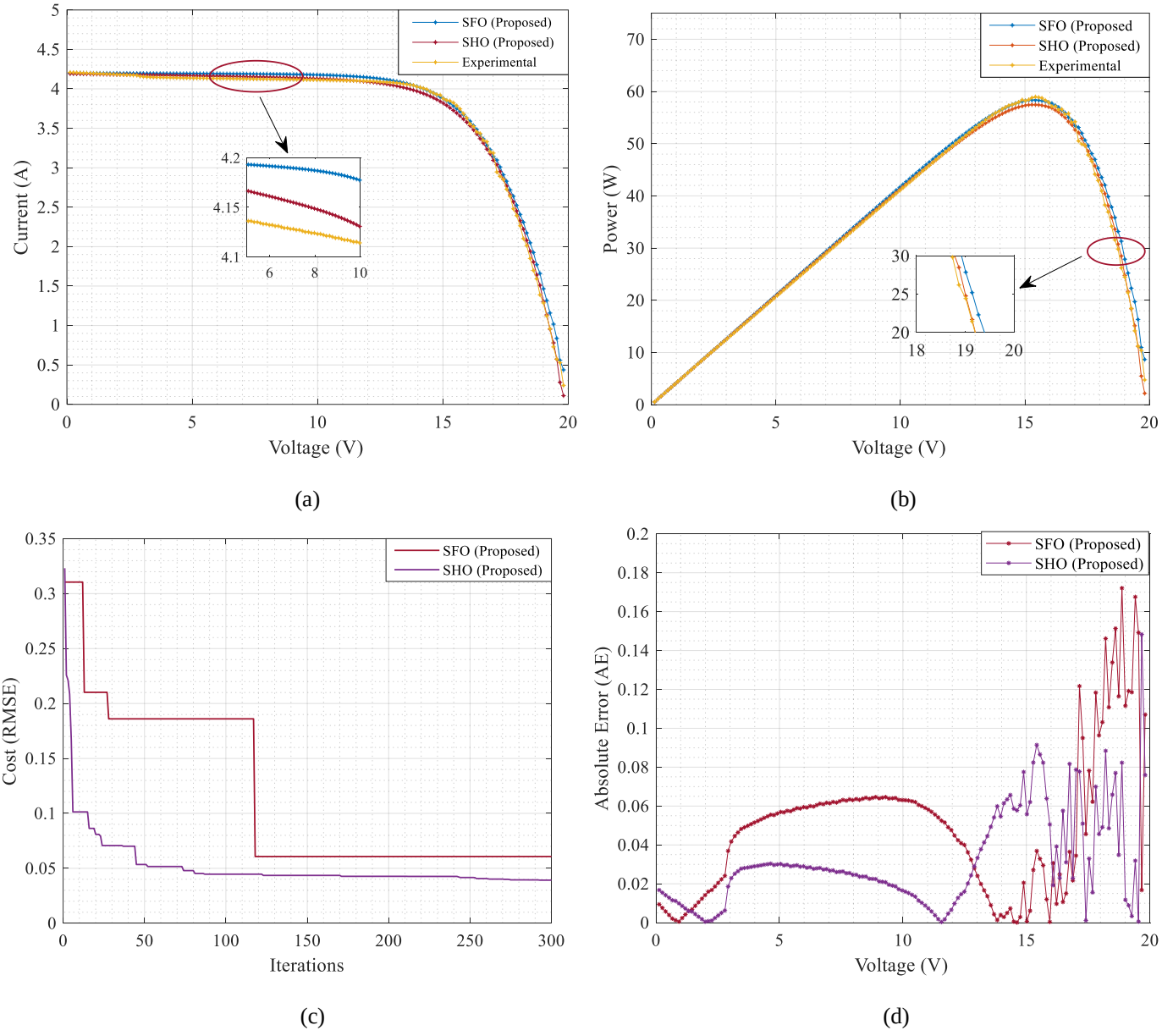

Fig. 5.13 Performance characteristics for EIL 75 W DDM (a) Comparison of *I-V* with experimental characteristic, (b) *P-V* characteristic comparison (c) Variation of OF with iterations, (d) Absolute error

Table 5.12 Comparison of error functions for SDM and DDM, of EIL 75W

E_f	EIL 75W			
	SDM	**DDM**	**SDM**	**DDM**
	(*h*-SHO)		(*h*-SFO)	
MAE	0.0222	0.0306	0.0502	0.0489
RMSE	0.0273	0.0392	0.0848	0.0607
MBE	0.0000	0.0005	0.0329	0.0449
SSE	0.1111	0.2291	1.0726	0.5496
NRME	0.0069	0.0099	0.0214	0.0153

5.4.5 Case study 5: Comparison of Sharp SFTI 60-P (SDM and DDM) using *h*-SHO and *h*-SFO methodologies

The experimental data for SFTI 60-P, is recorded, and already referred to in chapter 4, in this case, *h*-SHO exhibits a low RMSE of 0.0741 for SDM, when compared with the RMSE of 0.1492 through the *h*-SFO, and a similar scenario can be observed for the DDM *i.e.* well elaborated in table 5.13. High convergence with less error is the key feature of *h*-SHO, *i.e.* clearly observed for SDM and DDM in fig. 5.14 (c) and fig. 5.15 (c) respectively. Due to less error, the *I-V* and *P-V* characteristics are well in coordination with the experimental characteristics, which can be observed from fig. 5.14 (a) and fig. 5.14 (b) for SDM, whereas for the DDM fig. 5.15 (a) and fig. 5.15 (b) showcases comparatively higher errors. The estimated parameters for the SDM and DDM under various boundary conditions are well elucidated in table 5.4, for all the case studies.

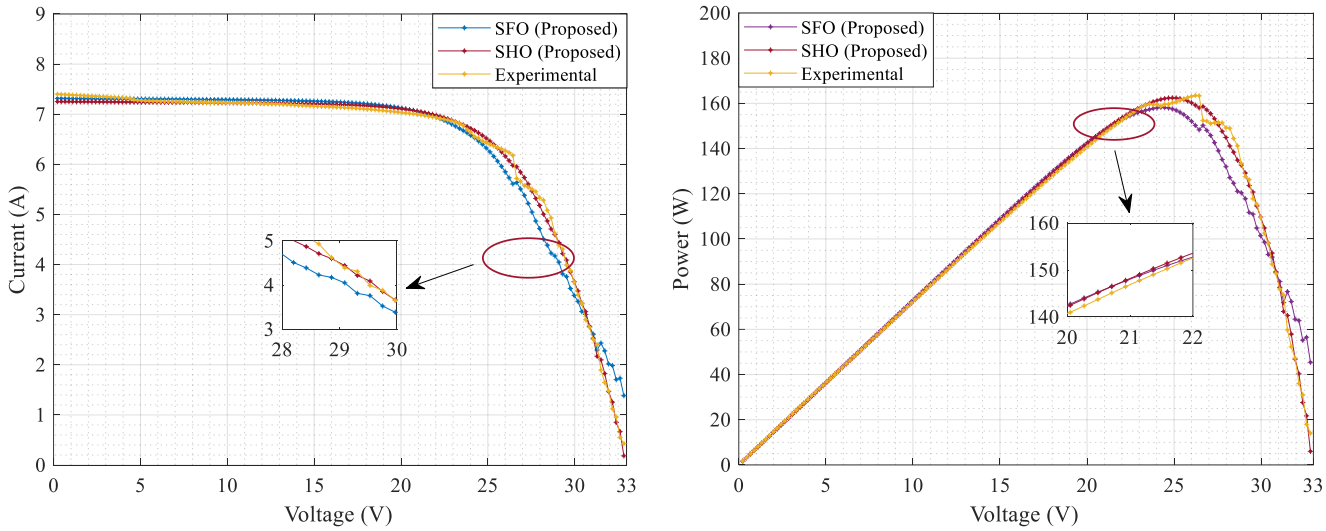

(a) (b)

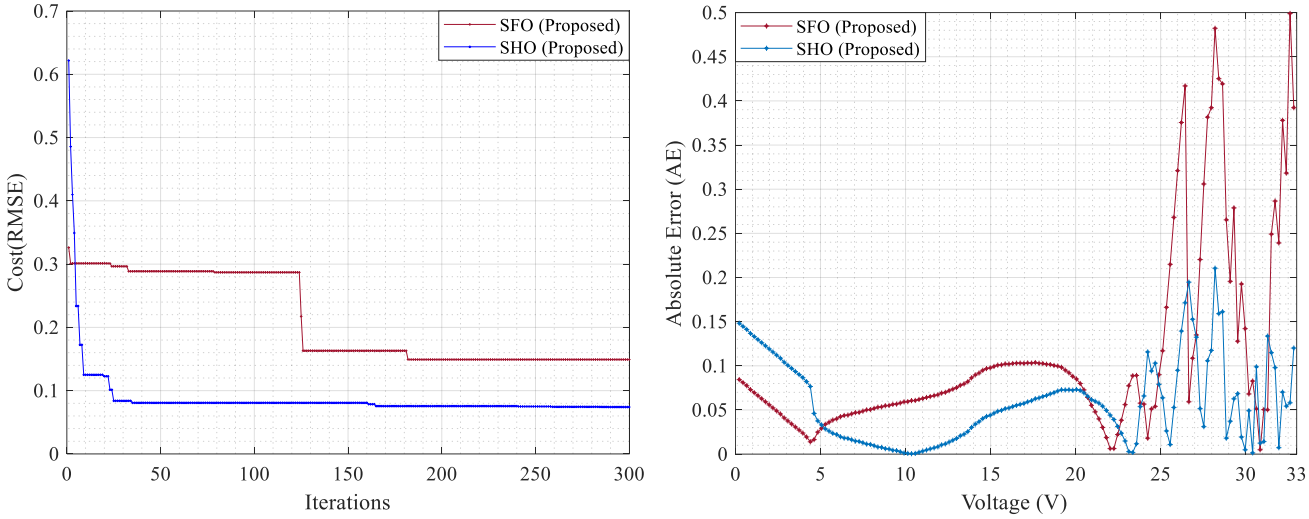

(c) (d)

Fig. 5.14 Performance characteristics for SFTI 60P DDM (a) Comparison of *I-V* with experimental characteristic, (b) *P-V* characteristic comparison (c) Variation of OF with iterations, (d) Absolute error

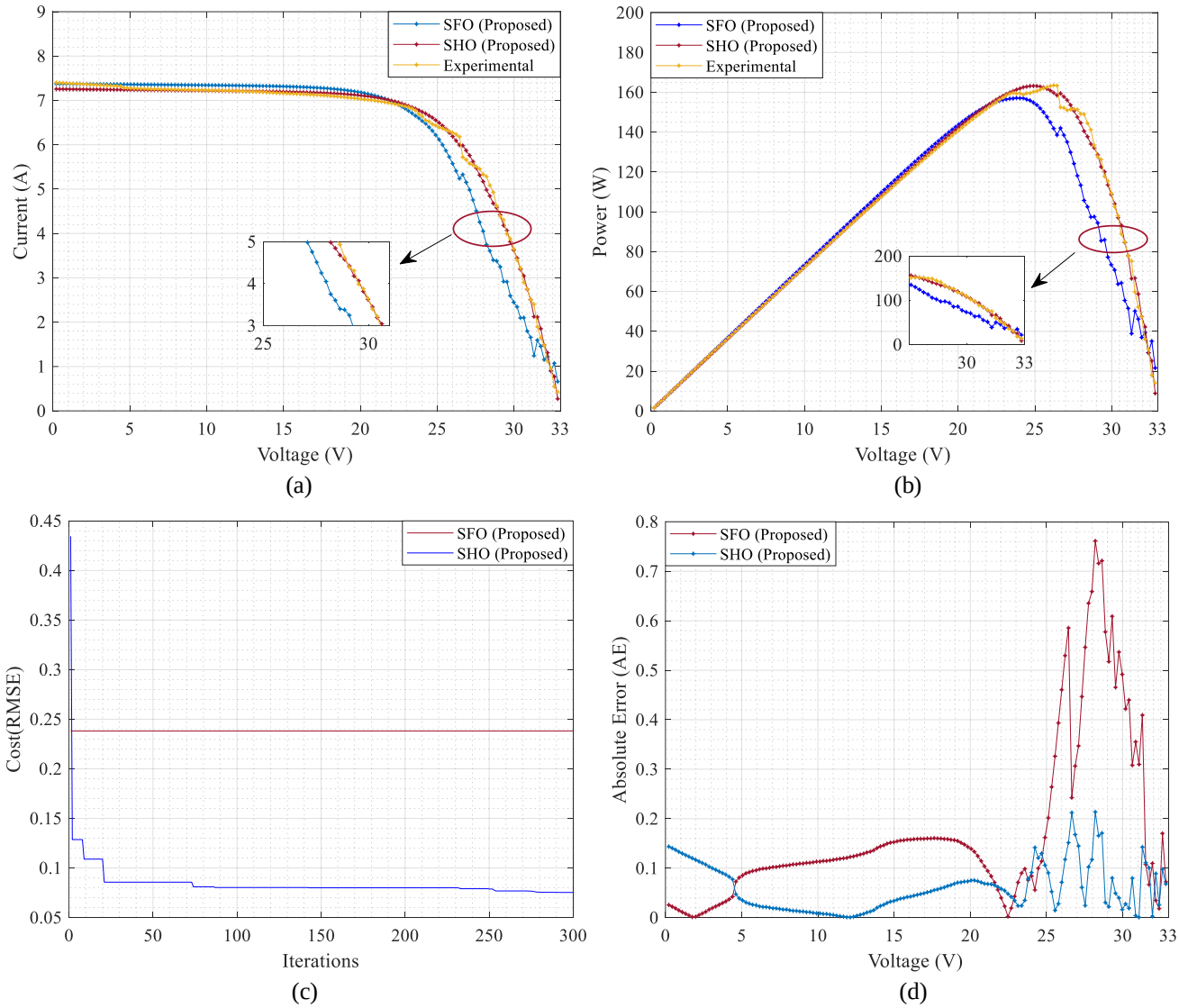

(a) (b) (c) (d)

Fig. 5.15 Performance characteristics for SFTI 60P DDM (a) Comparison of *I-V* with experimental characteristic, (b) *P-V* characteristic comparison (c) Variation of OF with iterations, (d) Absolute error

Table 5.13 Comparison of error functions for SDM and DDM, of SFTI 60P

E_f	SFTI 60-P			
	SDM	DDM	SDM	DDM
	(*h*-SHO)		(*h*-SFO)	
MAE	0.0576	0.0588	0.1071	0.1702
RMSE	0.0741	0.0753	0.1492	0.2382
MBE	0.0007	0.0001	0.0008	0.0299
SSE	0.8175	0.8449	3.3169	8.4519
NRME	0.0106	0.0108	0.0214	0.0342

5.4.6 Estimation of parameters for TDM using *h*-SHO methodology

In this section, the parameters are estimated using TDM through *h*-SHO, where the *I-V* and *P-V* characteristic for EIL75W is showcased in fig. 5.16 (a) and fig. 5.16 (b) respectively. Whereas, the performance characteristics for SFTI 60P are observed in fig. 5.17 (a) and fig. 5.17 (b), as it is evident from all the previous cases that *h*-SHO exhibits better convergence, and the same is observed in fig. 5.16 (c) and fig. 5.17 (c). Moreover, table 5.15, showcases higher RMSE values of 0.0058, 0.0502, and 0.0836 for PWP 201, EIL 75W, and SFTI 60P, respectively when compared with their respective SDM and DDM, in table 5.8, table 5.12, and table 5.13. So, in other words, we observe an increase in error with the increase in complexities associated with multi-diode models. The estimated parameters are well recorded in table 5.14.

Table 5.14 Estimated parameters for TDM

TDM						
S.No.	**'ρ'**	**RTC**	**PWP-201**	**Sharp ND-R250A5**	**EIL 75W**	**250 Watt**
1	I_{ph}	0.758538	1.040397	9.2055269	4.204162	7.307259
2	I_{s1}	1e-05	5.937251e-06	2.7009359e-06	5.300989e-06	8.64069e-06
3	I_{s2}	5.25353e-06	4.500185e-06	4.908462e-06	6.559105e-06	4.4006e-06
4	I_{s3}	5.42525e-07	1.064629e-12	9.8245738e-07	7.242609e-06	1.61287e-06
5	α_1	2.06986	1.515146	1.5694572	1.637246	1.371448
6	α_2	2.09143	1.912438	1.7217137	1.213168	1.3236
7	α_3	2.04085	2.167281	1.3890479	2.108739	2.14507
8	R_{se}	0.0011645	1.078282	0.55762356	0.249166	0.34041
9	R_{sh}	62.8079	531.2654	4739.1579	177.956	180.8418

Table 5.15 Comparison of error functions for TDM

TDM				
S.No	E_f	**PWP-201**	**EIL 75W**	**250 Watt**
1	MAE	0.0051	0.0369	0.0582
2	RMSE	0.0058	0.0502	0.0836
3	MBE	0.0001	0.0004	0.0005
4	SSE	0.0008	0.3751	1.0418
5	NRME	0.0043	0.0126	0.0120

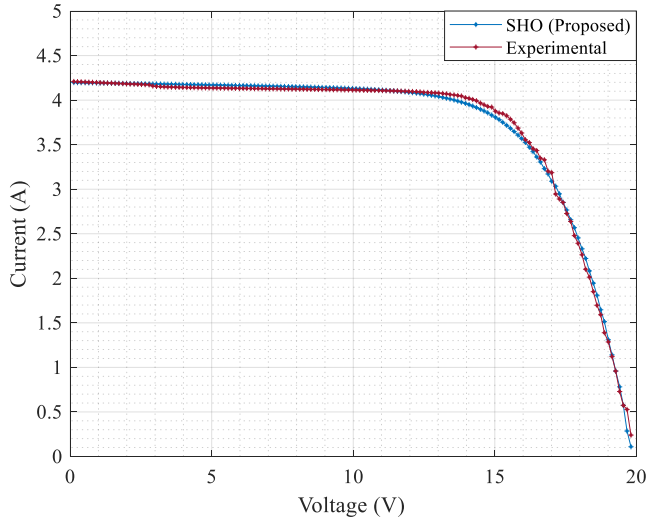

(a)

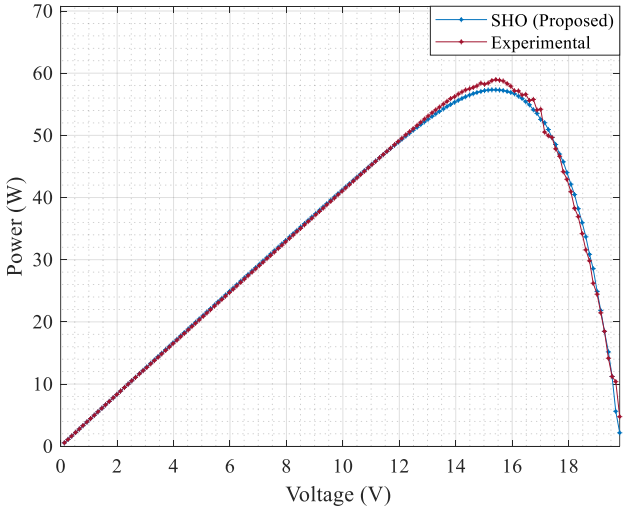

(b)

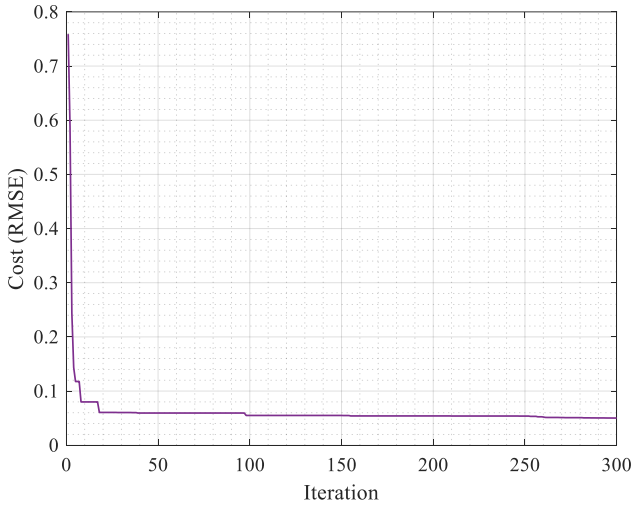

(c)

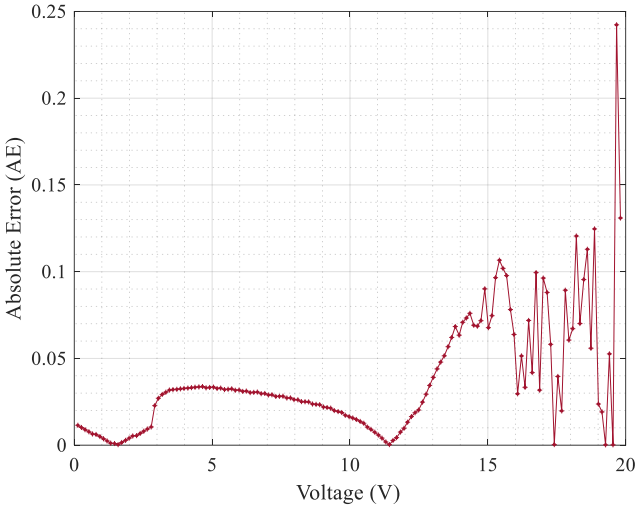

(d)

Fig. 5.16 Performance characteristics for EIL 75W TDM (a) Comparison of *I-V* with experimental characteristic, (b) *P-V* characteristic comparison (c) Variation of OF with iterations, (d) Absolute error

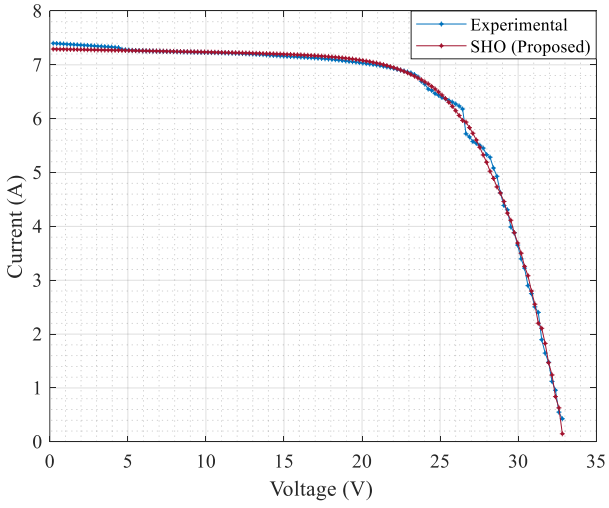

(a)

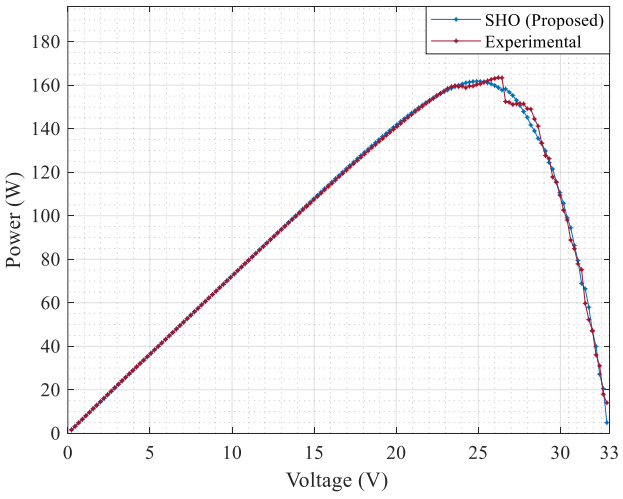

(b)

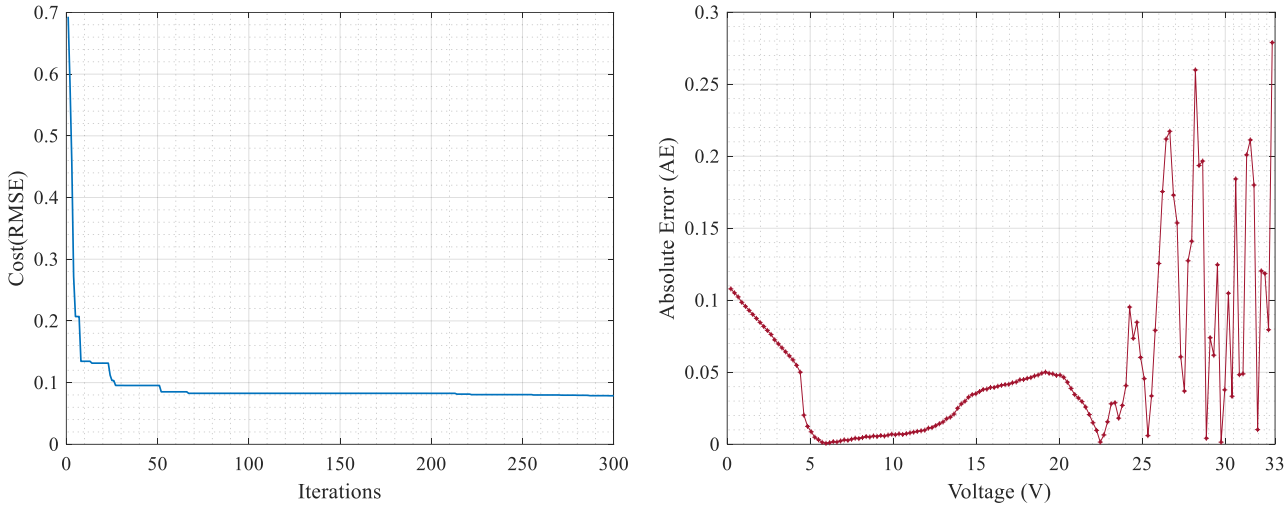

(c) (d)

Fig. 5.17 Performance characteristics for SFTI 60P TDM (a) Comparison of *I-V* with experimental characteristic, (b) *P-V* characteristic comparison (c) Variation of OF with iterations, (d) Absolute error curve

5.5 Chapter summary

This chapter presents a comparative analysis of two-hybrid approaches based on two new metaheuristic algorithms, *i.e.* SFO and SHO framework along with the NRM to estimate, precisely and quickly, the unknown parameter set for the mathematical models of the solar PV cell, module, or array. Both approaches were implemented by using the experimental dataset, to estimate the unknown parameters of the SDM and DDM. The NRM is incorporated with the SHO and SFO technique to estimate the current, where the estimated and experimental current is responsible for the evaluation of objective function *i.e.* the RMSE, and the proposed techniques are modified to hybrid SHO (*h*-SHO) and hybrid SFO (*h*-SFO). The validation of the proposed methodologies is carefully carried out through five different case studies, three case studies are extensively analyzed in various literature, whereas to examine the proposed methodologies the fourth and fifth case studies are performed with real outdoor experimental datasets recorded by the authors. For case study 1, the RMSE values of SDM are compared with *h*-SFO and a few existing techniques in the literature, and observed that the *h*-SHO methodology exhibits more promising results. The *I-V* and *P-V* characteristics of both SDM and DDM that are carried out through *h*-SHO, match more closely with the experimental data when compared with *h*-SFO, which showcases the preciseness of the proposed *h*-SHO methodology. Moreover, *h*-SHO exhibits high convergence when compared with *h*-SFO, and the same is observed with all case studies considered. With these case studies, we conclude that the *h*-SHO and *h*-SHO are among the newest, modern, and precisely tuned methods for the mathematical model parameter

estimation of solar PV cells, modules, or arrays, where *h*-SHO exhibits high converging ability, gives less erroneous results, under the same sets of boundary and environmental conditions when compared with the *h*-SFO and other well-known techniques in the literature. The parameters are also estimated for the TDM, using *h*-SHO where the complexity associated with the multi-diode models results in higher RMSE.

Chapter 6

CONCLUSION AND FUTURE SCOPE

6.1 Conclusions

This chapter includes the significant observations concluded through this research, which contributes toward a continuously developing field of renewable energy sources, where prominence is given to solar photovoltaics. Various observations are outlined in this section as,

1) With the growing challenges in the field of solar photovoltaics, the need for various simulation softwares are evolved, where the accuracy and robustness reside on the electrical PV model selected, the model parameter extraction technique incorporated, and the preciseness in estimated model parameters through various techniques. Hence, in this research SDM, DDM and TDM are selected and modeled for different case studies under different sets of environmental conditions through various modern metaheuristic and hybrid techniques.
2) Primarily, an Emperor penguin optimizer is considered for the parameter estimation problem, where the parameters are estimated for the KC200GT, PWP201, and STP6 120-36 solar PV arrays using SDM. Where it is asserted that the proposed method explores the objective of identifying minimum RMSE for the estimated output current when validated with the experimental data. The performance characteristics for the proposed case studies are also compared with well-established techniques like Hybrid BPFPA, ITLBO, ImCSA, ABSA, PG-Jaya, and ISCE through their *I-V* and *P-V* performance characteristics. Moreover, the impact of '*T*' and '*G*' on the estimated parameters is also recorded.
3) Moreover, the parameters are also estimated for six polycrystalline solar PV through SDM, DDM, and TDM, by using the *pv*-BWO and *cn*-BWO techniques. In the proposed methods two different aspects *i.e.* pheromone and cannibalism of the Black widow spider's lifecycle is considered. A comparative study is showcased that concludes the fast convergence ability of the *cn*-BWO algorithm over *pv*-BWO, whereas the preciseness in the estimated parameters is well established with the *pv*-BWO. The preciseness of the *pv*-BWO methodology for the parameter estimation is also validated with experimental *I-V* and *P-V* datasheet of the modules under consideration and also with well-engrained techniques for parameter estimation in literature *i.e.* GA, TLBO, MBA, PS, and NRM.

4) The exactness of the estimated parameters exists in the experimental data considered for comparison, hence to establish the accuracy of the proposed method, 149 pair experimental data is also recorded for EIL 75 W and SFTI 60P through the MECO9018BT PV analyser. The recorded data is considered to estimate the parameters of over mentioned modules, where SDM, DDM, and TDM parameters are extracted.
5) Literature suggests hybrid techniques as the most recent methodologies among researchers for parameter estimation, hence NRM is incorporated to estimate accurate solar PV output current. Accurate estimation of current results in the upsurge in the precision of RMSE identification which inturn increases the preciseness of the parameter estimation process. The NRM is further incorporated with SFO and SHO methodologies, where it is asserted on the basis of five case studies that *h*-SHO exhibits better convergence speed along with precise results when compared with *h*-SFO, IADE, MPCOA, ABC-DE, SA, TLBO, R*cr*-IJADE, LI, CS, CPSO, GA, etc. The comparison is carried out with the experimental *I-V* and *P-V* performance characteristics and various error functions *i.e.* RMSE, MAE, MBE, SSE, and NRME.
6) In all the methodologies it is observed that the complexities increase with an increase in the number of unknown parameters that are to be extracted, *i.e.* DDM and TDM over SDM, resulting in high computational time and computation cost, irrespective of the technique under consideration.

6.2 Future scope

Research is a multifarious and continuous endeavor, where the scope of enhancement is always accessible. After the successful accomplishment of Doctoral research work on 'Modeling and Parameter Estimation of Solar Photovoltaic Array' there is still scope for further research that is listed as,

1) A single-window user interface can be developed, where the user can easily enable to select the equivalent model to be used, the techniques to be implemented for parameter estimation, and analyse the comparison with the experimental data altogether.
2) Hybrid techniques are the most recent techniques for the parameter estimation problem where more exploration is still needed.
3) The availability of array data for research is still limited, hence the datasets for the arrays also can be recorded for standard modules.
4) The strategies can be developed for parameter estimation when different types of modules are connected to form an array.

LIST OF PUBLICATIONS

Journal Publication (SCI/SCIE)

1 Abhishek Chauhan and Surya Prakash, "A new emperor penguin optimization-based approach for solar photovoltaic parameter estimation" **Wiley: *International Transactions on Electrical Energy Systems***, vol. 31, issue 7, 3 May. 2021. **(IF: 2.63)**
DOI: doi.org/10.1002/2050-7038.12917.

2 Abhishek Chauhan and Surya Prakash, "Parameter Estimation and Analysis of Photovoltaics through a Hybrid Emperor Penguin Optimisation Approach under Different Environmental Constraints", Taylor and Francis: ***IETE Journal of Research***, vol. xx, no. xx, pp. xx, 18 Jul. 2021. **(IF: 2.33)**
DOI: doi.org/10.1080/03772063.2021.1951378.

3 Abhishek Chauhan & Surya Prakash, **"**A Novel Black Widow Optimisation Approach to Improve the Precision in Parameter Estimation Problem of Solar Photovoltaic Electrical Model", ***WILEY: Environmental Progress and Sustainable Energy,*** vol. xx, no. xx, pp. xx, e13846, 19 Mar. 2022, **(IF: 2.82)**
DOI: doi.org/10.1002/ep.13846, 2022.

4 Abhishek Chauhan & Surya Prakash, **"**Comparison and Performance Analysis of Pheromone Value and Cannibalism based Black Widow Optimisation Approaches for Modelling and Parameter Estimation of Solar Photovoltaic Mathematical Models", ***Elsevier: International Journal for Light and Electron Optics (Optik),*** *vol. 259,* Issn: 0030-4026, **(IF: 2.84)**
DOI: doi.org/10.1016/j.ijleo.2022.168943, 2022.

Book Chapter

Abhishek Chauhan and Surya Prakash, "Parameter Estimation of Solar Photovoltaic and Impact of Environmental Conditions on its Performance", ***World Scientific: Handbook of Renewable Energy Technology & Systems***, pp. 201–234, 14 Nov. 2021.
DOI: doi.org/10.1142/9781786349033_0008.

Conference

Abhishek Chauhan and Surya Prakash, "Considering Various Equivalent Circuits for Solar PV Array Modelling," *2nd IEEE International Conference on Power, Energy and Environment: Towards Smart Technology (ICEPE),* NIT Meghalaya, *pp*. 1-6, 2018.
DOI: doi.org/10.1109/EPETSG.2018.8658741.

SCI Journal (Revision Submitted)

Abhishek Chauhan and Surya Prakash**,** "Comparison of Nature Inspired Metaheuristic and Hybrid Approaches for Modeling and Equivalent Parameter Estimation of solar photovoltaics", ***Wiley: International Journal of Numerical Modelling: Electronic Networks, Devices, and Fields.***

REFERENCES

[1] S. Madan, S. Manimuthu and S. Thiruvengadam, "History of electric power in India (1890-1990)," *2007 IEEE Conference on the History of Electric Power*, 2007, pp. 152-165, doi: 10.1109/HEP.2007.4510263.

[2] *Total generation capacity*, https://www.powermin.gov.in/en/content/generation-capacity, accessed on 31/Aug/2021.

[3] Masters G.M, "Photovoltaic Materials and Electrical Characteristics", in *Renewable and Efficient Electric Power System*, 3rd Edition, John Wiley & Sons, Hoboken, New Jersey, 2004.

[4] Yetayew TT and Jyothsna TR, "Parameter extraction of photovoltaic modules using newton Raphson and simulated annealing techniques", in *proc. IEEE International Conference on Power, Communication, Information and Technology*, Bhubaneswar, India, *pp.* 239-244, Mar. 2015.

[5] Ulapane NN *et al*., "Extraction of parameters for simulating photovoltaic panels, *in proc. 6th IEEE International Conference on Industrial and Information Systems (ICIIS 2011)*", Kandy, Srilanka, pp. 539-544, Oct. 2011.

[6] Jordehi A.R, "Parameter estimation of solar photovoltaic (PV) cells: A review", in *Elsevier: Renewable and Sustainable Energy Reviews*, pp. 354-371, 2016.

[7] Jordehi A. R., "Maximum power point tracking in photovoltaic (PV) systems: A review of different approaches," *Renewable and Sustainable Energy Reviews*, *vol.* 65. Elsevier Ltd, *pp.* 1127–1138, *doi:* 10.1016/j.rser.2016.07.053, Nov. 01, 2016.

[8] Nunes H. G. G *et. al.*, "A new high-performance method for determining the parameters of PV cells and modules based on guaranteed convergence particle swarm optimization," *Applied Energy*, *vol.* 211, *pp.* 774–791, Feb. 2018.

[9] Jadli U, Thakur P, and Shukla R. D., "A new parameter estimation method of solar photovoltaic," *IEEE Journal of Photovoltaics*, *vol.* 8, no. 1, *pp.* 239-247, Jan. 2018.

[10] Rawat, N., Thakur, P., & Singh, A. K., "A novel hybrid parameter estimation technique of solar PV", *International Journal of Energy Research*, er.7485, 2021.

[11] Das, V., Karuppanan, P., Singh, A. K., & Thakur, P, "Optimal Sizing and Control of Solar PV-PEMFC Hybrid Power Systems", *International Journal of Mathematical, Engineering and Management Sciences*, vol. 6, no. 4, 2021.

[12] A. Chauhan and S. Prakash, "Considering Various Equivalent Circuits for Solar PV Array Modelling," *2018 2nd International Conference on Power, Energy and Environment: Towards Smart Technology (ICEPE)*, 2018, *pp.* 1-6.

[13] M. Badoni, A. Singh, S. Pandey and B. Singh, "Fractional-Order Notch Filter for Grid-Connected Solar PV System with Power Quality Improvement," in *IEEE Transactions on Industrial Electronics*, vol. 69, no. 1, pp. 429-439, Jan. 2022, doi: 10.1109/TIE.2021.3051585.

[14] Saxena, H., Singh, A., Rai, J. N., & Badoni, M., "PV integrated grid synchronization technique using modified SOGI-FLL and zero-crossing detector", *Electrical Engineering*, pp. 1–12, 2021.

[15] Mishra, S., Pullaguram, D., Buragappu, S. A., & Ramasubramanian, D, "Single-phase synchronverter for a grid connected roof top photovoltaic system", *IET Renewable Power Generation*, vol. 10, no. 8, pp.1187–1194, 2016.

[16] G.R Walker, "Evaluating MPPT converter topologies using a MATLAB PV model", in *Journal of Electrical and Electronics Australia*, vol. 21, no.1, pp. 49-55, 2001.

[17] K. Ding, X. Bian, H. Liu and T. Peng, "A MATLAB simulink based PV module model and its application under conditions of non-uniform irradiance", in *IEEE Trans. of Energy Conv.*, vol. 27, issues: 4, pp. 864-872, Dec. 2012.

[18] M. A., Torres, J. L., Prieto, E., & Garcia, A, "Selecting a suitable model for characterizing photovoltaic devices", *Renewable Energy, vol. 25,* issue 3, *pp.* 371-380.

[19] Brano, V., Orioli, A., Ciulla, G., & di Gangi, A., "An improved five-parameter model for photovoltaic modules", *Solar Energy Materials and Solar Cells*, vol. *94*, issue 8, pp. 1358-1370, 2010.

[20] A. Orioli and A.D Gangi, "A procedure to calculate the five-parameter model of crystalline silicon photovoltaic modules on the basis of the tabular performance data", in *Elsevier: Applied Energy*, vol. 102, pp. 1160-1177, 2013.

[21] A. Chouder *et al.*, "Modeling and simulation of a grid connected PV system based on the evaluation of main PV module parameters", in *Elsevier: Simulation Model Practice and Theory*, vol. 20, issue 1, pp. 46-58, Jan. 2012.

[22] O. Mares, M. Paulescu and V. Badescu, "A simple but accurate procedure for solving the five-parameter model", in *Elsevier: Energy Conversion and Management*, vol. 105, pp. 139-148, Nov 2015.

[23] J. Bai *et.al.*, "Development of a new compound method to extract the five parameters of PV modules", in *Elsevier: Energy Conversion and Management,* vol. 79, pp. 294-303, Mar. 2014.

[24] D. Sera, R. Teodorescu and P. Rodriguez, "PV panel model based on datasheet values", in *proc. IEEE International Symposium on Industrial Electronics (ISIE 2007)*, Vigo, Spain, pp. 2392-2396, 2007.

[25] F. Adamo *et al*., "Parameters estimation for a model of photovoltaic panels", in *proc. 11th IMEKO World Congress Fundamental Applied Metrology*, Lisbon, Portugal, Sept. 2009.

[26] Hansen C. Parameter Estimation for Single Diode Models of Photovoltaic Modules, Sandia National Laboratories, Albuquerque, NM, Forthcoming; 2015.

[27] Bashahu, M., & Nkundabakura, P., "Review and tests of methods for the determination of the solar cell junction ideality factors", *Solar Energy*, vol. 81, issue 7, pp. 856–863.

[28] Ortiz-Conde, A., Garcia-Sanchez, F. J., Muci, J., & Sucre-Gonzalez, A, "A review of diode and solar cell equivalent circuit model lumped parameter extraction procedures", *Facta Universitatis-Series: Electronics and Energetics*, vol. 27, issue 1, pp. 57–102, 2014.

[29] Cotfas, D. T., Cotfas, P. A., & Kaplanis, S., "Methods to determine the dc parameters of solar cells: A critical review", *Renewable and Sustainable Energy Reviews*, vol. 28, pp. 588-596, 2013.

[30] Li, Y., Huang, W., Huang, H., Hewitt, C., Chen, Y., Fang, G., & Carroll, D. L., "Evaluation of methods to extract parameters from current-voltage characteristics of solar cells", *Solar Energy*, vol. 90, pp. 51-57.

[31] A. A Elbaset, H. Ali and M. Abd-El Sattar, "Novel seven-parameter model for photovoltaic modules", in *Elsevier: Solar Energy Materials and Solar Cells*, vol. 130, pp. 442-455, Nov. 2014.

[32] Kumar, A., Jha, B. K., Singh, D., & Misra, R. K., "Current injection-based Newton–Raphson power-flow algorithm for droop-based islanded microgrids", *IET Generation, Transmission & Distribution*, vol. *13, no.* 23, pp. 5271–5283, 2019.

[33] L Peng, Y Sun and Z Meng, "An improved model and parameters extraction for photovoltaic cells using only three state points at standard test condition", in *Elsevier: Journal of Power Sources*, vol. 248, pp. 621-631, Feb. 2014.

[34] A. A Elbaset, H. Ali and M. Abd-El Sattar, “Novel seven-parameter model for photovoltaic modules”, in *Elsevier: Solar Energy Materials and Solar Cells*, vol. 130, pp. 442-455, Nov. 2014.

[35] D. Singh and K. S. Verma, "Multiobjective Optimization for DG Planning With Load Models," in *IEEE Transactions on Power Systems*, vol. 24, no. 1, pp. 427-436, Feb. 2009.

[36] Oliva, D., Cuevas, E., & Pajares, G., “Parameter identification of solar cells using artificial bee colony optimization”, *Energy*, vol. 72, pp. 93-102, 2014.

[37] Karaboga, D., & Basturk, B., “A powerful and efficient algorithm for numerical function optimization: artificial bee colony (ABC) algorithm”, *Journal of Global Optimization*, vol. 39, pp. 459-471, 2007.

[38] A. Formisano, J.C Hernandez, C. Petrarca and F. Sanchez-Sutil, “Modelling of PV module and DC/DC converter assembly for the analysis of induced transient response due to nearby lightning strike”, *Electronics*, vol. 10, 2021.

[39] M. G. Villalva, J. R. Gazoli, and E. R. Filho, “Comprehensive approach to modelling and simulation of photovoltaic arrays,” *IEEE Transactions on Power Electronics*, vol. 24, no. 5, pp. 1198–1208, 2009.

[40] Muhsen, D. H., Ghazali, A. B., Khatib, T., & Abed, I. A., “Extraction of photovoltaic module model’s parameters using an improved hybrid differential evolution/electromagnetism-like algorithm”, *Solar Energy*, vol. 119, pp. 286-297, 2015.

[41] Ishaque, K., Salam, Z., Mekhilef, S., & Shamsudin, A, “Parameter extraction of solar photovoltaic modules using penalty-based differential evolution”, *Applied Energy*, vol. 99, pp. 297-308, 2012.

[42] Gong, W., & Cai, Z., “Parameter extraction of solar cell models using repaired adaptive differential evolution”, *Solar Energy*, vol. 94, pp. 209-220, 2013.

[43] Khanna, V., Das, B. K., Bisht, D., Vandana, & Singh, P. K., “A three diode model for industrial solar cells and estimation of solar cell parameters using PSO algorithm”, *Renewable Energy*, vol. 78, pp. 105–113, 2015.

[44] Goyal, S., Nijhawan, P., & Ganguli, S., “A Harris Hawks Optimization (HHO)-Based Parameter Assessment for Modified Two-Diode Model of Solar Cells”, *Green Energy*, pp. 319–343, 2020.

[45] L.L Jiang, D.L Maskell and JC Patra, “Parameter estimation of solar cells and modules using an improved adaptive differential evolution algorithm”, in *Elsevier: Applied Energy*, vol. 112, pp. 185-193, 2013.

[46] Allam, D., Yousri, D. A., & Eteiba, M. B, "Parameters extraction of the three diode model for the multi-crystalline solar cell/module using Moth-Flame Optimization Algorithm", *Energy Conversion and Management*, vol. 123, pp. 535-548, 2016.

[47] Ali, E. E., El-Hameed, M. A., El-Fergany, A. A., & El-Arini, M. M., "Parameter extraction of photovoltaic generating units using multi-verse optimizer", *Sustainable Energy Technologies and Assessments*, vol. 17, pp. 68-76, 2016.

[48] Yu, K., Liang, J. J., Qu, B. Y., Chen, X., & Wang, H, "Parameters identification of photovoltaic models using an improved JAYA optimization algorithm", *Energy Conversion and Management*, vol. 150, pp. 742-753, 2017.

[49] Kler, D., Sharma, P., Banerjee, A., Rana, K. P. S., & Kumar, V, "PV cell and module efficient parameters estimation using Evaporation Rate based Water Cycle Algorithm", *Swarm and Evolutionary Computation*, vol. 35, pp. 93-110, 2017.

[50] Kang, T., Yao, J., Jin, M., Yang, S., & Duong, T, "A Novel Improved Cuckoo Search Algorithm for Parameter Estimation of Photovoltaic (PV) Models", *Energies*, vol. 11, 2018.

[51] G., Zhang, J., Shi, D., & He, Y, "Parameter extraction of solar photovoltaic models using an improved whale optimization algorithm", *Energy Conversion and Management*, vol. 174, pp. 388-405, 2018.

[52] Premkumar. M., Babu Thanikanti Sudhakar, Umashankar Subramaniam, Sowmya R., "A new metaphor-less algorithms for the photovoltaic cell parameter estimation", *Optik*, vol. 208, 164559, 2020.

[53] Hongliang Zhang, Ali Asghar Heidari, Mingjing Wang, Lejun Zhang, Huiling Chen, Chengye Li, "Orthogonal Nelder-Mead moth flame method for parameters identification of photovoltaic modules", *Energy Conversion and Management*, vol. 211, 112764, 2020.

[54] Ridha, H.M, Gomes, C. & Hizam, H, "Estimation of photovoltaic module model's parameters using an improved electromagnetic-like algorithm", *Neural Computer & Application*, vol. 32, pp. 12627-12642, 2020.

[55] Hsieh Y, Yu. L, Chang T, Liu W, Wu T, and Moo C., "Parameter Identification of One-Diode Dynamic Equivalent Circuit Model for Photovoltaic Panel," in *IEEE Journal of Photovoltaics*, vol. 10, no. 1, pp. 219-225, Jan. 2020.

[56] Sheng, H. Li, C. Wang, H. Yan, Z. Xiong, Y. Cao, Z. Kuang, Q, "Parameters Extraction of Photovoltaic Models Using an Improved Moth-Flame Optimization", *Energies*, vol. 12, 3527, 2019.

[57] Gupta, J., Nijhawan, P., & Ganguli, S., "Parameter extraction of solar PV cell models using novel metaheuristic chaotic tunicate swarm algorithm", *International Transactions on Electrical Energy Systems*, vol. 31, no. 12, 2021.

[58] M. Ismail, M. Moghavvemi and T. Mahlia, "Characterization of PV panel and global optimization of its model parameters using genetic algorithm", in *Elsevier: Energy Conversion and Management*, vol. 73, pp. 10-25, 2013.

[59] A.M Dizqah, A. Maheri and K. Busawon, "An accurate method for the PV model identification based on a genetic algorithm and the interior-point method", in *Elsevier: Renewable Energy*, vol. 72, pp. 212-222, 2014.

[60] N. Rajasekar, N.K Kumar and R. Venugopalan, "Bacterial foraging algorithm based solar PV parameter estimation", in *Elsevier: Solar Energy*, vol. 97, pp. 255-265, Nov. 2013.

[61] B. Nayak, A. Mohapatra, and K. B. Mohanty, "Parameter estimation of single diode PV module based on GWO algorithm," *Renewable Energy Focus*, vol. 30, pp. 1-12, Sep. 2019.

[62] K. Yu, B. Qu, C. Yue, S. Ge, X. Chen, and J. Liang, "A performance-guided JAYA algorithm for parameters identification of photovoltaic cell and module," *Applied Energy*, vol. 237, pp. 241-257, Mar. 2019.

[63] Shuhui Xu and Yong Wang, "Parameter estimation of photovoltaic modules using a hybrid flower pollination algorithm", An International Journal of Energy Conversion and Management, vol.144, pp.53–68, 2017.

[64] S. Li, W. Gong, X. Yan, C. Hu, D. Bai, and L. Wang, "Parameter estimation of photovoltaic models with memetic adaptive differential evolution," *Solar Energy*, vol. 190, pp. 465–474, Sep. 2019.

[65] X. Gao *et al.*, "Parameter extraction of solar cell models using improved shuffled complex evolution algorithm," *Energy Conversion and Management*, vol. 157, pp. 460-479, Feb. 2018.

[66] Kong, W., Jia, Y., Dong, Z. Y., Meng, K., & Chai, S., "Hybrid approaches based on deep whole-sky-image learning to photovoltaic generation forecasting", *Applied Energy*, vol. *280*, 115875, 2020.

[67] Ali, A., Twala, B., & Marwala, T., "Performance of MPPT in Photovoltaic Systems Using GA-ANN Optimization Scheme", *Advances in Intelligent Systems and Computing*, vol. 668, pp. 39–49, 2018.

[68] G. Dhiman and V. Kumar, “Emperor penguin optimizer: A bio-inspired algorithm for engineering problems,” *Knowledge-Based Systems*, vol. 159, pp. 20–50, Nov. 2018, doi: 10.1016/j.knosys.2018.06.001.

[69] M. Merchaoui, A. Sakly, and M. F. Mimouni, “Particle swarm optimisation with adaptive mutation strategy for photovoltaic solar cell/module parameter extraction,” *Energy Conversion and Management*, vol. 175, pp. 151–163, Nov. 2018, doi: 10.1016/j.enconman.2018.08.081.

[70] S. Li *et al.*, “Parameter extraction of photovoltaic models using an improved teaching-learning-based optimization,” *Energy Conversion and Management*, vol. 186, pp. 293–305, Apr. 2019, doi: 10.1016/j.enconman.2019.02.048

[71] J. Prasanth Ram, T. Sudhakar Babu, Tomislav Dragicevic and N. Rajasekar, "A new hybrid bee pollinator flower pollination algorithm for solar PV parameter estimation", *International Journal of Energy Conversion and Management*, vol.135, pp.463–476, 2017.

[72] Pena-Delgado, A. F., Peraza-Vazquez, H., Almazan-Covarrubias, J. H., Torres Cruz, N., Garcia-Vite, P. M., Morales-Cepeda, A. B., & Ramirez-Arredondo, J. M., “A Novel Bio-Inspired Algorithm Applied to Selective Harmonic Elimination in a Three-Phase Eleven-Level Inverter”, *Mathematical Problems in Engineering*, 2020.

[73] Hayyolalam, V., & Pourhaji Kazem, A. A. Black Widow Optimization Algorithm: A novel meta-heuristic approach for solving engineering optimization problems. *Engineering Applications of Artificial Intelligence*, vol. 87, 103249, 2020.

[74] MacLeod, E. C., & Andrade, M. C. B, Strong, “Convergent male mate choice along two preference axes in field populations of black widow spiders”, *Animal Behaviour*, vol. 89, pp. 163-169, 2014.

[75] Baruffaldi, L., & Andrade, M. C. B, “Contact pheromones mediate male preference in black widow spiders: avoidance of hungry sexual cannibals?”, *Animal Behaviour*, vol. 102, pp. 25-32, 2015.

[76] Easwarakhanthan, T., Bottin, J., Bouhouch, I., & Boutrit, C N, “Onlinear Minimization Algorithm for Determining the Solar Cell Parameters with Microcomputers”, *International Journal of Solar Energy*, vol. 4, no. 1, pp. 1-12, 2007.

[77] Askarzadeh, A., Rezazadeh, A., “Parameter identification for solar cell models using harmony search-based algorithms”, *Solar Energy*, vol. 86, pp. 3241-3249, 2012.

[78] AlRashidi, M.R., AlHajri, M.F., El-Naggar, K.M., Al-Othman, A.K., "A new estimation approach for determining the *I–V* characteristics of solar cells", *Solar Energy*, vol. 85, pp. 1543-1550, 2011.

[79] Rezk Hegazy, *et.* al, "A robust parameter estimation approach based on stochastic fractal search optimization algorithm applied to solar PV parameter", *Energy Reports*, vol. 7, pp. 620-640, 2021.

[80] Patel SJ, Panchal AK, Kheraj V., "Extraction of solar cell parameters from a single current–voltage characteristic using teaching learning based optimization algorithm" *Applied Energy*, vol. 119, pp. 384-93, 2014.

[81] Laudani A, Riganti Fulginei F, Salvini A., "High performing extraction procedure for the one-diode model of a photovoltaic panel from experimental *I-V* curves by using reduced forms", *Solar Energy*, vol. 103, pp. 316-26, 2014.

[82] El-Fergany A., "Efficient tool to characterize photovoltaic generating systems using mine blast algorithm", *Electric Power Components and Systems*, vol. 43, no. 8-10, pp. 890-901, 2015.

[83] Chen Y, Wang X, Li D, Hong R, Shen H., "Parameters extraction from commercial solar cells *I-V* characteristics and shunt analysis", *Applied Energy*, vol. 88, no. 6, pp. 2239-44, 2011.

[84] Peng L, Sun Y, Meng Z, Wang Y, Xu Y, "A new method for determining the characteristics of solar cells", *Journal of Power Sources*, vol. 227, pp. 131-6, 2013.

[85] Chegaar, M., Ouennoughi, Z., & Hoffmann, A, "A new method for evaluating illuminated solar cell parameters", *Solid-State Electronics*, vol. 45, no. 2, pp. 293–296.

[86] Bouzidi K, Chegaar M, Bouhemadou A, "Solar cells parameters evaluation considering the series and shunt resistance", *Solar Energy Materials and Solar Cells*, vol. 91,no. 18, pp. 1647-51, 2007.

[87] Dkhichi F, Oukarfi B, Fakkar A, Belbounaguia N, "Parameter identification of solar cell model using Levenberg-Marquardt algorithm combined with simulated annealing", *Solar Energy*, vol. 110, pp.781–788. 2014. doi.org/10.1016/j.solener.2014.09.033.

[88] S. X. Yang and C. Luo, "A neural network approach to complete coverage path planning," in *IEEE Transactions on Systems, Man, and Cybernetics, Part B (Cybernetics)*, vol. 34, no. 1, pp. 718-724, Feb. 2004, doi: 10.1109/TSMCB.2003.811769.

[89] Aderemi, B.A., Chowdhury, S.P.D., Olwal, T.O., Abu-Mahfouz, A.M, "Techno-Economic Feasibility of Hybrid Solar Photovoltaic and Battery Energy Storage Power

System for a Mobile Cellular Base Station in Soshanguve", South Africa, *Energies*, vol. *11*, pp. 1572, 2018, https://doi.org/10.3390/en11061572.

[90] Shadravan S., Naji H.R., Bardsiri V.K., "The Sailfish Optimizer: A novel nature-inspired metaheuristic algorithm for solving constrained engineering optimization problems", *Engineering Applications of Artificial Intelligence*, vol. 80, pp. 20-34, 2019. https://doi.org/10.1016/j.engappai.2019.01.001.

[91] Dhiman G, Kumar V, "Spotted hyena optimizer: A novel bio-inspired based metaheuristic technique for engineering applications", *Advances in Engineering Software*, vol. 114, pp. 48-70, 2017. https://doi.org/10.1016/j.advengsoft.2017.05.014.

[92] Dkhichi F, Oukarfi B, Fakkar A, Belbounaguia N, "Parameter identification of solar cell model using Levenberg-Marquardt algorithm combined with simulated annealing", *Solar Energy*, vol. 110, pp.781–788. 2014. doi.org/10.1016/j.solener.2014.09.033

[93] Yoon Y, Geem ZW, "Parameter optimization of single-diode model of photovoltaic cell using memetic algorithm", *International Journal of photo energy*, 2015, doi.org/10.1155/2015/963562.

[94] Hachana O, Hemsas KE, Tina GM, Ventura C. Comparison of different metaheuristic algorithms for parameter identification of photovoltaic cell/module. J *Renew Sustain Energy*, vol. 5, pp. 1–18, 2013.

[95] Chen Z, Wu L, Lin P, Wu Y, Cheng S. Parameters identification of photovoltaic models using hybrid adaptive Nelder-Mead simplex algorithm based on eagle strategy. *Appl Energy*, vol. 182, pp. 47–57, 2016.

[96] Xian-Kun G, Chuan-An Y, Xiang-Chuan G, Yong-Chang Y. Accuracy comparison between implicit and explicit single-diode models of photovoltaic cells and modules *Acta Phys* Sin, vol. 63, no. 17, pp. 1–10, 2014.

[97] Yu K, Chen X, Wang X, Wang Z. Parameters identification of photovoltaic models using self-adaptive teaching-learning-based optimization. *Energy Conv. Mgmt*. vol. 145, pp. 233–46, 2017.

[98] Yuan X, He Y, Liu L, "Parameter extraction of solar cell models using chaotic asexual reproduction optimization", *Neural Comput Appl*, vol. 26, no. 5, pp. 1227–39, 2015.

[99] Ma J. Optimization approaches for parameter estimation and maximum power point tracking (MPPT) of photovoltaic systems. University of Liverpool, 2014.

[100] Lim LHI, Ye Z, Ye J, Yang D, Du H, "A linear identification of diode models from single I-V characteristics of PV panels", *IEEE Trans Ind.* Electron, vol. 62, no. 7, pp. 4181–93, 2015.

[101] Cubas J, Pindado S, Victoria M, “On the analytical approach for modeling photovoltaic systems behaviour”, *Journal of Power Sources,* vol. 247, pp. 467–74, 2014.

[102] Tong NT, Pora W, “A parameter extraction technique exploiting intrinsic properties of solar cells”, *Appl Energy,* vol. 176, pp. 104–15, 2016.

[103] Fathabadi H, “Novel neural-analytical method for determining silicon/plastic solar cells and modules characteristics”, *Energy Convers Manage,* vol. 76, pp. 253, 2013.

[104] Wei H, Cong J, Lingyun X, Deyun S, “Extracting solar cell model parameters based on chaos particle swarm algorithm” *in International conference on electric information and control engineering,* pp. 398–40, 2011.

149 point *I-V* and *P-V* Data Recorded for EIL 75 W, at G=897W/m^2, T= 60.4 Deg. C

S. No.	Voltage (V)	Current (A)	Power (W)
1.	0.13	4.209	0.5596
2.	0.26	4.207	1.1187
3.	0.39	4.205	1.6774
4.	0.53	4.203	2.2356
5.	0.66	4.201	2.7933
6.	0.79	4.2	3.3505
7.	0.93	4.198	3.9072
8.	1.06	4.196	4.4634
9.	1.19	4.194	5.0192
10.	1.32	4.192	5.5745
11.	1.46	4.191	6.1293
12.	1.59	4.189	6.6836
13.	1.72	4.187	7.2374
14.	1.86	4.185	7.7908
15.	1.99	4.183	8.3436
16.	2.12	4.181	8.896
17.	2.26	4.18	9.4479
18.	2.39	4.178	9.9994
19.	2.52	4.176	10.5503
20.	2.65	4.174	11.1008
21.	2.79	4.172	11.6507
22.	2.92	4.159	12.1658
23.	3.05	4.154	12.7044
24.	3.19	4.151	13.2463
25.	3.32	4.149	13.7925
26.	3.45	4.147	14.3384
27.	3.58	4.146	14.8839
28.	3.72	4.145	15.4305
29.	3.85	4.144	15.9779
30.	3.98	4.143	16.5249
31.	4.12	4.142	17.0717
32.	4.25	4.141	17.6183
33.	4.38	4.14	18.1645
34.	4.52	4.139	18.7116
35.	4.65	4.138	19.2591
36.	4.78	4.138	19.8063
37.	4.91	4.137	20.3535
38.	5.05	4.136	20.9004
39.	5.18	4.136	21.4472
40.	5.31	4.135	21.9938
41.	5.45	4.135	22.5402
42.	5.58	4.134	23.0865

43.	5.71	4.133	23.6327
44.	5.84	4.133	24.1791
45.	5.98	4.132	24.7253
46.	6.11	4.132	25.2714
47.	6.24	4.131	25.8174
48.	6.38	4.131	26.3632
49.	6.51	4.13	26.9088
50.	6.64	4.129	27.4543
51.	6.78	4.129	27.9997
52.	6.91	4.128	28.5449
53.	7.04	4.128	29.09
54.	7.17	4.127	29.6348
55.	7.31	4.127	30.1793
56.	7.44	4.126	30.7237
57.	7.57	4.125	31.2679
58.	7.71	4.125	31.8119
59.	7.84	4.124	32.3558
60.	7.97	4.124	32.8995
61.	8.11	4.123	33.4431
62.	8.24	4.123	33.9865
63.	8.37	4.122	34.5297
64.	8.5	4.121	35.0728
65.	8.64	4.121	35.6152
66.	8.77	4.12	36.1572
67.	8.9	4.119	36.699
68.	9.04	4.119	37.2406
69.	9.17	4.118	37.782
70.	9.3	4.117	38.3233
71.	9.43	4.117	38.8643
72.	9.57	4.116	39.4052
73.	9.7	4.115	39.946
74.	9.83	4.115	40.4857
75.	9.97	4.114	41.0246
76.	10.1	4.113	41.5634
77.	10.23	4.112	42.1019
78.	10.37	4.111	42.6402
79.	10.5	4.11	43.1783
80.	10.63	4.11	43.7162
81.	10.76	4.109	44.2539
82.	10.9	4.108	44.7893
83.	11.03	4.107	45.3239
84.	11.16	4.106	45.8581
85.	11.3	4.105	46.3921
86.	11.43	4.104	46.9258
87.	11.56	4.103	47.4593
88.	11.69	4.101	47.9895
89.	11.83	4.1	48.5175

90.	11.96	4.098	49.045
91.	12.09	4.097	49.5722
92.	12.23	4.095	50.0979
93.	12.36	4.092	50.5979
94.	12.49	4.088	51.1001
95.	12.63	4.086	51.619
96.	12.76	4.084	52.1373
97.	12.89	4.082	52.6552
98.	13.02	4.079	53.1563
99.	13.16	4.075	53.6471
100.	13.29	4.07	54.12
101.	13.42	4.064	54.5803
102.	13.56	4.058	55.036
103.	13.69	4.052	55.496
104.	13.82	4.046	55.948
105.	13.96	4.027	56.2218
106.	14.09	4.02	56.6588
107.	14.22	4.007	57.0129
108.	14.35	3.993	57.3447
109.	14.49	3.967	57.4996
110.	14.62	3.947	57.7251
111.	14.75	3.929	57.993
112.	14.89	3.922	58.4102
113.	15.02	3.876	58.2334
114.	15.15	3.856	58.4447
115.	15.28	3.848	58.8458
116.	15.42	3.824	58.9862
117.	15.55	3.786	58.9084
118.	15.68	3.746	58.7775
119.	15.82	3.686	58.3252
120.	15.95	3.631	57.9341
121.	16.08	3.555	57.2064
122.	16.22	3.523	57.1516
123.	16.35	3.455	56.5028
124.	16.48	3.434	56.6177
125.	16.61	3.348	55.6521
126.	16.75	3.33	55.7935
127.	16.88	3.203	54.0975
128.	17.01	3.186	54.2316
129.	17.15	2.946	50.5275
130.	17.28	2.89	49.9672
131.	17.41	2.852	49.6827
132.	17.54	2.727	47.8676
133.	17.68	2.638	46.6546
134.	17.81	2.479	44.1739
135.	17.94	2.393	42.9599
136.	18.08	2.264	40.9373

137.	18.21	2.102	38.2943
138.	18.34	2.013	36.9436
139.	18.48	1.85	34.1981
140.	18.61	1.697	31.5872
141.	18.74	1.591	29.8388
142.	18.87	1.389	26.2333
143.	19.01	1.286	24.4622
144.	19.14	1.121	21.4708
145.	19.27	0.959	18.5006
146.	19.41	0.729	14.1534
147.	19.54	0.574	11.2309
148.	19.67	0.528	10.3905
149.	19.81	0.24	4.7664

149 point *I-V* and *P-V* Data Recorded for SFTI 60P, at G=985W/m^2, T= 51 Deg. C

S. No.	Voltage (V)	Current (A)	Power (W)
1.	0.22	4.209	0.5596
2.	0.26	4.207	1.1187
3.	0.39	4.205	1.6774
4.	0.53	4.203	2.2356
5.	0.66	4.201	2.7933
6.	0.79	4.2	3.3505
7.	0.93	4.198	3.9072
8.	1.06	4.196	4.4634
9.	1.19	4.194	5.0192
10.	1.32	4.192	5.5745
11.	1.46	4.191	6.1293
12.	1.59	4.189	6.6836
13.	1.72	4.187	7.2374
14.	1.86	4.185	7.7908
15.	1.99	4.183	8.3436
16.	2.12	4.181	8.896
17.	2.26	4.18	9.4479
18.	2.39	4.178	9.9994
19.	2.52	4.176	10.5503
20.	2.65	4.174	11.1008
21.	2.79	4.172	11.6507
22.	2.92	4.159	12.1658
23.	3.05	4.154	12.7044
24.	3.19	4.151	13.2463
25.	3.32	4.149	13.7925
26.	3.45	4.147	14.3384
27.	3.58	4.146	14.8839
28.	3.72	4.145	15.4305
29.	3.85	4.144	15.9779
30.	3.98	4.143	16.5249
31.	4.12	4.142	17.0717
32.	4.25	4.141	17.6183
33.	4.38	4.14	18.1645
34.	4.52	4.139	18.7116
35.	4.65	4.138	19.2591
36.	4.78	4.138	19.8063
37.	4.91	4.137	20.3535
38.	5.05	4.136	20.9004
39.	5.18	4.136	21.4472
40.	5.31	4.135	21.9938
41.	5.45	4.135	22.5402
42.	5.58	4.134	23.0865

43.	5.71	4.133	23.6327
44.	5.84	4.133	24.1791
45.	5.98	4.132	24.7253
46.	6.11	4.132	25.2714
47.	6.24	4.131	25.8174
48.	6.38	4.131	26.3632
49.	6.51	4.13	26.9088
50.	6.64	4.129	27.4543
51.	6.78	4.129	27.9997
52.	6.91	4.128	28.5449
53.	7.04	4.128	29.09
54.	7.17	4.127	29.6348
55.	7.31	4.127	30.1793
56.	7.44	4.126	30.7237
57.	7.57	4.125	31.2679
58.	7.71	4.125	31.8119
59.	7.84	4.124	32.3558
60.	7.97	4.124	32.8995
61.	8.11	4.123	33.4431
62.	8.24	4.123	33.9865
63.	8.37	4.122	34.5297
64.	8.5	4.121	35.0728
65.	8.64	4.121	35.6152
66.	8.77	4.12	36.1572
67.	8.9	4.119	36.699
68.	9.04	4.119	37.2406
69.	9.17	4.118	37.782
70.	9.3	4.117	38.3233
71.	9.43	4.117	38.8643
72.	9.57	4.116	39.4052
73.	9.7	4.115	39.946
74.	9.83	4.115	40.4857
75.	9.97	4.114	41.0246
76.	10.1	4.113	41.5634
77.	10.23	4.112	42.1019
78.	10.37	4.111	42.6402
79.	10.5	4.11	43.1783
80.	10.63	4.11	43.7162
81.	10.76	4.109	44.2539
82.	10.9	4.108	44.7893
83.	11.03	4.107	45.3239
84.	11.16	4.106	45.8581
85.	11.3	4.105	46.3921
86.	11.43	4.104	46.9258
87.	11.56	4.103	47.4593
88.	11.69	4.101	47.9895
89.	11.83	4.1	48.5175

90.	11.96	4.098	49.045
91.	12.09	4.097	49.5722
92.	12.23	4.095	50.0979
93.	12.36	4.092	50.5979
94.	12.49	4.088	51.1001
95.	12.63	4.086	51.619
96.	12.76	4.084	52.1373
97.	12.89	4.082	52.6552
98.	13.02	4.079	53.1563
99.	13.16	4.075	53.6471
100.	13.29	4.07	54.12
101.	13.42	4.064	54.5803
102.	13.56	4.058	55.036
103.	13.69	4.052	55.496
104.	13.82	4.046	55.948
105.	13.96	4.027	56.2218
106.	14.09	4.02	56.6588
107.	14.22	4.007	57.0129
108.	14.35	3.993	57.3447
109.	14.49	3.967	57.4996
110.	14.62	3.947	57.7251
111.	14.75	3.929	57.993
112.	14.89	3.922	58.4102
113.	15.02	3.876	58.2334
114.	15.15	3.856	58.4447
115.	15.28	3.848	58.8458
116.	15.42	3.824	58.9862
117.	15.55	3.786	58.9084
118.	15.68	3.746	58.7775
119.	15.82	3.686	58.3252
120.	15.95	3.631	57.9341
121.	16.08	3.555	57.2064
122.	16.22	3.523	57.1516
123.	16.35	3.455	56.5028
124.	16.48	3.434	56.6177
125.	16.61	3.348	55.6521
126.	16.75	3.33	55.7935
127.	16.88	3.203	54.0975
128.	17.01	3.186	54.2316
129.	17.15	2.946	50.5275
130.	17.28	2.89	49.9672
131.	17.41	2.852	49.6827
132.	17.54	2.727	47.8676
133.	17.68	2.638	46.6546
134.	17.81	2.479	44.1739
135.	17.94	2.393	42.9599
136.	18.08	2.264	40.9373

137.	18.21	2.102	38.2943
138.	18.34	2.013	36.9436
139.	18.48	1.85	34.1981
140.	18.61	1.697	31.5872
141.	18.74	1.591	29.8388
142.	18.87	1.389	26.2333
143.	19.01	1.286	24.4622
144.	19.14	1.121	21.4708
145.	19.27	0.959	18.5006
146.	19.41	0.729	14.1534
147.	19.54	0.574	11.2309
148.	19.67	0.528	10.3905
149.	19.81	0.24	4.7664